THÈSE POUR OBTENIR LE GRADE DE DOCTEUR DE L'UNIVERSITÉ DE MONTPELLIER

En Chimie et Physico-Chimie des Matériaux

École doctorale Sciences Chimiques Balard

Unité de recherche UMR 5253 CNRS-UM-ICGM

Investigation of new amine based double hydrophilic block copolymers and their self-assembly by Neutron and Light Scattering

Présentée par Ananthapadmanabhan UNNIKRISHNAN

Le 18 Avril 2025

Sous la direction de Dr. Corine GERARDIN, Dr. Ralf SCHWEINS et Dr. Julien SCHMITT

Devant le jury composé de

Dr. François Boué, Directeur de Recherche CNRS	Rapporteur
Dr. Christophe Schatz, Maitre de conférences, Bordeaux INP	Rapporteur
Dr. Najet Mahmoudi, Chargé de Recherches, ISIS	Examinateur
Dr. Marianne Impéror-Clerc, Directrice de Recherche, LPS	Président du jury
Dr. Corine Gerardin, Directrice de Recherche CNRS, ICGM	Directrice de thèse
Dr. Julien Schmitt, Chargé de Recherches CNRS, ICGM	Directeur de thèse
Dr. Ralf Schweins, Chef de Service Structures à Grande Echelle, LSS	Invité

UNIVERSITÉ DE MONTPELLIER

Acknowledgments

I would like to express my deepest gratitude to the Institut Laue-Langevin (ILL), the University of Montpellier, and Saint-Gobain Research Provence for their invaluable support and collaboration throughout my doctoral research. Their commitment to scientific progress and generosity in providing a stimulating research environment have been essential to the successful completion of this work. I am also sincerely grateful for the financial support provided by the European Union's Horizon 2020 research and innovation programme under the Marie Skłodowska-Curie grant agreement No. 847439, through the InnovaXN scheme. This funding played a crucial role in enabling my research and broadening my academic horizons.

I am especially thankful to my supervisors, Dr. Ralf Schweins, Dr. Julien Schmitt, and Dr. Corine Gerardin, for their exceptional mentorship, guidance, and constant encouragement. Their support went far beyond professional responsibilities—they were always patient and motivating, even during the most challenging moments. I know I must have tested their patience more than once, yet they never hesitated to offer kindness and support. Their dedication to research and mentorship has had a lasting impact on me, and as I reach the end of this journey, I truly appreciate everything they have done.

A special mention goes to Dr. Gaulthier Rydzek for his unwavering support throughout this project. His deep expertise in synthesis and his willingness to help whenever I faced challenges were invaluable. His commitment, both during my experimental work and throughout my time in Montpellier, is something I deeply appreciate.

I would also like to thank Dr. Julien Cambedouzou, Dr. Eric Clot, and Dr. Marc Cretin for being part of my CSI committee and for their guidance and support. I am incredibly grateful to my doctoral jury committee — Dr. Christophe Schatz, Dr. François Boué, Dr. Marianne Impéror-Clerc, and Dr. Najet Mahmoudi — for their time, expertise, and for kindly agreeing to be part of this process.

I also want to extend my gratitude to Dr. Lionel Porcar for generously providing internal beam time and assisting during crucial measurements. My appreciation also goes to Dr. Sylvain Prévost, Dr. Olga Matsarskaia, Dr. Krishna Batchu, and Khadeeja Mubashira for their support during experiments at ILL, as well as Dr. Martina Sandroni and Sandrine Verdon for their invaluable help in the ILL chemistry lab. I am also grateful to the ISIS Neutron and Muon Source for providing essential experimental facilities and support during my research.

To all my colleagues at ILL, the University of Montpellier, and Saint-Gobain Research Provence—thank you for your collaboration, encouragement, and support. A special thank you to my intern, Lynn Obeid, for her contributions to this project. I am also grateful to Dr. Anu Vashishtha, Sébastien Buys, and Amna Korbi for their help in Montpellier, especially during my time away.

I also want to take a moment to appreciate all my friends at ILL and beyond for their support throughout this journey—for all the laughter and fun moments that made this experience even more special.

Finally, my deepest appreciation goes to my family—Acha, Amma, Aams, and Scra—who have been my greatest pillars of strength. Their unwavering belief in me, countless sacrifices, and constant support have been the foundation of this journey. They have shared in my highest

achievements and stood by me during the toughest times, always offering love and encouragement. I know how much this journey has meant to them, and I am forever grateful. I also want to acknowledge the divine interventions that have guided me along the way.

This PhD journey has been one of the most transformative and rewarding experiences of my life. As this chapter comes to a close, I sincerely thank everyone who has been a part of this remarkable and memorable journey.

Table of Contents

List of Abbreviations
Résumé français de la thèse
General Introduction 1

Chapter 1: Synthesis of a double-hydrophilic block copolymer with a multifunctional block: spontaneous formation of polyion complex micelles from a single cationic-anionic copolymer 48

1.1 Introduction 52
1.2 Materials and methods 58
1.3 Results and discussion 77
1.4 Conclusion 110
1.5 References 113

Chapter 2: Design of primary amine-based double-hydrophilic block copolymer: from their synthesis to the formation of polyion complex micelles by electrostatic complexation with polyacids 126

2.1 Introduction 128
2.2 Materials and methods 132
2.3 Results and discussion 143
2.4 Conclusion 165
2.5 References 169

Chapter 3: Self-assembly of oppositely charged double hydrophilic block copolymers, tailoring the shape of the micelles 180

3.1 Introduction 182
3.2 Materials and methods 186
3.3 Results and discussion 199
3.4 Conclusion 213
3.5 References 216

General Conclusion & Perspectives 227
Annex 1 - Supporting information for Chapter 1 239
Annex 2 - Supporting information for Chapter 2 257
Annex 3 - Supporting information for Chapter 3 262

List of Abbreviations

^{1}H NMR	Proton nuclear magnetic resonance
ACPA	4,4'-Azobis(4-cyanopentanoic acid)
BCP	Block copolymers
BDMAT	2-(Butylthiocarbonothioylthio)-2-methylpropionic acid
CTA	Chain transfer agent
DHBC	Double-hydrophilic block copolymer
DLS	Dynamic light scattering
DP	Degree of polymerization
D_t	Translational diffusion coefficient
$\overline{D}_t$	Averaged translational diffusion coefficient
EA	Elemental analysis
EDC	N-(3-Dimethylaminopropyl)-N′-ethylcarbodiimide
EO	Ethylene oxide units
F(q)	Form factor amplitude
$g_1(q, \tau)$	Electric field-time auto-correlation function
$g_2(q,\tau)$	Normalized intensity time auto-correlation function
HPIC	Hybrid polyion complex micelles
I_0	Intensity at zero scattering angle
MALLS	Multi-angle laser light scattering
Mn	Number-averaged molecular weight
Mw	Weight-averaged molecular weight
N-Boc	N-Boc-ethylenediamine
NHS	N-Hydroxysuccinimide
NMR	Nuclear magnetic resonance
OC	Oligochitosan
PAA	Poly(acrylic acid)
PAEMA	Poly(2-aminoethyl methacrylate)
PDI	Polydispersity index

PEO	Poly(ethylene oxide)
PIC	Polyion complex
PNIPAM	Poly(N-isopropylacrylamide)
POEGMEA	Poly(oligoethylene glycol) methyl ether acrylate
P(q)	Form factor
PSS	Poly(styrene sulfonic acid)
q	Scattering vector
ΔR_θ	Rayleigh ratio
RAFT	Reversible addition-fragmentation chain transfer
Rg	Radius of gyration
R_H	Hydrodynamic radius
SANS	Small-angle neutron scattering
SAXS	Small-angle x-ray scattering
SDA	Structure directing agent
SEC	Size exclusion chromatography
SLD	Scattering length density
SLS	Static light scattering
S(q)	Structure factor

Résumé français de la thèse

Cette thèse a pour sujet la synthèse et caractérisation de nouveaux copolymères diblocs double hydrophiles (CBDH) composés d'un bloc neutre et d'un bloc riche en amine primaires, dans le but de les utiliser pour la synthèse de matériaux mésoporeux fonctionnels pour la capture du CO_2. Les CBDH sont un type spécifique de copolymères à blocs. Malgré l'hydrophilicité des deux blocs, ils peuvent s'auto-assembler en micelles en suspensions en fonction de certains *stimuli* tels la température, le pH ou la force ionique. Ces stimuli jouent sur l'hydrophilicité d'un des blocs uniquement, ce qui permet la micellisation contrôlée.

Parmi l'ensemble des CBDH disponibles, les CBDH avec un bloc ionique présentent un comportement spécifique : ils peuvent se micelliser par complexation électrostatique entre le bloc chargé du CBDH et un agent de micellisation de charge opposée, tels des poly-électrolytes. Les micelles formées sont appelées micelles PIC pour micelles à base de complexes de PolyIons. En jouant sur le pH de la suspension, on peut contrôler la charge du bloc chargé du CBDH ou de l'agent de micellisation, et donc obtenir une micellisation contrôlée. Ces micelles PIC peuvent être utilisées pour la fabrication de matériaux mésoporeux fonctionnels en jouant à la fois le rôle d'agents structurants et d'agents de fonctionnalisation. Brièvement, les matériaux sont synthétisés en mélangeant CBDH, agent de micellisation et précurseur de silice. En contrôlant le pH, on peut en même temps initier la micellisation et la condensation de la silice. Les espèces de silice interagissent par liaison hydrogène avec le bloc neutre du CBDH soigneusement choisi, ce qui permet la formation d'une mésophase hybride entre micelles PIC et silice. Une fois le matériau synthétisé, la variation de pH permet de dissocier les micelles, éliminer l'agent de micellisation et

libérer la porosité, tandis que le CBDH reste piégé dans les pores, et le bloc chargé donne sa fonctionnalité au matériau.

Dans l'équipe, nous avons précédemment particulièrement étudié la synthèse de CBDH avec un bloc polyacide chargé, de type poly(acide acrylique) (PAA) ou sulfonate de polystyrène (PSS). Le bloc neutre est à base de poly(oxyde d'éthylène) afin d'interagir avec la silice, soit sous forme linéaire (PEO), soit sous forme de peigne en utilisant le poly(acrylate de méthyl éther oligo(éthylène glycol)) ou P(OEGMEA). Nous avons également étudié en détails leur utilisation pour former des matériaux mésoporeux fonctionnels. Notre but était donc de remplacer le bloc polyacide chargé négativement par un bloc polybase chargé positivement, et particulièrement un bloc à base d'amines primaires. L'intérêt des amines primaires est quelles sont particulièrement prometteuses pour former des carbamates en présence de CO_2, ce qui rendrait ces CBDH particulièrement intéressants pour des applications de capture de CO_2.

Nous avons développé deux approches pour former ces nouveaux CBDH :

- via la modification d'un polymère parent, le P(OEGMEA)-*b*-P(AA), dont la synthèse est parfaitement contrôlée, par des méthodes dites d'activation/amidation (*Chapitre 1*),

- via la synthèse par polymérisation radicalaire contrôlée par transfert de chaîne réversible par addition-fragmentation (polymérisation RAFT) d'un nouveau CBDH (*Chapitre 2 et 3*).

Pour chaque CBDH, nous avons caractérisé leur structure par résonance magnétique nucléaire du proton (^{1}H-RMN), analyse élémentaire, voire la chromatographie d'exclusion couplée avec la mesure de la diffusion de la lumière sous multiples angles (SEC-MALLS). Ensuite, nous avons étudié les mécanismes de micellisation des CBDH en solution par diffusion dynamique/statique de la lumière (DLS/SLS) ainsi que par diffusion des neutrons aux petits angles (SANS) ou

diffusion des rayons x aux petits angles (SAXS). Nous avons ainsi caractérisé la morphologie ainsi que les dimensions des micelles en fonction du pH ou de la concentration.

Chapitre 1 – Synthèse d'un copolymère à block double-hydrophile avec un bloc multifonctionnel : formation spontanée de micelles de complexes de polyIons à partir un copolymère anionique-cationique

Dans ce chapitre, nous avons étudié la synthèse ainsi que les propriétés d'auto-assemblage d'un CBDH, le P(OEGMEA)-*b*-P(AA) modifié par l'ajout de groupements amines. Le copolymère parent, le P(OEGMEA)-*b*-P(AA), a été synthétisé par polymérisation RAFT en milieu aqueux, avec comme monomères l'OEGMEA et l'AA respectivement. L'ajout des groupements amines s'est fait par la méthode dite d'activation/amidation. L'activation a été effectuée en présence d'EDC (N-(3-Dimethylaminopropyl)-N′-ethylcarbodiimide hydrochloride) et de NHS (N-Hydroxysuccinimide) donnant le polymère activé P(OEGMEA)-*b*-P(AA-*s*-(AA-NHS)-*s*-(Acyl urea)), contenant à la fois des amines tertiaires par l'ajout de groupements d'urée N-acylé, et des esters activés par le greffage du NHS. Ce copolymère activé a montré des capacités d'autoassemblage en milieu aqueux sous certaines conditions en pH, à l'inverse du polymère parent. Ce comportement est attribué à la présence des groupements d'urée N-acylée (chargés positivement) qui réagissent avec les groupements acrylates résiduels (chargés négativement) par interactions électrostatiques. Ensuite, l'amidation, par ajout d'éthylène diamine N-Boc a donné le polymère amidé P(OEGMEA)-*b*-P(AA-*s*-(Acyl urea)-*s*-(N-Boc)). Ce copolymère contient, outre des groupements acrylates résiduels et les amines tertiaires précédentes, des amines primaires (protégées par le groupe Boc). Ces amines primaires peuvent être exposées par dé-protection, via hydrolyse des groupements Boc à pH=1.75 par ajout d'acide trichloracétique. Le polymère final déprotégé, noté P(OEGMEA)-*b*-P(AA-*s*-(Acyl urea)-*s*-(AA/NH_2)), a plusieurs applications

potentielles telles la purification ou la séparation d'espèces. Les propriétés d'autoassemblages observées pour le copolymère activé sont maintenues après amidation et dé-protection.

Alors que les degrés de polymérisation des deux blocs du polymère parent ont été obtenus par analyse des spectres de ^{1}H-RMN, les polymères activés, amidés et déprotégés ont été étudiés par combinaison de ^{1}H-RMN et d'analyse élémentaire pour déterminer le taux de modification du bloc ionisé. Les propriétés d'autoassemblage ont été étudiées par diffusion de la lumière et de neutrons, notamment en fonction du pH. La gamme de pH 5-7 a été trouvée comme gamme optimale pour la formation de micelles. S'éloigner de cette fenêtre de pH induit la dissociation progressive des micelles, avec une diminution de l'intensité diffusée, et une dissociation complète pour des pH $\leq$ 2. La dissociation n'a pas pu être étudiée pour des pH supérieurs à 9 afin d'éviter l'hydrolyse des esters du bloc P(OEGMEA). L'hydrophobicité modérée des groupements tert-butyl (Boc) et d'urée N-acylée ne semble pas jouer un rôle important dans la formation des micelles. Les données de SANS ont été modélisées grâce au modèle dit de « micelles sphériques polymères » comprenant un cœur de densité de longueur de diffusion moyen comprenant tous les composants du bloc ionique modifié et une couronne composée de plusieurs chaînes de P(OEGMEA). Ce sont les chaînes P(OEGMEA) qui assurent la stabilité des micelles en solution. Les ajustements des données ont permis d'obtenir des informations sur le rayon de cœur R des micelles ainsi que le rayon de gyration R_g des chaînes de P(OEGMEA). Les micelles ont aussi été étudiées en fonction de la concentration, dans la gamme 1-5 %pds. En augmentant la concentration, des interactions inter-micelles sont observées, modélisées par le modèle dit de « sphères dures ».

Ainsi, cette étude a permis de montrer qu'il était possible d'ajouter des groupements amines par activation/amidation, avec des taux de conversion de l'ordre de 13-30% en amine tertiaire et jusqu'à 34% en amines primaires (protégées). Également, l'ajout d'amines sur un bloc d'acide

polyacrylique induit des propriétés d'autoassemblage entre les amines tertiaires et les groupements acrylates. Enfin, nous avons vu que la dé-protection du polymère permet d'éliminer les groupements Boc qui protègent les amines primaires sans dénaturer le CBDH ou ses propriétés.

Chapitre 2 – Conception de copolymères à blocs double-hydrophiles à base d'amines primaires : de leur synthèse à la formation de micelles de complexes de PolyIons par complexation électrostatique avec des polyacides.

Dans ce second chapitre, nous avons étudié la synthèse par polymérisation RAFT d'un nouveau CBDH riche en amine primaires, le P(OEGMEA)-*b*-P(AEMA), obtenu à partir des monomères d'OEGMEA neutre et du méthacrylate d'aminoéthyl AEMA chargé positivement. La synthèse utilise comme initiateur l'acide 4,4'-azobis(4-cyanovalérique) (ACPA) et comme agent de transfert de chaîne l'acide 2-(butylthiocarbonothioylthio)-2-methylpropanoique (BDMAT). Le copolymère synthétisé a été d'abord caractérisé par SEC-MALLS pour prouver la formation d'un unique copolymère dibloc et non de deux homopolymères, et obtenir le poids moléculaire et l'indice de polydispersité du CBDH. Ensuite, des études en ^{1}H-RMN et en analyse élémentaire ont été faites pour déterminer précisément le degré de polymérisation de chaque bloc.

Le P(OEGMEA)-*b*-P(AEMA) permet la formation de micelles PIC en solution en présence de poly-électrolytes chargés négativement (i.e. l'acide polyacrylique PAA ou le sulfonate de polystyrène PSS). La taille, la morphologie et les conditions de micellisation ont été étudiées par diffusion de la lumière et des neutrons. En présence de PAA (de poids moléculaire 5.1 kD), l'influence du pH sur la micellisation du P(OEGMEA)$_{21}$-*b*-P(AEMA)$_{32}$ (où 21 et 32 sont les degrés de polymérisation de chaque bloc) a été étudiée pour une gamme de pH allant de 3 à 8, et une fenêtre de micellisation a été trouvée pour des pH de l'ordre de 5-7, avec un optimum à pH=6. Les études SANS ont montré que les micelles étaient allongées à pH=5 et sphériques à pH=6. Ce

système, ainsi que trois autres systèmes, variant la taille du PAA utilisé comme agent de micellisation (2.1 kD au lieu de 5.1 kD), le type d'agent de micellisation (le PSS au lieu du PAA) ou la longueur du bloc PAEMA du copolymère (avec un degré de polymérisation de 32 à 22) ont été étudiés par diffusion de lumière et neutrons à pH=5 pour déterminer l'influence de ces paramètres sur la forme des micelles obtenues. Toutes les courbes obtenues par SANS ont été modélisées en combinant deux modèles : un signal de sphères ou de cylindres simples pour décrire les micelles, et une contribution de chaînes de polymères en solution pour décrire le signal aux grands angles de diffusion. A pH 5, si le premier système présente des micelles allongées, les trois autres présentent des micelles sphériques mais avec des dimensions très différentes entre elles. Le changement de taille de l'agent de micellisation (passant d'un PAA 5.1 kD à 2.1 kD) induit une augmentation de la courbure des micelles, expliquant le changement de morphologie. De même, la diminution de la longueur du PAEMA (de 32 à 22 unités) a le même effet. Enfin, les tailles des micelles sont très différentes lorsque le PSS est utilisé comme agent de micellisation. Enfin, l'influence de la concentration sur les quatre systèmes a été étudiée, de 1 à 5 %pds.

Ainsi, cette étude permet de prouver qu'il est possible d'obtenir un polymère composé d'un bloc neutre et d'un bloc d'amines primaires par polymérisation RAFT, que ce polymère permet la formation de micelles PIC par complexation électrostatique en présence d'un poly-électrolyte chargé négativement et que la taille et la forme des micelles est hautement dépendante du poids moléculaire du CBDH et de l'agent de micellisation, ainsi que de la nature de l'agent de micellisation choisi.

Chapitre 3 – Formation de micelles de complexes de PolyIons à partir d'un mélange de deux copolymères à blocs double hydrophiles de charges opposées et l'influence des tailles de blocs sur la morphologie des micelles obtenues

Le dernier chapitre étudie la formation de micelles PIC par mélange entre deux CBDH, le P(OEGMEA)-*b*-P(AEMA) développé durant cette thèse avec le P(OEGMEA)-*b*-P(AA) étudié précédemment. Les deux CBDH, tous deux obtenus par polymérisation RAFT, présentent le même bloc neutre et deux blocs chargés de charges opposées, et ont été caractérisés par ^{1}H-RMN (et analyse élémentaire pour le P(OEGMEA)-*b*-P(AEMA)) pour extraire le degré de polymérisation de chaque bloc. Comme pour les chapitres précédents, les micelles ont été caractérisées par DLS/SLS et SANS, ainsi que par SAXS pour étudier l'effet de la longueur des blocs sur la morphologie des micelles. Pour ce dernier point, quatre systèmes ont été étudiés, en faisant varier la longueur du bloc P(AEMA) ou P(AA).

Des études de conditions optimales de micellisation ont été effectuées sur le premier système, $P(OEGMEA)_{21}$-*b*-$P(AEMA)_{32}$ et $P(OEGMEA)_{22}$-*b*-$P(AA)_{37}$. Spécifiquement, nous avons étudié l'influence du ratio AA/NH_2 qui caractérise le nombre de charges négatives par rapport aux charges positives. Des micelles sont obtenues par SANS pour des ratios > 0.6, avec un optimum caractérisé par le maximum de l'intensité à q=0 Å^{-1} pour une valeur de 1.1, donc avec un léger excès de charges négatives dans le système, probablement dû à une déprotonation incomplète des groupements acrylates au pH de travail. Ensuite, nous avons étudié l'influence du pH sur une gamme allant de 2.5 à 9.5. La formation de micelles est extrêmement sensible au pH, ce qui est attendu de par les valeurs de pKa du PAA et du PAEMA, de *ca.* 4.5 et 7.5 respectivement. Le pH optimum a été trouvé à 5.5.

Suite à cette optimisation des conditions de micellisation, une étude plus approfondie de la forme et des dimensions des micelles a été effectuée par SANS et SAXS. Un signal important est observé aux plus petits angles étudiés, avec une pente proche de $q^{-5/3}$ caractéristique de cylindres flexibles. Les courbes SANS ont donc été modélisées par la somme de deux contributions, de façon similaire aux micelles PIC du chapitre 2 : des cylindres flexibles (de rayon R, de longueur de Kuhn b_{Kuhn} et de longueur de contour L_c) plus une contribution de copolymères libres en suspension. La gamme de vecteur de diffusion utilisée ne permet pas de déterminer $L_{C,}$ mais les autres paramètres ont été obtenus. Ce même système a été étudié à différentes concentrations, allant de 0.5 à 2.5 %pds, et l'étude des données SANS indique une augmentation de la rigidité des cylindres, avec une baisse de la longueur de Kuhn (i.e. deux fois la longueur de persistance) avec la concentration. Nous avons noté qu'il est impossible de déterminer si cette rigidification est réelle, ou si la variation des courbes SANS en fonction de la concentration est due à l'émergence d'interactions inter-micellaires.

Enfin, nous avons comparé par SAXS les quatre systèmes pour des conditions similaires (pH=5.5, ratio de charge optimisé pour chaque système et concentration de 1%pds). Nous avons remarqué que pour un bloc P(AEMA) donnée, l'augmentation de la longueur du bloc P(AA) a peu d'influence sur la morphologie des micelles obtenus, les courbes SAXS se superposant totalement. A l'inverse, la diminution du bloc de P(AEMA) entraîne un changement drastique de la forme des micelles, qui deviennent sphériques, quelle que soit la longueur du bloc P(AA). Ces résultats montrent une différence de comportement importante comparée aux micelles PIC obtenues avec le même CBDH P(OEGMEA)-*b*-P(AEMA) mais en utilisant un homopolymère de P(AA) et étudié en Chapitre 2. En effet, dans ce cas la longueur de chaîne du P(AA) avait une influence drastique sur la forme des micelles, ce qui n'est pas observé lors du mélange des deux CBDH. Une hypothèse

qui permettrait d'expliquer ces résultats serait que le facteur limitant est le nombre de P(OEGMEA) qui peuvent composer une couronne polymère. A nombre constant, les micelles PIC faites d'un mélange de CBDH contiendraient deux fois moins de groupement P(AEMA) et P(AA) dans leur cœur, diminuant la courbure et promouvant la formation de micelles cylindriques. Le P(AEMA) présentant une structure plus volumineuse que le P(AA), il faut ainsi diminuer sa longueur de bloc pour promouvoir une morphologie sphérique.

Nous avons donc montré dans ce chapitre qu'il est possible de former des micelles PIC par mélange de deux CBDH présentant un bloc chargé de charges opposées et un bloc neutre sous forme de peigne. Les morphologies des micelles sont largement affectées par l'utilisation de deux CBDH au lieu d'un CBDH et un homopolymère comme dans le chapitre précédent, l'encombrement stérique dans la couronne favorisant la formation de micelles allongées.

En conclusion, au cours de cette thèse nous avons développé deux méthodes pour fabriquer des copolymères diblocs double hydrophile avec un bloc neutre et un bloc chargé (partiellement) par des amines primaires. Les CBDH ainsi que les micelles obtenues en solution ont été caractérisés en détails. Dans le futur, nous souhaiterions notamment utiliser ces CBDH pour la fabrication de matériaux mésoporeux fonctionnel, en les utilisant comme agent de synthèse et fonctionnalisation.

GENERAL INTRODUCTION

1. Block Copolymers

Block copolymers (BCPs) are a unique class of polymers, made of well-defined and chemically distinct polymer blocks, bonded covalently.[1–7] They have attracted significant attention in the recent past stemming from their contribution in building self-assembled nanostructures.[8–11] In the majority of the block copolymers, the difference in hydrophilicity between the blocks results in amphiphilicity; enabling spontaneous self-assembly into nanostructures of various shapes and scales including micelles, vesicles or micro-phase separated matrices, if the chemical nature and length of the blocks are carefully chosen.[12–16] BCPs, mostly synthesized by living/controlled polymerization techniques and coupling reactions, have been found to be structurally adaptable by themselves.[17–21] This structural versatility of BCPs, polymerized as linear,[1] miktoarm star,[22] cyclic[23] and comb-like structures,[24] along with their tuneable functionality,[25–27] and biocompatibility[28–32] make them suitable for applications ranging from thermoplastic elastomers,[33] soft lithography,[34] drug delivery[35] to controlled material synthesis.[36]

2. Double Hydrophilic Block Copolymers (DHBCs)

A specific type of BCPs are double hydrophilic block copolymers (DHBCs), known for their absolute hydrophilic nature. This lack of amphiphilicity impairs their capacity to spontaneously self-assemble when dispersed in a medium,[37–41] nonetheless this behaviour can be triggered using external or internal *stimuli*.[42,43] Indeed, although these block copolymers are fully hydrophilic, the sensitivity of one of the blocks to temperature, pH, or ionic-strength (among others) can induce a reduction of its hydrophilicity resulting in self-assembly, while the second block remains hydrophilic ensuring the stability of the well-defined core-shell structure formed.[44–49] As for all BCPs, controlling the block lengths, molecular weights, solvent conditions and chain architectures

of DHBCs can influence the size and shape of the self-assemblies made.[50–55] This character has been used to obtain nanostructures of distinct frameworks, namely spheres,[56] rods,[57] and vesicles.[58,59] This peculiar behaviour of DHBCs opens the field of applications to a wide range of domains including biology,[37] catalysis,[60] and functional material synthesis.[61,62] Often, a block made from poly(ethylene glycol) (PEG) is used for making the water soluble part of the DHBCs while the second block acting as the *stimuli* responsive group is chosen based on the targeted application.[63–66] A typical example are the DHBCs in which the responsive group is Poly(N-isopropylacrylamide) PNiPAM. PNiPAM is found to be a non-ionic thermo-responsive polymer, and displays inverse solubility when the temperature is increased. Notably, it exhibits a hydrophilic to hydrophobic transition at the so-called lower critical solution temperature, LCST at ca. 32 °C. When combined with a hydrophilic PEG, it dissolves in water below LCST but forms well-defined objects at higher temperatures, making them ideal for drug delivery.[67] Similarly, pH variation can also be used as a *stimulus* to influence the formation and dissociation of the self-assemblies, if appropriate responsive groups are chosen, as seen with poly(ethylene oxide)-*b*-poly(acrylic acid) PEO-*b*-PAA and poly(2-(methacryloyloxy)ethyl phosphorylcholine-*block*-2-(diisopropylamino)ethyl methacrylate) PMPC-*b*-PDPA block copolymers depicted in **Figure 1**.[68,69] Both the above copolymers form well defined self-assemblies at an optimum pH but dissociate as soon as there is a deviation from this optimum. Even though, poly(ethylene glycol) (PEG) is the most widely used water soluble block in DHBCs, others such as poly(vinyl pyrrolidone) (PVP), poly(vinyl caprolactam) (PVCL), poly(vinyl alcohol) (PVOH), poly(vinyl amine) (PVAm) and poly(oxazoline) (POx) have also been reported.[37]

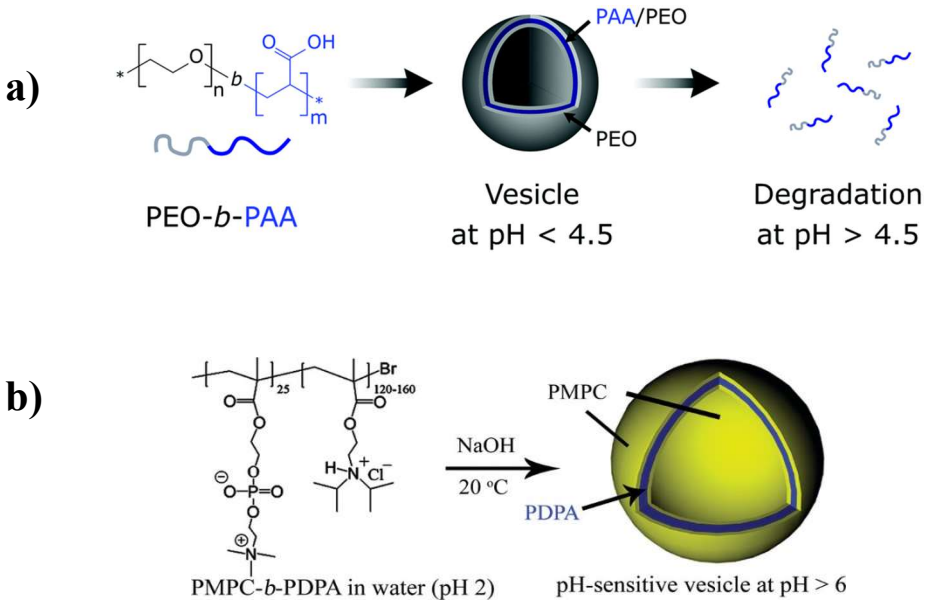


Figure 1. *(a) pH sensitive polymer vesicles from the self-assembly of a double hydrophilic block copolymer, poly(ethylene oxide)-b-poly(acrylic acid). Reprinted with permission from* [68]*. Copyright 2018 The Royal Society of Chemistry. (b) pH controlled self-assembly of biocompatible zwitterionic diblock copolymer, poly(2-(methacryloyloxy)ethyl phosphorylcholine-block-2-(diisopropylamino)ethyl methacrylate). Reprinted with permission from* [69]*. Copyright 2005 American Chemical Society.*

3. Ionic-Double Hydrophilic Block Copolymers (Ionic-DHBCs)

3.1. Ionic-DHBCs and the Formulation of (H)PIC Micelles

Among the various types of DHBCs, those containing a charged block and a neutral block are extensively studied due to the degree of tunability in their self-assembling properties.[70–76] Indeed, their self-assembly relies on electrostatic complexation in presence of a micellization partner (also called complexing agent) carrying opposite charges, forming well-defined objects. Mixing an ionic-DHBC with an oppositely-charged micellization partner results in spontaneous self-assembly, if pH of the medium falls between the pKa of the copolymer and the micellization

partner used (**Figure 2**). A pH in between the pKa of both species is important to ensure complete ionization of the components and proper charge neutralization in the final complex. A deviation from these conditions could result in structural, and functional instability of the species made. At extreme pH conditions, far from optimal, no characteristic interaction leading to self-assembly could be seen. This allows for a wide opening of applications depending on the DHBCs but also on the micellization partner used. Two main types of systems have been described depending on the micellization partner used. Polyion Complex Micelles (PIC)[64,77–81] are self-assemblies made from polyelectrolytes, while Hybrid Polyion Complexes (HPIC)[39,60,75,76,82–84] use multivalent metal ions.

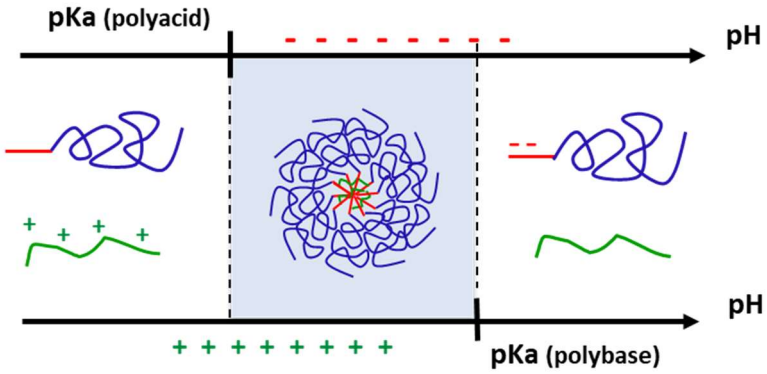


Figure 2. *Generalized scheme presenting the behaviour of typical PIC micelles, where the DHBC is made of a neutral block and a negatively-charged polyacid block. In that case, the micellization partner is a polybase.*

HPIC find notable application as nanoreactors in the synthesis of various nanomaterials including aluminium, manganese, cobalt, copper, zinc and lanthanides.[60] The growth of the nanoparticles takes place in the core of the micelle made from metal ion precursor along with the charged block of the DHBC, while the corona, made from the hydrophilic segment of the DHBC, controls the stability and dimension of the entire micelle as well as of the final nanoparticle.[76,83] Even though, HPIC micelles are primarily used in nanomaterial synthesis, they have also found application in

other fields including catalysis[85] and imaging.[75] Recently, Gadolinium ion Gd^{3+} based HPIC micelles were found to be excellent MRI contrast agent.[75,86] Gd^{3+}, when mixed with PEO-*b*-PAA, formed very stable colloids over a wide range of conditions (pH and ionic strength) and showed effectiveness as T^1 MRI contrast agent when tested *in vitro* and *in vivo*. In fact, researchers have gone one step further in this regard. They have prepared mixed HPIC nanostructures, in which two different metal ions are used simultaneously for the preparation of the HPIC micelles and have found success due to its ability to bring different properties into the same self-assembly. A good example is the preparation of HPIC micelles, again as a MRI contrast agent but this time by mixing Gd^{3+} with Zirconyl ions ZrO^{2+}, to make the core. Here, the ZrO^{2+} is used to increase the stability of the structure, while Gd^{3+} brings the desired character to the system.[75] The role of the HPIC micelles in catalysts also holds great promise but is yet to be fully utilized. The poor chemical stability in aqueous medium affects the catalytic activity of many metal ions, even after holding significant potential. This setback could be tackled using HPIC micelles, which ensures good stability of the ions in aqueous medium under a good range of pH and ionic conditions. A typical example is the HPIC micelles formed through the complexation of iron ion Fe^{3+} with PEO-*b*-PAA. This complex has been used as a homogeneous catalyst in a photo-Fenton degradation reaction of naphtol blue black and show good catalytic properties.[85]

PIC micelles find significant application in controlled synthesis of functionalized porous materials along with its notable contributions to medicine.[87–91] PIC micelles are found to be excellent carrier vehicles for the delivery of drugs, DNA and other biologically relevant species in the body, as they can electrostatically form self-assembled nanostructures with them. One of the earlier examples of these systems came from *Harada and Kataoka*, in 1995, when they mixed two poly(ethylene glycol) PEG based copolymers; PEG-poly(L-lysine) and PEG-poly(α, β-aspartic acid) block

copolymers (PEG-PLys and PEG-PAsp) to form well defined objects and discussed the potential ability of the system as carrier vehicles.[92] The above applicability of the PIC micelles even after studying for decades is still evolving and retains significant importance to this day.[51,93,94]

PIC micelles have heavily contributed to the synthesis of controlled and directly functionalized porous materials.[87] The traditional methodologies used for the synthesis of functionalized porous materials, often relying in post synthesis modification, were found to be effective but was not free of drawbacks; mainly due to the involvement of harsh methodologies including acid washing and calcination. Also, the product obtained through the traditional protocol is often not directly functionalized and require more steps for obtaining the final material. This makes the traditional methodologies less interesting. Porous materials synthesis carried out using PIC micelles is a suitable alternative to this.

Typical examples are materials synthesized using PIC micelles made from DHBCs comprising of a neutral poly(oligo(ethylene glycol) methyl ether acrylate) P(OEGMEA)) block along with a charged block (for instance poly(acrylic acid) P(AA) and poly(styrene sulphonate) P(SS)).[95–97] These micelles act simultaneously as structuring and functionalizing agent, during the formation of mesoporous materials, thanks to the specific features of each block. While the neutral P(OEGMEA)) block interacts with silica through hydrogen bonding, giving rise to a hybrid interface, the charged block provides functionality to the material formed. Since the formation of PIC micelles is sensitive to pH, after the material is made, the micellization partner can be removed by adjusting the pH, causing the micelles to dissociate and free the porosity, while the DHBC remains trapped on the pore surfaces, imparting its functionality to the material.[96] On top of giving a functional material, this method has the advantage of not employing any harsh techniques (e.g. acid washing or calcination) for freeing the porosity used in traditional protocols, making this

technique both economically and environmentally friendly. Functionalized mesoporous materials in general find applications in different domains including catalysis,[98] medicine,[99] separation & adsorption[98,100] and hence, their direct synthesis is a big step forward.

3.2. Anionic DHBCs: A Well-Studied System

Among the available DHBCs comprising of a charged block along with a neutral block, anionic systems based on polyacids, typically synthesized by Atom transfer radical polymerization (ATRP) or Reversible addition−fragmentation chain-transfer polymerization (RAFT), are the most prevalent ones; notable examples include poly(acrylic acid),[74,101] poly(methacrylic acid),[102] poly(vinyl phosphonic acid),[103] and poly(styrene sulphonate)[95] based DHBCs. Application of poly(acid) DHBCs in various fields, namely drug delivery, and colloidal stabilisation make them a very hot topic; despite being more readily available.

In the group, in depth studies on poly(acid)-based DHBCs have been carried out. Systems investigated include poly(ethylene oxide)-*b*-poly(acrylic acid) PEO-*b*-PAA,[74] poly(acrylic acid)-*b*-poly(acrylamide) PAA-*b*-PAM,[82] poly(acrylic acid)-block-poly(2-hydroxyethylacrylate) (PAA-*b*-PHEA),[82] (poly(oligoethylene glycol) methyl ether acrylate)-*b*-poly(acrylic acid) P(OEGMEA)-*b*-P(AA)[104] and poly(poly(ethylene glycol)-methyl ether acrylate)-*b*-poly(sodium 4-vinylbenzenesulfonate) P(OEGMEA)-*b*-P(SS).[95] All the copolymers mentioned above were well characterized and studied in order to understand their composition and to attain a efficient control over the degree of polymerization (DP) of each block. Understanding the composition and having control over the DP is crucial if self-assembling systems have to be made from them. A typical example of such micelles made is the polyion complex micelle derived from poly(ethylene oxide)-*b*-poly(acrylic acid) PEO-*b*-PAA and positively-charged complexing agent oligochitosan.[74]

The PIC micelles made in this fashion find applications in several fields including material functionalization[96] and drug delivery.[105] In the group the focus is more on : PIC micelles of PEO-*b*-PAA and oligochitosan allows synthesizing a –COOH functionalized porous material used in adsorption and separation studies.[104] Variation in the polymer and the micellization partner used could highly impact the size, shape and functionalities of the self-assembly made. This principle is used while choosing the DHBC and micellization agent and always depend upon its intended final application.

3.3. Cationic DHBCs: A System to Explore Further

Conversely, cationic DHBCs from straightforward synthesis protocols (in particular RAFT) are less common, although the few examples listed in the literature have found pivotal applications in various disciplines, namely drug or gene delivery.[66,106,107] Furthermore, the handful of cationic DHBCs known to date derive predominantly from secondary, tertiary, and quaternary amine groups: poly(dimethylaminoethyl methacrylate),[105] poly(ethylenimine),[108,109] and poly(3-acrylamidopropyltrimethylammonium chloride)[110]-based DHBCs.

Primary amines are found to have higher nucleophilicity and lesser steric hindrance compared to these higher order amine counterparts, making copolymers derived from them ideal for complexation, and further modifications. Notably, primary amines are well suited for CO_2 capture applications,[111] which would make this cationic DHBC highly appropriate for the design of functional mesoporous materials with anti-pollution applications. The major setback in the synthesis of the primary amine rich polymers is again its high reactivity compared to secondary, tertiary and quaternary amine groups. The high reactivity shown by primary amine groups can result in unwanted side-reactions deriving products with no interest, making its synthesis challenging.

3.4. PIC Micelles Made of a Mixture of Two DHBCs

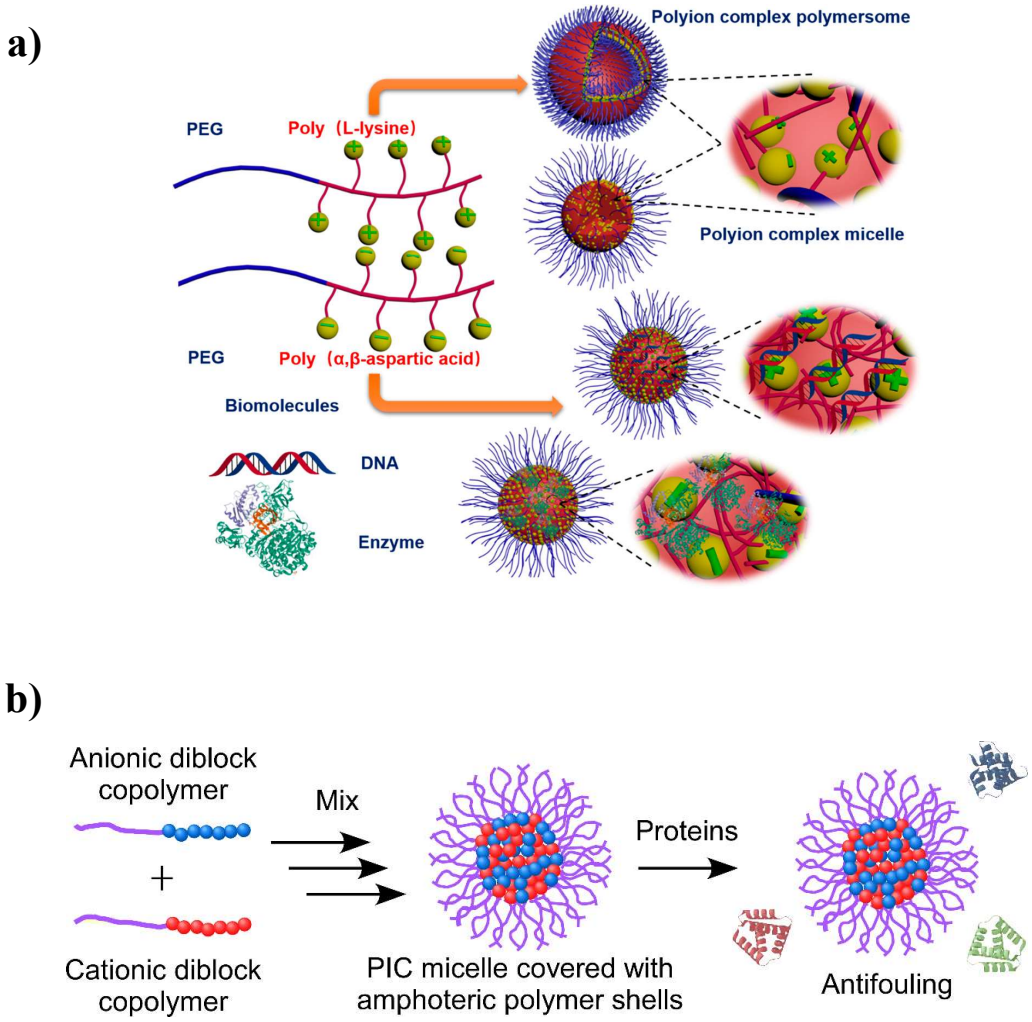


Figure 3. *(a) Consolidated presentation of research carried out by Kataoka et al. on the Polyion complex micelles and Polymersomes. Reprinted with permission from* [112]*. Copyright 2020 American Chemical Society. (b) Schematic representation of polyion complex (PIC) micelle formation from* $P(SA)_{91}S_{67}$ *and* $P(SA)_{91}A_{88}$*. The micelle displays protein antifouling character due to its amphoteric random copolymer shell (S = anionic sodium 2-acrylamido-2-methylpropanesulfonate; A = cationic 3-acrylamidopropyl trimethylammonium chloride). Adapted from* [113]*, licensed under CC BY 4.0.*

With the mastering of the synthesis of anionic-DHBCs and the development of cationic-DHBCs, a specific category of PIC micelles has emerged, based on the electrostatic complexation between

two ionic DHBCs of opposite charges (**Figure 3**).[79,107,112,114,115] Similar to PIC micelles made with a homopolymer, the charge neutralisation between the two charged blocks allows for the self-assembly of the system into PIC micelles: which requires a careful control of both DHBCs block lengths and charge ratios between the two DHBCs. Notably, as the core of the micelles is in this case composed of the two charged blocks, the corona is composed by the two neutral blocks. The nature, affinity and molecular weight of both neutral blocks have a strong influence on the shape and stability of the micelles formed by this approach.[116] By combining neutral blocks of both DHBCs together, a corona offering higher stability could be made. Also, it enables intriguing possibilities for the functionalization and the design of the corona. Through careful selection of the neutral blocks, multiple functionalities could be induced into the corona of fully DHBC-based PIC micelles, a character difficult to achieve in the traditional PIC/HPIC micelles, using either homopolymer or metals ions for self-assembly.[78,117–119] Combining two DHBCs with the same neutral block or neutral blocks exhibiting high compatibility will result in a uniform corona,[120] while choosing neutral blocks with a limited or poor affinity will interestingly lead to phase separation or asymmetry in the surface layer of the micelles.[119–121] Most of the studies carried out until now used linear polymers for building the fully DHBC-based PIC micelles. It has been already reported that the packing efficiency, size and shape of the self-assembled structures formed depend significantly on the architecture of the copolymers used.[122–125] Hence, investigating fully DHBC-based PIC micelles using comb-like neutral blocks to understand its effect on the shape, size and stability of the species formed deserves consideration (notably to evidence if a "crowding effect" in the corona influences the dimensions obtained).

4. Synthesis and Characterization of Polymers and DHBC-Based Systems

4.1. RAFT Polymerization

The Reversible Addition-Fragmentation Chain Transfer (RAFT) polymerization technique was developed in 1998 and enables access to complex polymer structures.[126,127] RAFT polymerization is a living radical polymerization, and hence mimics the characters of living polymerization while having the flexibility of radical process. Through RAFT polymerization, we gain significant control over the molecular weight of the polymers synthesized, with low polydispersity. The end-group fidelity and ability for continuous chain growth makes this technique even more useful for polymer scientists.

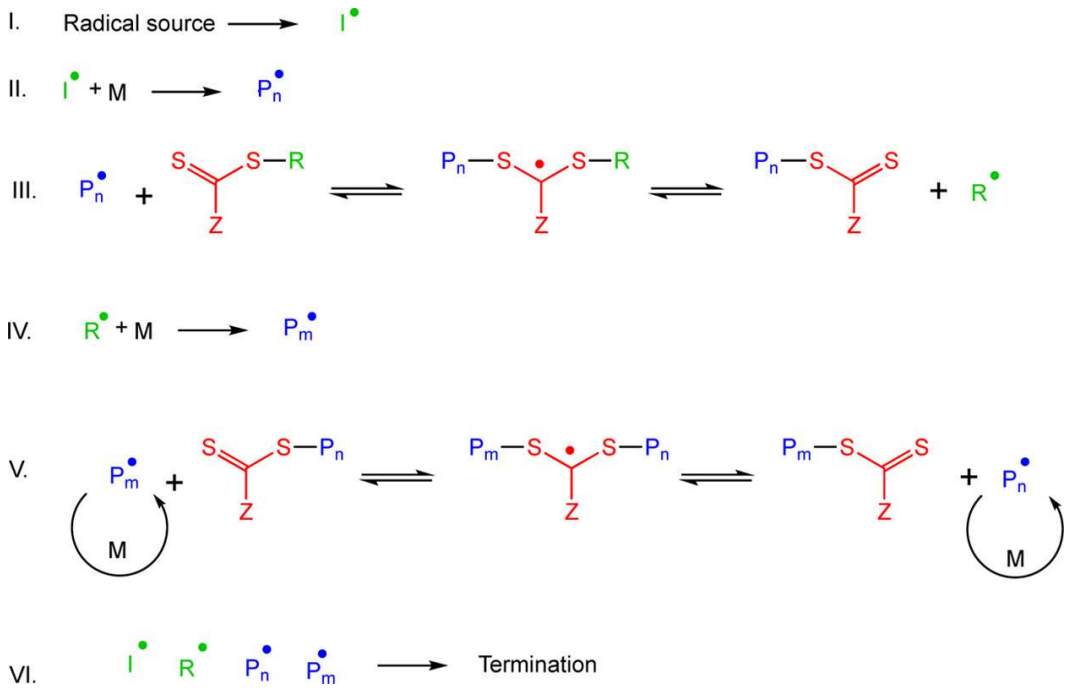


Figure 4. *Schematic representation of Reversible Addition-Fragmentation Chain Transfer (RAFT) polymerization mechanism. Reprinted from* [127]*, published under the ACS AuthorChoice License.*

The mechanism followed by RAFT polymerization, presented in **Figure 4**, could be divided stepwise:

Step I) *Radical Generation:* From an initiator a radical ($I^{\bullet}$) is generated

Steps II to IV) *CTA activation:*

Step II) The radical generated ($I^{\bullet}$) can react directly with the monomers (M) to give live oligomers ($P_n^{\bullet}$).

Step III) The live oligomers ($P_n^{\bullet}$) then react with the C=S group of the chain transfer agent (CTA, critical for regulating the molecular weight of the copolymer synthesized) to yield another intermediate radical. It is to be noted that the radical source ($I^{\bullet}$) can also directly attack the CTA to form another intermediate (*not shown in the scheme*). Both reactions are reversible and can give back the precursors. However, if the reactions proceed forward, each of them would produce different CTA along with radicals ($R^{\bullet}$).

Step IV) These radicals ($R^{\bullet}$) then can react with monomers to form other live oligomers ($P_m^{\bullet}$) and finish the CTA activation step.

Steps II to IV represents one addition-fragmentation cycle. Although, the reactions involved in this cycle are reversible, the direction described is the preferred one. Due to the stoichiometry involved in the RAFT polymerization the duration of this step is very short.

Step V) *RAFT equilibrium:* Live oligomers further polymerize by reacting with monomers until they react with a (modified) CTA species. Indeed, during this step, a live oligomer ($P_m^{\bullet}$) may react with a previously formed CTA-P_n species to form an intermediate (P_m-CTA-P_n). Since, the reaction is reversible we could revert back to the previous species, releasing the $P_m^{\bullet}$ live oligomer, or the P_m-CTA-P_n may release the previously attached $P_n^{\bullet}$ live oligomer. Then this oligomer propagates until it meets another CTA, which may retain it, through the release of another oligomer. This retain and release CTA equilibrium proceeds until all the monomers are used and

there are no monomers left for propagation. Via this protocol, RAFT polymerization confirms all the polymer chains to be of equal length, with a low polydispersity.

Step VI) *Termination of the reaction:* this may happen due to combination, disproportionation or conventional chain transfer. However, chances of these non-RAFT mechanisms to happen are very low due to the stoichiometry of the medium, which allows for the low polydispersity of the polymer chains synthesized.

The ability to synthesize polymers with distinct architectures, namely star, microgel, hyper branched and dendritic polymers, give this technique a special place in chemistry (**Figure 5**).

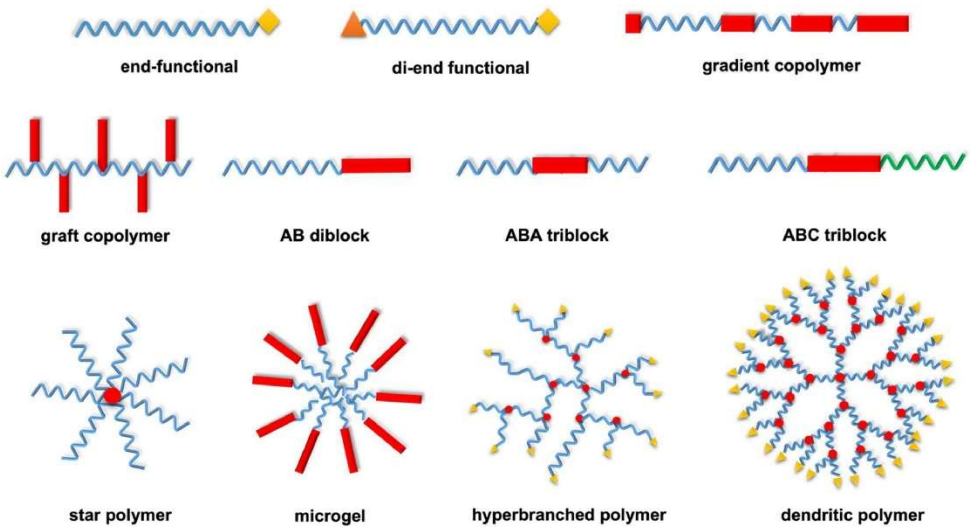


Figure 5. *Different polymer architectures that could be synthesized through RAFT polymerization. Reprinted from* [128]*, licensed under CC BY 4.0.*

4.2. Polymer Characterization

4.2.1. Size Exclusion Chromatography Multi Angle Laser Light Scattering (SEC-MALLS)

Size Exclusion Chromatography (SEC) is a powerful technique, used extensively in polymer chemistry for evaluating the molecular weight and molecular weight distribution of

macromolecules.[129,130] In a typical SEC measurement, the polymer sample is initially dissolved in a solvent, which is also used as the mobile phase (solvent passed through the column). The dissolved sample is then introduced into the column through injection (which could be either manual or automatic), where the constituents in the sample are separated based on the size. Larger populations (in terms of hydrodynamic volume) are found to elute faster than the smaller ones, due to limited interactions with the stationary phase. Generally, SEC experiments are carried out using well-defined linear polymers as standard (ideally identical in chemical nature to the sample polymer), and the molecular weight is reported on the basis of this calibration. Even though this methodology is usually considered optimal and has found success over decades, the drawbacks associated to it should not be neglected; the major one being the inability to provide the absolute molecular weight of polymers, if chemical structure or architecture of the sample analyzed is distinctly different from that of the standard. In such scenarios, instead of absolute molecular weight the instrument can only provide apparent molecular weight data. Even though correction parameters (Mark–Houwink–Sakurada, MHS) are available, their application is limited to specific cases, emphasizing the need for using other techniques which could extract absolute molecular weight of the samples.

Static light scattering (SLS) has evolved as a major contender for this, due to its ability to obtain absolute molecular weight of polymers with precision. SLS can be integrated to SEC experiments through in-line multi-angle laser light scattering (MALLS) detectors (**Figure 6**). SLS eliminates the need for accurate calibration, and calculation of the molecular weight based on the calibrated elution time. In SEC-MALLS, the molecular weight M_w is measured directly, while the details on molecular weight distribution and trace modality are obtained chromatographically. Hence, combining them together is of prime importance, for an efficient characterization of the polymer

samples. In the case of DHBCs, obtained by two successive block polymerization, SEC-MALLS is hence a powerful tool to ensure the compound synthesized is a di-block copolymer and not two separate blocks, as the former will give one population in the data analysis while the latter will result in two populations. Further, SEC-MALLS is able to evidence the presence of smaller species, that can indicate the presence of unpolymerized monomers. This factor, along with its ability to measure the distribution in size of polymers ($PDI = \frac{M_w}{M_n}$), makes SEC-MALLS an ideal route to understand the effectiveness of newly developed polymerization protocols.

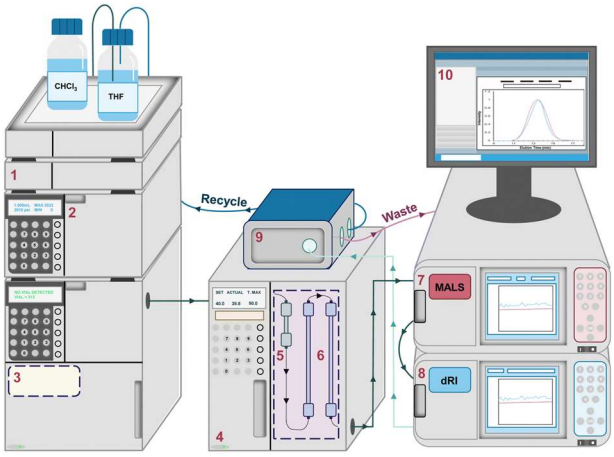


Figure 6. *Schematic representation of a typical SEC-MALLS instrument with (1) degassing unit, (2) solvent pump, (3) autosampler, (4) column oven, (5) guard column, (6) separation column, (7) MALLS detector, (8) dRI detector, (9) solvent recycling system, and (10) computer interface. Reprinted with permission from* [129]*. Copyright 2024 The Royal Society of Chemistry.*

4.2.2. Proton Nuclear Magnetic Resonance (^{1}H NMR)

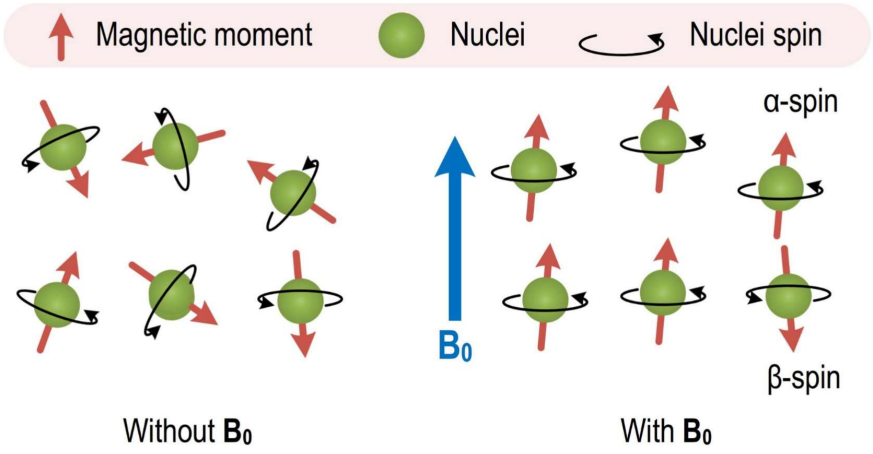


Figure 7. *Orientation of the magnetic moments based on the magnetic field provided B_0. Adapted with permission from* [131]*. Copyright 2022 Institute of Electrical and Electronics Engineers.*

Proton Nuclear Magnetic Resonance (^{1}H NMR) is a very important spectroscopic technique, widely used in chemistry for the elucidation of compound structures.[132] This versatile analytical technique holds the potential to detect the proton nuclei in the sample and determine their environment. Typically, in ^{1}H NMR, the sample is initially dissolved in a suitable solvent (deuterated), before being exposed to strong magnetic field. Under a field, the protons can either align themselves with the magnetic field (lowest energy level) or against the magnetic field (highest energy level), giving rise to two different energy levels (**Figure 7**). Indeed, the number of energy levels corresponding to an atomic nucleus depends on its nuclear spin (*I*). In case of ^{1}H, the energy level number is two ($I = \frac{1}{2}$, number of energy levels = $2I + 1$). The NMR sample is then irradiated with a pulse of radiofrequency energy, which destroys the existing equilibrium between the energy levels and promotes the jump of a few nuclei from the lowest energy to a higher energy level. The energy emitted when the nuclei fall back to their lower energy state is recorded using a sophisticated radio receiver and is represented in the form of intensity against

frequency. One might expect this energy to be constant for a nucleus at all scenarios, but interestingly it depends upon the environment around them, making structural analysis possible. The NMR spectrum when plotted is almost always represented in parts per million (p.p.m.) instead of frequency units, and the positions of the signals are noted with respect to a reference, giving rise to the chemical shift, δ.

The chemical shift δ, in p. p. m. of a given nucleus can be represented as:

$$\delta = \frac{(shift\ from\ TMS\ in\ Hz)}{(spectrometer\ frequency\ in\ MHz)} \qquad (1)$$

Generally, tetramethylsilane, TMS, is used as the reference in ^{1}H NMR. In TMS ($Si(CH_3)_4$), all four carbon atoms (as well as hydrogen atoms) are equivalent, and due to the electropositive nature of silicon when compared to carbon, resonate at a frequency lower than the value found for most of the organic compounds, making it an ideal chemical shift calibrant.

All the polymers synthesized during this project were characterized using ^{1}H NMR to obtain details about their structural composition. The degree of polymerization DP of each block in the polymers were found by integrating the peak areas in the NMR patterns with respect to an ideal reference chosen based on the scenario. Along with the DP, when needed the degree of modification carried out on the polymers were also evaluated using this technique.

4.2.3. Elemental Analysis (EA)

The determination of carbon, hydrogen, nitrogen and sulphur in the polymer samples can be carried out using CHNS elemental analyzers.[133] The analyzers are typically made allowing different configurations, ensuring the determination of the elements which are only of our interest; CHNS, CHN, CNS or N, being different possible setups, chosen depending on the application.

This robust technique works on the basis of classical Pregl-Dumas method. The high-temperature combustion (temperature of the furnace, ca. 1000 °C) in an oxygen abundant environment ensures the conversion of the carbon, hydrogen, nitrogen, and sulphur in the samples to carbon dioxide, water, nitrogen gas/oxides, and sulphur dioxide respectively. The supply of the oxygen for the combustion can be either static or dynamic. In static, a fixed volume of oxygen is introduced into the chamber while in dynamic, oxygen is introduced continuously, for a fixed period of time. Also, at times, during the combustion, catalysts are added to ensure full conversion of the elements present. Any other traces elements, if present in the sample, would also be converted to their combustion products during this process and could be removed using specific absorbents; typical example being chlorine which is converted into hydrogen chloride during combustion. Upon completion, the combusted product obtained is carried to a high purity copper at high temperature, either present in the base of the combustion chamber or in a separate furnace, by an inert carrier gas, typically Helium. The copper plays a critical role in the removal of surplus oxygen not consumed during the combustion and also, converts the nitrogen oxides present into nitrogen gas. The gases thus obtained are then passed through absorbent traps ensuring the presence of only the required emissions in the final product; carbon dioxide, water, nitrogen and sulphur dioxide. Finally, the detection and quantification of the gases follows.

4.3. Characterization of DHBC-Based Systems

4.3.1. Static and Dynamic Light Scattering (SLS and DLS)

Static and dynamic light scattering (SLS and DLS) are powerful techniques used to characterize soft matter systems such as polymers dispersed in a solvent. While dynamic light scattering studies the intensity of scattered light as a function of time at a particular angle θ, the fluctuations of which are related to the Brownian motion of the particles in solution, static light scattering measures the

temporally averaged intensity of scattered light as a function of scattering angle θ. From the former, the translation diffusion coefficient D is extracted, which is related to the hydrodynamic radius R_H of the particles along with their size distribution. From the latter, one can quantify the radius of gyration R_G, and molecular weight M_w associated to the particles. The second osmotic virial coefficient A_2 could also be calculated using static light scattering by measuring the sample at various concentrations (**Figure 8**).

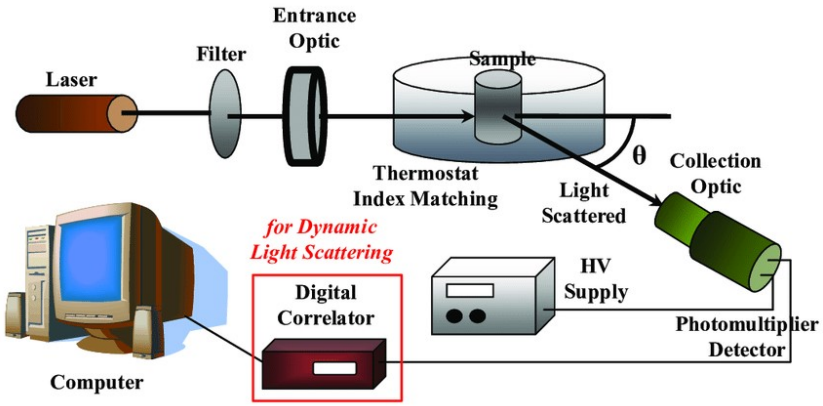


Figure 8. *Typical instrumental setup for static and dynamic light scattering measurements. Reprinted from* [134]*, licensed under CC BY 4.0.*

4.3.1.1. Static Light Scattering (SLS)

From the time-averaged scattering intensity <*I*> found experimentally, as a function of scattering vector q (a parameter associated with the scattering angle θ), the Rayleigh ratio (ΔR_θ) can be derived;

$$\Delta R_\theta = \frac{\langle I_{solution}\rangle - \langle I_{solvent}\rangle}{\langle I_{standard}\rangle}\left(\frac{n_{solvent}}{n_{standard}}\right)^2 RR_{standard} \qquad (2)$$

where, $\langle I_{solution}\rangle$, $\langle I_{solvent}\rangle$ and $\langle I_{standard}\rangle$ indicate the time-averaged scattering intensity of the solution, solvent and standard respectively at a scattering vector q, while $n_{solvent}$ and $n_{standard}$

are the refractive indexes associated to that of solvent and standard. $RR_{standard}$ is the Rayleigh ratio of the latter.

The Rayleigh ratio (ΔR_θ) can then be expressed using Zimm's approximation to extract the weight-averaged molecular weight M_w, and radius of gyration of the scattering objects R_G

$$\frac{Kc}{\Delta R_\theta} = \frac{1}{M_w} + \frac{1}{3M_w} R_G^2 q^2 \qquad (3)$$

In equation (3), q corresponds to the scattering vector related to the scattering angle θ, whereas c and K are the concentration of the object being analyzed and the associated optical constant, respectively. The scattering vector q and optical constant K can be obtained using the expressions given below;

$$q = \frac{4\pi n}{\lambda_0} sin\frac{\theta}{2} \qquad (4)$$

$$K = \frac{4\pi^2}{\lambda_0^4 N_A}\left(n\frac{dn}{dc}\right)^2 \qquad (5)$$

In equation (4) and (5), λ_0, N_A, n and $\frac{dn}{dc}$ correspond to the laser wavelength in vacuum, Avogadro's number, the refractive index of the solvent and the refractive index increment of the objects respectively.

From Zimm's plot (where $\frac{\mathrm{Kc}}{\Delta R_\theta}$ is plotted against q^2), the molecular weight (M_w) of the objects is extracted using the intercept ($M_w = \frac{1}{Intercept}$), while the slope gives information about the radius of gyration, $R_G = \sqrt{3.M_w.slope}$.

4.3.1.2. Dynamic Light Scattering (DLS)

Dynamic light scattering (DLS), investigates the scattering intensity of light from the particles against time *t* (*I(q)* against *t*), at a constant scattering angle θ (i.e. a constant scattering vector *q)*. The scattering intensity obtained can be used to extract the normalized intensity time auto-correlation function $g_2(q,\tau)$, associated to a time shift τ, which is related to the electric field-time auto-correlation function $g_1(q, \tau)$, through the Siegert's equation:

$$g_2(q,\tau) = \frac{\langle I\,(q,t) I(q,t+\,\tau)\rangle}{\langle I\,(q,t)\rangle^2} = 1 + |g_1(q,\tau)|^2 \qquad (6)$$

$I(q,t)$ and $I(q,t+\,\tau)$ are the scattering intensity at time *t* and $t + \tau$ respectively, and the temporal averaging over all the time t is presented using <>.

The electric field correlation function $g_1(q,\tau)$ collected can be used to derive the translational diffusion coefficient D_t of an object, a parameter indicating the rate at which an object is moving through the medium. This is usually done by a data treatment such as the CONTIN or cumulant analysis. CONTIN analysis is well suited for complex systems exhibiting more than one population while the cumulant analysis is used in less complex systems with a near monomodal distribution of population.

The CONTIN method was formulated using Laplace inverse by Provencher.[135,136] It links the electric field autocorrelation function $g_1(q,\tau)$ of a system to the translational diffusion coefficient D_t through the expression given below:

$$g_1(q,\tau) \;= \int_0^\infty G(D_t).\, e^{-D_t.\tau/q^2}\, dD_t \qquad (7)$$

with $G(D_t)$ the distribution function of translational diffusion coefficient D_t.

With the cumulant analysis, used for simpler systems with a quasi-monomodal distribution, the logarithm of electric field correlation function $g_1(q,\tau)$ is defined as a power sequence in terms of τ at a fixed scattering vector q and could be used to find the averaged translational diffusion coefficient $\overline{D}_t$.

$$ln\big(g_1(q,\tau)\big) = \Gamma_0 - \Gamma_1.\tau + \frac{\Gamma_2}{2!}.\tau^2 - \frac{\Gamma_3}{3!}.\tau^3 \qquad (8)$$

where Γ_0, Γ_1, Γ_2 and Γ_3 constitute the cumulants. While the average diffusion coefficient $\overline{D}_t$ is associated with the first cumulant through the expression; $\Gamma_1 = \overline{D}_t q^2$, polydispersity index PDI of the system could be derived from the ratio between the second cumulant and the square of the first cumulant ($PDI = \frac{\Gamma_2}{\Gamma_1^2}$).

Dynamic light scattering measurements carried out at different angles θ ensure the extraction of the translational diffusion coefficient extrapolated to zero-angle D_0, which is independent of the scattering vector q. D_0 for the dilute solutions can be derived using the linear approximation depicted below:

$$\overline{D}_t = D_0\big(1 + C.R_g^2.q^2\big) \qquad (9)$$

where C is a dimensionless constant related to shape of the object and its polydispersity. D_0 can be obtained from the intercept if $\overline{D}_t$ shows an angular dependence when plotted against q^2. If no angular dependencies is noted, D_0 is calculated through averaging $\overline{D}_t(q)$ collected over the angular range.

D_0 obtained is related to the hydrodynamic radius R_H of the object through the Stokes-Einstein equation:

$$R_H = \frac{K_B T}{6\pi\eta} \frac{1}{D_0} \qquad (10)$$

where k_B, T, η stands for Boltzmann constant, temperature and solvent viscosity in order.

Also, combining the results from static and dynamic light scattering ensures the deduction of a shape sensitive ratio $\frac{R_G}{R_H}$, hinting at the shape of the object probed. For homogeneous sphere the $\frac{R_G}{R_H}$ value expected is ca. 0.78, whereas for hollow sphere this value is ca. 1. Any deviation from these values indicate a distortion from sphere.

4.3.2. Small Angle Neutron/X-ray Scattering (SANS/SAXS)

Small Angle Scattering (SAS) of either neutron or x-ray is an elastic scattering technique used to investigate the structure and dynamics of soft matter samples, such as micelles in solution, based on the scattering of the collimated radiation through small angles (**Figure 9**).[137,138]

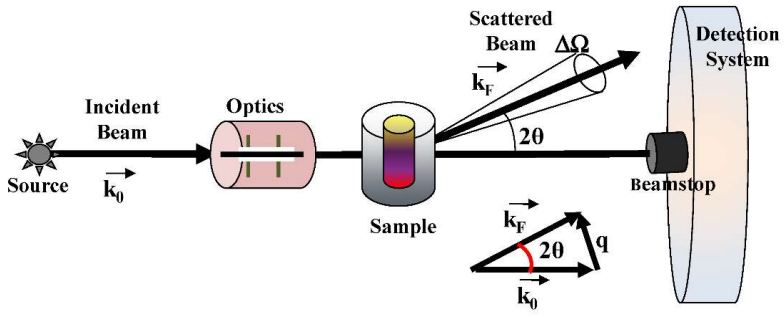


Figure 9. *General schematic representation of a Small Angle Scattering experiment. Reprinted from* [134]*, licensed under CC BY 4.0.*

In a typical SAS experiment, initially the sample is irradiated with either neutrons or x-rays. Even though, a large portion of the radiation passes through the sample with no interaction, a portion of it displays a deviation from its original path. These scattered radiations (at an angle θ) carry

information about the object probed and are collected using a 2D detector. Study of this scattered radiation intensity $I(\theta)$ as a function of the scattering angle θ, is the basis of SAS.

Scattering vector q, is a parameter associated with the scattering angle θ, and is related through the equation given below:

$$q = \frac{4\pi}{\lambda} sin\left(\frac{\theta}{2}\right) \qquad (11)$$

where λ corresponds to the wavelength associated with the incident radiation (either neutrons or x-rays).

Largely, $I(q)$ is studied as a function of scattering vector q, instead of θ, as θ is dependent of the wavelength used and hence of the experimental conditions. Scattering vector q, could also be represented in terms of initial (k_0) and final wave vectors (k_f), as depicted below:

$$q = k_f - k_0 \qquad (12)$$

The scattering intensity $I(q)$ depends largely on the molecular weight (M_w) and concentration (c) of the scattering objects along with the difference in scattering length density (SLD) between the object and the solvent in which it is dispersed. Also, it includes information about the form factor *P(q)* and the structure factor *S(q)*. While *P(q)* provides information about the size and shape of the objects, *S(q)* provides details about the interaction between objects. For samples measured in a very dilute regime, no interactions are recorded, and structure factor is reduced to $S(q) = 1$. In more concentrated systems, then interactions between objects are recorded and $S(q) \neq 1$. The scattering from SAS is collected as a 2D image. For isotropic systems, this image is azimuthally averaged to obtain the plot between $I(q)$ and the scattering vector q, containing details about size, shape, concentration, and molecular weight of the object probed.

Typically, in case of centrosymmetric objects at high concentration, where *S(q) ≠ 1*

$$I(q) \propto M_w c\left(SLD_{particle} - SLD_{solvent}\right)^2 P(q)S(q) \qquad (13)$$

while in dilute regime with *S(q) = 1,*

$$I(Q) \propto M_w c\left(SLD_{particle} - SLD_{solvent}\right)^2 P(q) \qquad (14)$$

where $SLD = \frac{b}{V_m}$, if V_m denotes the molecular volume and b the scattering length of neutrons or x-rays.

It is to be noted that, a good contrast between the solvent and the object probed is necessary for an efficient data collection. In SANS, the difference in SLDs (indicating the measure of scattering power) between the hydrogen and deuterium is often exploited to bring this contrast, while in SAXS the contrast depends upon the difference in electron density. If the contrast between the sample and solvent is not good, the scattering intensity drops drastically leading to poor data quality.

5. Objectives of the Thesis

The objective of this PhD work was to develop synthesis pathways for the design of aminated double hydrophilic block copolymers (DHBCs), specifically whose cationic block exhibits primary amines, followed by the complete evaluation of their self-assembling properties. Acknowledging this fact, two different protocols which could give amine rich DHBCs with self-assembling properties were investigated in depth.

5.1. Modification of a Parent Double Hydrophilic Block Copolymer

The first approach relies on the post-synthesis modification of a platform DHBC to introduce amine functionalities. Intrinsically amine rich cationic DHBCs are a rare find among the known DHBCs, mainly due to absence of simple synthesis procedures. We previously developed in the research group an optimized polymerization procedure to obtain polyacid-based DHBCs, fostering the inclusion of -COOH functionality.[74,96,97] Specifically, we can synthesize, via simple RAFT polymerization using (oligoethylene glycol) methyl ether acrylate (OEGMEA) and acrylic acid (AA) as monomers, with great control of the degree of polymerization, yielding the following DHBC: (poly(oligoethylene glycol) methyl ether acrylate)-*b*-poly(acrylic acid) P(OEGMEA)-*b*-P(AA).[104] This DHBC exhibits a comb-like neutral block, as this monomer allows using the same transfer agent to synthesize both blocks. As the synthesis of this DHBC is now perfectly controlled in our group, using it as a platform DHBC for further post-modification could allow obtaining several functionalities depending on the functions grafted on the PAA backbone. In the scope of the PhD, we focused on the addition of amine groups, but similar procedures could be used to add hydrophobic patches to the DHBC (for example by grafting of cyclodextrin).

In order to achieve an amine-containing copolymer through post-synthesis modification, first, the poly(acid) block of the parent copolymer, must be modified via the so-called activation/amidation route. This two-step protocol is as follows: first, the parent polymer is activated by reaction with N-(3-Dimethylaminopropyl)-N′-ethylcarbodiimide and N-Hydroxysuccinimide (EDC/NHS route) to introduce NHS activated esters into the copolymer backbone. Then, the amidation of these activated esters in presence of N-Boc-ethylenediamine (N-Boc), allows for the addition of protected primary amine species to the DHBC. Acid hydrolysis of the amidated copolymer allows removing the *tert*-butyl from the N-Boc group, and obtain the aminated DHBC. The method is

expected to give a partial amidation of the PAA backbone only, and our goal was to quantify the amount of N-Boc pendant groups obtained.

Chapter 1 focuses on this synthesis pathway, and we evidenced that, during the activation step, on top of the desired activated esters we introduced N-acyl urea, i.e. ternary amines, pendant chains to the PAA backbone. This side reaction, often neglected in the literature, has some crucial influence on the DHBCs obtained, as the presence of N-acyl urea allows for the activated and amidated DHBC to exhibit self-assembling properties in solution. We showed the micelle formation is due to electrostatic complexation between the unmodified acrylate and tertiary amine groups both present on the same DHBC. The characterization of the DHBCs was carried out after every modification step using Nuclear Magnetic Resonance (NMR) and Elemental Analysis (EA), while light (SLS/DLS), and neutron scattering techniques (SANS) were used to characterize the micelles obtained in aqueous suspensions and to study the micellization mechanisms. Ultimately, we designed a DHBC featuring acrylates, primary and tertiary amines as pendant chains in the ionic block, with potential application in various domains including separation and purification.

5.2. Direct Synthesis of Amine Rich Double Hydrophilic Block Copolymer

Our second approach lies on the direct synthesis of the primary amine rich DHBC in aqueous medium, using a straightforward RAFT polymerization procedure, which was lacking until now. Synthesis of primary amine rich DHBCs is often challenging, due to its high reactivity resulting in unwanted side reactions. Thus, only a handful of studies on the synthesis of intrinsically amine rich DHBCs have been reported yet and deserve further attention. The RAFT polymerization protocol for the synthesis of primary amine rich DHBC we developed is very straightforward, and relies again on the use of monomers that allows to work with the same chain transfer agent and initiator to polymerize both blocks. This reduces the possible chances of side-reactions to happen

and control the reactivity of primary amine entities. Here, direct synthesis of a novel amine rich DHBC, (Poly(oligoethylene glycol) methyl ether acrylate)-*b*-poly(aminoethyl methacrylate) P(OEGMEA)-*b*-P(AEMA) through a two-step RAFT polymerization is pursued. The polymer synthesis makes use of 4, 4′-azobis(4-cyano pentanoic acid) (ACPA) as initiator and 2-(butylthiocarbonothioylthio)-2-methylpropanoic acid (BDMAT) as chain transfer agent for both blocks. The cationic monomer, aminoethyl methacrylate, was chosen as it allows using similar chain transfer agents and initiator than our previously designed P(OEGMEA)-*b*-P(AA).

Chapter 2 focuses on the synthesis and characterization of this new DHBC, but also its use to form PIC micelles in presence of a negatively charged homopolymer. The copolymers synthesized were characterized using Size Exclusion Chromatography with Multi-Angle Laser Light Scattering (SEC-MALLS) to prove the successful design of a diblock copolymer and extract the molecular weight and polydispersity index of the DHBC, along with ^{1}H NMR and elemental analysis to obtain the degree of polymerization (DP) of each block. We studied the capacity of P(OEGMEA)-*b*-P(AEMA) to form micelles in presence of PAA or PSS as micellization partner, in aqueous medium under suitable pH conditions. The characterization of the micelles was conducted using light and neutron scattering experiments under various pHs and concentrations.

Finally, *Chapter 3* focuses on the formation of fully-DHBC PIC micelles by mixing the newly cationic copolymer prepared, P(OEGMEA)-*b*-P(AEMA), with the well investigated anionic comb-like copolymer, P(OEGMEA)-*b*-P(AA) using light scattering, small angle neutron and small angle x-ray scattering. By comparing the shape of the micelles obtained in that case with PIC micelles made using P(OEGMEA)-*b*-P(AEMA) with PAA alone, this allows studying the self-assembling properties between comb-like DHBC.

6. References

(1) Dau, H.; Jones, G. R.; Tsogtgerel, E.; Nguyen, D.; Keyes, A.; Liu, Y.-S.; Rauf, H.; Ordonez, E.; Puchelle, V.; Basbug Alhan, H.; Zhao, C.; Harth, E. Linear Block Copolymer Synthesis. *Chem. Rev.* **2022**, *122* (18), 14471–14553. https://doi.org/10.1021/acs.chemrev.2c00189.

(2) Kim, J. K.; Yang, S. Y.; Lee, Y.; Kim, Y. Functional Nanomaterials Based on Block Copolymer Self-Assembly. *Prog. Polym. Sci.* **2010**, *35* (11), 1325–1349. https://doi.org/10.1016/j.progpolymsci.2010.06.002.

(3) Kim, H.-C.; Park, S.-M.; Hinsberg, W. D. Block Copolymer Based Nanostructures: Materials, Processes, and Applications to Electronics. *Chem. Rev.* **2010**, *110* (1), 146–177. https://doi.org/10.1021/cr900159v.

(4) Pinna, M.; Hiltl, S.; Guo, X.; Böker, A.; Zvelindovsky, A. V. Block Copolymer Nanocontainers. *ACS Nano* **2010**, *4* (5), 2845–2855. https://doi.org/10.1021/nn901853e.

(5) Wang, X.; Guerin, G.; Wang, H.; Wang, Y.; Manners, I.; Winnik, M. A. Cylindrical Block Copolymer Micelles and Co-Micelles of Controlled Length and Architecture. *Science* **2007**, *317* (5838), 644–647. https://doi.org/10.1126/science.1141382.

(6) Bockstaller, M. R.; Mickiewicz, R. A.; Thomas, E. L. Block Copolymer Nanocomposites: Perspectives for Tailored Functional Materials. *Adv. Mater.* **2005**, *17* (11), 1331–1349. https://doi.org/10.1002/adma.200500167.

(7) *Developments in Block Copolymer Science and Technology*, 1st ed.; Hamley, I. W., Ed.; Wiley, 2004. https://doi.org/10.1002/0470093943.

(8) Lazzari, M.; López-Quintela, M. A. Block Copolymers as a Tool for Nanomaterial Fabrication. *Adv. Mater.* **2003**, *15* (19), 1583–1594. https://doi.org/10.1002/adma.200300382.

(9) Quémener, D.; Bonniol, G.; Phan, T. N. T.; Gigmes, D.; Bertin, D.; Deratani, A. Free-Standing Nanomaterials from Block Copolymer Self-Assembly. *Macromolecules* **2010**, *43* (11), 5060–5065. https://doi.org/10.1021/ma100809v.

(10) Deng, R.; Liang, F.; Zhu, J.; Yang, Z. Recent Advances in the Synthesis of Janus Nanomaterials of Block Copolymers. *Mater. Chem. Front.* **2017**, *1* (3), 431–443. https://doi.org/10.1039/C6QM00116E.

(11) Schnitzler, T.; Herrmann, A. DNA Block Copolymers: Functional Materials for Nanoscience and Biomedicine. *Acc. Chem. Res.* **2012**, *45* (9), 1419–1430. https://doi.org/10.1021/ar200211a.

(12) Klaikherd, A.; Nagamani, C.; Thayumanavan, S. Multi-Stimuli Sensitive Amphiphilic Block Copolymer Assemblies. *J. Am. Chem. Soc.* **2009**, *131* (13), 4830–4838. https://doi.org/10.1021/ja809475a.

(13) Zhu, J.; Hayward, R. C. Spontaneous Generation of Amphiphilic Block Copolymer Micelles with Multiple Morphologies through Interfacial Instabilities. *J. Am. Chem. Soc.* **2008**, *130* (23), 7496–7502. https://doi.org/10.1021/ja801268e.

(14) Zhang, W.; Shi, L.; An, Y.; Gao, L.; Wu, K.; Ma, R. A Convenient Method of Tuning Amphiphilic Block Copolymer Micellar Morphology. *Macromolecules* **2004**, *37* (7), 2551–2555. https://doi.org/10.1021/ma035801b.

(15) Zou, Y.; Zhou, X.; Ma, J.; Yang, X.; Deng, Y. Recent Advances in Amphiphilic Block Copolymer Templated Mesoporous Metal-Based Materials: Assembly Engineering and Applications. *Chem. Soc. Rev.* **2020**, *49* (4), 1173–1208. https://doi.org/10.1039/C9CS00334G.

(16) Choucair, A.; Eisenberg, A. Control of Amphiphilic Block Copolymer Morphologies Using Solution Conditions. *Eur. Phys. J. E* **2003**, *10* (1), 37–44. https://doi.org/10.1140/epje/e2003-00002-5.

(17) Hillmyer, M. Block Copolymer Synthesis. *Curr. Opin. Solid State Mater. Sci.* **1999**, *4* (6), 559–564. https://doi.org/10.1016/S1359-0286(00)00006-1.

(18) Keddie, D. J. A Guide to the Synthesis of Block Copolymers Using Reversible-Addition Fragmentation Chain Transfer (RAFT) Polymerization. *Chem Soc Rev* **2014**, *43* (2), 496–505. https://doi.org/10.1039/C3CS60290G.

(19) Jennings, J.; He, G.; Howdle, S. M.; Zetterlund, P. B. Block Copolymer Synthesis by Controlled/Living Radical Polymerisation in Heterogeneous Systems. *Chem. Soc. Rev.* **2016**, *45* (18), 5055–5084. https://doi.org/10.1039/C6CS00253F.

(20) Krishnan, A.; Roy, S.; Menon, S. Amphiphilic Block Copolymers: From Synthesis Including Living Polymerization Methods to Applications in Drug Delivery. *Eur. Polym. J.* **2022**, *172*, 111224. https://doi.org/10.1016/j.eurpolymj.2022.111224.

(21) Taskin, O. S.; Temel, B. A.; Tasdelen, M. A.; Yagci, Y. Synthesis of Block Copolymers by Selective H-Abstraction and Radical Coupling Reactions Using Benzophenone/Benzhydrol Photoinitiating System. *Eur. Polym. J.* **2015**, *62*, 304–311. https://doi.org/10.1016/j.eurpolymj.2014.07.007.

(22) Xu, Y.; Wang, C.; Zhong, S.; Li, W.; Lin, Z. Self-Assembly of Miktoarm Star-Like AB_n Block Copolymers: From Wet to Dry Brushes. *Langmuir* **2015**, *31* (9), 2905–2913. https://doi.org/10.1021/acs.langmuir.5b00081.

(23) Poelma, J. E.; Ono, K.; Miyajima, D.; Aida, T.; Satoh, K.; Hawker, C. J. Cyclic Block Copolymers for Controlling Feature Sizes in Block Copolymer Lithography. *ACS Nano* **2012**, *6* (12), 10845–10854. https://doi.org/10.1021/nn304217y.

(24) López-Barrón, C. R.; Brant, P.; Shivokhin, M.; Lu, J.; Kang, S.; Throckmorton, J. A.; Mouton, T.; Pham, T.; Savage, R. C. Long-Chain Hyperbranched Comb Block Copolymers: Synthesis, Microstructure, Rheology, and Thermal Behavior. *Macromolecules* **2018**, *51* (15), 5720–5731. https://doi.org/10.1021/acs.macromol.8b00068.

(25) Romulus, J.; Henssler, J. T.; Weck, M. Postpolymerization Modification of Block Copolymers. *Macromolecules* **2014**, *47* (16), 5437–5449. https://doi.org/10.1021/ma5009918.

(26) Durkin, T. J.; Barua, B.; Savagatrup, S. Modification of Amphiphilic Block Copolymers for Responsive and Biologically Active Surfactants in Complex Droplets. *Giant* **2023**, *13*, 100134. https://doi.org/10.1016/j.giant.2022.100134.

(27) Mons, P. J.; Poudel, P.; Hingel, M.; Schacher, F. H. Synthesis and Post-Polymerization Modification of Star-Shaped Poly(Ethylene Glycol)- *Block* -Polydehydroalanine Block

Copolymers: A Versatile Template for Designing Multifunctional Polymers. *Polym. Chem.* **2023**, *14* (31), 3600–3609. https://doi.org/10.1039/D3PY00622K.

(28) Signori, F.; Chiellini, F.; Solaro, R. New Self-Assembling Biocompatible–Biodegradable Amphiphilic Block Copolymers. *Polymer* **2005**, *46* (23), 9642–9652. https://doi.org/10.1016/j.polymer.2005.07.071.

(29) Elluru, M.; Ma, H.; Hadjiargyrou, M.; Hsiao, B. S.; Chu, B. Synthesis and Characterization of Biocompatible Hydrogel Using Pluronics-Based Block Copolymers. *Polymer* **2013**, *54* (8), 2088–2095. https://doi.org/10.1016/j.polymer.2013.02.017.

(30) Kidd, B. E.; Li, X.; Piemonte, R. C.; Cooksey, T. J.; Singh, A.; Robertson, M. L.; Madsen, L. A. Tuning Biocompatible Block Copolymer Micelles by Varying Solvent Composition: Dynamics and Populations of Micelles and Unimers. *Macromolecules* **2017**, *50* (11), 4335–4343. https://doi.org/10.1021/acs.macromol.6b02579.

(31) Aryal, S.; Prabaharan, M.; Pilla, S.; Gong, S. Biodegradable and Biocompatible Multi-Arm Star Amphiphilic Block Copolymer as a Carrier for Hydrophobic Drug Delivery. *Int. J. Biol. Macromol.* **2009**, *44* (4), 346–352. https://doi.org/10.1016/j.ijbiomac.2009.01.007.

(32) Du, J.; Fan, L.; Liu, Q. pH-Sensitive Block Copolymer Vesicles with Variable Trigger Points for Drug Delivery. *Macromolecules* **2012**, *45* (20), 8275–8283. https://doi.org/10.1021/ma3015728.

(33) Shi, W.; Lynd, N. A.; Montarnal, D.; Luo, Y.; Fredrickson, G. H.; Kramer, E. J.; Ntaras, C.; Avgeropoulos, A.; Hexemer, A. Toward Strong Thermoplastic Elastomers with Asymmetric Miktoarm Block Copolymer Architectures. *Macromolecules* **2014**, *47* (6), 2037–2043. https://doi.org/10.1021/ma402566g.

(34) Banik, M.; Shenhar, R. Nanoparticle Assembly by Transient Topography Induced by Applying Soft Lithography to Block Copolymer Films. *Soft Matter* **2024**, *20* (19), 4035–4042. https://doi.org/10.1039/D4SM00234B.

(35) Volokhova, A. S.; Edgar, K. J.; Matson, J. B. Polysaccharide-Containing Block Copolymers: Synthesis and Applications. *Mater. Chem. Front.* **2020**, *4* (1), 99–112. https://doi.org/10.1039/C9QM00481E.

(36) Schacher, F. H.; Rupar, P. A.; Manners, I. Functional Block Copolymers: Nanostructured Materials with Emerging Applications. *Angew. Chem. Int. Ed.* **2012**, *51* (32), 7898–7921. https://doi.org/10.1002/anie.201200310.

(37) El Jundi, A.; Buwalda, S. J.; Bakkour, Y.; Garric, X.; Nottelet, B. Double Hydrophilic Block Copolymers Self-Assemblies in Biomedical Applications. *Adv. Colloid Interface Sci.* **2020**, *283*, 102213. https://doi.org/10.1016/j.cis.2020.102213.

(38) Cölfen, H. Double-Hydrophilic Block Copolymers: Synthesis and Application as Novel Surfactants and Crystal Growth Modifiers. *Macromol. Rapid Commun.* **2001**, *22* (4), 219–252. https://doi.org/10.1002/1521-3927(20010201)22:4<219::AID-MARC219>3.0.CO;2-G.

(39) Nakashima, K.; Bahadur, P. Aggregation of Water-Soluble Block Copolymers in Aqueous Solutions: Recent Trends. *Adv. Colloid Interface Sci.* **2006**, *123–126*, 75–96. https://doi.org/10.1016/j.cis.2006.05.016.

(40) An, Z.; Shi, Q.; Tang, W.; Tsung, C.-K.; Hawker, C. J.; Stucky, G. D. Facile RAFT Precipitation Polymerization for the Microwave-Assisted Synthesis of Well-Defined, Double Hydrophilic Block Copolymers and Nanostructured Hydrogels. *J. Am. Chem. Soc.* **2007**, *129* (46), 14493–14499. https://doi.org/10.1021/ja0756974.

(41) Reinhold, F.; Kolb, U.; Lieberwirth, I.; Gröhn, F. Assemblies of Double Hydrophilic Block Copolymers and Oppositely Charged Dendrimers. *Langmuir* **2009**, *25* (3), 1345–1351. https://doi.org/10.1021/la8027594.

(42) Al Nakeeb, N.; Willersinn, J.; Schmidt, B. V. K. J. Self-Assembly Behavior and Biocompatible Cross-Linking of Double Hydrophilic Linear-Brush Block Copolymers. *Biomacromolecules* **2017**, *18* (11), 3695–3705. https://doi.org/10.1021/acs.biomac.7b01094.

(43) Casse, O.; Shkilnyy, A.; Linders, J.; Mayer, C.; Häussinger, D.; Völkel, A.; Thünemann, A. F.; Dimova, R.; Cölfen, H.; Meier, W.; Schlaad, H.; Taubert, A. Solution Behavior of Double-Hydrophilic Block Copolymers in Dilute Aqueous Solution. *Macromolecules* **2012**, *45* (11), 4772–4777. https://doi.org/10.1021/ma300621g.

(44) Nadal, C.; Gineste, S.; Coutelier, O.; Tourrette, A.; Marty, J.-D.; Destarac, M. A Deeper Insight into the Dual Temperature- and pH-Responsiveness of Poly(Vinylamine)-b-Poly(N-

Isopropylacrylamide) Double Hydrophilic Block Copolymers. *Colloids Surf. Physicochem. Eng. Asp.* **2022**, *641*, 128502. https://doi.org/10.1016/j.colsurfa.2022.128502.

(45) Ge, Z.; Xie, D.; Chen, D.; Jiang, X.; Zhang, Y.; Liu, H.; Liu, S. Stimuli-Responsive Double Hydrophilic Block Copolymer Micelles with Switchable Catalytic Activity. *Macromolecules* **2007**, *40* (10), 3538–3546. https://doi.org/10.1021/ma070550i.

(46) Marková, P.; Uchman, M. Synthesis and Self-Assembly of Polyzwitterionic Phenylboronic Acid-Containing Double Hydrophilic Block Copolymers. *Eur. Polym. J.* **2021**, *151*, 110439. https://doi.org/10.1016/j.eurpolymj.2021.110439.

(47) Maruya-Li, K.; Shetty, C.; Moini Jazani, A.; Arezi, N.; Oh, J. K. Dual Reduction/Acid-Responsive Disassembly and Thermoresponsive Tunability of Degradable Double Hydrophilic Block Copolymer. *ACS Omega* **2020**, *5* (7), 3734–3742. https://doi.org/10.1021/acsomega.9b04430.

(48) Yin, J.; Chen, Y.; Zhang, Z.-H.; Han, X. Stimuli-Responsive Block Copolymer-Based Assemblies for Cargo Delivery and Theranostic Applications. *Polymers* **2016**, *8* (7), 268. https://doi.org/10.3390/polym8070268.

(49) Han, J.; An, B.; Wang, Y.; Bao, X.; Ni, L.; Li, C.; Wang, L.; Xie, X. A Novel Type of Responsive Double Hydrophilic Block Copolymer-Based Multifunctional Fluorescence Chemosensor and Its Application in Biological Samples. *Sens. Actuators B Chem.* **2017**, *250*, 436–445. https://doi.org/10.1016/j.snb.2017.04.174.

(50) Kim, Y.; Pyun, J.; Fréchet, J. M. J.; Hawker, C. J.; Frank, C. W. The Dramatic Effect of Architecture on the Self-Assembly of Block Copolymers at Interfaces. *Langmuir* **2005**, *21* (23), 10444–10458. https://doi.org/10.1021/la047122f.

(51) Nabiyan, A.; Max, J. B.; Schacher, F. H. Double Hydrophilic Copolymers – Synthetic Approaches, Architectural Variety, and Current Application Fields. *Chem. Soc. Rev.* **2022**, *51* (3), 995–1044. https://doi.org/10.1039/D1CS00086A.

(52) Xu, Z.; Dong, Q.; Li, W. Architectural Design of Block Copolymers. *Macromolecules* **2024**, *57* (5), 1869–1884. https://doi.org/10.1021/acs.macromol.3c01730.

(53) Booth, C.; Attwood, D. Effects of Block Architecture and Composition on the Association Properties of Poly(Oxyalkylene) Copolymers in Aqueous Solution. *Macromol. Rapid Commun.* **2000**, *21* (9), 501–527. https://doi.org/10.1002/1521-3927(20000601)21:9<501::AID-MARC501>3.0.CO;2-R.

(54) Zehm, D.; Ratcliffe, L. P. D.; Armes, S. P. Synthesis of Diblock Copolymer Nanoparticles via RAFT Alcoholic Dispersion Polymerization: Effect of Block Copolymer Composition, Molecular Weight, Copolymer Concentration, and Solvent Type on the Final Particle Morphology. *Macromolecules* **2013**, *46* (1), 128–139. https://doi.org/10.1021/ma301459y.

(55) Rager, T.; Meyer, W. H.; Wegner, G.; Winnik, M. A. Influence of Chain Length and Salt Concentration on Block Copolymer Micellization. *Macromolecules* **1997**, *30* (17), 4911–4919. https://doi.org/10.1021/ma961866l.

(56) Chang, T.; Lord, M. S.; Bergmann, B.; Macmillan, A.; Stenzel, M. H. Size Effects of Self-Assembled Block Copolymer Spherical Micelles and Vesicles on Cellular Uptake in Human Colon Carcinoma Cells. *J Mater Chem B* **2014**, *2* (19), 2883–2891. https://doi.org/10.1039/C3TB21751E.

(57) Mihut, A. M.; Drechsler, M.; Möller, M.; Ballauff, M. Sphere-to-Rod Transition of Micelles Formed by the Semicrystalline Polybutadiene- *Block* -Poly(Ethylene Oxide) Block Copolymer in a Selective Solvent. *Macromol. Rapid Commun.* **2010**, *31* (5), 449–453. https://doi.org/10.1002/marc.200900571.

(58) Sohn, H.; Shin, H.-W.; Lee, S.-M. Metal-Mediated Morphology Regulation of Self-Assembled Double-Hydrophilic Block Copolymers. *ACS Macro Lett.* **2020**, *9* (4), 600–605. https://doi.org/10.1021/acsmacrolett.0c00120.

(59) Schmidt, B. V. K. J. Double Hydrophilic Block Copolymer Self-Assembly in Aqueous Solution. *Macromol. Chem. Phys.* **2018**, *219* (7), 1700494. https://doi.org/10.1002/macp.201700494.

(60) Gineste, S.; Mingotaud, C. Double-Hydrophilic Block Copolymer–Metal Ion Associations: Structures, Properties and Applications. *Adv. Colloid Interface Sci.* **2023**, *311*, 102808. https://doi.org/10.1016/j.cis.2022.102808.

(61) Karayianni, M.; Pispas, S. Block Copolymer Solution Self-assembly: Recent Advances, Emerging Trends, and Applications. *J. Polym. Sci.* **2021**, *59* (17), 1874–1898. https://doi.org/10.1002/pol.20210430.

(62) Tauer, K.; Khrenov, V.; Shirshova, N.; Nassif, N. Preparation and Application of Double Hydrophilic Block Copolymer Particles. *Macromol. Symp.* **2005**, *226* (1), 187–202. https://doi.org/10.1002/masy.200550818.

(63) Harada, A.; Kataoka, K. Novel Polyion Complex Micelles Entrapping Enzyme Molecules in the Core: Preparation of Narrowly-Distributed Micelles from Lysozyme and Poly(Ethylene Glycol)−Poly(Aspartic Acid) Block Copolymer in Aqueous Medium. *Macromolecules* **1998**, *31* (2), 288–294. https://doi.org/10.1021/ma971277v.

(64) Bayó-Puxan, N.; Dufresne, M.-H.; Felber, A. E.; Castagner, B.; Leroux, J.-C. Preparation of Polyion Complex Micelles from Poly(Ethylene Glycol)-Block-Polyions. *J. Controlled Release* **2011**, *156* (2), 118–127. https://doi.org/10.1016/j.jconrel.2011.07.027.

(65) Itaka, K.; Yamauchi, K.; Harada, A.; Nakamura, K.; Kawaguchi, H.; Kataoka, K. Polyion Complex Micelles from Plasmid DNA and Poly(Ethylene Glycol)–Poly(l-Lysine) Block Copolymer as Serum-Tolerable Polyplex System: Physicochemical Properties of Micelles Relevant to Gene Transfection Efficiency. *Biomaterials* **2003**, *24* (24), 4495–4506. https://doi.org/10.1016/S0142-9612(03)00347-8.

(66) Katayose, S.; Kataoka, K. Water-Soluble Polyion Complex Associates of DNA and Poly(Ethylene Glycol)−Poly(L -Lysine) Block Copolymer. *Bioconjug. Chem.* **1997**, *8* (5), 702–707. https://doi.org/10.1021/bc9701306.

(67) Bayati, S.; Bergquist, K.-E.; Zhu, K.; Nyström, B.; Skov Pedersen, J.; Galantini, L.; Schillén, K. Mixed Micelles of Oppositely Charged Poly(*N* -Isopropylacrylamide) Diblock Copolymers. *J. Polym. Sci. Part B Polym. Phys.* **2017**, *55* (19), 1457–1470. https://doi.org/10.1002/polb.24403.

(68) Shin, S. H. R.; McAninch, P. T.; Henderson, I. M.; Gomez, A.; Greene, A. C.; Carnes, E. C.; Paxton, W. F. Self-Assembly/Disassembly of Giant Double-Hydrophilic Polymersomes at

Biologically-Relevant pH. *Chem. Commun.* **2018**, *54* (65), 9043–9046. https://doi.org/10.1039/C8CC05155K.

(69) Du, J.; Tang, Y.; Lewis, A. L.; Armes, S. P. pH-Sensitive Vesicles Based on a Biocompatible Zwitterionic Diblock Copolymer. *J. Am. Chem. Soc.* **2005**, *127* (51), 17982–17983. https://doi.org/10.1021/ja056514l.

(70) Harada, A.; Kataoka, K. Pronounced Activity of Enzymes through the Incorporation into the Core of Polyion Complex Micelles Made from Charged Block Copolymers. *J. Controlled Release* **2001**, *72* (1–3), 85–91. https://doi.org/10.1016/S0168-3659(01)00264-4.

(71) Kakizawa, Y.; Kataoka, K. Block Copolymer Micelles for Delivery of Gene and Related Compounds. *Adv. Drug Deliv. Rev.* **2002**, *54* (2), 203–222. https://doi.org/10.1016/S0169-409X(02)00017-0.

(72) Read, E.; Lonetti, B.; Gineste, S.; Sutton, A. T.; Di Cola, E.; Castignolles, P.; Gaborieau, M.; Mingotaud, A.-F.; Destarac, M.; Marty, J.-D. Mechanistic Insights into the Formation of Polyion Complex Aggregates from Cationic Thermoresponsive Diblock Copolymers. *J. Colloid Interface Sci.* **2021**, *590*, 268–276. https://doi.org/10.1016/j.jcis.2021.01.028.

(73) Karayianni, M.; Koufi, D.; Pispas, S. Development of Double Hydrophilic Block Copolymer/Porphyrin Polyion Complex Micelles towards Photofunctional Nanoparticles. *Polymers* **2022**, *14* (23), 5186. https://doi.org/10.3390/polym14235186.

(74) Reboul, J.; Nugay, T.; Anik, N.; Cottet, H.; Ponsinet, V.; In, M.; Lacroix-Desmazes, P.; Gérardin, C. Synthesis of Double Hydrophilic Block Copolymers and Induced Assembly with Oligochitosan for the Preparation of Polyion Complex Micelles. *Soft Matter* **2011**, *7* (12), 5836. https://doi.org/10.1039/c1sm05230f.

(75) Yon, M.; Gineste, S.; Parigi, G.; Lonetti, B.; Gibot, L.; Talham, D. R.; Marty, J.-D.; Mingotaud, C. Hybrid Polymeric Nanostructures Stabilized by Zirconium and Gadolinium Ions for Use as Magnetic Resonance Imaging Contrast Agents. *ACS Appl. Nano Mater.* **2021**, *4* (5), 4974–4982. https://doi.org/10.1021/acsanm.1c00495.

(76) Markiewicz, K. H.; Marmuse, L.; Mounsamy, M.; Billotey, C.; Destarac, M.; Mingotaud, C.; Marty, J.-D. Assembly of Poly(Vinylphosphonic Acid)-Based Double Hydrophilic Block

Copolymers by Gadolinium Ions for the Formation of Highly Stable MRI Contrast Agents. *ACS Macro Lett.* **2022**, *11* (12), 1319–1324. https://doi.org/10.1021/acsmacrolett.2c00489.

(77) Du, Y.; Yan, W.; Lian, H.; Xiang, C.; Duan, L.; Xiao, C. 2,2′-Dithiodisuccinic Acid-Stabilized Polyion Complex Micelles for pH and Reduction Dual-Responsive Drug Delivery. *J. Colloid Interface Sci.* **2018**, *522*, 74–81. https://doi.org/10.1016/j.jcis.2018.03.049.

(78) Luo, Y.-L.; Yuan, J.-F.; Shi, J.-H.; Gao, Q.-Y. Synthesis and Characterization of Polyion Complex Micelles and Their Controlled Release of Folic Acid. *J. Colloid Interface Sci.* **2010**, *350* (1), 140–147. https://doi.org/10.1016/j.jcis.2010.06.014.

(79) Nakamura, N.; Mochida, Y.; Toh, K.; Fukushima, S.; Cabral, H.; Anraku, Y. Effect of Mixing Ratio of Oppositely Charged Block Copolymers on Polyion Complex Micelles for In Vivo Application. *Polymers* **2020**, *13* (1), 5. https://doi.org/10.3390/polym13010005.

(80) Luo, Y.; Wang, A.; Yuan, J.; Gao, Q. Preparation, Characterization and Drug Release Behavior of Polyion Complex Micelles. *Int. J. Pharm.* **2009**, *374* (1–2), 139–144. https://doi.org/10.1016/j.ijpharm.2009.03.019.

(81) Nguyen, V. T. A.; De Pauw-Gillet, M.-C.; Sandre, O.; Gauthier, M. Biocompatible Polyion Complex Micelles Synthesized from Arborescent Polymers. *Langmuir* **2016**, *32* (50), 13482–13492. https://doi.org/10.1021/acs.langmuir.6b03683.

(82) Sanson, N.; Bouyer, F.; Destarac, M.; In, M.; Gérardin, C. Hybrid Polyion Complex Micelles Formed from Double Hydrophilic Block Copolymers and Multivalent Metal Ions: Size Control and Nanostructure. *Langmuir* **2012**, *28* (8), 3773–3782. https://doi.org/10.1021/la204562t.

(83) Layrac, G.; Destarac, M.; Gérardin, C.; Tichit, D. Highly Stable Layered Double Hydroxide Colloids: A Direct Aqueous Synthesis Route from Hybrid Polyion Complex Micelles. *Langmuir* **2014**, *30* (32), 9663–9671. https://doi.org/10.1021/la502159x.

(84) Gineste, S.; Lonetti, B.; Yon, M.; Giermanska, J.; Di Cola, E.; Sztucki, M.; Coppel, Y.; Mingotaud, A.-F.; Chapel, J.-P.; Marty, J.-D.; Mingotaud, C. Hybrid Polymeric Micelles Stabilized by Gallium Ions: Structural Investigation. *J. Colloid Interface Sci.* **2022**, *609*, 698–706. https://doi.org/10.1016/j.jcis.2021.11.077.

(85) Peng, L.; Mingotaud, C.; Benoît-Marquié, F.; Marty, J.-D. Hybrid Polymeric Nanostructures Stabilized by Ferric Cations with Photo-Fenton Performance: Implications for Recoverable Multicatalyst Design. *ACS Appl. Nano Mater.* **2022**, *5* (8), 11458–11464. https://doi.org/10.1021/acsanm.2c02501.

(86) Frangville, C.; Li, Y.; Billotey, C.; Talham, D. R.; Taleb, J.; Roux, P.; Marty, J.-D.; Mingotaud, C. Assembly of Double-Hydrophilic Block Copolymers Triggered by Gadolinium Ions: New Colloidal MRI Contrast Agents. *Nano Lett.* **2016**, *16* (7), 4069–4073. https://doi.org/10.1021/acs.nanolett.6b00664.

(87) Houssein, D.; Warnant, J.; Molina, E.; Cacciaguerra, T.; Gérardin, C.; Marcotte, N. Mesoporous Silica Templated by Polyion Complex Micelles: A Versatile Approach for Controlling the Mesostructure. *Microporous Mesoporous Mater.* **2017**, *239*, 244–252. https://doi.org/10.1016/j.micromeso.2016.10.013.

(88) Molina, E.; Mathonnat, M.; Richard, J.; Lacroix-Desmazes, P.; In, M.; Dieudonné, P.; Cacciaguerra, T.; Gérardin, C.; Marcotte, N. pH-Mediated Control over the Mesostructure of Ordered Mesoporous Materials Templated by Polyion Complex Micelles. *Beilstein J. Nanotechnol.* **2019**, *10*, 144–156. https://doi.org/10.3762/bjnano.10.14.

(89) Birault, A.; Molina, E.; Trens, P.; Cot, D.; Toquer, G.; Marcotte, N.; Carcel, C.; Bartlett, J. R.; Gérardin, C.; Wong Chi Man, M. Periodic Mesoporous Organosilicas from Polyion Complex Micelles – Effect of Organic Bridge on Nanostructure. *Eur. J. Inorg. Chem.* **2019**, *2019* (27), 3157–3164. https://doi.org/10.1002/ejic.201900487.

(90) Wang, J.; Xu, W.; Guo, H.; Ding, J.; Chen, J.; Guan, J.; Wang, C. Selective Intracellular Drug Delivery from pH-Responsive Polyion Complex Micelle for Enhanced Malignancy Suppression in Vivo. *Colloids Surf. B Biointerfaces* **2015**, *135*, 283–290. https://doi.org/10.1016/j.colsurfb.2015.07.065.

(91) Dai, Y.; Ren, T.; Wang, Y.; Zhang, X. Polyion Complex Micelles to Stabilize Gold Nanoparticles for Catalytic Reduction of 4-Nitrophenol. *Gold Bull.* **2018**, *51* (1–2), 21–26. https://doi.org/10.1007/s13404-017-0225-9.

(92) Harada, A.; Kataoka, K. Polyion Complex Micelle Formation from Double-Hydrophilic Block Copolymers Composed of Charged and Non-Charged Segments in Aqueous Media. *Polym. J.* **2018**, *50* (1), 95–100. https://doi.org/10.1038/pj.2017.67.

(93) Ohno, S.; Ishihara, K.; Yusa, S. Formation of Polyion Complex (PIC) Micelles and Vesicles with Anionic pH-Responsive Unimer Micelles and Cationic Diblock Copolymers in Water. *Langmuir* **2016**, *32* (16), 3945–3953. https://doi.org/10.1021/acs.langmuir.6b00637.

(94) Wibowo, A.; Osada, K.; Matsuda, H.; Anraku, Y.; Hirose, H.; Kishimura, A.; Kataoka, K. Morphology Control in Water of Polyion Complex Nanoarchitectures of Double-Hydrophilic Charged Block Copolymers through Composition Tuning and Thermal Treatment. *Macromolecules* **2014**, *47* (9), 3086–3092. https://doi.org/10.1021/ma500314d.

(95) Richard, J.; Phimphachanh, A.; Schneider, J.; Nandi, S.; Laurent, E.; Lacroix-Desmazes, P.; Trens, P.; Devautour-Vinot, S.; Marcotte, N.; Gérardin, C. Integrated Process for Structuring and Functionalizing Ordered Mesoporous Silica to Achieve Superprotonic Conductivity. *Chem. Mater.* **2022**, *34* (17), 7828–7836. https://doi.org/10.1021/acs.chemmater.2c01352.

(96) Richard, J.; Vashishtha, A.; Phimphachanh, A.; Rydzek, G.; Lacroix-Desmazes, P.; Marcotte, N.; Gérardin, C. Mesoporous Silica for Sustainable Dye Removal: Fast and Reversible Adsorption from Ordered Mesopores Densely Functionalized with Polymers. *Microporous Mesoporous Mater.* **2024**, *379*, 113254. https://doi.org/10.1016/j.micromeso.2024.113254.

(97) Witecka, A.; Schmitt, J.; Courtien, M.; Gérardin, C.; Rydzek, G. Hybrid Mesoporous Silica Materials Templated with Surfactant Polyion Complex (SPIC) Micelles for pH-Triggered Drug Release. *Microporous Mesoporous Mater.* **2024**, *365*, 112913. https://doi.org/10.1016/j.micromeso.2023.112913.

(98) Yokoi, T.; Kubota, Y.; Tatsumi, T. Amino-Functionalized Mesoporous Silica as Base Catalyst and Adsorbent. *Appl. Catal. Gen.* **2012**, *421–422*, 14–37. https://doi.org/10.1016/j.apcata.2012.02.004.

(99) Yang, P.; Gai, S.; Lin, J. Functionalized Mesoporous Silica Materials for Controlled Drug Delivery. *Chem. Soc. Rev.* **2012**, *41* (9), 3679. https://doi.org/10.1039/c2cs15308d.

(100) Hu, Y.; Misal Castro, L. C.; Drouin, E.; Florek, J.; Kählig, H.; Larivière, D.; Kleitz, F.; Fontaine, F.-G. Size-Selective Separation of Rare Earth Elements Using Functionalized Mesoporous Silica Materials. *ACS Appl. Mater. Interfaces* **2019**, *11* (26), 23681–23691. https://doi.org/10.1021/acsami.9b04183.

(101) Warnant, J.; Reboul, J.; Aqil, A.; Cacciaguerra, T.; Jerome, C.; Gerardin, C. Nanostructured Silica Templated by Double Hydrophilic Block Copolymers with a Comb-like Architecture. *Powder Technol.* **2011**, *208* (2), 461–466. https://doi.org/10.1016/j.powtec.2010.08.043.

(102) Zhang, P.; Zhong, X.; Chai, Y.; Liu, Y. The Effect of PVP-b-PMAA Block Copolymer on Morphologies Control of Calcium Carbonate. *Colloid Polym. Sci.* **2008**, *286* (10), 1135–1141. https://doi.org/10.1007/s00396-008-1875-1.

(103) Markiewicz, K. H.; Seiler, L.; Misztalewska, I.; Winkler, K.; Harrisson, S.; Wilczewska, A. Z.; Destarac, M.; Marty, J.-D. Advantages of Poly(Vinyl Phosphonic Acid)-Based Double Hydrophilic Block Copolymers for the Stabilization of Iron Oxide Nanoparticles. *Polym. Chem.* **2016**, *7* (41), 6391–6399. https://doi.org/10.1039/C6PY01558A.

(104) Richard, J.; Phimphachanh, A.; Jamet-Fournier, A.; Cacciaguerra, T.; Dieudonné-George, P.; Cot, D.; Destarac, M.; Lacroix-Desmazes, P.; In, M.; Marcotte, N.; Gérardin, C. Dual Control of External Surface and Internal Pore Structure of Small Ordered Mesoporous Silica Particles Directed by Mixed Polyion Complex Micelles. *Microporous Mesoporous Mater.* **2022**, *338*, 111915. https://doi.org/10.1016/j.micromeso.2022.111915.

(105) Luo, Y.; Yao, X.; Yuan, J.; Ding, T.; Gao, Q. Preparation and Drug Controlled-Release of Polyion Complex Micelles as Drug Delivery Systems. *Colloids Surf. B Biointerfaces* **2009**, *68* (2), 218–224. https://doi.org/10.1016/j.colsurfb.2008.10.014.

(106) Kataoka, K.; Togawa, H.; Harada, A.; Yasugi, K.; Matsumoto, T.; Katayose, S. Spontaneous Formation of Polyion Complex Micelles with Narrow Distribution from Antisense Oligonucleotide and Cationic Block Copolymer in Physiological Saline. *Macromolecules* **1996**, *29* (26), 8556–8557. https://doi.org/10.1021/ma961217+.

(107) Voets, I. K.; Keizer, A. D.; Leermakers, F. A. M.; Debuigne, A.; Jérôme, R.; Detrembleur, C.; Cohen Stuart, M. A. Electrostatic Hierarchical Co-Assembly in Aqueous Solutions of Two Oppositely Charged Double Hydrophilic Diblock Copolymers. *Eur. Polym. J.* **2009**, *45* (10), 2913–2925. https://doi.org/10.1016/j.eurpolymj.2009.06.020.

(108) Delecourt, G.; Plet, L.; Guen, Y. L.; Tezgel, O.; Tresset, G.; Midoux, P.; Montier, T.; Bennevault, V.; Guégan, P. Synthesis of Double Hydrophilic Block Copolymers Poly(2-isopropyl-2-oxazoline- *b* -ethylenimine) and Their DNA Transfection Efficiency. *Macromol. Biosci.* **2023**, *23* (1), 2200296. https://doi.org/10.1002/mabi.202200296.

(109) Gao, Y.-X.; Yu, S.-H.; Guo, X.-H. Double Hydrophilic Block Copolymer Controlled Growth and Self-Assembly of $CaCO_3$ Multilayered Structures at the Air/Water Interface. *Langmuir* **2006**, *22* (14), 6125–6129. https://doi.org/10.1021/la060005v.

(110) Guinaudeau, A.; Coutelier, O.; Sandeau, A.; Mazières, S.; Nguyen Thi, H. D.; Le Drogo, V.; Wilson, D. J.; Destarac, M. Facile Access to Poly(*N* -Vinylpyrrolidone)-Based Double Hydrophilic Block Copolymers by Aqueous Ambient RAFT/MADIX Polymerization. *Macromolecules* **2014**, *47* (1), 41–50. https://doi.org/10.1021/ma4017899.

(111) Ko, Y. G.; Shin, S. S.; Choi, U. S. Primary, Secondary, and Tertiary Amines for CO2 Capture: Designing for Mesoporous CO2 Adsorbents. *J. Colloid Interface Sci.* **2011**, *361* (2), 594–602. https://doi.org/10.1016/j.jcis.2011.03.045.

(112) Sun, J.; Li, Z. Polyion Complexes via Electrostatic Interaction of Oppositely Charged Block Copolymers. *Macromolecules* **2020**, *53* (20), 8737–8740. https://doi.org/10.1021/acs.macromol.0c02031.

(113) Nakahata, R.; Yusa, S. Preparation of Water-Soluble Polyion Complex (PIC) Micelles Covered with Amphoteric Random Copolymer Shells with Pendant Sulfonate and Quaternary Amino Groups. *Polymers* **2018**, *10* (2), 205. https://doi.org/10.3390/polym10020205.

(114) Ando, T.; Vu, T. N.; Nishimura, T.; Takahashi, R.; Yusa, S. Synthesis and Characterization of Polyion Complex Micelles with Glycopolymer Shells for Drug Delivery Carriers. *Langmuir* **2024**, *40* (49), 26249–26258. https://doi.org/10.1021/acs.langmuir.4c03795.

(115) Yusa, S.; Yokoyama, Y.; Morishima, Y. Synthesis of Oppositely Charged Block Copolymers of Poly(Ethylene Glycol) via Reversible Addition−Fragmentation Chain Transfer Radical Polymerization and Characterization of Their Polyion Complex Micelles in Water. *Macromolecules* **2009**, *42* (1), 376–383. https://doi.org/10.1021/ma8021162.

(116) Nakai, K.; Nishiuchi, M.; Inoue, M.; Ishihara, K.; Sanada, Y.; Sakurai, K.; Yusa, S. Preparation and Characterization of Polyion Complex Micelles with Phosphobetaine Shells. *Langmuir* **2013**, *29* (31), 9651–9661. https://doi.org/10.1021/la401063b.

(117) Voets, I. K.; Moll, P. M.; Aqil, A.; Jérôme, C.; Detrembleur, C.; Waard, P. D.; Keizer, A. D.; Stuart, M. A. C. Temperature Responsive Complex Coacervate Core Micelles With a PEO and PNIPAAm Corona. *J. Phys. Chem. B* **2008**, *112* (35), 10833–10840. https://doi.org/10.1021/jp8014832.

(118) De Santis, S.; Diana Ladogana, R.; Diociaiuti, M.; Masci, G. Pegylated and Thermosensitive Polyion Complex Micelles by Self-Assembly of Two Oppositely and Permanently Charged Diblock Copolymers. *Macromolecules* **2010**, *43* (4), 1992–2001. https://doi.org/10.1021/ma9026542.

(119) Voets, I. K.; Fokkink, R.; Hellweg, T.; King, S. M.; Waard, P. D.; Keizer, A. D.; Cohen Stuart, M. A. Spontaneous Symmetry Breaking: Formation of Janus Micelles. *Soft Matter* **2009**, *5* (5), 999–1005. https://doi.org/10.1039/B812793J.

(120) Pergushov, D. V.; Müller, A. H. E.; Schacher, F. H. Micellar Interpolyelectrolyte Complexes. *Chem. Soc. Rev.* **2012**, *41* (21), 6888. https://doi.org/10.1039/c2cs35135h.

(121) Schrage, S.; Sigel, R.; Schlaad, H. Formation of Amphiphilic Polyion Complex Vesicles from Mixtures of Oppositely Charged Block Ionomers. *Macromolecules* **2003**, *36* (5), 1417–1420. https://doi.org/10.1021/ma0255940.

(122) Steinschulte, A. A.; Gelissen, A. P. H.; Jung, A.; Brugnoni, M.; Caumanns, T.; Lotze, G.; Mayer, J.; Pergushov, D. V.; Plamper, F. A. Facile Screening of Various Micellar Morphologies by Blending Miktoarm Stars and Diblock Copolymers. *ACS Macro Lett.* **2017**, *6* (7), 711–715. https://doi.org/10.1021/acsmacrolett.7b00328.

(123) Chen, F.; Raveendran, R.; Cao, C.; Chapman, R.; Stenzel, M. H. Correlation between Polymer Architecture and Polyion Complex Micelle Stability with Proteins in Spheroid Cancer Models as Seen by Light-Sheet Microscopy. *Polym. Chem.* **2019**, *10* (10), 1221–1230. https://doi.org/10.1039/C8PY01565A.

(124) Harada, A.; Kataoka, K. Effect of Charged Segment Length on Physicochemical Properties of Core−Shell Type Polyion Complex Micelles from Block Ionomers. *Macromolecules* **2003**, *36* (13), 4995–5001. https://doi.org/10.1021/ma025737i.

(125) Gioldasis, C.; Gergidis, L. N.; Vlahos, C. Micellization through Complexation of Oppositely Charged Diblock Copolymers: Effects of Composition, Polymer Architecture, Salt of Different Valency, and Thermoresponsive Block. *J. Polym. Sci.* **2021**, *59* (2), 191–204. https://doi.org/10.1002/pol.20200754.

(126) Lowe, A. B.; McCormick, C. L. Reversible Addition–Fragmentation Chain Transfer (RAFT) Radical Polymerization and the Synthesis of Water-Soluble (Co)Polymers under Homogeneous Conditions in Organic and Aqueous Media. *Prog. Polym. Sci.* **2007**, *32* (3), 283–351. https://doi.org/10.1016/j.progpolymsci.2006.11.003.

(127) Perrier, S. *50th Anniversary Perspective*: RAFT Polymerization—A User Guide. *Macromolecules* **2017**, *50* (19), 7433–7447. https://doi.org/10.1021/acs.macromol.7b00767.

(128) Zhao, W.; Li, C.; Chang, J.; Zhou, H.; Wang, D.; Sun, J.; Liu, T.; Peng, H.; Wang, Q.; Li, Y.; Whittaker, A. K. Advances and Prospects of RAFT Polymerization-Derived Nanomaterials in MRI-Assisted Biomedical Applications. *Prog. Polym. Sci.* **2023**, *146*, 101739. https://doi.org/10.1016/j.progpolymsci.2023.101739.

(129) Matson, J. B.; Steele, A. Q.; Mase, J. D.; Schulz, M. D. Polymer Characterization by Size-Exclusion Chromatography with Multi-Angle Light Scattering (SEC-MALS): A Tutorial Review. *Polym. Chem.* **2024**, *15* (3), 127–142. https://doi.org/10.1039/D3PY01181J.

(130) D'Atri, V.; Imiołek, M.; Quinn, C.; Finny, A.; Lauber, M.; Fekete, S.; Guillarme, D. Size Exclusion Chromatography of Biopharmaceutical Products: From Current Practices for Proteins to Emerging Trends for Viral Vectors, Nucleic Acids and Lipid Nanoparticles. *J. Chromatogr. A* **2024**, *1722*, 464862. https://doi.org/10.1016/j.chroma.2024.464862.

(131) Fan, S.; Zhou, Q.; Lei, K.-M.; Mak, P.-I.; Martins, R. P. Miniaturization of a Nuclear Magnetic Resonance System: Architecture and Design Considerations of Transceiver Integrated Circuits. IEEE Trans. Circuits Syst. I Regul. Pap. 2022, 69 (9), 3752–3765. https://doi.org/10.1109/TCSI.2022.3187041.

(132) Clayden, J. Organic Chemistry.

(133) Analytical Methods Committee. Evaluation of Analytical Instrumentation. Part XIX CHNS Elemental Analysers. *Accreditation Qual. Assur.* **2006**, *11* (11), 569–576. https://doi.org/10.1007/s00769-006-0185-x.

(134) Lombardo, D.; Calandra, P.; Kiselev, M. A. Structural Characterization of Biomaterials by Means of Small Angle X-Rays and Neutron Scattering (SAXS and SANS), and Light Scattering Experiments. *Molecules* **2020**, *25* (23), 5624. https://doi.org/10.3390/molecules25235624.

(135) Provencher, S. W. CONTIN: A General Purpose Constrained Regularization Program for Inverting Noisy Linear Algebraic and Integral Equations. *Comput. Phys. Commun.* **1982**, *27* (3), 229–242. https://doi.org/10.1016/0010-4655(82)90174-6.

(136) Provencher, S. W. A Constrained Regularization Method for Inverting Data Represented by Linear Algebraic or Integral Equations. *Comput. Phys. Commun.* **1982**, *27* (3), 213–227. https://doi.org/10.1016/0010-4655(82)90173-4.

(137) McDowall, D.; Adams, D. J.; Seddon, A. M. Using Small Angle Scattering to Understand Low Molecular Weight Gels. *Soft Matter* **2022**, *18* (8), 1577–1590. https://doi.org/10.1039/D1SM01707A.

(138) Wei, Y.; Hore, M. J. A. Characterizing Polymer Structure with Small-Angle Neutron Scattering: A Tutorial. *J. Appl. Phys.* **2021**, *129* (17), 171101. https://doi.org/10.1063/5.0045841.

CHAPTER 1

Synthesis of a double-hydrophilic block copolymer with a multifunctional block: spontaneous formation of polyion complex micelles from a single cationic-anionic copolymer

Ananthapadmanabhan Unnikrishnan,[1,2] Mateus Garcia Rodolfo,[2] Najet Mahmoudi,[3] Gaulthier Rydzek,[2,*] Julien Schmitt,[2,4,*] Ralf Schweins[1] and Corine Gérardin[2]

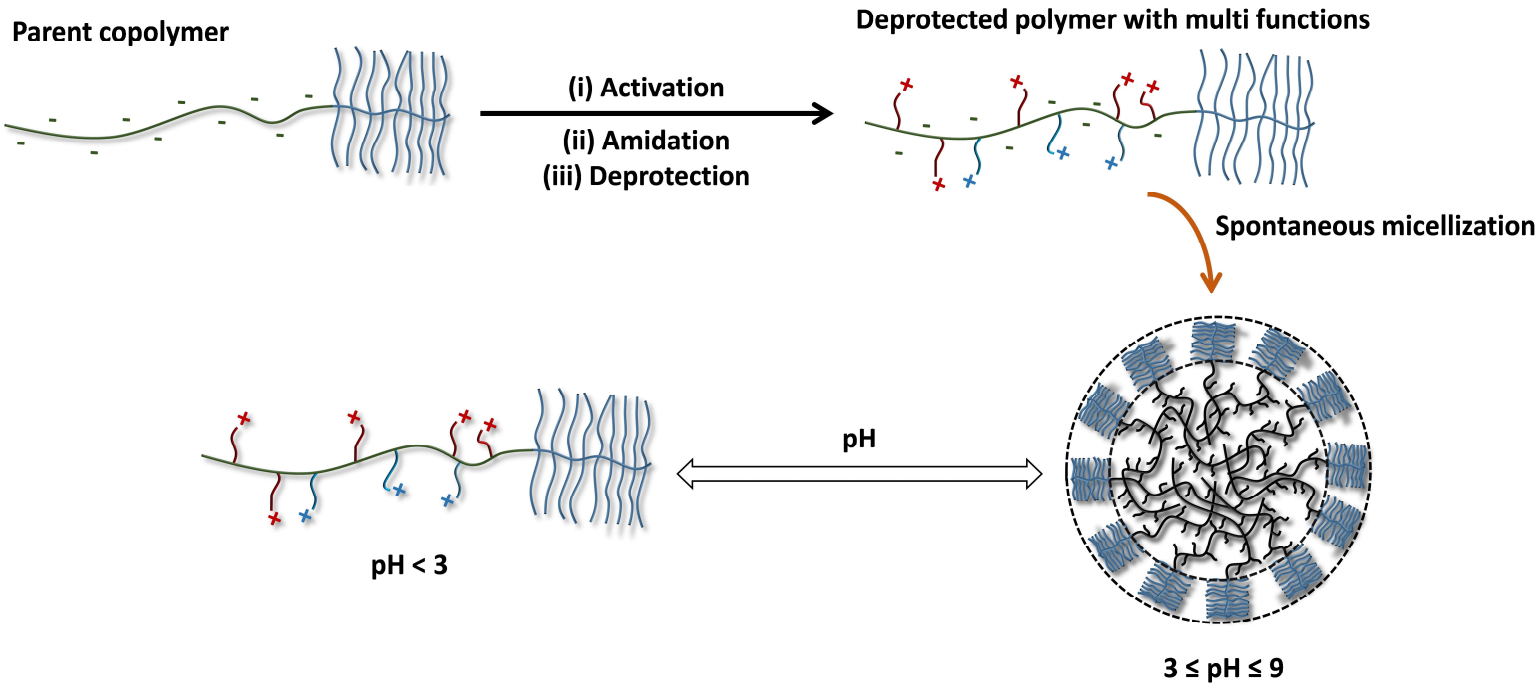
[1] Institut Laue − Langevin, DS / LSS Group, 71 Avenue des Martyrs, CS 20156, Grenoble Cedex 9, 38042, France

[2] Institut Charles Gerhardt, UMR 5253, CNRS-ENSCM-UM, University of Montpellier, Cedex, F-34295, France

[3] ISIS Neutron and Muon Source, Science and Technology Facilities Council, Rutherford Appleton Laboratory, Didcot OX11 0QX, United Kingdom

[4] LSFC – Laboratoire de Synthèse et Fonctionnalisation des Céramiques, UMR 3080 CNRS/Saint-Gobain CREE, Saint-Gobain Research Provence, 550 Avenue Alphonse Jauffret, Cavaillon, France

Schematic representation of the dynamics of polyion complex micelles



Polyion Complex micelles from a DHBC with multi anionic-cationic functions

ABSTRACT

A double-hydrophilic block copolymer (DHBC) exhibiting a multifunctional block was obtained via a multi-step synthesis. First, a parent copolymer, Par. Pol., P(OEGMA)-*b*-PAA, made of a neutral block of poly(oligo(ethylene glycol)) methyl ether acrylate (P(OEGMA)) and a weak polyacid block of poly(acrylic acid) (PAA) was synthesized by RAFT polymerization. Then, the PAA block was modified via the activation/amidation route, using N-(3-Dimethylaminopropyl)-N′-ethylcarbodiimide (EDC) and N-Hydroxysuccinimide (NHS) to activate the DHBC, giving the activated copolymer Act. Pol., before reaction with N-Boc ethylene diamine. The resulting amidated copolymer, named Ami. Pol. and made of P(OEGMEA)-*b*-P(AA-*s*-(Acyl urea)-*s*-(N-Boc)), exhibits several functional groups on the second block : acrylates from the PAA backbone, pending N-acyl urea and finally pending N-Boc-ethylenediamine. N-acyl urea exhibits tertiary amines. N-Boc-ethylenediamine adds primary amine, protected by a tert-butyl group, that can be later removed by a deprotection step using trichloroacetic acid (TCA), yielding the final P(OEGMEA)-*b*-P(AA-*s*-(Acyl urea)-*s*-(AA/NH_2)) copolymer, labelled De. Pol.. We characterized the DHBC at every stage of the modification (i.e. parent copolymer, activated copolymer, amidated copolymer and deprotected copolymer) using a combination of NMR and elemental analysis to assess the number of units of each groups in the second block. After activation/amidation, N-acyl urea groups represent ca. 13 - 32% of the second block, depending on the activation conditions, while the amount of N-Boc-ethylenediamine groups is ca. 8 - 34% depending on the amidation conditions. We evidenced the efficient removal of the tert-butyl protection groups after deprotection without any damage to the DHBC. Due to the presence of acrylates and amines functions, the activated, amidated and deprotected copolymers exhibit pH-tuneable self-assembling properties. Samples were studied at pHs ranging from 2 to 9, using dynamic light

scattering (DLS), ζ-potential measurements and ATR-FTIR and well defined micelles were observed at pH ranging from 4 – 9. The combination of measurements, coupled with DLS studies as a function of salt, allows evidencing that micelles were formed by electrostatic complexation between the positively charged N-acyl urea pending groups and the unmodified negatively-charged acrylate species. Micelles were then characterized using a combination of light and small angle neutron scattering (SANS). Notably, an optimum pH range of micellization of 5 - 7 with a single population was obtained by dynamic light scattering (DLS). SANS data were successfully fitted using a model of polymer micelles, which allows obtaining information about the core radius of the micelles R (6.3 ± 0.1 nm for amidated copolymer at pH = 5), the gyration radius of the P(OEGMA) chains in the micelles shell R_g (3.3 ± 0.1 nm) and the polydispersity in size σ (13 ± 1%). SANS patterns of amidated copolymers as a function of concentration were also studied, and data were successfully fitted adding a hard-sphere structure factor, evidencing inter-micellar interactions. Finally, SANS patterns of the deprotected copolymer show a decrease of the core radius (R = 5.3 ± 0.1 nm at pH = 5), consistent with the removal of the bulky tert-butyl groups. The method developed here allows forming DHBCs that not only exhibit self-assembling properties in water due to the addition of N-acyl urea groups, but also present extra functional groups (in our case primary amines).

1.1. INTRODUCTION

Block copolymers, composed of well-defined blocks of different chemical natures, have attracted a particular attention as structuring agents for self-assembled nanomaterials.[1–3] Many of them display an amphiphilic behaviour due to a difference of hydrophilicity of the copolymer blocks. Controling finely the chemical structure and relative mass fraction of each block allows those copolymers to spontaneously self-assemble in aqueous solutions to form micelles, fibres, vesicles

and micro-phase separated matrices.[4–6] A specific type of block copolymers, the double hydrophilic block-copolymers (DHBC), are distinguished by their entirely hydrophilic nature, but some of them can still be micellized in aqueous solvent under specific conditions.[7,8] Indeed, DHBC can self-assemble in water in response to internal or external *stimuli* (such as pH,[9,10] ionic strength,[9,11] temperature[10,11] or nature of added solvents[12]), which selectively decrease the hydrophilicity of one of the blocks and trigger the self-assembly, while the second block remains hydrophilic and ensures the formation of stable core-shell micelles. Thanks to a judicious choice of the two blocks of the DHBC, researchers have been able to form pH sensitive vesicles (using zwitterionic polymers)[13] or even structure-reversible micelles, whose core and corona can be switched using a DHBC with a dual thermosensitivity.[14] This paved the way for multi-*stimuli* responsive DHBC,[15–17] with applications as drug carriers that often require breaking of the carrier at a controlled pH or temperature,[18–20] or as catalytic nanoreactors, where micellization enhances the catalytic properties of the polymer.[21]

Some DHBC, exhibiting a charged block and a neutral block, require a micellization partner to form micelles in solution, via electrostatic interaction between the charged block of the DHBC and a micellization partner of opposite charge. Depending on the type of micellization partner, polyelectrolyte or multivalent metal ion, the micelles formed are labelled as Polyion complex (PIC)[22–24] or Hybrid Polyion complex (HPIC)[25,26] micelles respectively. HPIC micelles have found a natural application in the field of nanoparticle synthesis, by using the micelle core as a nanoreactor for the particle growth (with the metal ions as precursors), while the corona of the micelles controls the size of the nanoparticles and the overall shape of the micelles influencing that of the nanoparticles.[27–31] PIC (and HPIC) micelles have also found a fascinating application in the formation of mesoporous functional materials.[32–36] An example lies in DHBC comprising

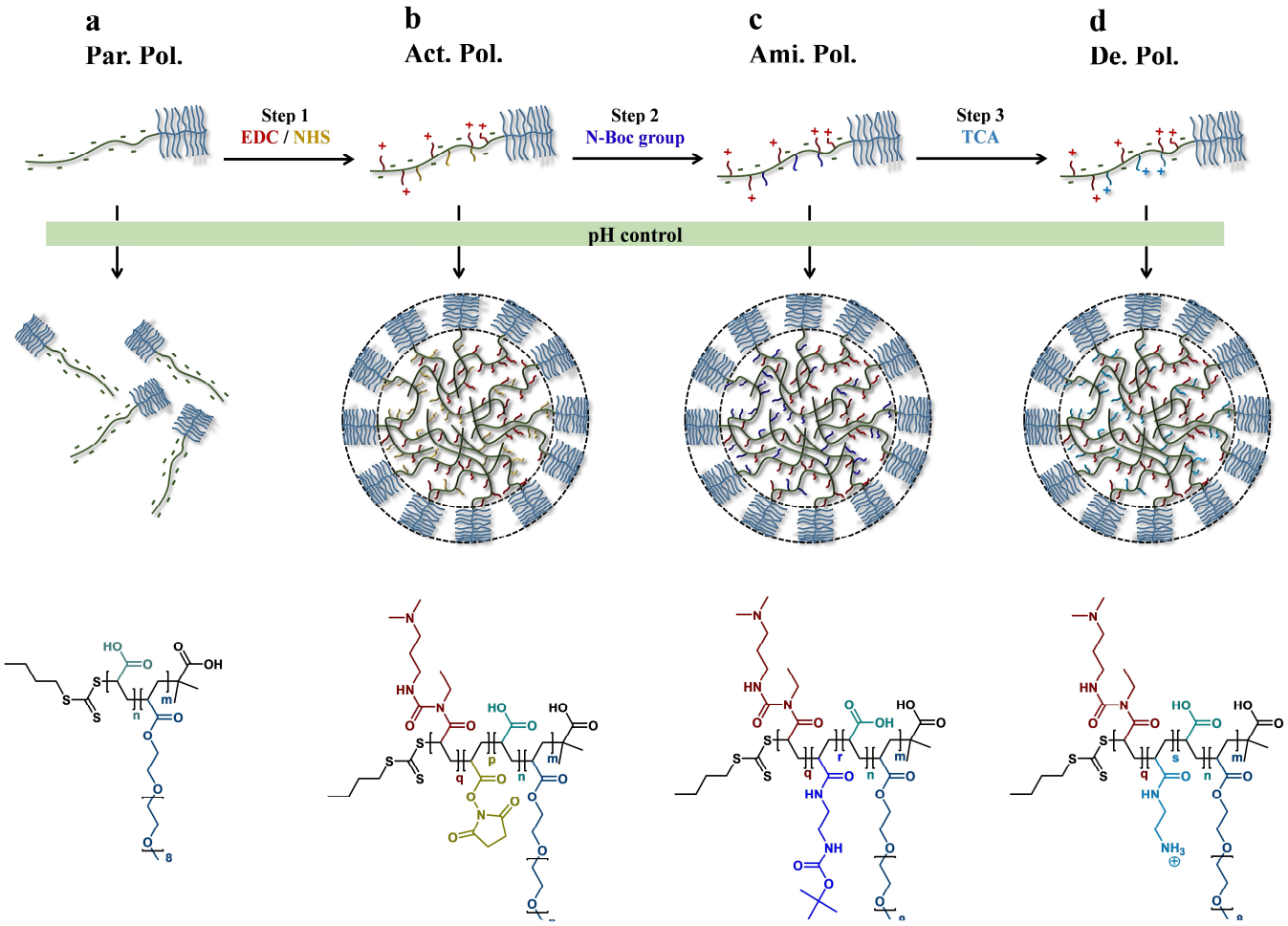
of a neutral ethylene oxide-based hydrophilic block (for instance poly(oligo(ethylene glycol) methyl ether acrylate) P(OEGMEA)) and a polyelectrolyte block (for instance poly(acrylic acid) P(AA)). PIC micelles formed with these DHBC can be used as both structure-directing and functionalizing agents for the formation of an ordered mesoporous structure whose pores are functionalized by polyelectrolytes.[37] These dual features are related to the specific properties of the two blocks of the DHBC: the ethylene oxide units of the neutral block strongly interact with silicic species in aqueous solution *via* hydrogen bonding to form the hybrid interface of the material, while the polyelectrolyte block gives its functionality to the final material.[32,33] In the case of weak polyelectrolytes, the pH-dependent ionisation rate of the charged block of the DHBC and of the micellization partner controls the range of pH associated to H(PIC) micelles formation. This mechanism places requirements on the micellization partner, such as good coacervation properties, but also on the formulation, including the fine control of the ratio of micellization partner to DHBC in solution, a controlled pH window, and the efficient removal of the micellization partner after material formation. Further, a salient limitation of this approach is that the nature of the polyelectrolyte block of the DHBC chosen must be adapted each time to the targeted application; this implies designing new polymer synthesis procedures for each new DHBC. Since direct polymerization with target functions is not always easily reachable, this methodological drawback limits the variety of functions that can be integrated in PIC micelles and their arising functional hybrid materials. Hence, it prevents versatile use of the functional materials. Thus, our goal is to design a P(OEGMEA)-based DHBC whose polyelectrolyte block exhibits several complementary functional groups in order to provide both direct self-assembly properties in aqueous solution and versatility in targeted application.

This goal can be achieved by post-synthesis modification of the DHBC, in order to specifically tune the physico-chemical properties of its polyelectrolyte block without degrading its neutral block.[38–40] For instance, introducing specific hydrophilic and hydrophobic sections within the copolymer allows its self-assembly under aqueous conditions.[23,24,41,42] Post-synthesis modification also allows the addition of functional groups that are not easily accessible by direct polymerization.[38] In the case of acrylic and methacrylic polymers, a common method is to activate carboxylic acids using N-Hydroxysuccinimide (NHS),[43–45] to form active esters that enhance their amidation reaction with nucleophilic amine species under mild aqueous conditions, due to the stability of NHS-activated esters against hydrolysis.[38,46] NHS activation is typically achieved by using N-(3-Dimethylaminopropyl)-N′-ethylcarbodiimide (EDC), which increases the reactivity of carboxylic acids with NHS.[43–45] Examples of nucleophilic amines used for this amidation procedure include aliphatic and cycloaliphatic amines for therapeutic applications[47] while ethylenediamine gives access to pendant primary amines, unlocking applications ranging from CO_2 capture[48] to removal of metallic pollutants.[49,50] In the latter case, the homobifunctional nature of ethylenediamine poses the challenge of cross-linking the polymer chains. It is therefore worth replacing it with N-Boc-ethylenediamine, where one of the amines is protected by the Boc ($(CH_3)_3COCO$) group, which can be removed at a later stage to free the primary amine.[51–54]

Here, post-synthesis modification has been developed as a novel and effective approach to form poly(acrylic acid) based-DHBCs that exhibit self-assembly capabilities with pH-sensitive micellization behaviour, while containing additional functional primary amine pendant groups. We followed a several steps strategy that is summarized in **Scheme 1**. First, the polyacid block of the parent P(OEGMEA)-*b*-P(AA)[35,55,56] copolymer, named Par. Pol. (a in **Scheme 1**) was activated via the EDC/NHS route in aqueous medium. We demonstrated that the reaction of EDC with

carboxylic acids also introduces N-acyl urea pendant groups into the polymer, resulting in the activated copolymer, or Act. Pol. (b), composed of P(OEGMEA)-*b*-P(AA-*s*-(AA-NHS)-*s*-(Acyl urea)), with AA-NHS corresponding to 2,5-dioxopyrrolidin-1-yl acrylate species from the grafting of NHS to the backbone and Acyl urea to N-((3-(dimethylamino)propyl)carbamoyl)-N-ethylacrylamide groups formed by the reaction of EDC with acrylates.[57–59] The introduced N-acyl urea groups contain a tertiary amine with a pKaH of 9.76, which can provide positive charges to the modified polymer under mild pH conditions.[60,61] Meanwhile, NHS-activated esters are also formed on the PAA block and can further react by amidation with N-Boc-ethylenediamine. After this amidation step, the resulting amidated copolymer was named Ami. Pol. (c), composed of P(OEGMEA)-*b*-P(AA-*s*-(Acyl urea)-*s*-(N-Boc)), with N-Boc corresponding to tert-butyl (2-acrylamidoethyl)carbamate groups in the polymer. This copolymer was found to not only self-assemble in aqueous solutions as a result of the new interactions between acrylates from the PAA backbone and tertiary amines from grafted N-acyl urea, but also to contain additional protected primary amines. Finally, a simple deprotection step allows the primary amines to be exposed, resulting in the deprotected copolymer, or De. Pol. (d), composed of P(OEGMEA)-*b*-P(AA-*s*-(Acyl urea)-*s*-(AA/NH_2)), where AA/NH_2 are N-(2-aminoethyl)acrylamide groups obtained after removal of the tert-butyl group.[51–54] The self-assembling behaviour observed for the amidated copolymer is maintained after deprotection, while the primary amine groups can act as extra functional groups. Each DHBC modification step was characterized by nuclear magnetic resonance (NMR) and elemental analysis, while self-assembly properties were assessed by light scattering. The shape of the micelles was fully characterized using small angle neutron scattering (SANS). Finally, the mechanisms of micellization were studied using ζ-potential measurements and ATR-FTIR as a function of pH, and by DLS as a function of salt concentration. This new

DHBC has great potential for the direct formation of multifunctional mesoporous materials whose properties can be adjusted as a function of pH, depending on the need to expose the initial acrylic acid function or the new primary or tertiary amine functions obtained after modifications in the mesopores.



Scheme 1. *Methodology to design a DHBC which exhibits self-assembling properties in water while presenting several functions on its second block. Step 1) Activation of a previously synthesized P(OEGMEA)-b-P(AA) parent polymer (Par. Pol.) (a) with EDC/NHS allows the formation of an activated copolymer (Act. Pol.) made of P(OEGMEA)-b-P(AA-s-(AA-NHS)-s-(Acyl urea)) (b). Step 2) Amidation of Act. Pol. by reaction with N-Boc-ethylenediamine to form an amidated polymer (Ami. Pol.) made of P(OEGMEA)-b-P(AA-s-(Acyl urea)-s-(N-Boc)) (c). Step 3) Deprotection by reaction with TCA to remove the tert-butyl of the N-Boc-ethylenediamine,*

freeing primary amine functions of the final deprotected polymer (De. Pol.), P(OEGMEA)-b-P(AA-s-(Acyl urea)-s-(AA/NH_2)) DHBC (d). P(OEGMEA) comb-like block is given in classic blue, PAA linear block in green, NHS activated esters in yellow, N-acyl urea pendant functions in red, protected amine in navy blue and primary amine functions in turquoise. At the bottom of the scheme, chemical structure of each DHBC is given.

1.2. MATERIALS AND METHODS

1.2.1. Chemicals Used

Oligo(ethylene glycol) methyl ether acrylate (OEGMEA, 99%, M_n = 480 g/mol, 9 EO units on average) and acrylic acid (AA, 99%, M_n = 72.06 g/mol) were purchased from Sigma-Aldrich. Removal of radical inhibitors by adsorption with alumina particles (Sigma-Aldrich) was carried out before their use for polymerization. The initiator, 4,4′-azobis(4-cyano pentanoic acid) (ACPA, 98%) was purchased from Sigma-Aldrich while the chain transfer agent, 2-(butylthiocarbonothioylthio)-2-methylpropanoic acid (BDMAT), was synthesized according to protocols already documented.[62,63] N-(3-Dimethylaminopropyl)-N′-ethylcarbodiimide (EDC, 98%), was purchased from AlfaAesar and used as received. Meanwhile N-Hydroxysuccinimide (NHS, 98%) and N-Boc-ethylenediamine (≥ 98%) were also purchased from Sigma Aldrich. Milli-Q water with a resistivity of 18.2 MΩ·cm at 25 °C was used for chemical synthesis and sample preparation. pH modification was carried out using NaOH and HCl (1M and 5M) solutions. For small angle neutron scattering and NMR analysis, D_2O from Sigma-Aldrich was used as solvent.

1.2.2. P(OEGMEA)-*b*-P(AA) Synthesis

The parent copolymer, (Poly(oligoethylene glycol) methyl ether acrylate)-*b*-poly(acrylic acid) or P(OEGMEA)-*b*-P(AA), was synthesized using reversible addition-fragmentation chain-transfer polymerization (RAFT) in an aqueous solvent.[64] The synthesis of $P(OEGMEA)_{24}$-*b*-$P(AA)_{53}$ (35 wt% polymeric solution) was carried out as shown below: BDMAT (0.1705 g, 7×10^{-4} mol) acting

as chain transfer agent, ACPA (0.0186 g, 7×10^{-5} mol) acting as radical initiator, OEGMEA (7.59 g, 1.6×10^{-2} mol) monomer and 14.4 mL of Milli-Q water were added to a 250 mL round bottom flask. The reaction medium was stirred at *ca.* 250 rpm and purged with nitrogen for 30 minutes followed by heating at 80 °C for 4.5 hours. Then, the second block was obtained by adding ACPA (0.0178 g, 6×10^{-5} mol), AA (2.40 g, 3.3×10^{-2} mol) and 4.5 mL of Milli-Q water to the reaction medium at room temperature. The reaction medium was then degassed again with nitrogen for 30 minutes followed by heating at 80 °C under stirring. A 1 mL portion of the samples was collected after the synthesis of each block of the DHBC for ^{1}H NMR and elemental analysis. The degree of polymerization of each block, given in **Table 1**, was determined from the ^{1}H NMR data as described in supplementary information, SI. The sample is labelled Par. Pol. for parent polymer.

Sample name	Type of polymer	DP P(OEGMEA)	DP P(AA)
Par. Pol.	P(OEGMEA)-*b*-P(AA)	24	53

Table 1. *Description of the parent polymer Par. Pol. obtained by RAFT polymerization, with (for each block) the degree of polymerization (DP) extracted from the analysis of the NMR spectra given in Figure S1, SI.*

1.2.3. Amidation of the Copolymer

Amidation of Par. Pol. (P(OEGMEA)-*b*-P(AA)) was carried out using the EDC/NHS carboxylic acid activation, followed by an amidation reaction with N-Boc-ethylenediamine. We have carried six synthesis, one with solely the activation step, yielding the activated copolymer Act. Pol., and five with the activation and amidation procedure, varying the reaction time and pH, yielding the 5 amidated polymers or Ami. Pol. 1 - 5. The six polymers with their synthesis conditions are

presented in **Table 2**. Ami. Pol. 5 was synthesized for complementary measurements and was characterized only by NMR.

A typical amidation procedure, corresponding to P(OEGMEA)$_{24}$-*b*-P((AA)$_{28}$-*s*-(Acyl urea)$_{17}$-*s*-(N-Boc)$_8$) (Ami. Pol. 1 in **Table 2**), is described as follows: P(OEGMEA)-*b*-P(AA) (2.55 g of 35 wt% Par. Pol. solution, 6×10^{-5} mol) was mixed in 10.0 mL of Milli-Q water in a 250 mL round bottom flask and was stirred at 200 rpm (temp. 50 °C) for 15 min. Then, EDC (0.823 g, 5×10^{-3} mol) diluted to 30 wt% (using 1.92 mL Milli-Q water) was added. 5 min later NHS (0.610 g, 5×10^{-3} mol) at 30 wt% (using 1.42 mL Milli-Q water) was introduced. After a certain activation time t_{act} (overnight for Ami. Pol. 1, 15 min for the others), a 30 wt% aqueous solution of N-Boc-ethylenediamine (0.832 g, 5×10^{-3} mol) was added to the reaction medium, which was left at 50 °C for > 2 days to obtain the final amidated copolymer. The pH of all solutions except N-Boc-ethylenediamine (DHBC, EDC, NHS) was adjusted to pH_{act} (= 7 for Ami. Pol. 1 and 2) using 1 M HCl or 1 M NaOH beforehand. Further, after the addition of N-Boc-ethylenediamine solution without pH regulation, the pH of the total reaction medium was adjusted to pH_{amid} (8 for Ami.Pol. 1). After synthesis, the amidated copolymer Ami. Pol., P(OEGMEA)-*b*-P(AA-*s*-(Acyl urea)-*s*-(N-Boc)), was dialysed against Milli-Q water for 3 days (with six solvent exchanges) using a dialysis bag with a molar mass cut off of 2.5 kDa (from CelluSep membranes). Let us note that in the case of Act. Pol., the dialysis was carried for one-day only (involving two water exchanges) to try to avoid the removal of activated ester groups. Finally, the sample was freeze-dried.

Each sample was characterized by NMR and elemental analysis to calculate the number of units for each group and hence determine their precise chemical structure.

* The number of units was found using EA for this sample (see main text)
** Activation time t_{act} = 16 hours for this sample (vs 15 minutes for all the other Ami. Pol. samples)

Sample name	Block copolymer modified (number of units from NMR)	pH_{act}	pH_{amid}	N-Acyl Urea percentage	N-Boc amination percentage	Atomic ratios from EA			Ratios calculated from NMR		
						N/C	S/C	H/C	N/C	S/C	H/C
Act. Pol.	$P(OEGMEA)_{24}$-*b*-$P((AA)_{25}$-*s*-$(AA\text{-}NHS)_{17}$-*s*-$(Acryl\ urea)_{11})$ *	7	---	21	---	0.111	0.00119	2.25	0.111	0.00294	1.80
Ami. Pol. 1	$P(OEGMEA)_{24}$-*b*-$P((AA)_{28}$-*s*-$(Acryl\ urea)_{17}$-*s*-$(N\text{-}Boc)_8)$ **	7	8	32	15	0.132	0.00010	2.28	0.102	0.00307	1.87
Ami. Pol. 2	$P(OEGMEA)_{24}$-*b*-$P((AA)_{28}$-*s*-$(Acryl\ urea)_{17}$-*s*-$(N\text{-}Boc)_8)$	7	8	32	15	0.130	0.00123	1.99	0.102	0.00307	1.87
Ami. Pol. 3	$P(OEGMEA)_{24}$-*b*-$P((AA)_{23}$-*s*-$(Acryl\ urea)_{12}$-*s*-$(N\text{-}Boc)_{18})$	9	9	23	34	0.110	0.00010	2.21	0.119	0.00282	1.88
Ami. Pol. 4	$P(OEGMEA)_{24}$-*b*-$P((AA)_{32}$-*s*-$(Acryl\ urea)_7$-*s*-$(N\text{-}Boc)_{14})$	8	8	13	26	0.111	0.00067	2.01	0.101	0.00304	1.87
Ami. Pol. 5	$P(OEGMEA)_{24}$-*b*-$P((AA)_{32}$-*s*-$(Acryl\ urea)_{17}$-*s*-$(N\text{-}Boc)_4)$	7	7	32	08	---	---	---	---	---	---

Table 2. *List of activated (Act. Pol.) and amidated (Ami. Pol.) polymers prepared, with their experimental conditions and the key results obtained from NMR and elemental analysis (EA). Excess ratios used were ca. 1.70 for EDC, NHS and N-Boc. The reaction time was 60 hours in all cases except for Ami. Pol. 1, in which reaction time was 84 hours. The pH conditions for both activation (pH_{act}) and amidation (pH_{amid}) are provided. For all samples, the number of units of each block was obtained by NMR ; this allowed estimating the percentage of activation and amidation obtained ($^{N}/_{N_{AA}}.100$ with N the number of N-acyl urea or N-Boc pending groups and N_{AA} the number of acrylates in Par. Pol.). The number of units also allowed calculating the elemental atomic ratios N/C, S/C and H/C, which were compared to the ratios found by EA.*

1.2.4. Deprotection of the Amidated Copolymer

Deprotection of the amidated copolymer Ami. Pol. (P(OEGMEA)-*b*-P(AA-*s*-(Acyl urea)-*s*-(N-Boc))), was undertaken with trichloroacetic acid (TCA). In a 50 mL beaker, a ca. 1 wt% solution of Ami. Pol. was prepared in 10 mL of Milli-Q water and the solution was stirred at room temperature for 1 hour after the pH was adjusted at 1.75 using a 1 M TCA aqueous solution. After deprotection, the sample was purified by dialysis with Milli-Q water for 1 day (two water exchanges) using a cellulose dialysis bag with a molar mass cutoff of 2.5 kDa. Eventually, the sample was freeze-dried to obtain the final deprotected copolymer, De. Pol., with a chemical

composition of P(OEGMEA)-*b*-P(AA-*s*-(Acyl urea)-*s*-(AA/NH_2)). The deprotection rate was evaluated by NMR and elemental analysis. **Table 3** gives the list of deprotected samples prepared.

Sample name	Amidated copolymer used	Amidated copolymer used (DPs from NMR)	Conditions of deprotection (acid, reaction time)	Atomic ratios from EA		
				N/C	S/C	H/C
De. Pol. 1	Ami. Pol. 1	$P(OEGMEA)_{24}$-*b*-$P((AA)_{28}$-*s*-$(Acyl\ urea)_{17}$-*s*-$(N\text{-}Boc)_8)$	TCA, 1 hour	0.115	0.00052	2.11
De. Pol. 2	Ami. Pol. 2	$P(OEGMEA)_{24}$-*b*-$P((AA)_{28}$-*s*-$(Acyl\ urea)_{17}$-*s*-$(N\text{-}Boc)_8)$	TCA, 1 hour	0.114	0.00078	2.07
De. Pol. 3	Ami. Pol. 2	$P(OEGMEA)_{24}$-*b*-$P((AA)_{28}$-*s*-$(Acyl\ urea)_{17}$-*s*-$(N\text{-}Boc)_8)$	TCA, 1 day	0.119	0.00043	2.05
De. Pol. 4	Ami. Pol. 2	$P(OEGMEA)_{24}$-*b*-$P((AA)_{28}$-*s*-$(Acyl\ urea)_{17}$-*s*-$(N\text{-}Boc)_8)$	HCl, 1 day	0.116	0.00095	2.04

Table 3. *List of deprotected copolymers prepared (De. Pol. 1 to 4). For each sample is given the amidated polymer (Ami. Pol.) used for deprotection, the conditions of deprotection (acid used and reaction time), the number of units of each block from NMR and the atomic ratios N/C, S/C and H/C obtained by elemental analysis (EA).*

1.2.5. Preparation of Suspensions

Polymers (Par. Pol., Act. Pol., Ami. Pol. 1 - 5 or De. Pol. 1 - 4) were dispersed in aqueous suspensions for DLS/SLS or SANS analysis. Suspensions were prepared at room temperature. For DLS/SLS analysis, H_2O was used as solvent, while D_2O was used for SANS. In light scattering experiments, samples were prepared at a concentration of 0.1 wt% in DHBC, while in neutron scattering, the typical concentration used was 1 wt%, unless stated otherwise. Similarly, for ζ-potential measurements made as a function of pH, samples were prepared at 1wt%.

Regarding Act. Pol., suspensions for DLS/SLS and SANS were prepared at three various pHs: 3, 5 and 9, to evidence the formation of micelles at pH = 5 and the effect of acidic (3) or basic (9) conditions on these micelles.

For the amidated polymers, several suspensions were prepared: for Ami. Pol. 1, the first samples were prepared again at pH = 5, then a complete study of the role of pH was carried by varying the

pH between 2 to 9 by increments of 1. Similarly, for the same polymer, the role of concentration was studied in SANS at pH = 5 by studying concentrations ranging from 1 to 5 wt% in DHBC by increments of 1 wt%. To compare the different amidated polymers, Ami. Pol. 2 to 4 were also prepared at 1wt% and pH = 5 for SANS studies. As Ami. Pol. 1 – 4 were used totally, in DLS and SANS, complementary ζ-potential measurements were carried on a fifth sample, Ami. Pol. 5, at 1wt% and pH ranging from 2 – 9. Finally, the effect of salt was studied in DLS on suspensions of Ami. Pol. 5 at 0.1 wt% and pH=5 by adding NaCl in order to reach concentrations of 0, 0.1, 0.5 and 1 M.

Concerning the deprotected polymers, De. Pol. 1 was studied both in DLS/SLS and SANS at three pHs (3, 5 and 9) to compare results with the activated and amidated copolymers.

Finally, the parent polymer Par. Pol. was also briefly studied at pH = 5 in DLS to prove that micelles are not formed prior to the DHBC modification. This sample was dispersed in 0.1 M NaCl to avoid electrostatic repulsion between PAA blocks.

Samples were prepared by mixing the needed amount of DHBC with the solvent before pH adjustement by addition of HCl or NaOH (1M or 5M).

1.2.6. Characterization Techniques

1.2.6.1. NMR Spectroscopy

^{1}H NMR spectra of the copolymers were collected using Bruker Advance III 600 MHz NMR Spectrometer using D_2O as the solvent. Regarding the parent copolymer, samples collected during polymerization were dried in an oven at 50 ºC overnight and about 10 mg were dissolved in 1 mL D_2O for characterization. Other samples (activated, amidated and deprotected copolymers) were

not directly dried to avoid unwanted reaction but were characterized by NMR after dialysis at neutral pH and freeze-drying (ca. 10 mg in 1 mL D_2O). The NMR data were treated using Topspin 4.1.4 and chemical shifts δ are presented in ppm.

NMR data analysis allows extracting the number of units of each pending group on the polymers. For Act. Pol., Ami. Pol. and De. Pol., conversion rates in N-acyl urea and N-Boc pending groups corresponds to the number of units of said group *N*, divided by N_{AA} = 53, the overall number of acrylate units in the parent polymer (see **Table 2**).

1.2.6.2. ATR-FTIR Spectroscopy

Attenuated total reflectance Fourier transformed infrared spectroscopy (ATR-FTIR) was performed in the 4000 – 400 cm^{-1} region using a Thermo Scientific Nicolet 4700 apparatus (USA) with a 0.5 cm^{-1} scan resolution. Act. Pol. and Ami. Pol. 1 were freeze-dried following the same procedure than for NMR analysis. For the studies as a function of pH, suspensions at 1wt% of Ami. Pol. 5 at pH ranging from 2 to 9 were prepared, homogenised before freeze-drying. To determine the ionisation coefficient of the polyacrylic acid block for each pH, the carbonyl region of each spectrum was investigated extensively. The spectra were normalized using their most intense vibrational band (C-O stretching at ca 1050 cm^{-1}) and the region from 1350 to 1800 cm^{-1} was isolated. The Origin software was used to convert the transmittance spectra into absorbance, define their baseline and substract it. The carbonyl region (eg 1500 to 1800 cm^{-1}) exhibited 3 broads peaks that were deconvoluted using 5 gaussians corresponding to the carbonyl stretching in esters (1730 cm^{-1}), carboxylic acids (ca 1700 cm^{-1}), amides (1640-1650 cm^{-1}), bound carboxylic acids (1620 cm^{-1}), and carboxylates (1560 cm^{-1}) as well as N-H bending from amides (1560 cm^{-1}).[65–67] An example of peak deconvolution is given in supporting information. The positions and

areas of the components corresponding to the ester and the amide carbonyl bands were determined on the spectrum acquired at pH 9 and set as constraints for fitting the spectra at other pH values. No contraint was set to other components for the peak fitting. Due to the overlap of carboxylates and N-H bending bands, these two species were fitted within the same gaussian component. At pH 2, that band almost disappeared and its area was attributed to N-H bending only. This allowed to provide a minor correction to the peak areas measured at higher pH values, giving access to the contribution of carboxylate species. The ionisation coefficient was determined by using the following equation where the factor 1.8 takes account for the different molar extinction coefficients of carboxylic acid and carboxylate species:[66]

$$\alpha = A(COO^-)/[A(COO^-) + 1.8.\,(A(COOH) + A(COOH)_{Bound})] \qquad (1)$$

1.2.6.3. Elemental Analysis

Atomic percentage of C, H, N, S of the dried samples were obtained via elemental analysis (approximately 50 mg of sample used for measurement) employing a ThermoFisher Scientific spectrometer iCE 3000. Drying procedure was the same than for NMR analysis.

1.2.6.4. ζ-Potential Measurements

The zeta potential of Ami. Pol. 5 at 1wt% and at pH ranging from 2 – 9 were measured using an AMERIGO system, Cordouan technologies, France. All measurements were done at room temperature. Laser Doppler electrophoresis measurements were performed using a laser at 638 nm and at 20.27 $V \cdot cm^{-1}$ applied electric field. The zeta potentials were extracted from the electrophoretic mobility using Smoluchovski equation. Results are given as the average of 6 experiments with their standard deviations.

1.2.6.5. Small Angle Neutron Scattering (SANS)

All samples were dispersed in D_2O and studied in 2 mm thick quartz cuvettes. The signal of D_2O alone was always recorded first. Concentrations between 1 to 5 wt% were used for the concentration studies while pH dependence of the samples was confirmed using 1 wt% solutions with a pH range from 2 to 9. A pH meter calibrated using H_2O was used to measure the samples. The pH of the micellar solution in D_2O can be obtained using the expression pD = 0.929 × pH* + 0.42, where pH* is the direct reading of H_2O-calibrated pH meter.[68] The samples were studied using SANS without any pre-experimental filtration.

SANS measurements were mainly carried out at the D22 beamline of the Institut Laue – Langevin, Grenoble, France along with supplementary measurements on Larmor and Sans2d at ISIS Neutron and Muon Source at the Rutherford Appleton Laboratory, Oxford, UK.

At D22, experiments were carried out using a circular neutron beam with a diameter of 13 mm. The wavelength of the neutron beam and the q range investigated were 6 Å ($\Delta\lambda/\lambda = 0.1$) and 0.002 to 0.641 $Å^{-1}$ respectively. The two different detectors in D22, i) a fixed front detector and ii) a rear detector, were having a sample to detector distance of 1.4 m and 17.6 m (with a collimation distance of 17.6 m) respectively, enabling the access to a wide q range. The neutrons were recorded using ^{3}He multitube detectors made of Reuter−Stokes tubes, the front detector consists of 96 tubes, while the rear one has 128 (tube diameter: 8 mm and a pixel size of 8 mm × 8 mm). Using the GRASP software,[69] the two-dimensional multi detector data were corrected for direct beam transmission, empty cell scattering, background scattering and detector efficiencies before being scaled to absolute intensity, and azimuthally averaged. Finally, incoherent scattering was subtracted from each averaged data obtained.

The measurements performed on the time-of-flight instrument Larmor at the ISIS Neutron and Muon Source used a square beam of 6 mm × 6 mm with a neutron wavelength range of 0.9 – 13.5 Å. The sample-to-detector distance of 4.1 m enabled an effective q-range of $0.004 - 0.680$ $Å^{-1}$ (the source-to-detector distance was also set to 4 m). Scattered neutrons were recorded in event mode on a ^{3}He tube array detector (64×64 cm^2) with a 4 mm × 8 mm pixel size. The raw data obtained were converted to scattering cross-section data and set onto an absolute scale after being corrected for transmission, empty cell scattering, background scattering, detector efficiencies, and radially averaged using Mantid Workbench software.[70] Further, at Sans2d small-angle neutron diffractometer at ISIS,[71] the beamline operated with a neutron beam diameter of 12 mm and the wavelength range used was 1.75 – 16.5 Å. The use of two 1 m^2 detectors at 2.4 m and 4 m from the sample gave access to a q-range of 0.004 – 1 $Å^{-1}$, with a q-resolution varying from ca. 2% at the highest q-values to ca. 19% with decreasing q-values, calculated using the Mildner Carpenter equation.[72] The same protocol was used to correct the 2D patterns (using transmissions, empty cell scattering, background scattering, detector efficiencies), which were then radially averaged, converted to scattering cross-section and absolutely scaled using a standard polymer in the Mantid software.[70] Subsequently, the incoherent scattering was subtracted from all the corrected scattering curves from ISIS instruments as well.

1.2.6.6. Light Scattering

Light scattering measurements of the 0.1 wt% aqueous polymer suspensions, gently stirred overnight at the required pH, filtered using 0.45 μm PTFE membrane based Millipore filters (for the corresponding buffer solutions, 0.22 μm PTFE filters were utilized), were carried out using an ALV CGS3 goniometer with an ALV 5004 correlator (ALV GmbH, Langen, Germany). Multiple tau digital correlators in the equipment allow measurements of static and dynamic light scattering

in parallel. The instrument is equipped with a HeNe laser, of wavelength λ = 632.8 nm and a maximum output power of 23 mW. Samples were measured at 21.5 ± 1.0 °C and at an angular range between 30° and 150°.

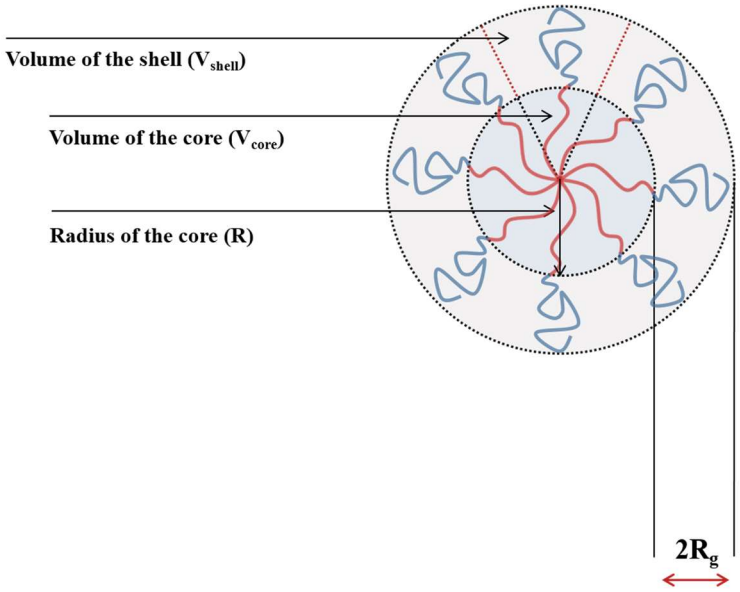
Complementary measurements of the effect of salt were carried on an AMERIGO, Cordouan technologies, France, using a laser at 638 nm with a laser power of 100% for all samples. Samples (Ami. Pol 5 at pH=5 with [NaCl] ranging from 0 to 1 M) were filtered using a 0.8 mm PTFE membrane based Millipore filters. The data were measured at a scattering angle of 170°. The scattered intensity was averaged over 45 s measurements.

1.2.7. Scattering Data Analysis

1.2.7.1. Models Used to Fit the SANS Data

1.2.7.1.1. Polymer Micelles Model

The SANS data were fitted using the model of polymer micelles described by *Pedersen and Gerstenberg*.[73] This model is well-suited to describe micelles made of diblock copolymers, where one block forms the core of the micelle of radius R and scattering length density (SLD) ρ_{core} and the second block forms a shell of SLD ρ_{shell} made of solvated chains, each with a radius of gyration R_g (see **Scheme 2**). N_{agg}, the aggregation number, is the number of copolymers in each micelle, while v_{core} is the volume occupied by one block within the micelle core and v_{shell} the volume occupied by one chain in the shell.



Scheme 2. *Sketch of a polymer micelle of core radius R and shell block gyration radius* R_g

By considering the total volume of the core $V_{core} = 4/3\pi R^3$ (2), the volume occupied by one block in the core v_{core} can be rewritten as $v_{core} = \frac{V_{core}}{N_{agg}} = \frac{^4/_3\pi R^3}{N_{agg}}$ (3)

Moreover, the scattering length densities can be estimated as follows:

$$\rho_{core} = 0.5\rho_{AU} + 0.5\rho_{AA} \quad (4)$$

$$\rho_{shell} = 0.25\rho_{POEGMEA} + 0.75\rho_{D_2O} \quad (5)$$

with ρ_{AU}, ρ_{AA}, $\rho_{POEGMEA}$ and ρ_{D_2O} the SLD of N-acyl urea, acrylic acid, the P(OEGMEA) block and heavy water respectively. To simplify the model, we neglected any presence of water within the core, while we estimated the amount of water in the shell to be 75%.[74] We also neglected the possible presence of N-Boc-ethylenediamine within the core, due to its relatively low amount. **Table 4** gives the densities and SLD for each compound and the final SLD estimated for the core and shell.

* Density of urea used

Component name	Density (g/ml)	SLD (10^{-6}/Å^2)
Oligo(ethylene glycol) methyl ether acrylate (OEGMEA)	1.087	0.719
Acrylic Acid (AA)	1.051	1.45
Acyl Urea*	1.320	1.19
N-Boc-ethylenediamine	1.012	0.647
$\rho_{core} = 0.5\rho_{AU} + 0.5\rho_{AA}$	----	1.32
$\rho_{shell} = 0.25\rho_{POEGMEA} + 0.75\rho_{D_2O}$	----	4.97

Table 4. *Scattering length density of the components used in the copolymer (SLDs of core and shell included)*

For non-interacting micelles, the scattered intensity $I(cm^{-1})$ can be described as follows:

$$I(q) = nP_{mic}(q) \qquad (6)$$

with n the number of objects per unit volume (cm^{-3}) and $P_{mic}(q)$ the form factor of the micelles, with:

$$P_{mic}(q) = N_{agg}^2 v_{core}^2 \Delta\rho_{core}^2 P_{spher}\ (q,R) + N_{agg} v_{shell}^2 \Delta\rho_{shell}^2 P_{ch}(q,R_g) + N_{agg}(N_{agg}-1) v_{shell}^2 \Delta\rho_{shell}^2 S_{cc}(q,R,R_g) + 2N_{agg}^2 v_{core}\Delta\rho_{core} v_{shell}\Delta\rho_{shell} S_{sc}(q,R,R_g) \qquad (7)$$

where $\Delta\rho_X = \rho_X - \rho_{D_2O}$ is the SLD difference between the object (X = core or shell) and the solvent.

P_{sphere} is the form factor of a simple sphere of radius R that describes the core, with $P_{sphere}(q,R) = F^2_{sphere}(q,R)$, with F_{sphere} the form factor amplitude:

$$F_{sphe}\ (q,R) = \frac{3[\sin(qR) - qR\cos(qR)]}{(qR)^3} \qquad (8)$$

P_{ch} describes the form factor of one polymer chain composing the shell

$$P_{ch}(q, R_g) = P_{ch}\left(x = \left(qR_g\right)^2\right) = \frac{2[\exp(-x) - 1 + x]}{x^2} \qquad (9)$$

while S_{cc} and S_{sc} are cross terms between two different chains and the core and one chain, respectively, arising when passing from the form factor amplitude to the full form factor:

$$S_{cc}(q) = \psi(q, R_g)^2 \left[\frac{\sin\left(q\left(R + dR_g\right)\right)}{q\left(R + dR_g\right)}\right]^2 \qquad (10)$$

and

$$S_{sc}(q) = F_{sphere}(q, R)\psi\left(q, R_g\right)\frac{\sin\left(q\left(R + dR_g\right)\right)}{q\left(R + dR_g\right)} \qquad (11)$$

with

$$\psi\left(q, R_g\right) = \psi\left(x = \left(qR_g\right)^2\right) = \frac{1 - \exp(-x)}{x} \qquad (12)$$

and $0 \leq d \leq 1$ the interpenetration parameter characterizing how much of the outside chain interpenetrates within the core. In our case, we always fixed *d = 1* (no interpenetration).

The polydispersity in size over the micelle radius *R* was taken into account using the Schulz-Zimm distribution, i.e.:

$$\langle P(q, R)\rangle_\sigma = \int f_{SZ}\left(r, R, \frac{1}{\sigma^2} - 1\right) P(q, r)dr \qquad (13)$$

with

$$f_{SZ}(x, x_0\,, z) = \frac{x^z}{\Gamma(z + 1)}\left(\frac{z + 1}{x_0}\right)^{z+1} \exp\left(-(z + 1)\frac{x}{x_0}\right) \qquad (14)$$

and σ the polydispersity index in %. Schulz-Zimm distribution was previously used successfully to characterize the polydispersity in size of core-shell micelles.[75]

The model can be adapted to ellipsoidal or even cylindrical polymer micelles.[76]

When studying micelles as a function of concentration, interactions between micelles arise and the structure factor has to be considered. Due to the complex nature of the model, the intensity cannot be described as the product of the form factor and the structure factor. Instead, the analytical calculation from *Pedersen*[77] should be used:

$$I = n\left(P_{mic}(q) + \left(A_{mic}^{AV}(q)\right)^2[S(q) - 1]\right) \qquad (15)$$

with

$$A_{mic}^{AV}(q) = N_{agg}\left[v_{core}\Delta\rho_{core}F_{spher}\ (q,R) + v_{shell}\Delta\rho_{shell}\psi\left(q,R_g\right)\frac{\sin\left(q\left(R+dR_g\right)\right)}{q\left(R+dR_g\right)}\right] \qquad (16)$$

with $A_{mic}^{AV}(q)$ the form factor amplitude of the average radial scattering length density distribution.

The structure factor was accounted for by a hard-sphere model, using the well-known Percus-Yevick solution.[78] The structure factor $S(q, R_{HS}, \varphi_{HS})$ depends on the hard-sphere radius R_{HS} and the volume fraction of interacting micelles φ_{HS}.

Data were fitted using a home-made Fortran program.[79]

1.2.7.1.2. Secondary Models: Guinier Approximation and Polymer Chains with Excluded Volume

In a few cases, shape-independent models were used to characterize the SANS data. The well-known Guinier approximation[80] was used to obtain the radius of gyration R_G of the micelle to compare with SLS data. In the Guinier approximation, the intensity can be written

$$I(q) = A.e^{-\frac{q^2 R_G^2}{3}} + B \qquad (17)$$

with A a scaling factor and B a background term. R_G is not to be confused with the with the radius of gyration R_g of the P(OEGMA) chains that composes the corona of the micelles used in the polymer micelles model ($R_G >> R_g$).

On the other side, when micelles are not formed, the DHBC remains free in suspension. This free polymer was described using the polymer chains with excluded volume model.[81] This model, which analytical form was given by Hammouda in 1993 depends on the radius of gyration R'_g of the complete polymer chain (i.e. the complete DHBC) in solution and the Porod exponent α that characterizes the signal at high angles ($I \propto q^{-\alpha}$). For a linear polymer in good solvent, $\alpha \approx 5/3$, but is higher for comb-like polymers.[22] R'_g is not to be confused with the radius of gyration R_g of the P(OEGMA) chains that composes the corona of the micelles used in the polymer micelles model ($R'_g > R_g$).

Those models are readily available on Sasview.

1.2.7.2. Static Light Scattering

The weight-averaged molecular weight M_w, and radius of gyration of the scattering objects R_G could be obtained from SLS data depicted using Zimm's approximation

$$\frac{Kc}{\Delta R_\theta} = \frac{1}{M_w} + \frac{1}{3M_w} R_G^2 q^2 \qquad (18)$$

where *c* and *K* are the concentration of the scattering objects and optical constant respectively, and q is the scattering vector, that depends on the scattering angle θ:

$$q = \frac{4\pi n}{\lambda_0} sin\frac{\theta}{2} \qquad (19)$$

The optical constant K can be written as:

$$K = \frac{4\pi^2}{\lambda_0^4 N_A}\left(n\frac{dn}{dc}\right)^2 \qquad (20)$$

where λ_0, N_A, n and $\frac{dn}{dc}$ are the laser wavelength in vacuum, Avogadro's number, the refractive index of the solvent and the refractive index increment of the self-assembled species respectively. Experimentally, we measured the scattering intensity <*I*> as a function of the scattering vector q. The Rayleigh ratio (ΔR_θ) was then obtained using equation (21)

$$\Delta R_\theta = \frac{\langle I_{solution}\rangle - \langle I_{solvent}\rangle}{\langle I_{standard}\rangle}\left(\frac{n_{solvent}}{n_{standard}}\right)^2 RR_{standard} \qquad (21)$$

with $\langle I_{solution}\rangle$, $\langle I_{solvent}\rangle$ and $\langle I_{standard}\rangle$ the scattering intensities of the solution, solvent (i.e. water) and standard (i.e. toluene) respectively. $n_{solvent}$ = 1.33 and $n_{standard}$ = 1.49 are the

respective refractive indexes while $RR_{standard}$ = 1.36 × 10^{-5} cm^{-1} for λ = 632.8 nm at 21.5 ± 1.0 °C is the Rayleigh ratio of the toluene standard.

Plotting $\frac{Kc}{\Delta R_\theta}$ against q^2 shows a linear dependence. The slope ($\frac{R_g^2}{3}$) yields the radius of gyration and the intercept gives the molecular weight ($\frac{1}{Mw}$) of the self-assembled entities. $\frac{dn}{dc}$ value was not determined experimentally. Hence, we extracted only the radius of gyration R_G. Let us note that the radius of gyration R_G obtained in SLS is different from the radius of gyration of polymer chains in the shell of the micelles R_g from the SANS analysis made using the polymer-micelles model. In SLS, R_G corresponds to the radius of gyration of the scattering objects, in most cases the micelles. At pH values where micelles are not formed, it would correspond to the radius of gyration of the DHBC soluble in water.

1.2.7.3. Dynamic Light Scattering

In DLS, we measured the scattered intensity as a function of time at a specific scattering vector q. From the scattered intensity, the normalized intensity-time correlation function, $g_2(q,\tau)$ is obtained as a function of time shift τ. Utilizing Siegert's equation, the electric field-time correlation function $g_1(q,\tau)$ could be extracted.

$$g_2(q,\tau) = \frac{\langle I\,(q,t) I(q,t+\tau)\rangle}{\langle I\,(q,t)\rangle^2} = 1 + |g_1(q,\tau)|^2 \qquad (22)$$

where $I(q,t)$ and $I(q,t+\tau)$ are the scattering intensity at time t and $t + \tau$ respectively. <> indicates temporal averaging over all the times t.

The electric field correlation function relates to the particle translational diffusion coefficient which can be obtained either using the CONTIN method, or the cumulant analysis. The latter is

well-suited for a quasi monomodal distribution of population, while the former is better tailored for system that exhibit several populations.

In CONTIN, developed by Provencher based on Laplace inverse, the electric field correlation function $g_1(q,\tau)$ is related to the translational diffusion coefficient D_t by:

$$g_1(q,\tau) = \int_0^\infty G(D_t).e^{-D_t.\tau/q^2} dD_t \qquad (23)$$

with $G(D_t)$ being the distribution function of D_t.[82]

The cumulant fit describes the logarithm of $g_1(q,\tau)$ at fixed q as a power series in τ

$$ln\big(g_1(q,\tau)\big) = \Gamma_0 - \Gamma_1.\tau + \frac{\Gamma_2}{2!}.\tau^2 - \frac{\Gamma_3}{3!}.\tau^3 \qquad (24)$$

with Γ_0, Γ_1, Γ_2 and Γ_3 the cumulants. The first cumulant is related to the z-averaged translational diffusion coefficient D through $\Gamma_1 = Dq^2$, while the ratio between the second and square of the first cumulant unveils the polydispersity index $PDI = \frac{\Gamma_2}{\Gamma_1^2}$.

Here the translational diffusion coefficient D is obtained at a single scattering vector q. To extract the translational diffusion coefficient with more accuracy, it is required to study the sample at different scattering vectors and extract the translational diffusion coefficient extrapolated at zero-angle D_0. For dilute solutions, D_0 is calculated through the linear approximation method given below:

$$D = D_0\big(1 + C.R_g^2.q^2\big) \qquad (25)$$

where C is a dimensionless constant which relies on polydispersity and particle shape. By plotting D as a function of q^2, the intercept allows extracting D_0. If there is no angular dependence, D_0 is obtained by averaging over the angular range.

Once D_0 is obtained, the hydrodynamic radius R_H is obtained via the Stokes-Einstein relationship:

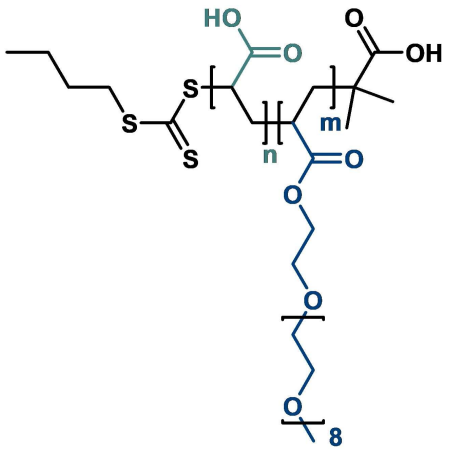
$$R_H = \frac{K_B T}{6\pi\eta} \frac{1}{D_0} \qquad (26)$$

with k_B, T, η denoting Boltzmann constant, temperature and solvent viscosity respectively. Finally, combining static and dynamic light scattering data allows extracting the shape reliant ratio $\frac{R_G}{R_H}$. [82–84] Spherical objects usually exhibit a ratio of ca. 0.78.

1.3. RESULTS AND DISCUSSION

1.3.1. Parent Block Copolymer, Par. Pol. (P(OEGMEA)-*b*-P(AA))

The parent diblock copolymer, Par. Pol., made of P(OEGMEA)-*b*-P(AA), whose chemical structure is given in **Scheme 3**, was synthesized by RAFT polymerization following previously established protocols.[55,56] The degree of polymerization of each block was determined using ^{1}H NMR and results give 24 units of P(OEGMEA) and 53 of P(AA) respectively (see **Table 1**), with a monomer conversion rate ca. 99% for both blocks. This corresponds to a total molecular weight of 15.6 kDa (including the terminal groups) for the DHBC, with a contribution of 11.5 kDa and 3.8 kDa from P(OEGMEA) and P(AA), respectively (**Figure S1**, supplementary information).



***Scheme 3**. Structure of the parent polymer, Par. Pol., P(OEGMEA)$_m$-b-P(AA)$_n$*

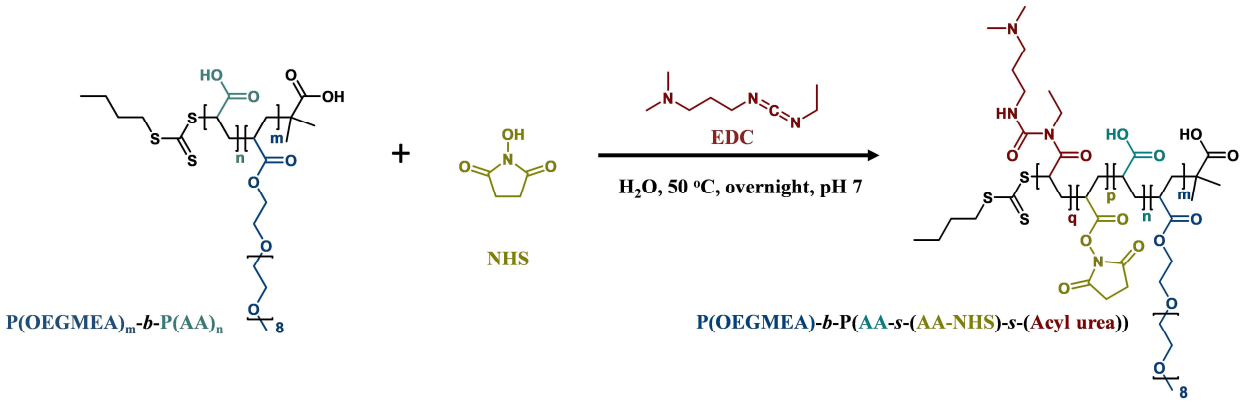
1.3.2. Modification of the Parent Polymer by Activation and Amidation of the Acrylic Acid Functions

1.3.2.1. Activated and Amidated Copolymers, Act. Pol. (P(OEGMEA)-*b*-P(AA-*s*-(AA-NHS)-*s*-(Acyl urea))) and Ami. Pol. (P(OEGMEA)-*b*-P(AA-*s*-(Acyl urea)-*s*-(N-Boc)))

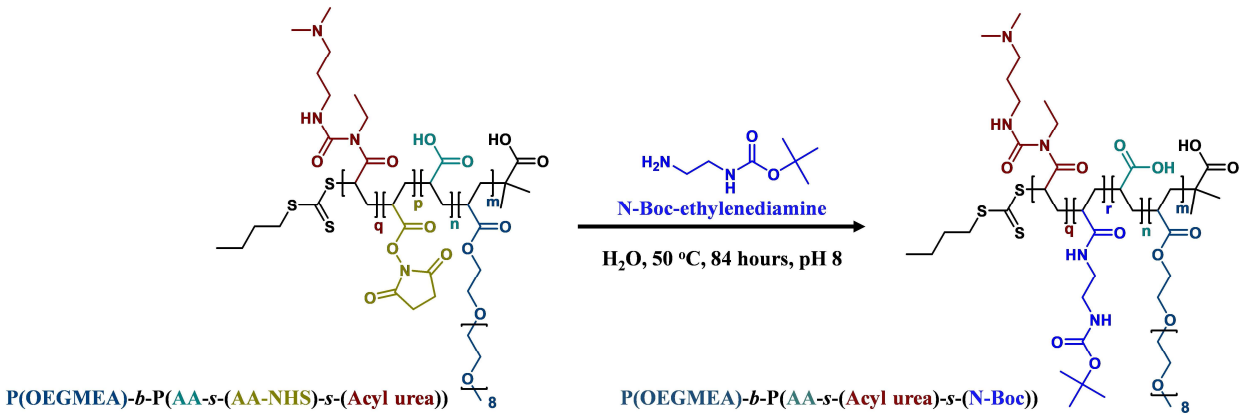
In order to introduce new functional groups to the ionic block and impart self-micellization capabilities to P(OEGMEA)-*b*-P(AA) copolymers, a specific modification of the P(AA) block was carried out by activation/amidation of the carboxylic acid groups. Since both blocks of the DHBC are based on acrylate monomers, mild reaction conditions were necessary to achieve specific reactions on the polyacid block P(AA) while leaving the comb polyester block P(OEGMEA) untouched. In addition, since the copolymer synthesis was achieved in water, an aqueous functionalization route was favoured to reduce the environmental impact of the synthesis. Activation of carboxylic acid groups was achieved through successive reactions with 1-Ethyl-3-(3-dimethylaminopropyl) carbodiimide (EDC) and N-hydroxysuccinimide (NHS) in order to reach

two aims: *(i)* forming reactive esters P(OEGMEA)-*b*-(PAA-NHS) for subsequent amidation and *(ii)* forming stable N-acyl urea pendant functions P(OEGMEA)-*b*-(PAA-Acyl urea), which contain a tertiary amine (pKaH = 9.76). The presence of amine functions together with acrylate functions is expected to provide the necessary conditions for inducing intramolecular complexation-driven self-micellization to the newly formed DHBC.

Indeed, while the reaction of EDC on carboxylic acid forms O-acyl urea esters, these moieties can undergo hydrolysis or, more importantly, rearrangement (N → O displacement), before reacting with NHS. As a result, AA and N-acyl urea-grafted AA are obtained, respectively. These side reactions are typically controlled by NHS addition, as it reacts with O-acyl urea esters to give an activated ester that can conveniently react with primary amines.[59] In contrast, the N-acyl urea and the carboxylic acid side products do not react with primary amines under mild conditions. Here, in our amidation protocol, after EDC was added, there was a subsequent delay before NHS addition to the reaction medium in order to ensure the formation of both stable N-acyl urea and activated ester**.** *Sam et al.* in their study of the EDC/NHS activation of acid end groups (at 15 °C for 1.50 hours in water), reported that the excess of added EDC and NHS favours rearrangement and formation of N-acyl urea rather than the activated ester.[43] Consequently, in the present study, an excess of EDC and NHS (excess ratio of ca. 1.70 for both) was used for the activation of the parent copolymer. Therefore, the typical activated copolymer, Act. Pol., obtained has a fraction of the three possible products, giving P(OEGMEA)-*b*-P(AA-*s*-(AA-NHS)-*s*-(Acyl urea)), see **Scheme 4a**. To graft primary amines on the DHBC, the activated copolymer was subsequently reacted with N-Boc-ethylenediamine, forming the amidated copolymer or Ami. Pol. exhibiting both N-Boc-protected amine and N-acyl urea pendant groups, with the following chemical formula, P(OEGMEA)-*b*-P(AA-*s*-(Acyl urea)-*s*-(N-Boc)), see **Scheme 4b**.



Scheme 4a. *Step 1) Activation of Par. Pol. (P(OEGMEA)$_m$-b-P(AA)$_n$) into Act. Pol. (P(OEGMEA)-b-P(AA-s-(AA-NHS)-s-(Acyl urea))).*



Scheme 4b. *Step 2) Amidation of Act. Pol. (P(OEGMEA)-b-P(AA-s-(AA-NHS)-s-(Acyl urea))) into Ami. Pol. (P(OEGMEA)-b-P(AA-s-(Acyl urea)-s-(N-Boc))).*

Although amidation of carboxylic acids can be achieved by direct reaction with primary amines, it is virtually impossible to achieve in water because the chemical equilibrium is strongly biased in favour of the hydrolysis of the acid groups. To overcome this problem, direct amidation in the absence of EDC/NHS activation requires high temperatures (160 °C - 180 °C), which would lead to the alteration of both blocks in the case of a P(OEGMEA)-*b*-P(AA) copolymer.[59] Therefore, activation of the copolymer using the above protocol is essential to achieve both amidation and grafting of N-acyl urea groups onto DHBC under mild and aqueous conditions.

1.3.2.2. ATR-FTIR Analysis

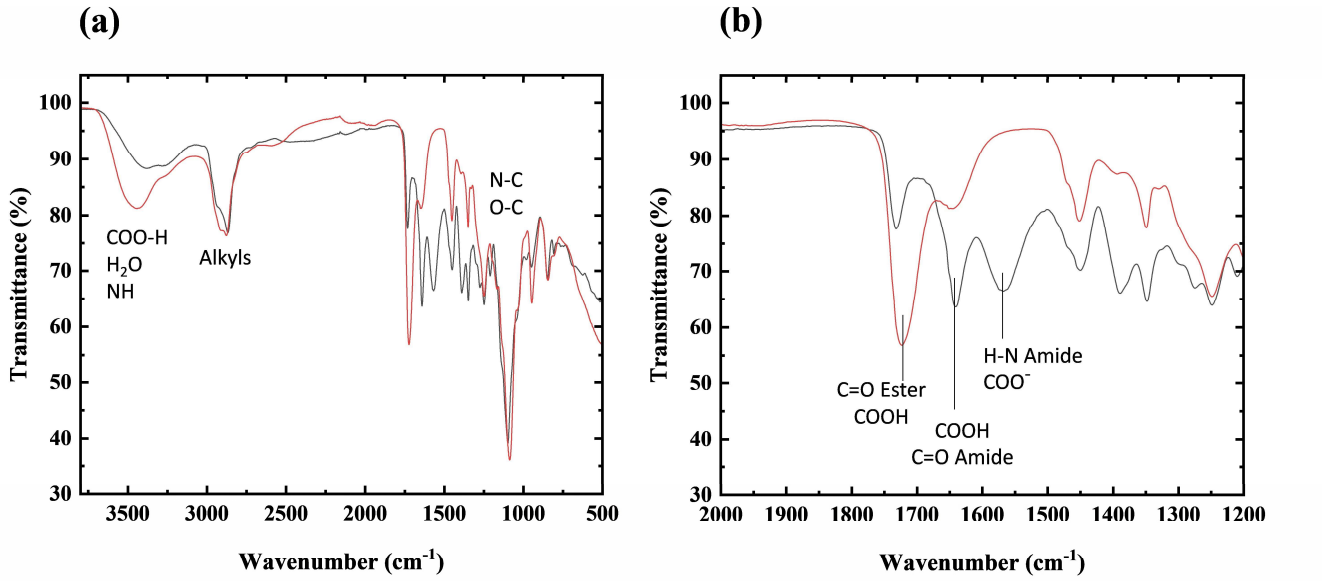


Figure 1. *ATR-FTIR spectra of Par. Pol. (red line) and Ami. Pol. 1 (black line) (a) over the entire wavenumber range and (b) over 2000 - 900 cm^{-1}. The main bands contributions have been highlighted.*

The polymers before (Par. Pol.) and after amidation (Ami. Pol. 1) were studied in ATR-FTIR (**Figure 1**). After amidation, new bands can be observed between ca. 1500 and 2000 cm^{-1} characteristics of H-N and C=O bonds in amides, proving the successful amidation of the P(AA) block. Further, the signal at ca. 1700 cm^{-1}, associated notably to the carbonyl stretching in the esters of the P(OEGMEA) block is still present after amidation, suggesting the first block was not damaged by the procedure. On top of those bands, the rest of the pattern is similar before and after amidation (notably the presence of alkyls groups between 2800 - 3000 cm^{-1} and O-C stretching from ethylene glycol units at around 1050 cm^{-1}), again hinting at the absence of damage to the copolymer. A quantification of the modification of DHBC was made using ^{1}H NMR.

1.3.2.3. NMR Analysis

Figure 2 shows the ^{1}H NMR spectra of (a) the parent copolymer P(OEGMEA)-*b*-P(AA) (b) the activated copolymer P(OEGMEA)-*b*-P(AA-*s*-(AA-NHS)-*s*-(Acyl urea)) and (c) the amidated copolymer P(OEGMEA)-*b*-P(AA-*s*-(Acyl urea)-*s*-(N-Boc)) labelled Par. Pol., Act. Pol. and Ami. Pol. 1 respectively (see **Tables 1 and 2**). In **Figure 2**, the insets highlights for each copolymer the concerned protons for the peaks used to characterize the copolymer (and labelled *a* to *h*).

In all three NMR spectra, the peaks between 0.2 - 3.2 ppm are predominantly the contribution from the acrylate backbone of the copolymer (protons identified as *c*), while the peaks in the range 3.2 - 4.4 are ascribed to the protons from the oligo(ethylene oxide) methyl ether comb in the P(OEGMEA) block (*a, b* and *e*). In particular, the separated peak at 4.30 ppm is the contribution from the two α-hydrogen atoms adjacent to the ester bond in P(OEGMEA) (*a*).

In **Figure 2b**, a triplet at ca. 1.2 ppm, related to the protons of the methyl end group of N-acyl urea and labelled as *g* allows extracting the number of units of N-acyl urea in the activated copolymer (which gives a conversion rate of ca. 20% for Act. Pol.). Further, the prominent peak at 2.90 ppm could be a collective contribution from three different types of protons: the protons in the tertiary amine group of the N-acyl urea (*f 1*), the same protons from the tertiary amine of EDC present in excess and not removed by dialysis, and the equivalent protons in the NHS ring (*f 2*), makes it impossible to discriminate the signal from both NHS and free EDC at this stage. In **Figure 2c** associated to the spectrum of Ami. Pol. 1, four series of peaks can be noted: first, the same triplet at 1.2 ppm related to the methyl group of N-acyl urea (*g*) that allows extracting the number of N-acyl urea groups in the copolymer. Second, the one at 2.90 ppm associated to the protons in the tertiary amine group of N-acyl urea and the same protons on EDC in excess (*f*). Indeed, we assume

all the NHS-activated sites to have been either hydrolysed or amidated. A zoom on the peak at 2.90 ppm reveals that it is composed of a broad peak (probably from protons of the immobilized N-acyl urea groups) and a sharp peak (from the same protons but on the remaining EDC), proving that EDC in excess is not fully removed after dialysis but is not covalently attached to the DHBC. Once the contribution from N-acyl urea is known, this peak can hence be used to extract the amount of EDC still present. Thirdly, another peak at 1.47 ppm corresponding to the tert-butyl group in the N-Boc-ethylenediamine group (*h*). Finally, the peak at ca. 3.4 ppm is this time not only due to the 3 protons of the methyl terminal group of the P(OEGMEA), but also from the 4 protons before the amine function in the Boc pending group (*e*). Those last two peaks (*h* and *e*) gives two methods to extract the number of N-Boc pending groups, and we took the average of those two methods.

Using the peak at 4.30 ppm in the spectrum of Ami. Pol. 1, P(OEGMEA)-*b*-P(AA-*s*-(Acyl urea)-*s*-(N-Boc)), for calibration, the conversion rates of acrylic acids to N-acyl urea and amide groups were found to be ca. 32% and ca. 15%, respectively. Hence, Ami. Pol. 1 may be descripted as $P(OEGMEA)_{24}$-*b*-$P((AA)_{28}$-*s*-$(Acyl\ urea)_{17}$-*s*-$(N\text{-}Boc)_8)$. Let us note that a strong contribution from not covalently bound EDC can still be monitored, as for one DHBC, 11 EDC molecules contributes to the NMR pattern. The relative abundances of the three possible units obtained after transformation of AA groups, statistically arranged in the ionic block of the copolymers have been quantified for all samples (see **Table 2**). In order to confirm the percentage values of activation and amidation, it is essential to check that the P(OEGMEA) block is not damaged by the amidation step. Hence, the peak at 4.30 ppm, was again used as the reference, (corresponding to the two α-hydrogens adjacent to the ester bond in P(OEGMEA) labelled *a*) to find the area of the peak between 3.6 – 4.0, before and after amidation, and similar values were obtained, confirming the absence of damage (**Figure S2**), in agreement with ATR-FTIR results.

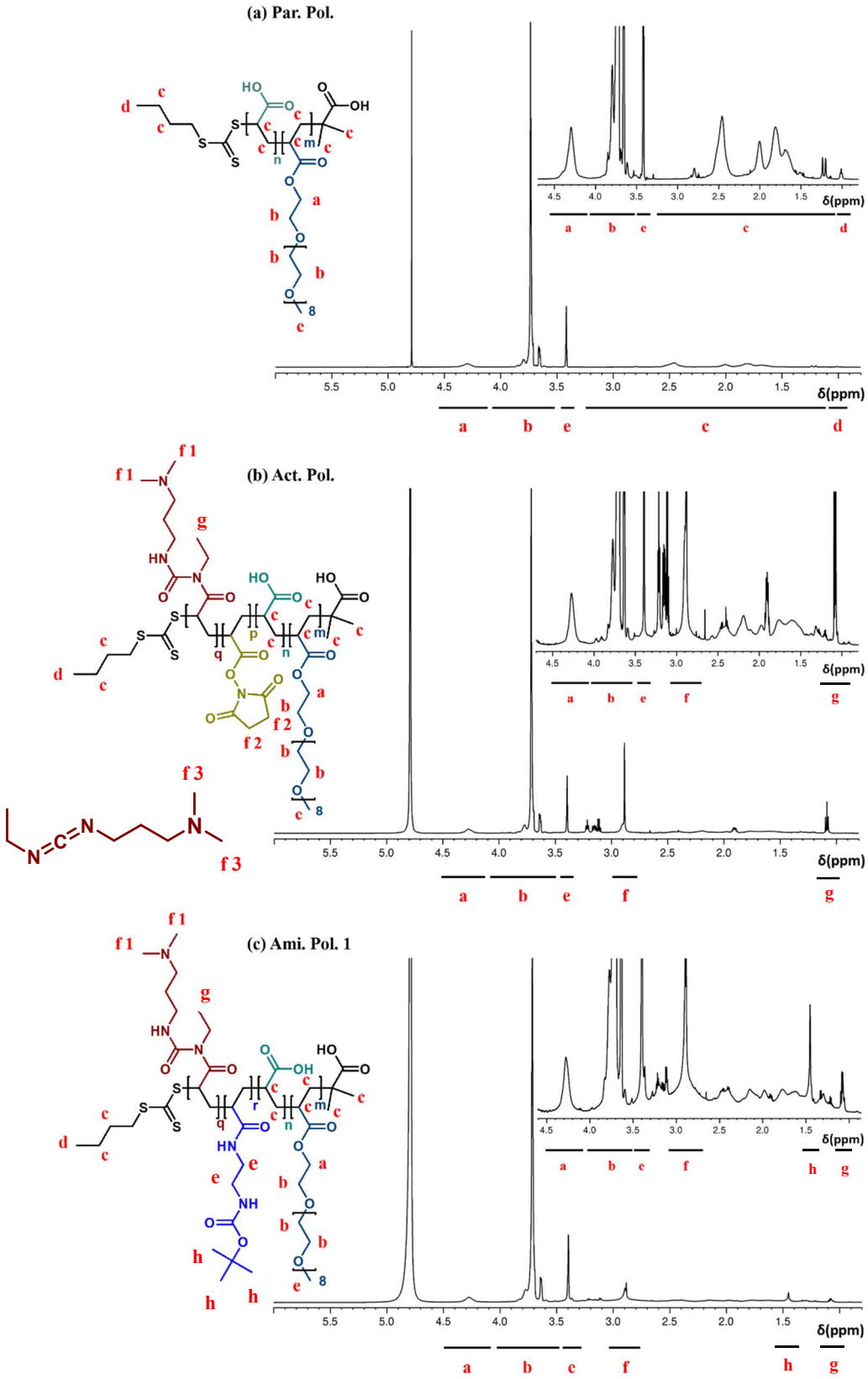

(a) Par. Pol.
(b) Act. Pol.
(c) Ami. Pol. 1
δ(ppm)

Figure 2. *NMR spectra of a) the parent copolymer P(OEGMEA)$_{24}$-b-P(AA)$_{53}$ (Par. Pol.) b) the activated polymer, P(OEGMEA)$_{24}$-b-P((AA)$_{25}$-s-(AA-NHS)$_{17}$-s-(Acyl urea)$_{11}$) (Act. Pol.) and (c) the amidated polymer, P(OEGMEA)$_{24}$-b-P((AA)$_{28}$-s-(Acyl urea)$_{17}$-s-(N-Boc)$_{8}$) (Ami. Pol. 1). The number of units for each groups were calculated using the peaks highlighted using alphabetical characters. The insets, showing the chemical formula of each copolymer, indicate the protons attribution to each peak. The peak at 4.30 ppm is used for calibration.*

After amidation, the copolymers contain an unmodified P(OEGMEA) polyester block and a transformed P(AA) block containing randomly distributed protected amine species, tertiary amine species, and acrylic acid units. For moderate pH values, the resulting P(OEGMEA)-*b*-P(AA-*s*-(Acyl urea)-*s*-(N-Boc)) copolymer thus simultaneously presents positive and negative charges.

1.3.2.4. Elemental Analysis

The activated and amidated copolymers were also characterized using elemental analysis (EA) for their CHNS composition. The main purpose of these results (presented in **Table 2** and **Table S1**) was to complement the NMR analysis to accurately determine the relative abundance of each possible product unit within the P(AA) block after activation with EDC/NHS (Act. Pol.) and subsequent amidation with N-Boc-ethylenediamine (Ami. Pol. 1 - 4), which introduced protected amine species into the poly(acrylic acid) block. In the case of Act. Pol., which corresponds to P(OEGMEA)-*b*-P(AA-*s*-(AA-NHS)-*s*-(Acyl urea)), the measured weight percentages were 46.95% carbon, 8.79% Hydrogen and 6.08% Nitrogen, which gives atomic ratios of N/C = 0.111 and H/C = 2.25. As the amount of N-acyl urea pending groups is known by NMR, these elemental ratios within the copolymer were used to estimate the amount of activated ester groups. Act. Pol. was thus characterized as P(OEGMEA)$_{24}$-*b*-P((AA)$_{25}$-*s*-(AA-NHS)$_{17}$-*s*-(Acyl urea)$_{11}$), which complemented the NMR measurements. In the amidated copolymers P(OEGMEA)-*b*-P(AA-*s*-(Acyl urea)-*s*-(N-Boc)) (Ami. Pol. 1 - 4), the obtained atomic ratios typically indicated equal or

higher content of nitrogen atoms compared to the activated copolymer. For example, in Ami. Pol. 1, atomic ratios determined by elemental analyses were found at N/C = 0.132 and H/C = 2.28 (from 48.84% Carbon, 9.28% Hydrogen and 7.52% Nitrogen weight ratios). These values are in relatively good agreement with the calculated atomic ratios using the number of units deduced from NMR data and taking into account the contribution from EDC not removed by dialysis (N/C_{NMR} 0.102 and N/C_{EA} 0.132). This approach of data-crossing between NMR and EA analysis was done for the 4 amidated polymers (see **Table 2**). Let us note that ratios from EA are always found slightly higher than the calculation made from the number of units obtained by analysis of the NMR patterns, probably as we underestimate the amount of EDC impurities in the final sample.

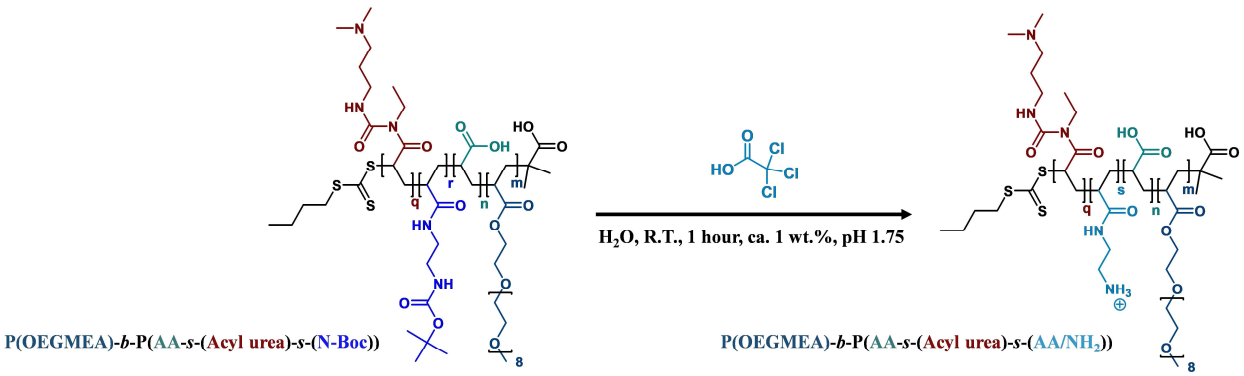
Elemental analysis along with NMR, fully confirm the incorporation of amine entities in the activated and amidated copolymers. The highest N-acyl urea content is recorded in Ami. Pol. 2 (32%) and the lowest in Ami. Pol. 4 (13%). For Act. Pol., Ami. Pol. 1 and Ami. Pol. 3, the conversion rates to N-acyl urea are found to be 21%, 32%, and 23% respectively (see **Table 2**). These results may be related to the pH of the suspension during the addition of EDC and NHS (pH_{act}), as Ami. Pol. 2 activation step was carried at pH_{act} = 7, while Ami. Pol. 4 and Ami. Pol. 3 were done at pH_{act} = 8 and 9 respectively. The activation pH chosen could influence the balance between NHS and N-acyl urea grafting and hence the final ratio of N-acyl urea. Let us note that Ami. Pol. 1, 2 and 5, all activated at pH = 7, show the same conversion rate in N-acyl urea, proving the consistency of the method. It should be noted that having a longer activation step (t_{act}) does not improve the final N-acyl urea content, as Ami. Pol. 2 was activated for 15 min before N-Boc-ethylenediamine addition while Ami. Pol. 1 was activated overnight, without a significant alteration of the amount of N-acyl urea content in the amidated polymer. Finally, the activated

copolymer shows a lower conversion rate, probably as some O-acylurea groups are removed during the dialysis prior to their modification into N-acyl urea. Further, Ami. Pol. 1, 2, 3, 4 and 5 also reported 15%, 15%, 34%, 26% and 8% N-Boc conversions rates respectively, see **Table 2**. Ami. Pol. 1 and 2 exhibit the same amidation rate, showing that a longer activation time t_{act} has little influence on this, while the higher amidation rates for Ami. Pol. 3 and 4 compared to Ami. Pol. 1, 2 and 5 hints again at the role of the pH both during the activation (pH_{act}) or most importantly the amidation step (pH_{amid}), with basic pH (9 and especially 8) favouring higher conversion rates. This trend may be rationalized by a better nucleophilic character of N-Boc-ethylenediamine when pH conditions are more favourable for the existence of unprotonated amines. Controlling the activation and amidation steps will be crucial to tailor the number of N-acyl urea and primary amines available in the final copolymer.

1.3.3. Deprotection of P(OEGMEA)-*b*-P(AA-*s*-(Acyl urea)-*s*-(N-Boc))

1.3.3.1. Deprotected Copolymer, De. Pol. (P(OEGMEA)-*b*-P(AA-*s*-(Acyl urea)-*s*-(AA/NH_2)))

In order to free the primary amine groups grafted with N-Boc-ethylenediamine, the deprotection of the copolymer was carried out by selective acidic hydrolysis of the N-Boc protective group. This was done by adding trichloroacetic acid (TCA) to a suspension of the amidated copolymer at ca. 1 wt% until a pH of 1.75 was reached. These acidic conditions were maintained for one hour at room temperature. The success of the deprotection was assessed by checking the removal of the tert-butyl from the Boc group by NMR spectroscopy. The deprotected copolymer presents thus both primary and tertiary amines as pendant groups in their P(AA) block, yielding P(OEGMEA)-*b*-P(AA-*s*-(Acyl urea)-*s*-(AA/NH_2)), see **Scheme 5**.



Scheme 5. *Deprotection of Ami. Pol. (P(OEGMEA)-b-P(AA-s-(Acyl urea)-s-(N-Boc))), to obtain the targeted deprotected polymer De. Pol. (P(OEGMEA)-b-P(AA-s-(Acyl urea)-s-(AA/NH₂))).*

1.3.3.2. Characterization Using NMR and Elemental Analysis

The deprotection of Ami. Pol. 1 using TCA for 1 hour (see **Table 3**), yielding the copolymer labelled De. Pol. 1, was confirmed initially using ^{1}H NMR, with the disappearance of the peak at 1.47 ppm, associated to the 9 protons from the tert-butyl group of Boc, see **Figure 3**. A complete disappearance of this peak contribution was found, suggesting total deprotection. In addition, NMR analysis showed that the contribution from protons of the P(OEGMEA) block was unchanged, showing that the deprotection conditions did not lead to hydrolysis of the polyester comb. Finally, the contribution from EDC impurities, although still present, is found much lower that before deprotection (11 EDC for one DHBC before deprotection, whereas only 2 are measured after), proving the acidic treatment followed by further dialysis help removing these impurities. The abundance of Nitrogen in the copolymer composition was checked using elemental analysis, where 50.77% Carbon, 8.95% Hydrogen and 6.79% Nitrogen weight fractions were found (De. Pol. 1, **Table S2**). The high Nitrogen content even after deprotection confirms that the amide links on the P(AA) block remain intact even at the low pH of 1.75 used for the deprotection. The atomic N/C ratio obtained from elemental analysis decreased after deprotection: it passes from

N/C = 0.132 before deprotection (Ami. Pol. 1) to 0.114 (De. Pol. 1), again hinting at the removal of extra impurities such as EDC. Assuming all the Boc groups are removed, we can use the number of units obtained before deprotection (from Ami. Pol. 1) and the number of units from EDC still present in the sample to calculate an atomic ratio N/C = 0.0844, again lower than the actual ratio found in elemental analysis. To further explore the deprotection step, we attempted two other deprotection procedures, using TCA for 1 hour, 1 day or HCl for 1 day and Ami. Pol. 2 as polymer studied. In all cases, the Boc groups was successfully removed as seen by NMR (see **Figure S3** in SI), and the elemental analysis showed an atomic N/C ratio lower after deprotection (see **Table 3**).

We noted that in the activated and amidated DHBC, some EDC impurities are still present. Note that due to the electrostatic nature of the interactions between acrylate species and these impurities, a full removal of those impurities by dialysis would require a pH of at least 2 to avoid the formation of micelles that could entrap these impurities in the core (see **Section 3.4**). But the different deprotection tests indicate that it is not possible to reach such pHs without also removing the Boc groups, hence why dialysis at a pH not lower than 3 was carried out with the amidated copolymers.

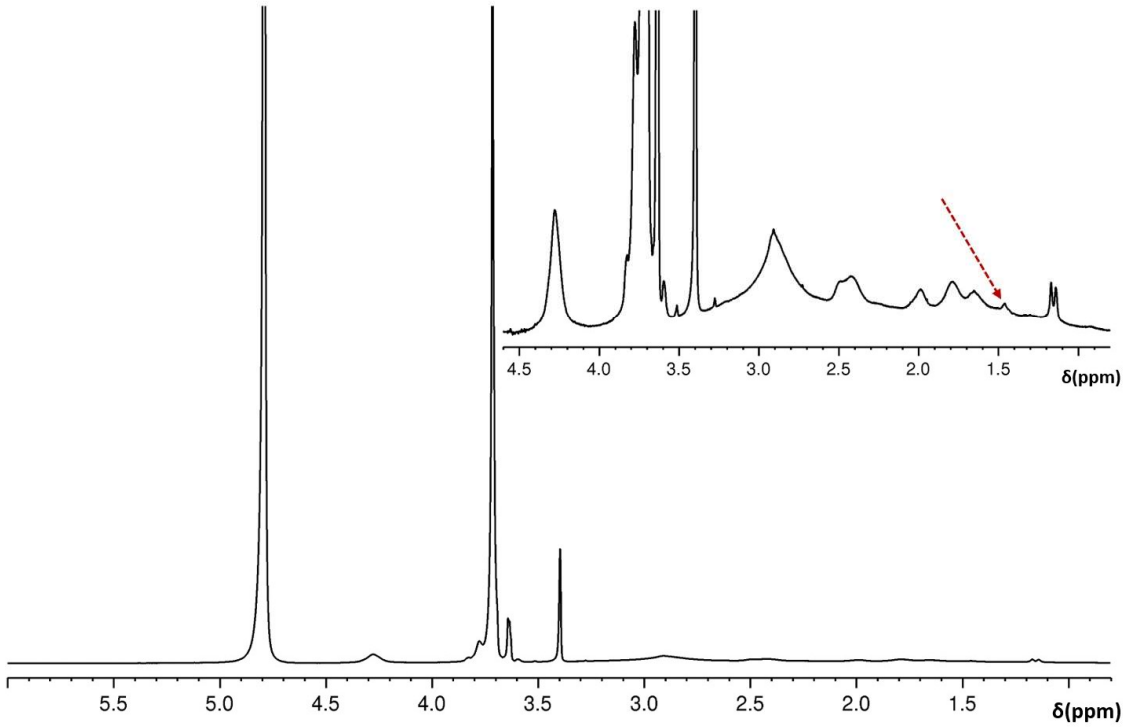


Figure 3. *^{1}H NMR spectra of De. Pol. 1 from the deprotection of Ami. Pol. 1. The graduation in red (1.47 ppm) is the position where a peak associated to the 9 protons of the tert-butyl group would be seen, highlighting its absence.*

1.3.4. Self-Assembly Properties of the Different Polymers Studied via Static & Dynamic Light Scattering and Small Angle Neutron Scattering

The addition of N-acyl urea and N-Boc-ethylenediamine groups to the DHBC may both influence drastically its behaviour in solution, notably by giving self-assembling properties to the activated or amidated copolymers. Notably, N-acyl urea bears positive charges at pH < pKaH of the tertiary amine,[60,85] while the tert-butyl group of N-Boc-ethylenediamine is known for its hydrophobicity.[53]

Both phenomena could hence induce self-assembling properties to the copolymer in aqueous solution, which were investigated using light and small-angle neutron scattering.

1.3.4.1. Characterization of Par. Pol. and Act. Pol.: Emergence of Self-Assembling Mechanisms After Polymer Modification

The parent copolymer, Par. Pol. (P(OEGMEA)-*b*-P(AA)), is double hydrophilic and lacks the ability to self-assemble (as confirmed by dynamic light scattering, **Figure S5**); it requires an external additive, such as a polyion of opposite charge, to induce a co-assembly process and form polyion complex micelles.

However, modification of the macromolecule by activation with EDC/NHS, gives a copolymer that can self-assemble naturally. As a first step, Act. Pol. was studied to determine the influence of N-acyl urea tertiary amine groups in the P(AA) block on the self-assembled micellar structures. The autocorrelation function $g_2(\tau)$ of intensity *vs* time and the corresponding relaxation time distributions were measured using DLS at pH 5 and a scattering angle of 90°. Results are depicted in **Figure 4a**. The CONTIN fit shows a single peak corresponding to a stable and well-defined population of colloids with a hydrodynamic radius R_H = 13.4 ± 0.3 nm at pH 5. The data were analyzed at different scattering angles (**Figure 4b**) to extract more precisely the translational diffusion coefficient of the particles. D_0 was obtained via averaging over the angular range (see *Materials and Methods*). This gave D_0 (m^2s^{-1}) = (1.9 ± 0.1) × 10^{-11} m^2/s^{-1} and hence the hydrodynamic radius was found at R_H = 12.5 ± 0.5 nm. The sample was also studied by SLS, and fitting of the Zimm plot was attempted to extract the radius of gyration of the scattering particles R_G (**Figure S6**). Nevertheless, the SLS data show that R_G is very small (<< λ/20); the scattering intensity was found to be independent of the scattering vector, which prevents extracting an

accurate value. To calculate R_G/R_H and get some indication on the topology of the species, we hence have to rely on small angle neutron scattering. The SANS data for the same sample, Act. Pol., measured at 1 wt% in D_2O were therefore fitted first using the Guinier model to extract the radius of gyration of particles R_G (**Figure S7**). At pH 5, R_G was found at 7.8 ± 0.1 nm, acquired in the very low q region ($0.004 < q < 0.016$ Å^{-1}) of the scattering curve. This gives a ratio R_G/R_H = 0.62 ± 0.03, which corresponds to spherical species with a non-homogeneous distribution, as usually seen for micelles. The values of R_G, R_H and of the R_G/R_H ratio all suggest that micelles have spontaneously formed from the self-assembly of Act. Pol. alone at pH 5.

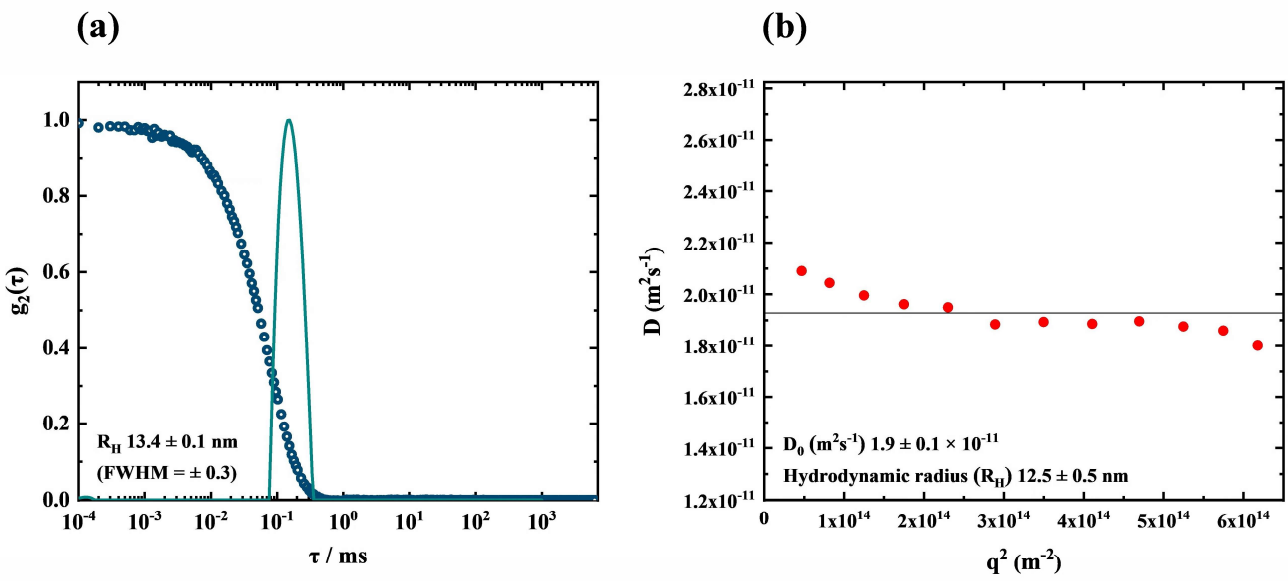


Figure 4. *SLS/DLS data of Act. Pol. at 0.1 wt% and pH 5 in H_2O: (a) Intensity-time autocorrelation function $g_2(\tau)$ measured at a scattering angle $\theta = 90^o$ with distribution of relaxation times obtained from the CONTIN method (in inset, the hydrodynamic radius R_H and full width at half maximum (FWHM) from the CONTIN analysis are given), (b) Diffusion coefficient D as a function of the scattering angle from the second order Cumulant analysis (in inset, the diffusion coefficient at the zero angle D_0 and its corresponding hydrodynamic radius R_H is given).*

Considering that Act. Pol., P(OEGMEA)-*b*-P(AA-*s*-(AA-NHS)-*s*-(Acyl urea)), contains both weak acid (pKa (AA monomer) = 4.30) and basic (Acyl urea pKaH = 9.76) sites, the effect of pH

on the stability, shape and size of the micellar species was studied in DLS at 90° and three different pHs: pH = 3 (acidic conditions), pH = 5 and pH = 9 (alkaline conditions). This pH window prevented any hydrolysis of the copolymer during the experiment. The data obtained were fitted using the CONTIN analysis to obtain the particle size distributions (**Figure 5a**). The emergence of a second small population at pH = 3 (R_H = 84.3 ± 0.2 nm) and the significant increase in polydispersity at pH = 9 both indicate a pH sensitive character of the micellization, which we attribute to electrostatic interactions between the tertiary amine and the carboxylate groups of the diblock.

Small angle neutron scattering (SANS) experiments performed on Act. Pol. at the same pHs further confirm the result obtained from light scattering (**Figure 5b)**. For all pH, the signal in the low q region ($0.005 < q < 0.040$ Å^{-1}) is characteristic of quasi spherical objects, with a plateau at the smallest angles and an oscillation at ca. 0.010 - 0.020 Å^{-1}. Using the Guinier approximation, we find radii of gyration of micelles R_G of 7.1 ± 0.1 nm, 7.8 ± 0.1 nm and 8.1 ± 0.2 nm at pH = 3, 5 and 9. Furthermore, the very low q region ($0.004 < q < 0.010$ Å^{-1}) displays a clear plateau and the absence of an upturn, confirming no aggregation in all three solutions. At higher values of q ($0.120 < q < 0.430$ Å^{-1}), the data show a power-law dependence $I \sim q^{-\alpha}$ with an exponent α of ca. 2.77, 3.23, and 3.45 at pH = 3, 5, and 9, respectively. This slope could be related to the contribution from polymer chains in the shell of the micelles. Indeed, in the case of comb-like chains such as P(OEGMEA) forming the micelle corona, the slope is higher than in the case of linear polymers in a good solvent where it is typically of $\alpha = 5/3$.[86] For that reason, data were fitted using the model for polymer micelle described in the *Materials and Methods* section. This model is well-suited for micelles made of block copolymers, notably to describe accurately the corona of micelles (see **Scheme 2**).

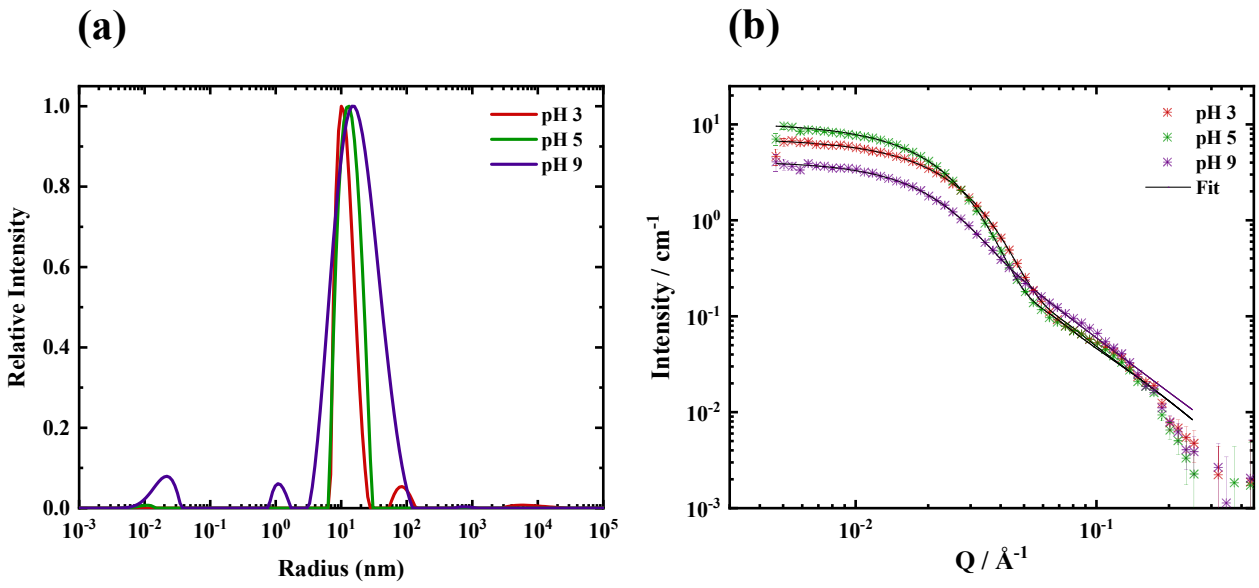


Figure 5. *(a) Distribution in size of Act. Pol. micelles (0.1 wt%) obtained from the CONTIN analysis of intensity-time autocorrelation functions $g_2(\tau)$ studied at a scattering angle of $\theta = 90°$ at 3 different pHs in H_2O (associated correlograms are provided in Figure S8) and (b) SANS data of Act. Pol. suspensions (1 wt%) at the same pHs in D_2O. In (b), the fit using the polymer micelle model is shown as black lines.*

Compared to the optimum pH = 5, the scattering intensity shows a noticeable decrease in the low to medium q region ($0.010 < q < 0.050$ Å^{-1}) for pH = 3 and pH = 9, with an even more pronounced decrease for the latter. This phenomenon could be due to fewer micelles in solution, while more polymer chains remain free in solution. At pH 5, both the acrylic acid species and amine entities are mainly in their ionic form, unlike at pH 3 and pH 9, where one species or the other is much less charged. The shape of the neutron scattering curves, characteristic of core-shell morphologies, is similar for the three pH levels; nevertheless, it is less marked at pH 3 and 9 than at pH 5. At pH 5, the difference in intensity between the low q domain and the high q domain is higher and better marked, as expected for core-corona micelles with a well-defined interface between the core and the corona. The three curves could be fitted using the polymer micelle model, indicating a

micellar structure even as the pH is changed, with the results of the fits given in **Table 5**. Nevertheless, when moving from a lower to a higher pH, a strong variation in the core radius R and radius of gyration of the P(OEGMEA) chains R_g was observed. Indeed, the core radius was determined as R = 4.3 ± 0.2 nm, 5.2 ± 0.3 nm and 4.4 ± 1.3 nm and the radius of gyration as R_g = 1.6 ± 0.2 nm, 1.8 ± 0.2 nm and 0.6 ± 0.1 nm at pH = 3, 5 and 9, respectively. Let us note that the surprisingly low value of R_g at pH = 9 is accompanied by a similar decrease in the volume of one chain in the shell v_{shell} and is related to the very high polydispersity index at this pH, which prevents extracting a completely accurate value for the shell of the micelles. Indeed, the polydispersity in size σ varies from ca. 35% (at pH = 3 and 5) to ca. 74% (at pH = 9). The lower intensity associated to a large increase of the polydispersity in size confirms that at pH = 9, the system starts to lose its self-assembling properties, in agreement with the DLS data. This can be related to the value of the pH which is close to the pKa of acyl urea.

Sample name	pH	Scale (std. error)	Radius R nm (std. error)	Radius of gyration R_g nm (std. error)	Volume of shell v_{shell} nm^3 (std. error)	Polydispersity σ % (std. error)	Structural factor	
							Volume fraction % (std. error)	Hard sphere radius nm (std. error)
$P(OEGMEA)_{24}$-*b*-$P((AA)_{25}$-*s*-$(AA\text{-}NHS)_{17}$-*s*-$(Acyl\ urea)_{11})$ (Act. Pol.)	3	0.40×10^{-7} (0.06×10^{-7})	4.3 (0.2)	1.6 (0.2)	0.12×10^{3} (0.02×10^{3})	37 (1)	------	------
	5	0.48×10^{-7} (0.03×10^{-7})	5.2 (0.3)	1.8 (0.2)	0.14×10^{3} (0.02×10^{3})	36 (1)	------	------
	9	0.82×10^{-7} (0.88×10^{-7})	4.4 (1.3)	0.6 (0.1)	0.64×10^{2} (0.48×10^{2})	74 (30)	------	------
$P(OEGMEA)_{24}$-*b*-$P((AA)_{28}$-*s*-$(Acyl\ urea)_{17}$-*s*-$(N\text{-}Boc)_{8})$ (Ami. Pol. 1)	3	0.65×10^{-8} (0.83×10^{-8})	3.5 (0.1)	2.1 (0.1)	0.75×10^{3} (0.85×10^{3})	55 (3)	------	------
	4	0.29×10^{-6} (0.02×10^{-6})	3.3 (0.2)	3.6 (0.1)	0.26×10^{2} (0.01×10^{2})	28 (5)	------	------
	5	0.14×10^{-6} (0.01×10^{-6})	6.3 (0.1)	3.3 (0.1)	0.72×10^{2} (0.01×10^{2})	13 (2)	------	------
	6	0.15×10^{-6} (0.01×10^{-6})	6.5 (0.1)	2.5 (0.1)	0.84×10^{2} (0.02×10^{2})	36 (2)	------	------
	7	0.16×10^{-6} (0.01×10^{-6})	5.7 (0.1)	3.9 (0.1)	0.86×10^{2} (0.01×10^{2})	16 (2)	6 (1)	19.4 (0.2)
	8	0.20×10^{-6} (0.01×10^{-6})	4.7 (0.1)	4.2 (0.1)	0.70×10^{2} (0.01×10^{2})	22 (4)	5 (1)	18.1 (0.3)
	9	0.26×10^{-6} (0.03×10^{-6})	3.8 (0.4)	4.5 (0.1)	0.52×10^{2} (0.01×10^{2})	32 (11)	5 (1)	17.8 (0.5)
$P(OEGMEA)_{24}$-*b*-$P((AA)_{28}$-*s*-$(Acyl\ urea)_{17}$-*s*-$(AA/NH_2)_{8})$ (De. Pol. 1)	3	0.39×10^{-7} (0.09×10^{-7})	4.0 (0.2)	1.5 (0.2)	0.12×10^{3} (0.03×10^{3})	40 (1)	------	------
	5	0.19×10^{-6} (0.01×10^{-6})	5.3 (0.1)	3.5 (0.1)	0.62×10^{2} (0.01×10^{2})	17 (1)	5 (1)	15.0 (0.2)
	9	0.49×10^{-7} (0.07×10^{-7})	5.3 (0.3)	1.4 (0.3)	0.13×10^{3} (0.03×10^{3})	37 (1)	------	------

Table 5. *Parameters obtained from the SANS data fitting using the model of polymer micelle for suspensions at 1 wt% and various pHs of 3 different polymers: Act. Pol., Ami. Pol. 1, and De. Pol. 1. Table S4 in supplementary information compares the micelles dimension probed by DLS and SANS.*

1.3.4.2. Characterization of Ami. Pol.: Probing the Micellization Mechanisms as a Function of pH and Salinity

The pH sensitivity of this system was explored in more detail with the amidated copolymer Ami. Pol. 1, P(OEGMEA)$_{24}$-*b*-P((AA)$_{28}$-*s*-(Acyl urea)$_{17}$-*s*-(N-Boc)$_{8}$). The self-assembling properties are maintained after the addition of the N-Boc group (see **Figure 6**), and the pH sensitive nature of the self-assembled structures was studied in detail using DLS while varying the pH between 2 - 9 (**Figure 7**).

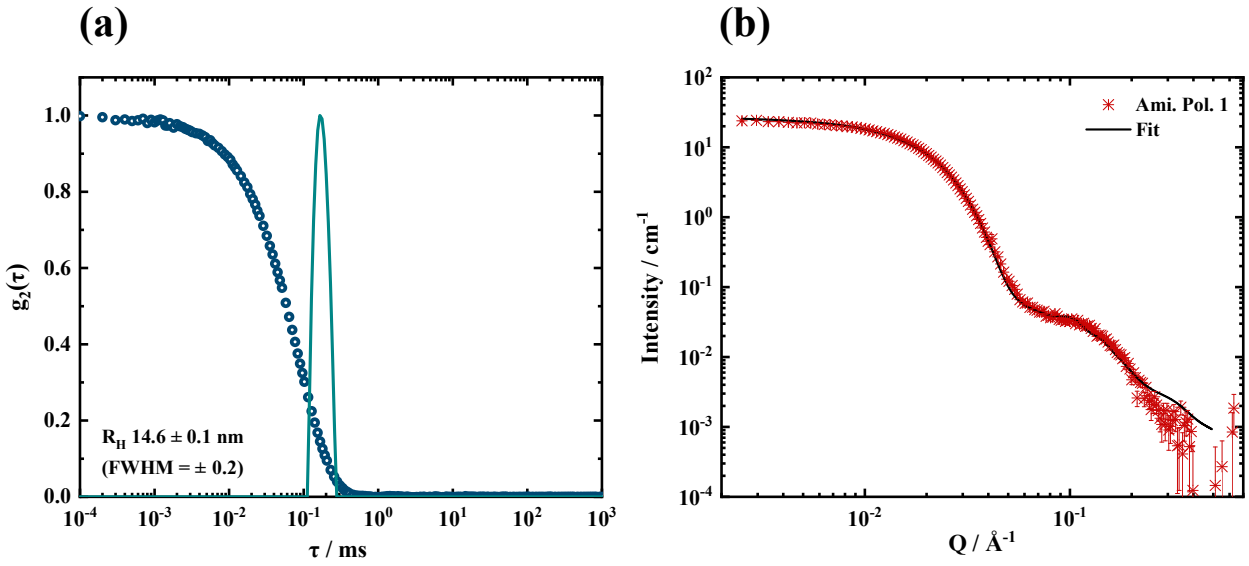


Figure 6. *a) Intensity-time autocorrelation function $g_2(\tau)$ of Ami. Pol. 1 at 0.1 wt% and pH 5 in H_2O, measured at a scattering angle $\theta = 90^o$ and its distribution in relaxation time from the CONTIN analysis (in inset, the hydrodynamic radius R_H and full width at half maximum (FWHM) from the CONTIN are given). (b) SANS pattern of Ami. Pol. 1 at 1 wt%, pH = 5 in D_2O. In black, the fit made using the polymer micelle model.*

First, the variation of the normalized scattered light intensity was studied as a function of pH (see **Figure 7a**). One can observe an increase of the intensity with pH up to pH 5 - 6 before a decrease in alkaline conditions. This pH dependence of the self-assembly of the copolymer further suggests

that electrostatic complexation between the negatively charged acrylate species and the positively charged N-acyl urea groups is mainly responsible for the micelle formation, similar to Polyion complex micelles,[36,55,87] rather than an intrinsic amphiphilic property of the polymer, which could also be expected from both the N-Boc-ethylenediamine and N-acyl urea grafting on the copolymer,[53,88,89] as tert-butyl group in N-Boc and N-acyl urea are seen to exhibit moderate hydrophobicity. Indeed, the highest value of the scattered intensity is obtained at an intermediate pH range of 5 - 6, a pH range between the pKa of the acrylic acid monomer (ca. 4.30)[90] and that of the amine in N-acyl urea (ca. 9 - 10).[60,61] Moving away from this ideal pH range leads to the progressive dissociation of the micelles into individual polymer chains, resulting in a decrease in scattered intensity. Notably, the scattered intensity at pH = 2 is very weak, suggesting that at this pH no micelles are formed in solution. This is further evidenced by studying the results from the CONTIN analysis of the DLS data at different pHs (**Figure 7b**). In a specific pH window between 4 and 9, particles with a monomodal size distribution and low polydispersity are observed, further confirming an optimal pH range for micellization around pH 5. As soon as one moves away from this pH range, the peaks widen, which may be due to multiple populations or high polydispersity. At pH = 5, the hydrodynamic radius obtained was similar to the one obtained for the activated copolymer (Act. Pol.) with a R_H of 14.6 ± 0.2 nm at the same pH (even though bulky N-Boc groups are grafted to the copolymer). The CONTIN analysis shows a narrower size distribution for the amidated copolymer (see **Figure 6a**) than for the activated copolymer (**Figure 4a**). This narrow size distribution could be due to the fact that the grafting of the N-Boc species would reinforce the self-assembling behaviour of the copolymers (through its hydrophobicity). As with the activated copolymer, the hydrodynamic radius R_H obtained by DLS was compared with the radius of gyration of micelles R_G obtained by using the Guinier approximation on the SANS data at pH = 5

to characterize the shape of the species (again corresponding to a non-homogeneous but spherical population, $R_G/R_H = 0.63 \pm 0.03$, **Figure S9**).

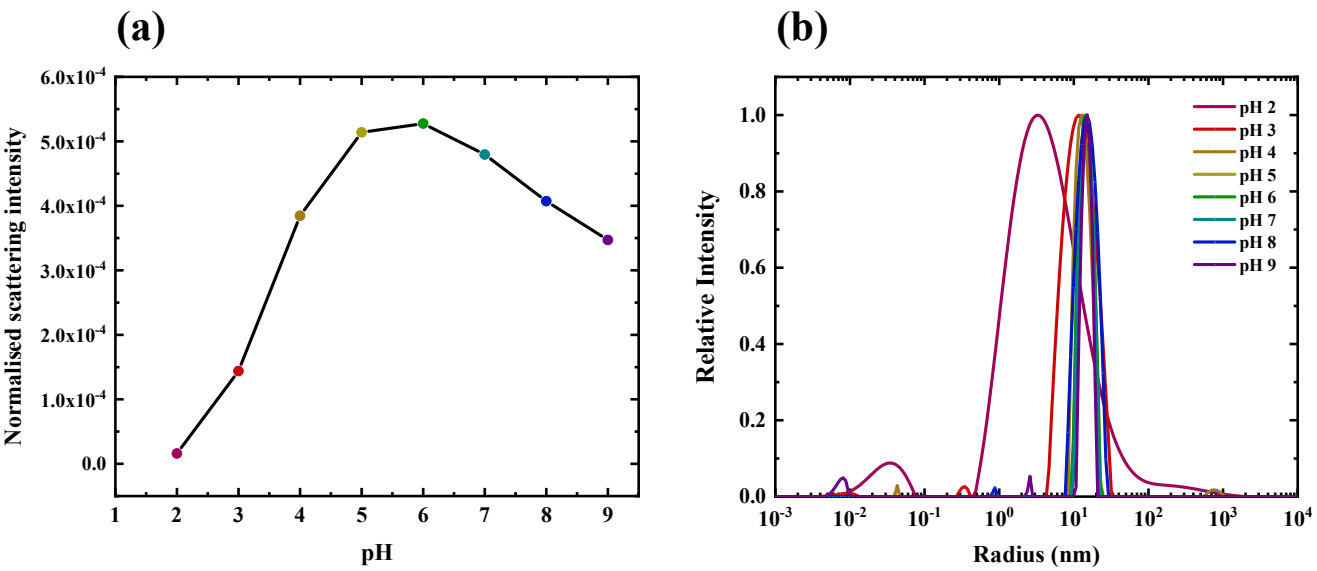


Figure 7. *(a) Variation of the scattered light intensity of Ami. Pol. 1 suspensions normalized by the primary laser intensity as a function of pH (2 - 9) in H_2O (0.1 wt%) and (b) associated size distribution from the intensity time autocorrelation function $g_2(\tau)$ at a scattering angle of $\theta = 90^o$ analyzed using CONTIN (associated correlograms are provided in Figure S8).*

In order to further characterize the micelles, SANS measurements of Ami. Pol. 1 at 1 wt% in D_2O and pH ranging from 2 to 9 were performed (**Figure 8**). Once again, scattering curves from pH 3 to 9 were fitted with the polymer micelle model. At pH 5, the scattering curve for Ami. Pol. 1 is similar to the one of Act. Pol. at the same pH, albeit a slightly higher overall intensity at low q for the amidated copolymer micelles. From the fit of the sample at pH 5, the core radius R and chain gyration radius R_g were found to be 6.3 ± 0.1 nm and 3.3 ± 0.1 nm respectively (with a polydispersity in size $\sigma = 13 \pm 2\%$). In the range pH 3 - 9, the shape of the scattering curves remains about the same. However, the overall intensity is found lower at pH = 3 and 4 notably than at pH 5, which could be due to a partial assembly in solution, as P(AA) is only partially charged at those pH values. According to the model, the radius of the core R and the gyration radius R_g of the

polymers in the corona were 3.5 ± 0.2 nm and 2.1 ± 0.1 nm, with a polydispersity in size σ = 55 ± 3% for pH 3. For pH 4, the core radius R was 3.3 ± 0.2 nm, while R_g was found at 3.6 ± 0.1 nm, with a polydispersity in size σ = 28 ± 5%. In the pH 5 - 9, the shape and intensity are more constant and change less. Nevertheless, the addition of a structure factor is required to fit the data for pH 7 - 9, due to the appearance of a weak but notable correlation peak at q ca. 0.010 $Å^{-1}$, which was interestingly absent at pH 5 and 6. The fitting values obtained for the above pHs have been displayed in **Table 5**. At pH = 2, the high intensity at low to medium q-range disappears, proving the absence of well-defined micelles at this pH. Moreover, the oscillation observed at ca. q = 0.1 $Å^{-1}$ does not correspond as well to the second oscillation from the micellar corona seen at the other pHs. It was hence associated with a signal from free polymers in solution. Further, upon focussing on the low q region ($0.004 < q < 0.008$ $Å^{-1}$), the SANS pattern indicates an upturn suggesting inter-polymeric interactions and therefore aggregation of polymers. Therefore, the curve was fitted using a free polymer chain model with a polymer of radius of gyration R'_g = 2.7 ± 0.1 nm which is in line with the size of the polymer chain. Let us note that at high q ($0.1 < q < 0.4$ $Å^{-1}$), the intensity follows a $q^{-\alpha}$ behaviour, with α = 3.1 ± 0.1, in agreement with a copolymer presenting a comb-like block.

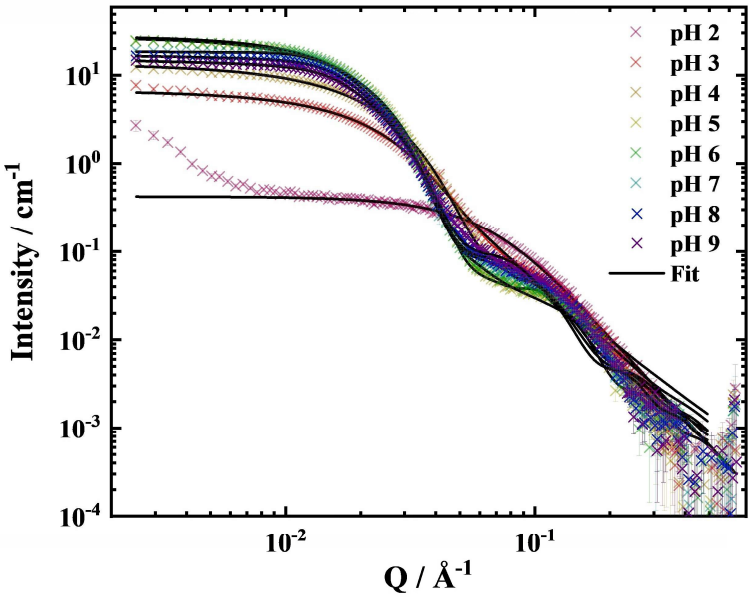


Figure 8. *SANS patterns of Ami. Pol. 1 suspensions at 1 wt% and various pHs (2 - 9) in D_2O. In black, the fits made using the polymer micelle model (pH 3 - 9) or the model of free polymer in solution (pH 2).*

The prevailing effect of pH on the formation and dissociation of micelles from the modified copolymers (activated and amidated) all concur with the hypothesis that the self-assembly results from the electrostatic interactions between the unmodified acrylate groups and the tertiary amine entities of grafted N-acyl urea, rather than from the mild hydrophobicity of N-Boc and N-acyl urea. Indeed, the behaviour of the modified micelles described here is similar to that of the well-studied polyion complex micelles, however it surpasses them in their ability to self-assemble without the need for a complexation partner. To validate unambiguously this hypothesis, we studied the ζ-potential and the ionisation coefficient of the acrylates groups of another amidated copolymer, Ami. Pol. 5 as a function of pH (**Figure 9**). The ionisation coefficient, i.e. the ratio $COO^-/(COOH + COO^-)$ in the polymer, was calculated by a careful study of the COOH and COO^- bands monitored in ATR-FTIR between 1800 and 1500 cm^{-1} (see **Figure S10**). In acidic

conditions, ζ-potential measurements give an overall positive charge of ca. +10 mV, in agreement with the low ionisation coefficient of the polyacrylic acid block (found at 0 % at pH 2 and ca. 15% at pH 3), indicating the predominance of the positive charges of tertiary amines. With increasing pH values, the polyacrylic acid block in the copolymer is gradually deprotonated, resulting in a larger ionisation coefficient and a decreasing ζ-potential. Interestingly, the isoelectric point of the macromolecule was detected by ζ-potential measurements for pH = 5-6, which corresponds to ionisation coefficients of ca. 20 to 45%. NMR studies of Ami. Pol. 5 give conversion rates of 32 % in N-acyl urea pending groups and ca 8 % in N-boc leaving around 60 % of acryclic acid functions on the polymer. From these values, we could calculate a theoretical isoelectric point for this polymer at a ionisation coefficient of 30%, which is indeed reached at pH = 5-6, corroborating with the ζ-potential experimental data. In alkaline conditions, the ionisation coefficient further increases, reaching ca. 80% at pH=9, while the ζ-potential becomes strongly negative, as the negative charges from acrylates become predominant over positive charges from tertiary amines. From the ionisation coefficient curve, we could determine the apparent pKa of the polyacid block in the copolymer at 6.4, in good agreement with the litterature.[66] Although it was not possible to similarly determine the ionisation coefficient of the tertiary amine, their known high pKaH (around 9.76) suggests that positive charges should be present in the entire pH range probed. When compared with DLS and SANS studies, these results demonstrate that micellization occurs around pH=3-4 once Ami. Pol. starts exhibiting negative charges by the partial ionisation of the polyacid block that can interact with the positively charged tertiary amines. Further, the micellization optimum at ca. pH=6 monitored in DLS and SANS is consistant with the point of charge equivalence in the electrostatic balance of the polymer, as seen by the low value of the ζ-potential and closeness to the theoretical isoelectric point.

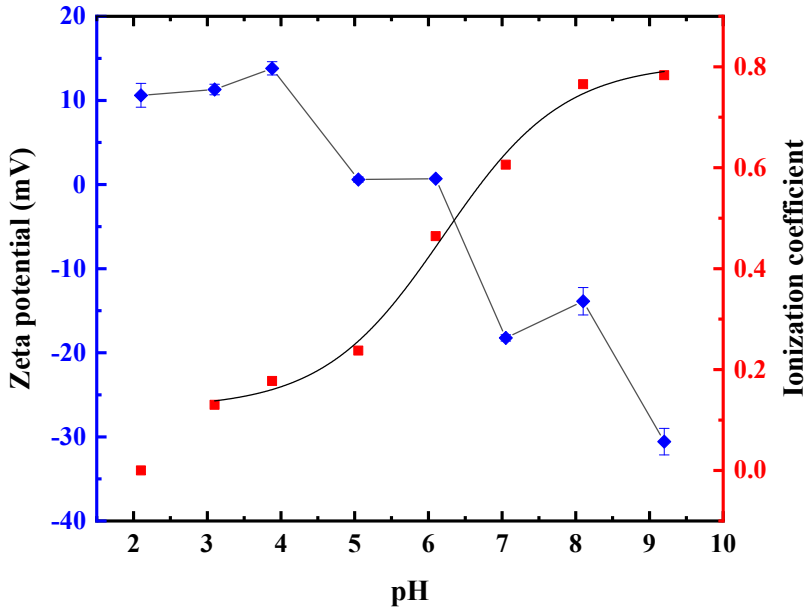


Figure 9. *Comparison between the ζ-potential and the ionisation coefficient of the COOH/COO⁻ groups in Ami. Pol. 5 as a function of pH. The lines are for guiding the eye only.*

A micellization that depends on electrostatic complexation should be sensitive to the ionic strength of the system, as the addition of salt can screen the charges present on the DHBC. We have hence studied in DLS Ami. Pol. 5 at pH = 5 and different concentrations of NaCl, ranging from 0 to 1 M. **Figure S11** gives the averaged scattered intensity as a function of the salt concentration and the associated correlation functions in intensity $g_2(\tau)$. The scattered intensity shows a clear decrease when increasing concentration, which is consistent with a decrease in number of micelles in the suspension. Accordingly, the correlation function goes from a signal of one well-defined population at 0 M to a signal from very polydisperse systems at [NaCl] = 1 M, again in agreement with the loss of micellization properties with increasing salt concentration.

When thoroughly compared, these results establish conclusively that micellization occurs due to electrostatic complexation, and as soon as the DHBC exhibit both positive and negative charges, even if charges are not completely balanced within the polymer.

1.3.4.3. Characterization of Ami. Pol.: Probing the Effect of Concentration

The effect of concentration on the size and shape of the self-assembling species was studied using Ami. Pol. 1 suspensions at pH = 5 in D_2O (1 - 5 wt%), measured by SANS. As shown in **Figure 10**, the absolute scattering intensity of the solutions increases with concentration, as expected due to the increase in number of scattering objects. At 1 wt%, no characteristics of inter-micellar interaction was observed and the data could be fitted using only the form factor of polymer micelles ($S(q)$ = 1). However, by increasing the copolymer concentration, from 2 wt% to 5 wt%, a structure factor peak at q ca. 0.02 $Å^{-1}$ becomes increasingly more pronounced, indicating the emergence of inter-micellar interactions, modeled with a hard sphere structure factor (see *Materials and Methods*).

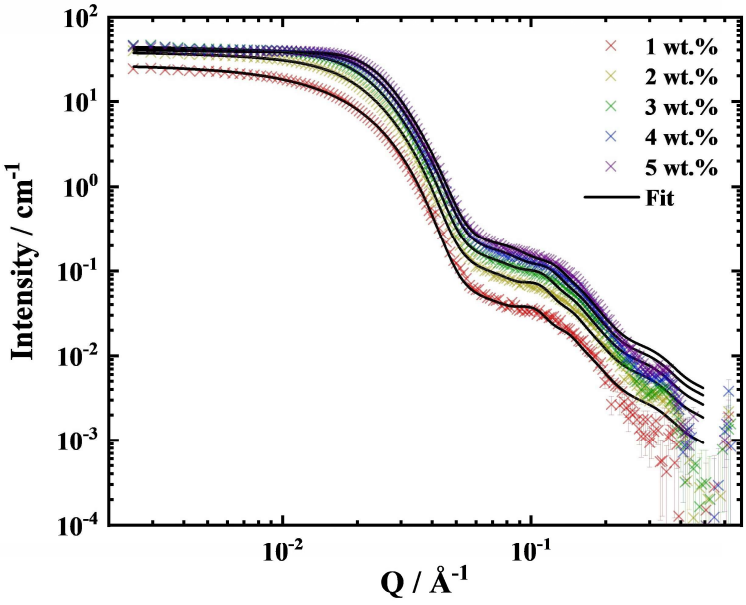


Figure 10. *SANS patterns for Ami. Pol. 1 micelles made at pH = 5 in D_2O at different concentrations (1 - 5 wt%).*

The core radius of the micelles *R* was found to decrease with concentration (from 6.3 ± 0.1 nm at 1 wt% to 4.9 ± 0.1 nm at 5 wt%) while the gyration radius of the chains in the corona R_g remains roughly constant at ca. 3.3 nm. This has been observed previously for micelles formed by electrostatic interaction between the charged block of a DHBC and an oppositely charged micellization partner, because increasing the concentration results in less water in the micelle core, thus reducing its size.[74] This suggests that these self-assembled micelles, also formed by electrostatic complexation between positively and negatively charged units present within the same block, follow the same trend. Hence, one could expect the micelle core to be rich in water, as it was previously observed with PIC micelles, reaching in some cases up to 50 vol% of the core.[74] It should be noted that, in our model, the SLD of the core was calculated neglecting the presence of water. Although probably being incorrect, this would have little influence on the other

parameters of the fits, except regarding the overall scaling factor (related to the volume fraction of particles), which would be influenced by an error in SLDs. As SLDs cannot be accurately extracted with a single contrast, the actual value of the scale is not discussed here, but only the trends will be. Notably, with concentration, the scale factor increases almost linearly, which is expected because it would follow the increase in volume fraction. More surprisingly, the volume of the shell v_{shell} decreases with concentration, which may be related to some decrease of the water content in the corona.[74] As for the inter-micelles interactions, they were modelled with the hard-sphere structure factor, which is the simplest possible model. The hard sphere radius of interactions R_{HS} decreases as the concentration increases (from 15.1 ± 0.3 nm at 2 wt% to 12.5 ± 0.1 nm at 5 wt%), as expected. By defining $R_{tot} = R + 2R_g$ the total radius of one micelle, it is interesting to study the variation of $\frac{R_{HS}}{R_{tot}}$ with concentration. $\frac{R_{HS}}{R_{tot}}$ decreases from 1.19 ± 0.03 at 2 wt% to 1.09 ± 0.02 at 5 wt%, but remains > 1, indicating that micelles are not yet at close contact or interpenetrating. On the other hand, the volume fraction of interacting particles φ_{HS} increases almost monotonously with concentration as expected. All the parameters from the fits are given in **Table 6**.

Concentration wt.%	Scale (std. error)	Radius R nm (std. error)	Radius of gyration R_g nm (std. error)	Volume of shell v_{shell} nm^3 (std. error)	Polydispersity σ % (std. error)	Structural factor	
						Volume fraction % (std. error)	Hard sphere radius nm (std. error)
1	0.14×10^{-6} (0.01×10^{-6})	6.3 (0.1)	3.3 (0.1)	0.72×10^{2} (0.01×10^{2})	13 (2)	------	------
2	0.29×10^{-6} (0.01×10^{-6})	5.9 (0.1)	3.4 (0.1)	0.71×10^{2} (0.01×10^{2})	14 (1)	3 (1)	15.1 ± 0.3
3	0.42×10^{-6} (0.01×10^{-6})	5.7 (0.1)	3.3 (0.1)	0.67×10^{2} (0.01×10^{2})	15 (2)	5 (1)	14.0 ± 0.2
4	0.58×10^{-6} (0.02×10^{-6})	5.3 (0.1)	3.3 (0.1)	0.61×10^{2} (0.01×10^{2})	16 (2)	8 (1)	13.1 ± 0.1
5	0.73×10^{-6} (0.02×10^{-6})	4.9 (0.1)	3.3 (0.1)	0.58×10^{2} (0.01×10^{2})	18 (2)	10 (1)	12.5 ± 0.1

Table 6. *Parameters obtained from the SANS data fitting of micelles from Ami. Pol. 1 at various concentrations (1 - 5 wt%) using the model of polymer micelles.*

1.3.4.4. Characterization of Ami. Pol.: Comparison Between Ami. Pol. 1 – 4

The self-assembling nature of the P(OEGMEA)-*b*-P(AA-*s*-(Acyl urea)-*s*-(N-Boc)) copolymer was further substantiated using multiple batches of the amidated copolymer (Ami. Pol. 1 to 4) comprising different degrees of N-Boc grafting (up to 34% of the block units). **Figure S12** depicts the NMR pattern of the N-Boc incorporated copolymers and **Figure S13** shows the SANS plot of the above polymers at 1 wt% in D_2O, pH 5. The shape and scattering intensity of the different batches did not evolve drastically (see fitting parameters in **Table S5**) proving the consistency of the results discussed above even at higher amount of N-Boc grafted. An interesting feature can nevertheless be noted: **Figure S13** shows that the self-assembly process of the amidated copolymers is favoured when the fractions of N-acyl urea are the highest, as evidenced by the highest intensity at low q values and the much more marked interface suggested by the higher slope at q ca. 0.04 $Å^{-1}$ when the fraction of acyl urea is higher. These results highlight that micellization is favoured when the ratio between negative charges (from the remaining acrylate groups) and positive charges (from N-acyl urea) is closer to one.

1.3.4.5. Characterization of De. Pol.: Influence of Primary Amines on the Self-Assemblies

Light and small angle neutron scattering experiments were run on De. Pol. 1 suspensions to investigate the effect of deprotection on the self-assembling properties of the copolymer. DLS results indicate matching features for both samples at pH = 5, before and after deprotection (see **Figure 6a** for the sample before deprotection and **Figure S14a** for the one after deprotection). The pH behaviour is also similar for protected and deprotected samples (see **Figure 5b** and **Figure 11a**). Notably, both samples at pH = 5 exhibit similar hydrodynamic radii with $R_H = 14.6 \pm 0.2$ nm

before deprotection and R_H = 13.8 ± 0.3 nm after deprotection (from the CONTIN analysis). Also, both samples display the same pH response, with an optimal range at 5 - 6. Likewise, SANS patterns before (see **Figure 6b**) and after deprotection (**Figure 11b**, and **Figure S14b**) show the same features, with a plateau at small angles followed by a marked intensity decrease at ca. q = 0.02 Å^{-1} corresponding to the size of the micelles and a second oscillation at ca. q = 0.1 Å^{-1} followed by a slope $q^{-\alpha} \geq q^{-3}$ (α = 3.0, 3.2 and 3.0 at pH = 3, 5 and 9 respectively for the deprotected sample) associated to the shell of P(OEGMEA) comb-like chains of the micelles. The highly similar results obtained before and after deprotection are consistent with the low fraction of protected N-Boc groups in the functional block for this particular polymer (8 units in a 53 unit block): neither the overall size *(R_H)*, the shape (spherical) or the pH-dependence of the micelle objects seems very much affected by the deprotection step. The self-association behaviour observed is likely primarily due to the electrostatic complexation between the acyl urea-amine groups and the acrylate groups, which are present in more comparable amounts.

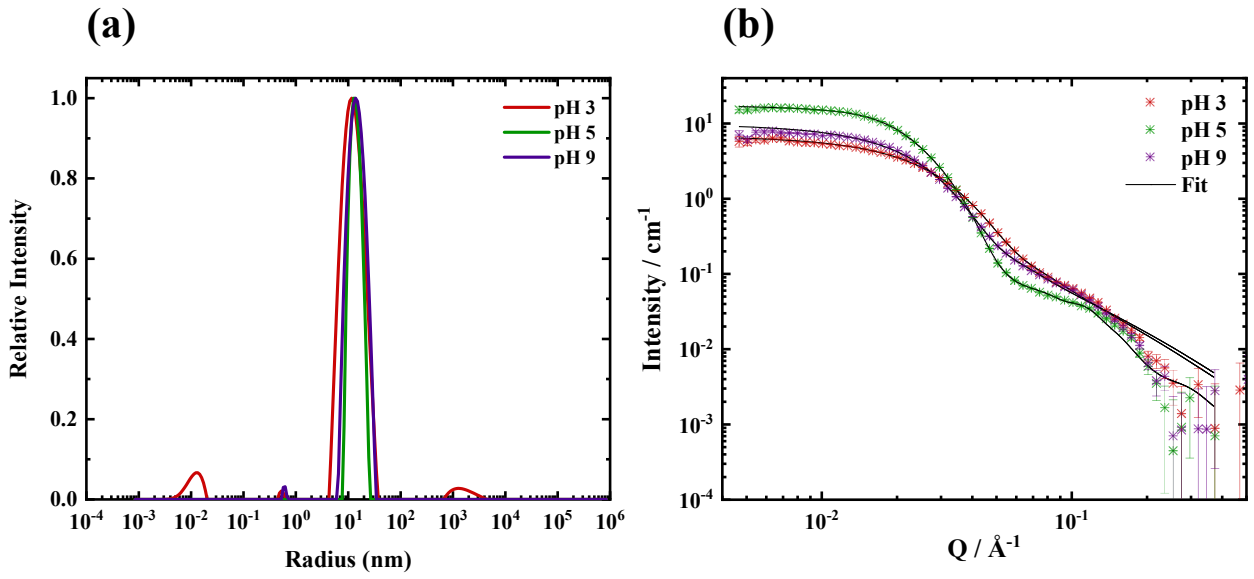


Figure 11. *(a) Distribution of size from intensity-time autocorrelation functions $g_2(\tau)$ studied at a scattering angle of θ = 90° for De. Pol. 1 micelles at 0.1 wt% in H_2O and various pH using the*

CONTIN method (associated correlograms are provided in Figure S8) and (b) corresponding SANS curves at 1 wt% in D_2O. In (b), the fit made using the polymer micelle model is given in black lines. The pH studied are pH = 3 (red), 5 (green) and 9 (purple).

Nonetheless, overlapping SANS patterns of the polymer before and after deprotection measured at pH = 5 (see **Figure S15**) allows one to observe some subtle differences, notably the emergence of a very weak correlation peak at ca. q = 0.012 $Å^{-1}$ after deprotection. The fit of the data at pH = 5 of De. Pol. 1 was carried out using the polymer micelle model taking into account the structure factor and its results were compared with the conclusions from the corresponding amidated copolymer before deprotection (see Ami. Pol. 1 and De. Pol. 1 at pH = 5 in **Table 5**).

Upon fitting, a drop in core radius R from 6.3 ± 0.1 to 5.3 ± 0.1 nm could be seen, moving from protected to the deprotected sample, that we link to the removal of bulky N-Boc groups from the protected copolymer. The radius of gyration of the polymer chains in the corona R_g remained nearly similar in both cases (3.3 ± 0.1 and 3.5 ± 0.1 nm respectively) and the polydispersity was also found in the same range (13 ± 2% and 17 ± 1% respectively). The weakly emerged correlation peak in the deprotected sample refers to the developing inter-micellar interactions and has been modelled using a hard sphere structural factor, giving a volume fraction 5 ± 1% and a hard sphere radius 15.0 ± 0.2 nm. The emergence of inter-micellar interactions could suggest the formation of more micelles in the deprotected sample compared to its precursor (in agreement with the increase in scale factor, see **Table 5**) and may be related to changes in the charge balance and hydrophobicity within the micelle core due to the removal of N-Boc species. Notably, the deprotection of the co-polymer brings more positively charged species into the core, which is possibly anchoring the formation of the well-defined micelles.

To conclude, we have shown that it is possible to perform a post-synthesis modification using the EDC/NHS activation route followed by N-Boc-ethylenediamine and with this method modify a P(OEGMA)-*b*-P(AA) DHBC by grafting N-acyl urea groups and N-Boc-ethylenediamine. We have seen that modifying the conditions of activation and amidation, and notably their pH, influences the amount of both functional groups in the amidated copolymer. Notably, by working at pH 8 for both the activation and amidation, a total amount of ca. 34 % of N-Boc-ethylenediamine species can be grafted to the polymer. We demonstrated that the addition of N-acyl urea groups gives self-assembling properties to the polymer, allowing it to form well-defined spherical micelles in suspensions. pH variation studies, associated with salt concentration studies evidenced that electrostatic complexation bonding between N-acyl urea and acrylate groups of the DHBC was responsible for these self-assembling properties, while further modification with N-Boc-ethylenediamine shows that extra functional groups can be added to the DHBC. We also verified that the deprotection step, mandatory to remove the tert-butyl from the N-Boc-ethylenediamine does not damage the DHBC, and that the self-assembling properties are maintained after deprotection. The final DHBC, P(OEGMEA)-*b*-P(AA-*s*-(Acyl urea)-*s*-(AA/NH_2)), hence displays acrylate groups, primary amine and tertiary amines, three different functional groups that could be passed on to a functional mesoporous material, following procedures put in place for materials templated with PIC micelles,[37,91] for example for removing a wide range of pollutants in wastewaters. The amount of primary amines (8 to 34 % depending on the amidation conditions) could be improved by further optimisation of both activation and amidation protocols. Finally, the amidation procedure could be adapted to other nucleophilic amine-containing molecules to add other functions to the DHBC.

1.4. CONCLUSION

In the present study, the self-assembly behaviour of the double hydrophilic block copolymer, P(OEGMEA)-*b*-P(AA) after functionalization by partial amidation in aqueous medium, has been studied in detail. P(OEGMEA)-*b*-P(AA) synthesized by RAFT polymerization using OEGMEA and AA as the precursors, was initially modified using EDC/NHS to derive an activated P(OEGMEA)-*b*-P(AA-*s*-(AA-NHS)-*s*-(Acyl urea)) copolymer that contains N-acyl urea groups formed by the rearrangement of O-acylurea esters. This activated DHBC can self-assemble into well-defined micelles at controlled pH. This activated polymer was then transformed using N-Boc-ethylenediamine to yield the amidated copolymer, P(OEGMEA)-*b*-P(AA-*s*-(Acyl urea)-*s*-(N-Boc)), grafted with protected primary amine species, while retaining its self-assembling properties. The parent copolymer, P(OEGMEA)-*b*-P(AA), was characterized using ^{1}H NMR to determine the number of units of each block along with the conversion rate, while the modified macromolecules (activated and amidated copolymers) obtained were studied using both NMR and elemental analysis to confirm the degree of modifications.

The self-assembling properties of both the activated and amidated copolymers were investigated using light and neutron scattering. The pH sensitivity of the self-assembling structures was studied using light scattering and further complemented by neutron experiments and ζ-potential measurements, varying the pH between 2 and 9. For both activated and amidated polymers, well-defined core-shell spherical micelles were obtained over a wide range of pH (5 – 9, alongside an optimum at pH = 5 - 7), with the modified acrylic acid ionic block composing the core and P(OEGMEA) building the corona, as inferred from the SANS experiments carried out. However, moving away from this optimal pH range led to the progressive dissociation of the self-assembled structures. All the data for micellar suspensions obtained by SANS were fitted using a polymer

micelle model and a structure factor, using a model of hard-sphere, was used when necessary. Specific information including core radius R and the gyration radius R_g of the P(OEGMEA) polymer chains composing the corona of the micelles were collected from the neutron data. Additionally, we observed the effect of concentration in the amidated copolymer (Ami. Pol. 1) at pH 5 using SANS, confirming that increasing the concentration induced the rise of inter-micelle interactions, which could be effectively modelled using a hard-sphere structure factor.

The induced self-assembling character of the polymers is expected mainly through complexation, deriving from the positively charged tertiary amine species in the N-acyl urea chain and negatively charged remaining acrylate functions, as confirmed by the pH and salt susceptible nature of the micelles. Notably, the gradual loss of micellization properties at pH < 5, associated to a gradual loss of the ionisation coefficient of the acrylate groups, is well-explained by the uncharged nature of the acrylic acid groups at these pHs. A similar trend seems to emerge towards pH = 9, due to the gradual loss of the positive charges of the tertiary amine. Nonetheless, studies at higher pH (≥ 10) were not performed to avoid possible degradation of the P(OEGMEA) block. Micellization can also be controlled by the addition of salt, DLS measurements at various salt concentration showed a gradual loss of the micelles, due to charge screening. The mild hydrophobicity of the tert-butyl group and the N-acyl urea added to the polymer seem to have only a minor impact on the self-assembling character of the micelle.

Acid hydrolysis on amidated copolymer using TCA at pH = 1.75 removes the tert-butyl from the N-Boc group of the copolymer and gives the final deprotected structure, P(OEGMEA)-*b*-P(AA-*s*-(Acyl urea)-*s*-(AA/NH_2)) featuring both primary and tertiary amines as pendant functions in the ionic block of the copolymer, promising applications in diverse domains including separation, and purification.[92–94] TCA as a mild acid is preferred over HCl or trifluoroacetic acid, as it is able to

selectively remove the tert-butyl group of the N-Boc, while preserving the esters of the P(OEGMEA) block. Characterization of the copolymer using NMR, EA and scattering confirms efficient deprotection while the self-assembling properties are maintained. So, new DHBC polymers comprised of a neutral comb-type block and a multifunctional ionic block that displays in similar amounts anionic and cationic functions concomitantly present in a large pH domain were successfully synthesized. Their self-assembly behaviour leads to the formation of original electrostatically driven - polyion complex micelles formed from a unique polymer, which can be dissociated in acidic medium when acrylate functions are neutralized.

SUPPORTING INFORMATION

^{1}H NMR spectra of the parent copolymer and modified samples; composition details of activated, amidated and deprotected samples through elemental analysis; static and dynamic light scattering data along with neutron scattering data of specific samples; fitting parameters used for specific samples in SANS; comparing methods of deprotection

ACKNOWLEDGMENTS

The authors express sincere gratitude to the Physical Measurement Laboratory (Chemical Analysis Platform) at Universite de Montpellier, France for supporting the NMR and elemental analysis. Also, the authors are grateful to the Partnership for Soft Condensed Matter (PSCM) facilities at Grenoble, France for facilitating all preliminary sample characterizations. The authors thank warmly Jan Skov Pedersen who designed the Fortran software for SANS data analysis that was modified by the authors to fit polymer micelles. This project has received funding from the European Union's Horizon 2020 research and innovation programme under the Marie Skłodowska-Curie grant agreement No 847439, through the InnovaXN scheme (Project XN2020-

ILL30). All the authors, thankfully acknowledge the beamtimes allotted by Institut Laue-Langevin (D22) and ISIS Neutron and Muon Source (Larmor, https://doi.org/10.5286/ISIS.E.RB2320268-2 and Sans2d, https://doi.org/10.5286/ISIS.E.RB2320268-1). This work benefited from the use of the SasView application, originally developed under NSF award DMR-0520547. SasView contains code developed with funding from the European Union's Horizon 2020 research and innovation programme under the SINE2020 project, grant agreement No 654000.

1.5. REFERENCES

(1) Lu, Y.; Lin, J.; Wang, L.; Zhang, L.; Cai, C. Self-Assembly of Copolymer Micelles: Higher-Level Assembly for Constructing Hierarchical Structure. *Chem. Rev.* **2020**, *120* (9), 4111–4140. https://doi.org/10.1021/acs.chemrev.9b00774.

(2) Boles, M. A.; Engel, M.; Talapin, D. V. Self-Assembly of Colloidal Nanocrystals: From Intricate Structures to Functional Materials. *Chem. Rev.* **2016**, *116* (18), 11220–11289. https://doi.org/10.1021/acs.chemrev.6b00196.

(3) Kötz, J.; Kosmella, S.; Beitz, T. Self-Assembled Polyelectrolyte Systems. *Progress in Polymer Science* **2001**, *26* (8), 1199–1232. https://doi.org/10.1016/S0079-6700(01)00016-8.

(4) *Amphiphilic Block Copolymers*; Elsevier, 2000. https://doi.org/10.1016/B978-0-444-82441-7.X5000-2.

(5) Mai, Y.; Eisenberg, A. Self-Assembly of Block Copolymers. *Chem. Soc. Rev.* **2012**, *41* (18), 5969. https://doi.org/10.1039/c2cs35115c.

(6) Malmsten, M.; Lindman, B. Self-Assembly in Aqueous Block Copolymer Solutions. *Macromolecules* **1992**, *25* (20), 5440–5445. https://doi.org/10.1021/ma00046a049.

(7) Al Nakeeb, N.; Willersinn, J.; Schmidt, B. V. K. J. Self-Assembly Behavior and Biocompatible Cross-Linking of Double Hydrophilic Linear-Brush Block Copolymers. *Biomacromolecules* **2017**, *18* (11), 3695–3705. https://doi.org/10.1021/acs.biomac.7b01094.

(8) Casse, O.; Shkilnyy, A.; Linders, J.; Mayer, C.; Häussinger, D.; Völkel, A.; Thünemann, A. F.; Dimova, R.; Cölfen, H.; Meier, W.; Schlaad, H.; Taubert, A. Solution Behavior of Double-Hydrophilic Block Copolymers in Dilute Aqueous Solution. *Macromolecules* **2012**, *45* (11), 4772–4777. https://doi.org/10.1021/ma300621g.

(9) Boudier, A.; Aubert-Pouëssel, A.; Gérardin, C.; Devoisselle, J.-M.; Bégu, S. pH-Sensitive Double-Hydrophilic Block Copolymer Micelles for Biological Applications. *International Journal of Pharmaceutics* **2009**, *379* (2), 212–217. https://doi.org/10.1016/j.ijpharm.2009.05.032.

(10) Bathfield, M.; Warnant, J.; Gérardin, C.; Lacroix-Desmazes, P. Asymmetric Neutral, Cationic and Anionic PEO-Based Double-Hydrophilic Block Copolymers (DHBCs): Synthesis and Reversible Micellization Triggered by Temperature or pH. *Polym. Chem.* **2015**, *6* (8), 1339–1349. https://doi.org/10.1039/C4PY01502A.

(11) Khimani, M.; Patel, H.; Patel, V.; Parekh, P.; Vekariya, R. L. Self-Assembly of Stimuli-Responsive Block Copolymers in Aqueous Solutions: An Overview. *Polym. Bull.* **2020**, *77* (11), 5783–5810. https://doi.org/10.1007/s00289-019-03046-w.

(12) Hoogenboom, R.; Rogers, S.; Can, A.; Becer, C. R.; Guerrero-Sanchez, C.; Wouters, D.; Hoeppener, S.; Schubert, U. S. Self-Assembly of Double Hydrophobic Block Copolymers in Water–Ethanol Mixtures: From Micelles to Thermoresponsive Micellar Gels. *Chem. Commun.* **2009**, No. 37, 5582. https://doi.org/10.1039/b911858f.

(13) Rodríguez-Hernández, J.; Lecommandoux, S. Reversible Inside−Out Micellization of pH-Responsive and Water-Soluble Vesicles Based on Polypeptide Diblock Copolymers. *J. Am. Chem. Soc.* **2005**, *127* (7), 2026–2027. https://doi.org/10.1021/ja043920g.

(14) Arotçaréna, M.; Heise, B.; Ishaya, S.; Laschewsky, A. Switching the Inside and the Outside of Aggregates of Water-Soluble Block Copolymers with Double Thermoresponsivity. *J. Am. Chem. Soc.* **2002**, *124* (14), 3787–3793. https://doi.org/10.1021/ja012167d.

(15) Nabiyan, A.; Max, J. B.; Schacher, F. H. Double Hydrophilic Copolymers – Synthetic Approaches, Architectural Variety, and Current Application Fields. *Chem. Soc. Rev.* **2022**, *51* (3), 995–1044. https://doi.org/10.1039/D1CS00086A.

(16) Zhuang, J.; Gordon, M. R.; Ventura, J.; Li, L.; Thayumanavan, S. Multi-Stimuli Responsive Macromolecules and Their Assemblies. *Chem. Soc. Rev.* **2013**, *42* (17), 7421. https://doi.org/10.1039/c3cs60094g.

(17) Cheng, R.; Meng, F.; Deng, C.; Klok, H.-A.; Zhong, Z. Dual and Multi-Stimuli Responsive Polymeric Nanoparticles for Programmed Site-Specific Drug Delivery. *Biomaterials* **2013**, *34* (14), 3647–3657. https://doi.org/10.1016/j.biomaterials.2013.01.084.

(18) Karimi, M.; Sahandi Zangabad, P.; Ghasemi, A.; Amiri, M.; Bahrami, M.; Malekzad, H.; Ghahramanzadeh Asl, H.; Mahdieh, Z.; Bozorgomid, M.; Ghasemi, A.; Rahmani Taji Boyuk, M. R.; Hamblin, M. R. Temperature-Responsive Smart Nanocarriers for Delivery Of Therapeutic Agents: Applications and Recent Advances. *ACS Appl. Mater. Interfaces* **2016**, *8* (33), 21107–21133. https://doi.org/10.1021/acsami.6b00371.

(19) El Jundi, A.; Buwalda, S. J.; Bakkour, Y.; Garric, X.; Nottelet, B. Double Hydrophilic Block Copolymers Self-Assemblies in Biomedical Applications. *Advances in Colloid and Interface Science* **2020**, *283*, 102213. https://doi.org/10.1016/j.cis.2020.102213.

(20) Felber, A. E.; Dufresne, M.-H.; Leroux, J.-C. pH-Sensitive Vesicles, Polymeric Micelles, and Nanospheres Prepared with Polycarboxylates. *Advanced Drug Delivery Reviews* **2012**, *64* (11), 979–992. https://doi.org/10.1016/j.addr.2011.09.006.

(21) Ge, Z.; Xie, D.; Chen, D.; Jiang, X.; Zhang, Y.; Liu, H.; Liu, S. Stimuli-Responsive Double Hydrophilic Block Copolymer Micelles with Switchable Catalytic Activity. *Macromolecules* **2007**, *40* (10), 3538–3546. https://doi.org/10.1021/ma070550i.

(22) Warnant, J.; Marcotte, N.; Reboul, J.; Layrac, G.; Aqil, A.; Jerôme, C.; Lerner, D. A.; Gérardin, C. Physicochemical Properties of pH-Controlled Polyion Complex (PIC) Micelles of Poly(Acrylic Acid)-Based Double Hydrophilic Block Copolymers and Various Polyamines. *Anal Bioanal Chem* **2012**, *403* (5), 1395–1404. https://doi.org/10.1007/s00216-012-5947-1.

(23) Zhang, X. A.; Chen, M. R.; Zhao, H.; Gao, Y.; Wei, Q.; Zhang, S.; Qin, A.; Sun, J. Z.; Tang, B. Z. A Facile Synthetic Route to Functional Poly(Phenylacetylene)s with Tunable Structures and Properties. *Macromolecules* **2011**, *44* (17), 6724–6737. https://doi.org/10.1021/ma2014657.

(24) Zhu, Z.; Pan, X.; Zhang, W.; Li, H.; Wang, W.; He, Y. Amphiphilic Block Copolymer with Diazonium Salt Pendant Groups: Synthesis, Self-Assembly and Post-Modification. *Reactive and Functional Polymers* **2022**, *179*, 105377. https://doi.org/10.1016/j.reactfunctpolym.2022.105377.

(25) Sanson, N.; Bouyer, F.; Destarac, M.; In, M.; Gérardin, C. Hybrid Polyion Complex Micelles Formed from Double Hydrophilic Block Copolymers and Multivalent Metal Ions: Size Control and Nanostructure. *Langmuir* **2012**, *28* (8), 3773–3782. https://doi.org/10.1021/la204562t.

(26) Gineste, S.; Lonetti, B.; Yon, M.; Giermanska, J.; Di Cola, E.; Sztucki, M.; Coppel, Y.; Mingotaud, A.-F.; Chapel, J.-P.; Marty, J.-D.; Mingotaud, C. Hybrid Polymeric Micelles Stabilized by Gallium Ions: Structural Investigation. *Journal of Colloid and Interface Science* **2022**, *609*, 698–706. https://doi.org/10.1016/j.jcis.2021.11.077.

(27) Layrac, G.; Destarac, M.; Gérardin, C.; Tichit, D. Highly Stable Layered Double Hydroxide Colloids: A Direct Aqueous Synthesis Route from Hybrid Polyion Complex Micelles. *Langmuir* **2014**, *30* (32), 9663–9671. https://doi.org/10.1021/la502159x.

(28) Bouyer, F.; Sanson, N.; Destarac, M.; Gérardin, C. Hydrophilic Block Copolymer-Directed Growth of Lanthanum Hydroxide Nanoparticles. *New J. Chem.* **2006**, *30* (3), 399. https://doi.org/10.1039/b516368d.

(29) Tarasov, K.; Houssein, D.; Destarac, M.; Marcotte, N.; Gérardin, C.; Tichit, D. Stable Aqueous Colloids of ZnS Quantum Dots Prepared Using Double Hydrophilic Block Copolymers. *New J. Chem.* **2013**, *37* (2), 508–514. https://doi.org/10.1039/C2NJ40738H.

(30) Antonietti, M.; Breulmann, M.; Göltner, C. G.; Cölfen, H.; Wong, K. K. W.; Walsh, D.; Mann, S. Inorganic/Organic Mesostructures with Complex Architectures: Precipitation of Calcium Phosphate in the Presence of Double-Hydrophilic Block Copolymers. *Chem. Eur. J.* **1998**, *4* (12), 2493–2500. https://doi.org/10.1002/(SICI)1521-3765(19981204)4:12<2493::AID-CHEM2493>3.0.CO;2-V.

(31) Bronstein, L. M.; Chernyshov, D. M.; Timofeeva, G. I.; Dubrovina, L. V.; Valetsky, P. M.; Obolonkova, E. S.; Khokhlov, A. R. Interaction of Polystyrene- *Block* -Poly(Ethylene Oxide) Micelles with Cationic Surfactant in Aqueous Solutions. Metal Colloid Formation in Hybrid Systems. *Langmuir* **2000**, *16* (8), 3626–3632. https://doi.org/10.1021/la991191q.

(32) Bathfield, M.; Reboul, J.; Cacciaguerra, T.; Lacroix-Desmazes, P.; Gérardin, C. Thermosensitive and Drug-Loaded Ordered Mesoporous Silica: A Direct and Effective Synthesis Using PEO- *b* -PNIPAM Block Copolymers. *Chem. Mater.* **2016**, *28* (10), 3374–3384. https://doi.org/10.1021/acs.chemmater.6b00595.

(33) Baccile, N.; Reboul, J.; Blanc, B.; Coq, B.; Lacroix-Desmazes, P.; In, M.; Gérardin, C. Ecodesign of Ordered Mesoporous Materials Obtained with Switchable Micellar Assemblies. *Angewandte Chemie* **2008**, *120* (44), 8561–8565. https://doi.org/10.1002/ange.200802431.

(34) Molina, E.; Mathonnat, M.; Richard, J.; Lacroix-Desmazes, P.; In, M.; Dieudonné, P.; Cacciaguerra, T.; Gérardin, C.; Marcotte, N. pH-Mediated Control over the Mesostructure of Ordered Mesoporous Materials Templated by Polyion Complex Micelles. *Beilstein J. Nanotechnol.* **2019**, *10*, 144–156. https://doi.org/10.3762/bjnano.10.14.

(35) Richard, J.; Phimphachanh, A.; Jamet-Fournier, A.; Cacciaguerra, T.; Dieudonné-George, P.; Cot, D.; Destarac, M.; Lacroix-Desmazes, P.; In, M.; Marcotte, N.; Gérardin, C. Dual Control of External Surface and Internal Pore Structure of Small Ordered Mesoporous Silica Particles Directed by Mixed Polyion Complex Micelles. *Microporous and Mesoporous Materials* **2022**, *338*, 111915. https://doi.org/10.1016/j.micromeso.2022.111915.

(36) Houssein, D.; Warnant, J.; Molina, E.; Cacciaguerra, T.; Gérardin, C.; Marcotte, N. Mesoporous Silica Templated by Polyion Complex Micelles: A Versatile Approach for Controlling the Mesostructure. *Microporous and Mesoporous Materials* **2017**, *239*, 244–252. https://doi.org/10.1016/j.micromeso.2016.10.013.

(37) Richard, J.; Phimphachanh, A.; Schneider, J.; Nandi, S.; Laurent, E.; Lacroix-Desmazes, P.; Trens, P.; Devautour-Vinot, S.; Marcotte, N.; Gérardin, C. Integrated Process for Structuring and Functionalizing Ordered Mesoporous Silica to Achieve Superprotonic Conductivity. *Chem. Mater.* **2022**, *34* (17), 7828–7836. https://doi.org/10.1021/acs.chemmater.2c01352.

(38) Gauthier, M. A.; Gibson, M. I.; Klok, H. Synthesis of Functional Polymers by Post-Polymerization Modification. *Angew Chem Int Ed* **2009**, *48* (1), 48–58. https://doi.org/10.1002/anie.200801951.

(39) Liu, X.; Hu, D.; Jiang, Z.; Zhuang, J.; Xu, Y.; Guo, X.; Thayumanavan, S. Multi-Stimuli-Responsive Amphiphilic Assemblies through Simple Postpolymerization Modifications. *Macromolecules* **2016**, *49* (17), 6186–6192. https://doi.org/10.1021/acs.macromol.6b01397.

(40) Zhong, Y.; Zeberl, B. J.; Wang, X.; Luo, J. Combinatorial Approaches in Post-Polymerization Modification for Rational Development of Therapeutic Delivery Systems. *Acta Biomaterialia* **2018**, *73*, 21–37. https://doi.org/10.1016/j.actbio.2018.04.010.

(41) Riemer, S.; Prévost, S.; Dzionara, M.; Gasser, U.; Gradzielski, M. Hydrophobically Modified Polyacrylates (hmPAAs) with Long Alkyl Chains – Self-Assembly in Aqueous Solution. *Polymer* **2017**, *128*, 78–86. https://doi.org/10.1016/j.polymer.2017.09.005.

(42) McCormick, C. L.; Middleton, J. C.; Cummins, D. F. Water-Soluble Copolymers. 37. Synthesis and Characterization of Responsive Hydrophobically Modified Polyelectrolytes. *Macromolecules* **1992**, *25* (4), 1201–1206. https://doi.org/10.1021/ma00030a001.

(43) Sam, S.; Touahir, L.; Salvador Andresa, J.; Allongue, P.; Chazalviel, J.-N.; Gouget-Laemmel, A. C.; Henry De Villeneuve, C.; Moraillon, A.; Ozanam, F.; Gabouze, N.; Djebbar, S. Semiquantitative Study of the EDC/NHS Activation of Acid Terminal Groups at Modified Porous Silicon Surfaces. *Langmuir* **2010**, *26* (2), 809–814. https://doi.org/10.1021/la902220a.

(44) Oh, E. J.; Park, K.; Kim, K. S.; Kim, J.; Yang, J.-A.; Kong, J.-H.; Lee, M. Y.; Hoffman, A. S.; Hahn, S. K. Target Specific and Long-Acting Delivery of Protein, Peptide, and Nucleotide Therapeutics Using Hyaluronic Acid Derivatives. *Journal of Controlled Release* **2010**, *141* (1), 2–12. https://doi.org/10.1016/j.jconrel.2009.09.010.

(45) Martin, J.; Desfoux, A.; Martinez, J.; Amblard, M.; Mehdi, A.; Vezenkov, L.; Subra, G. Bottom-up Strategies for the Synthesis of Peptide-Based Polymers. *Progress in Polymer Science* **2021**, *115*, 101377. https://doi.org/10.1016/j.progpolymsci.2021.101377.

(46) Pedone, E.; Li, X.; Koseva, N.; Alpar, O.; Brocchini, S. An Information Rich Biomedical Polymer Library. *J. Mater. Chem.* **2003**, *13* (11), 2825–2837. https://doi.org/10.1039/B306857A.

(47) Ferruti, P.; Bettelli, A.; Feré, A. High Polymers of Acrylic and Methacrylic Esters of N-Hydroxysuccinimide as Polyacrylamide and Polymethacrylamide Precursors. *Polymer* **1972**, *13* (10), 462–464. https://doi.org/10.1016/0032-3861(72)90084-5.

(48) Yuan, S.; Wang, Z.; Qiao, Z.; Wang, M.; Wang, J.; Wang, S. Improvement of CO2/N2 Separation Characteristics of Polyvinylamine by Modifying with Ethylenediamine. *Journal of Membrane Science* **2011**, *378* (1–2), 425–437. https://doi.org/10.1016/j.memsci.2011.05.023.

(49) Chethan, P. D.; Vishalakshi, B. Synthesis of Ethylenediamine Modified Chitosan and Evaluation for Removal of Divalent Metal Ions. *Carbohydrate Polymers* **2013**, *97* (2), 530–536. https://doi.org/10.1016/j.carbpol.2013.04.102.

(50) Parlar, E. D.; Özten, Ö.; Kızılaslan, A.; Can, M. Synthesis of an Ethylene Diamine Modified Tannin Polymer and Recovery of Gold(III) Ions from Electronic Wastes. *React. Chem. Eng.* **2023**, *8* (5), 1134–1151. https://doi.org/10.1039/D2RE00538G.

(51) Schelhaas, M.; Waldmann, H. Protecting Group Strategies in Organic Synthesis. *Angew. Chem. Int. Ed. Engl.* **1996**, *35* (18), 2056–2083. https://doi.org/10.1002/anie.199620561.

(52) Isidro-Llobet, A.; Álvarez, M.; Albericio, F. Amino Acid-Protecting Groups. *Chem. Rev.* **2009**, *109* (6), 2455–2504. https://doi.org/10.1021/cr800323s.

(53) Wu, X.; Hong, R.; Meng, J.; Cheng, R.; Zhu, Z.; Wu, G.; Li, Q.; Wang, C.; Chen, S. Hydrophobic Poly(*Tert* -butyl Acrylate) Photonic Crystals towards Robust Energy-Saving Performance. *Angew Chem Int Ed* **2019**, *58* (38), 13556–13564. https://doi.org/10.1002/anie.201907464.

(54) Becker, G.; Wurm, F. R. Functional Biodegradable Polymers *via* Ring-Opening Polymerization of Monomers without Protective Groups. *Chem. Soc. Rev.* **2018**, *47* (20), 7739–7782. https://doi.org/10.1039/C8CS00531A.

(55) Witecka, A.; Schmitt, J.; Courtien, M.; Gérardin, C.; Rydzek, G. Hybrid Mesoporous Silica Materials Templated with Surfactant Polyion Complex (SPIC) Micelles for pH-Triggered Drug Release. *Microporous and Mesoporous Materials* **2024**, *365*, 112913. https://doi.org/10.1016/j.micromeso.2023.112913.

(56) Warnant, J.; Reboul, J.; Aqil, A.; Cacciaguerra, T.; Jerome, C.; Gerardin, C. Nanostructured Silica Templated by Double Hydrophilic Block Copolymers with a Comb-like Architecture. *Powder Technology* **2011**, *208* (2), 461–466. https://doi.org/10.1016/j.powtec.2010.08.043.

(57) Panda, S. S.; Hall, C. D.; Oliferenko, A. A.; Katritzky, A. R. Traceless Chemical Ligation from *S* -, *O* -, and *N* -Acyl Isopeptides. *Acc. Chem. Res.* **2014**, *47* (4), 1076–1087. https://doi.org/10.1021/ar400242q.

(58) Raiford, L. Chas.; Clark, E. P. Behavior Of Mixed O-Acyl-N-Acyl Derivatives In Which The Reacting Groups Are Not On Adjacent Carbon Atoms [1]. *J. Am. Chem. Soc.* **1926**, *48* (2), 483–489. https://doi.org/10.1021/ja01413a027.

(59) Watté, J.; Van Gompel, W.; Lommens, P.; De Buysser, K.; Van Driessche, I. Titania Nanocrystal Surface Functionalization through Silane Chemistry for Low Temperature Deposition on Polymers. *ACS Appl. Mater. Interfaces* **2016**, *8* (43), 29759–29769. https://doi.org/10.1021/acsami.6b08931.

(60) Clark, J.; Perrin, D. D. Prediction of the Strengths of Organic Bases. *Q. Rev., Chem. Soc.* **1964**, *18* (3), 295. https://doi.org/10.1039/qr9641800295.

(61) Hall, H. K. Correlation of the Base Strengths of Amines [1]. *J. Am. Chem. Soc.* **1957**, *79* (20), 5441–5444. https://doi.org/10.1021/ja01577a030.

(62) Bray, C.; Peltier, R.; Kim, H.; Mastrangelo, A.; Perrier, S. Anionic Multiblock Core Cross-Linked Star Copolymers via RAFT Polymerization. *Polym. Chem.* **2017**, *8* (36), 5513–5524. https://doi.org/10.1039/C7PY01062A.

(63) Lowe, A. B.; McCormick, C. L. Reversible Addition–Fragmentation Chain Transfer (RAFT) Radical Polymerization and the Synthesis of Water-Soluble (Co)Polymers under Homogeneous Conditions in Organic and Aqueous Media. *Progress in Polymer Science* **2007**, *32* (3), 283–351. https://doi.org/10.1016/j.progpolymsci.2006.11.003.

(64) Phimphachanh, A.; Chamieh, J.; Leclercq, L.; Harrisson, S.; Destarac, M.; Lacroix-Desmazes, P.; Gérardin, C.; In, M.; Cottet, H. Characterization of Diblock Copolymers by Capillary Electrophoresis: From Electrophoretic Mobility Distribution to Distribution of Composition. *Macromolecules* **2020**, *53* (1), 334–345. https://doi.org/10.1021/acs.macromol.9b01978.

(65) Rydzek, G.; Pakdel, A.; Witecka, A.; Awang Shri, D. N.; Gaudière, F.; Nicolosi, V.; Mokarian-Tabari, P.; Schaaf, P.; Boulmedais, F.; Ariga, K. pH-Responsive Saloplastics Based on

Weak Polyelectrolytes: From Molecular Processes to Material Scale Properties. *Macromolecules* **2018**, *51* (12), 4424–4434. https://doi.org/10.1021/acs.macromol.8b00609.

(66) Dong, R.; Lindau, M.; Ober, C. K. Dissociation Behavior of Weak Polyelectrolyte Brushes on a Planar Surface. *Langmuir* **2009**, *25* (8), 4774–4779. https://doi.org/10.1021/la8039384.

(67) Crouzier, T.; Picart, C. Ion Pairing and Hydration in Polyelectrolyte Multilayer Films Containing Polysaccharides. *Biomacromolecules* **2009**, *10* (2), 433–442. https://doi.org/10.1021/bm8012378.

(68) Krężel, A.; Bal, W. A Formula for Correlating p K a Values Determined in D 2 O and H 2 O. *Journal of Inorganic Biochemistry* **2004**, *98* (1), 161–166. https://doi.org/10.1016/j.jinorgbio.2003.10.001.

(69) Dewhurst, C. D. Graphical Reduction and Analysis Small-Angle Neutron Scattering Program: *GRASP*. *J Appl Crystallogr* **2023**, *56* (5), 1595–1609. https://doi.org/10.1107/S1600576723007379.

(70) Arnold, O.; Bilheux, J. C.; Borreguero, J. M.; Buts, A.; Campbell, S. I.; Chapon, L.; Doucet, M.; Draper, N.; Leal, R. F.; Gigg, M. A.; Lynch, V. E.; Markvardsen, A.; Mikkelson, D. J.; Mikkelson, R. L.; Miller, R.; Palmen, K.; Parker, P.; Passos, G.; Perring, T. G.; Peterson, P. F.; Ren, S.; Reuter, M. A.; Savici, A. T.; Taylor, J. W.; Taylor, R. J.; Tolchenov, R.; Zhou, W.; Zikovsky, J. Mantid - Data Analysis and Visualization Package for Neutron Scattering and $μSR$ Experiments. **2014**. https://doi.org/10.48550/ARXIV.1407.5860.

(71) Heenan, R. K.; Rogers, S. E.; Turner, D.; Terry, A. E.; Treadgold, J.; King, S. M. Small Angle Neutron Scattering Using Sans2d. *Neutron News* **2011**, *22* (2), 19–21. https://doi.org/10.1080/10448632.2011.569531.

(72) Mildner, D. F. R.; Carpenter, J. M. Optimization of the Experimental Resolution for Small-Angle Scattering. *J Appl Crystallogr* **1984**, *17* (4), 249–256. https://doi.org/10.1107/S0021889884011468.

(73) Pedersen, J. S.; Gerstenberg, M. C. Scattering Form Factor of Block Copolymer Micelles. *Macromolecules* **1996**, *29* (4), 1363–1365. https://doi.org/10.1021/ma9512115.

(74) Mathonnat, M. Le Rôle de l'eau Dans La Structuration Des Silices Mésoporeuses Par Des Complexes Électrostatiques, 2017.

(75) Manet, S.; Lecchi, A.; Impéror-Clerc, M.; Zholobenko, V.; Durand, D.; Oliveira, C. L. P.; Pedersen, J. S.; Grillo, I.; Meneau, F.; Rochas, C. Structure of Micelles of a Nonionic Block Copolymer Determined by SANS and SAXS. *J. Phys. Chem. B* **2011**, *115* (39), 11318–11329. https://doi.org/10.1021/jp200212g.

(76) Pedersen, J. S. Form Factors of Block Copolymer Micelles with Spherical, Ellipsoidal and Cylindrical Cores. *J Appl Crystallogr* **2000**, *33* (3), 637–640. https://doi.org/10.1107/S0021889899012248.

(77) Pedersen, J. S. Structure Factors Effects in Small-Angle Scattering from Block Copolymer Micelles and Star Polymers. *The Journal of Chemical Physics* **2001**, *114* (6), 2839–2846. https://doi.org/10.1063/1.1339221.

(78) Kinning, D. J.; Thomas, E. L. Hard-Sphere Interactions between Spherical Domains in Diblock Copolymers. *Macromolecules* **1984**, *17* (9), 1712–1718. https://doi.org/10.1021/ma00139a013.

(79) Manet, S.; Schmitt, J.; Impéror-Clerc, M.; Zholobenko, V.; Durand, D.; Oliveira, C. L. P.; Pedersen, J. S.; Gervais, C.; Baccile, N.; Babonneau, F.; Grillo, I.; Meneau, F.; Rochas, C. Kinetics of the Formation of 2D-Hexagonal Silica Nanostructured Materials by Nonionic Block Copolymer Templating in Solution. *J. Phys. Chem. B* **2011**, *115* (39), 11330–11344. https://doi.org/10.1021/jp200213k.

(80) Guinier, A.; Fournet, G.; Walker, C. B.; Vineyard, G. H. *Small-Angle Scattering of X-Rays*. *Physics Today* **1956**, *9* (8), 38–39. https://doi.org/10.1063/1.3060069.

(81) Hammouda, B. SANS from Homogeneous Polymer Mixtures: A Unified Overview. In *Polymer Characteristics*; Advances in Polymer Science; Springer-Verlag: Berlin/Heidelberg, 1993; Vol. 106, pp 87–133. https://doi.org/10.1007/BFb0025862.

(82) Schweins, R.; Hollmann, J.; Huber, K. Dilute Solution Behaviour of Sodium Polyacrylate Chains in Aqueous NaCl Solutions. *Polymer* **2003**, *44* (23), 7131–7141. https://doi.org/10.1016/j.polymer.2003.07.005.

(83) Burchard, W. Static and Dynamic Light Scattering from Branched Polymers and Biopolymers. In *Light Scattering from Polymers*; Advances in Polymer Science; Springer Berlin Heidelberg: Berlin, Heidelberg, 1983; Vol. 48, pp 1–124. https://doi.org/10.1007/3-540-12030-0_1.

(84) Schweins, R.; Lindner, P.; Huber, K. Calcium Induced Shrinking of NaPA Chains: A SANS Investigation of Single Chain Behavior. *Macromolecules* **2003**, *36* (25), 9564–9573. https://doi.org/10.1021/ma0347722.

(85) Tshepelevitsh, S.; Kütt, A.; Lõkov, M.; Kaljurand, I.; Saame, J.; Heering, A.; Plieger, P. G.; Vianello, R.; Leito, I. On the Basicity of Organic Bases in Different Media. *Eur J Org Chem* **2019**, *2019* (40), 6735–6748. https://doi.org/10.1002/ejoc.201900956.

(86) Tan, W. L.; Tang, L.; Matsidik, R.; Bryant, G.; Martin, T. B.; Sommer, M.; Huang, D. M.; McNeill, C. R. Small-Angle Neutron Scattering of P(NDI2OD-T2) Solutions: Importance of Network Structure for Data Interpretation and Film Morphology. *Macromolecules* **2024**, *57* (2), 691–706. https://doi.org/10.1021/acs.macromol.3c01435.

(87) Schwiertz, D.; Angelina, J.; Zhang, H.; Barz, M. Miktoarm Star-Polypept(o)Ide-Based Polyion Complex Micelles for the Delivery of Large Nucleic Acids. *Biomacromolecules* **2024**, acs.biomac.4c00695. https://doi.org/10.1021/acs.biomac.4c00695.

(88) Tonegawa, A.; Tamura, A.; Zhang, S.; Yui, N. Hydrophobicity of Acyl Groups in α-Cyclodextrin-Threaded Polyrotaxanes Dominates the Formation and Stability of Self-Assembled Nanoparticles. *Polymer* **2020**, *200*, 122537. https://doi.org/10.1016/j.polymer.2020.122537.

(89) Bader, R. A.; Silvers, A. L.; Zhang, N. Polysialic Acid-Based Micelles for Encapsulation of Hydrophobic Drugs. *Biomacromolecules* **2011**, *12* (2), 314–320. https://doi.org/10.1021/bm1008603.

(90) Améndola, I. F.; Velasco, M. I.; Acosta, R. H.; Soler Illia, G. J. A. A.; Contreras, C. B. Smart Hybrid Copolymer-Coated Silica Nanosystems with Dual Responsiveness as a Carrier for Positive Charged Molecules. *European Polymer Journal* **2024**, *204*, 112717. https://doi.org/10.1016/j.eurpolymj.2023.112717.

(91) Molina, E.; Warnant, J.; Mathonnat, M.; Bathfield, M.; In, M.; Laurencin, D.; Jérôme, C.; Lacroix-Desmazes, P.; Marcotte, N.; Gérardin, C. Drug–Polymer Electrostatic Complexes as New Structuring Agents for the Formation of Drug-Loaded Ordered Mesoporous Silica. *Langmuir* **2015**, *31* (47), 12839–12844. https://doi.org/10.1021/acs.langmuir.5b03221.

(92) Yang, Y.; Qi, P.; Ding, Y.; Maitz, M. F.; Yang, Z.; Tu, Q.; Xiong, K.; Leng, Y.; Huang, N. A Biocompatible and Functional Adhesive Amine-Rich Coating Based on Dopamine Polymerization. *J. Mater. Chem. B* **2015**, *3* (1), 72–81. https://doi.org/10.1039/C4TB01236D.

(93) Elhalwagy, M. E.; Elsherbiny, A. S.; Gemeay, A. H. Amine-Rich Polymers for Water Purification Applications. *Materials Today Chemistry* **2023**, *27*, 101344. https://doi.org/10.1016/j.mtchem.2022.101344.

(94) Darabi, A.; Jessop, P. G.; Cunningham, M. F. CO_2 -Responsive Polymeric Materials: Synthesis, Self-Assembly, and Functional Applications. *Chem. Soc. Rev.* **2016**, *45* (15), 4391–4436. https://doi.org/10.1039/C5CS00873E.

CHAPTER 2

Design of primary amine-based double-hydrophilic block copolymer: from their synthesis to the formation of polyion complex micelles by electrostatic complexation with polyacids

Ananthapadmanabhan Unnikrishnan,[1,2] Lynn Obeid,[1] Amna Korbi,[2] Gaulthier Rydzek,[2] Julien Schmitt,[2,3] Ralf Schweins[1] and Corine Gérardin[2]

[1] Institut Laue − Langevin, DS / LSS Group, 71 Avenue des Martyrs, CS 20156, Grenoble Cedex 9, F-38042, France

[2] Institut Charles Gerhardt, UMR 5253, CNRS-ENSCM-UM, University of Montpellier, Cedex, F-34295, France

[3] LSFC – Laboratoire de Synthèse et Fonctionnalisation des Céramiques, UMR 3080 CNRS/Saint-Gobain CREE, Saint-Gobain Research Provence, 550 Avenue Alphonse Jauffret, Cavaillon, France

2.1. INTRODUCTION

Ordered mesoporous materials are a group of materials that exhibits well-defined and organised porous structures, with pore diameters ranging between 2 – 50 nm and a high surface area that makes them highly compatible for applications including catalysis,[1,2] adsorption,[3–5] storage[6,7] and drug delivery.[8–10] Among the substantial collection of mesoporous materials available, silica-based structures are particularly studied due to their fine tunability, chemical strength, high surface area and chemical stability.[11–14] In order to tailor the mesoporous silica materials to their application, they are often functionalized with active sites, resulting in organic-inorganic hybrids.[15–17] The functionalization is traditionally carried out using two different approaches, both involving organo-substituted trialkoxysilanes: a) post-synthesis grafting or b) co-condensation synthesis.[18–20] While these methodologies provide significant benefits, they also present certain disadvantages, that need to be carefully considered. Through post-synthesis grafting, materials with a good control over morphology, pore size, distribution, shape and orientation can be ensured, however, applications are limited due to its inability to build materials with homogenous distribution of active groups.[20,21] Unlike the former, the latter technique, co-condensation synthesis, can fabricate functionalized materials exhibiting a homogenous distribution of active sites, on both the inner and outer surface of the materials, but it requires careful and precise synthesis protocol to gain control over the material morphology, making this route challenging.[22,23] A suitable alternative lies in the structuring agent assisted synthesis and functionalization, which allows a direct and homogenous functionalization of the porous materials with a good control of the sample morphology.[24–28] In this route, the silica is initially allowed to condense over the carefully selected structuring agent, that comprises the desired functions. After silica condensation, the structuring

agent is partially removed, leaving the function moiety in the sample. The functionalized materials of desired pore size, shape and orientation is thus obtained.[29–31]

Among the various types of structuring agents used to form mesoporous materials, those based on block copolymers allow, by finely tuning the mass fraction of each block and altering their chemical nature, adjusting the pore size and architecture in the materials.[32–34] Double hydrophilic block copolymers (DHBC) are a specialised category of block copolymers comprising two separate hydrophilic blocks in the polymer backbone that generally lacks the ability to self-assemble spontaneously in aqueous medium. However, modifying DHBCs using external or internal *stimuli* such as pH, temperature and solvent can trigger micellization, generally due to the difference in hydrophilicity introduced.[35–38] DHBCs, comprising a neutral block along with a charged block, are extensively used as functionalized structuring agents for mesoporous silica material synthesis.[11,39–41] These DHBCs can form well-defined structures called PolyIon Complex (PIC) micelles[42–44] in presence of a micellization partner (polyelectrolyte), through electrostatic complexation between the charged block of the DHBC and the opposite charges of the micellization partner, while the neutral block interacts with silica through hydrogen bonding. pH influences the net charge of both DHBC and micellization partner, which allows controlling the micellization of the system.[45] Thanks to this pH sensitivity, after material synthesis, a pH change allows for the elution of the micellization partner, freeing the porosity, while the DHBC remains trapped at the pore surface, imparting them functionality from the charged block. Functionalities such as carboxyl group (-COOH),[24,33,40] and sulfonic group ($-SO_3H$)[39] were successfully grafted to mesoporous silica by this approach. While carboxyl group is often used in drug delivery,[46,47] and adsorption[48,49], sulfonic group has applications in catalysis[50,51] and proton conductivity[52,53] when

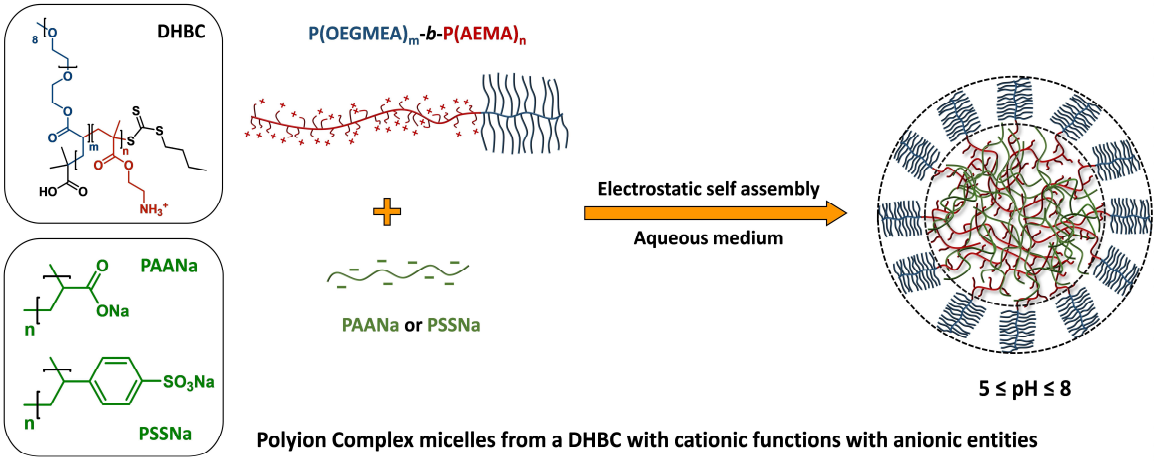
incorporated into the materials, demonstrating the wide range of fields where functionalized porous systems find application.

Owing to its extensive applicability, mesoporous materials exhibiting amines directly crafted from structuring agents would be a perfect addition to this long-standing group of functionalized ordered porous materials. Amine functionalized porous materials are well suited for CO_2 capture,[54–56] which with the rise of climate change is a crucial application, along with many alternative purposes including catalysis,[57,58] water treatment,[59,60] separation[61] and drug delivery,[9,62]. Consequently, developing new DHBCs that could build structuring agents with amine functions has become a top priority.

Even though several cationic DHBCs with secondary and quaternary amines have been previously reported,[36,63,64] a simple methodology developing intrinsically primary amine-rich cationic DHBCs is still lacking. Primary amine shows a higher nucleophilicity and is sterically less hindered than its counterparts (secondary, tertiary and quaternary amines), which can have significant applications in separation and adsorption when incorporated into materials.[65,66] The few primary amine rich DHBCs devised find application in biological projects,[67,68] and their use as structuring agents for directly developing amine rich porous materials is scarcely investigated.

Reported in this study is the synthesis and self-assembling character of a new double hydrophilic block copolymer (DHBC), namely P(OEGMEA)$_m$-*b*-P(AEMA)$_n$, made of a neutral poly(oligo(ethylene glycol) methyl ether acrylate) P(OEGMEA) block and a charged poly(aminoethyl methacrylate) P(AEMA) block via Reversible Addition Fragmentation Chain Transfer (RAFT) polymerization. The inherent amine functionalities give positive charges to the P(AEMA) block of the copolymer, a distinguished attribute among the DHBCs used till date as combined structuring and functionalization agents. The positive charges enable the copolymer to

complex electrostatically with negatively charged polyelectrolytes such as poly(acrylic acid) sodium salt and poly(styrene sulphonate) sodium salt of varying molecular weight in aqueous medium at controlled pH (see **Scheme 1**). The copolymer synthesized was initially characterized using Size Exclusion Chromatography with Multi-Angle Laser Light Scattering (SEC-MALLS) to estimate the molecular weight and polydispersity index of the macromolecule. Further, characterization using ^{1}H NMR and elemental analysis were used to obtain the degree of polymerization of each block. The pH sensitive nature of the self-assembly was studied using Static and Dynamic Light Scattering (SLS/DLS) along with Small Angle Neutron Scattering (SANS), allowing the characterization of the structure formed in aqueous suspensions ranging from alkaline to acidic conditions. Along with pH, the effect of concentration, micellization partner used and length of the copolymer chain in the shape and size of the micelles were also investigated. The new DHBC developed is a big leap and holds key potential for introducing a high fraction of amine functionalities into mesoporous materials via a one-pot synthesis, something which has been missing until now.



Scheme 1. *Schematic representation of Polyion complex (PIC) micelle formation using a cationic double hydrophilic block copolymer (DHBC, P(OEGMEA)$_m$-b-P(AEMA)$_n$) with oppositely charged micellization partner.*

2.2. MATERIALS AND METHODS

2.2.1. Chemicals Used

Oligo(ethylene glycol) methyl ether acrylate (OEGMEA, 99%, M_n = 480 g/mol, 9 EO units on average) and 2-Aminoethyl methacrylate hydrochloride (AEMA, 90%, M_n = 165.62 g/mol) were secured from Sigma-Aldrich. AEMA was dissolved in water before being used for polymerization. Radical inhibitors were removed from the reagents before synthesis by adsorption with alumina particles (Sigma-Aldrich) to prepare them for polymerization. The initiator, 4, 4′-azobis(4-cyano pentanoic acid) (ACPA, 98%) was also purchased from Sigma-Aldrich while the chain transfer agent, 2-(butylthiocarbonothioylthio)-2-methylpropanoic acid (BDMAT), was synthesized in accordance with already reported protocols.[69,70] Negatively charged polyelectrolytes used for micellization include i) poly(acrylic acid) sodium salts (5.1 kDa and 2.1 kDa) from Sigma-Aldrich and ii) poly(styrene sulphonate) sodium salt (1.1 kDa) from Polymer Standards Service GmBH (now a part of Agilent). Chemical synthesis and analytical preparation of samples were carried out using Milli-Q water with a resistivity of 18.2 MΩ·cm at 25 °C. NaOH (1M) and HCl (1M) solutions were used for the pH alteration of samples when necessary. D_2O purchased from Sigma-Aldrich was used as solvent for small angle neutron scattering and NMR experiments.

2.2.2. Synthesis of P(OEGMEA)-*b*-P(AEMA)

Double hydrophilic block copolymers (DHBC) labelled P(OEGMEA)-*b*-P(AEMA), comprising a positively charged poly(aminoethyl methacrylate) P(AEMA) block and a neutral comb block of poly(oligo(ethylene glycol) methyl ether acrylate) P(OEGMEA) were synthesized using reversible addition-fragmentation chain-transfer polymerization (RAFT), in aqueous medium. Two polymers (Pol. 1 and Pol. 2) were made with the following targets for each block:

1) $P(OEGMEA)_{21}$-*b*-$P(AEMA)_{40}$ and 2) $P(OEGMEA)_{21}$-*b*-$P(AEMA)_{20}$ (see **Table 1**). Depicted below is the synthesis route for the first polymer (30 wt% polymeric solution): In a round bottom flask of 250 mL, chain transfer agent BDMAT (0.171 g, 7.0×10^{-4} mol), radical initiator ACPA (0.019 g, 7.0×10^{-5} mol), monomer OEGMEA (6.68 g, 1.4×10^{-2} mol) and 16.0 mL of Milli-Q water were added. The reaction medium was stirred at *ca.* 250 rpm, flushed with nitrogen for 30 minutes and heated at 80 °C for 4.5 hours in order to synthesize the initial P(OEGMEA) block. As for the second block, ACPA (0.018 g, 6.0×10^{-5} mol), AEMA (4.83 g, 2.6×10^{-2} mol) and 11.0 mL of Milli-Q water were added to the initial mixture. The reaction medium was then degassed again with nitrogen for 30 minutes followed by heating at 80 °C under stirring for another 4.5 hours. After the synthesis of each block of the DHBC, 1 mL of samples were collected for ^{1}H NMR and elemental analysis. The molecular weight and polydispersity index of the DHBC were obtained using Size Exclusion Chromatography with Multi-Angle Laser Light Scattering (SEC-MALLS), the degree of polymerization (DP) of each block was determined from ^{1}H-NMR and the results obtained were confirmed using Elemental Analysis. DP obtained by both methods are given in **Table 1** and the methods for obtaining them is detailed in the later section.

Sample name	Target block copolymer	Results according to NMR	Results according to NMR + EA
Pol. 1	$P(OEGMEA)_{21}$-*b*-$P(AEMA)_{40}$	$P(OEGMEA)_{21}$-*b*-$P(AEMA)_{23}$	$P(OEGMEA)_{21}$-*b*-$P(AEMA)_{32}$
Pol. 2	$P(OEGMEA)_{21}$-*b*-$P(AEMA)_{20}$	$P(OEGMEA)_{25}$-*b*-$P(AEMA)_{17}$	$P(OEGMEA)_{25}$-*b*-$P(AEMA)_{22}$

Table 1. *Targeted degree of polymerization of each block in the DHBCs, along with the results obtained from NMR alone, and by combining NMR with elemental analysis.*

2.2.3. Sample Preparation

Sample preparation was carried out at room temperature. Even though all the samples were prepared in D_2O, depending upon the characterization technique, namely light and neutron scattering, the concentration of the final sample varied. In light scattering the concentration of the

sample used was 0.1 wt% with respect to the P(OEGMEA)-*b*-P(AEMA) copolymer, while in neutron scattering the typical concentration used was 1 wt%, unless stated otherwise. Four different systems, depending on the DHBC and micellization partner used, were studied Agg. 1 - 4 (see **Table 2**). Let us note that the degree of polymerization (DP) given in **Table 1** of the two DHBCs used are the ones obtained after analysis of the NMR and elemental analysis data and not the targets (see *Results* section).

The initial studies on the micelles were performed on Agg. 1, made by $P(OEGMEA)_{21}$-*b*-$P(AEMA)_{32}$ and PAA 5.1 kDa, at the optimal condition of pH = 5 and charge ratio acid/NH_2 = ca. 1.1. The charge ratio is the ratio between the acid (acrylates for Agg. 1) and amine species in the polyelectrolyte and P(OEGMEA)-*b*-P(AEMA) respectively. Agg. 1 was also used to investigate the influence of pH (3 - 8) in SLS/DLS and SANS. Finally, the four different systems (Agg. 1 - 4) were studied at pH = 5 and various concentration (1 – 5 wt%) in SANS. While, pH controls the micelle formation and dissociation, concentration could play a significant role in the shape and size of the species made. The comparison between the four systems allowed probing the influence of the polymer chain length and chemical composition on the characteristics of the micelles formed. It is important to note that depending on the micellization partner and copolymer used, the optimal charge ratio acid/NH_2 varies. For poly(acrylic acid) PAA polyelectrolyte based micelles, the ratio was ca. 1.1, while in poly(styrene sulfonate) PSS based system it is ca. 0.7.

A typical sample preparation has been detailed here for Agg. 1 at optimal conditions (pH = 5 and acid/NH_2 = ca. 1.1): Initially, stock solutions of $P(OEGMEA)_{21}$-*b*-$P(AEMA)_{32}$ and PAA 5.1 kDa were prepared in D_2O. In light scattering the stock solutions prepared were at 1 and 5 wt% for PAA 5.1 kDa and $P(OEGMEA)_{21}$-*b*-$P(AEMA)_{32}$ respectively, while in neutron scattering 2 and 15 wt% solutions were used. Next, to a small vial containing $P(OEGMEA)_{21}$-*b*-$P(AEMA)_{32}$

solution, PAA 5.1 kDa was added dropwise with stirring until the optimum charge ratio is reached. The overall solution was then diluted to the required final concentration using the solvent. Finally, the pH of the solution made was adjusted to pH = 5.5 and was stirred overnight before characterization. In general, the pH of the all the solutions prepared in this experiment was adjusted when required, using either HCl or NaOH solutions at 1 M.

Sample name	Block copolymer used	Block copolymer (results according to NMR + EA)	Polyelectrolyte, molecular weight (kDa)	acid/NH_2 ratio used
Agg. 1	Pol. 1	$P(OEGMEA)_{21}$-*b*-$P(AEMA)_{32}$	PAA, 5.1	1.0
Agg. 2	Pol. 1	$P(OEGMEA)_{21}$-*b*-$P(AEMA)_{32}$	PSS, 1.1	0.7
Agg. 3	Pol. 1	$P(OEGMEA)_{21}$-*b*-$P(AEMA)_{32}$	PAA, 2.1	1.1
Agg. 4	Pol. 2	$P(OEGMEA)_{25}$-*b*-$P(AEMA)_{22}$	PAA, 2.1	1.2

Table 2. *Agg. 1 - 4 sample composition with the corresponding acid/NH_2 ratio used*

2.2.4. Characterization Techniques

2.2.4.1. Size Exclusion Chromatography (SEC) Coupled with Multi-Angle Laser Light Scattering (MALLS) Detection

The SEC/MALLS experiments were performed on a Shimadzu Nexera GPC System (Shimadzu, Tokyo, Japan) equipped with a SHODEX SB-G column guard (50 × 6.0 mm, 10 µm) and SHODEX SB-G column (300 × 8.0 mm, 6 µm) (SHODEX, Germany) thermostatically controlled at 30 °C in association with a UV detector Shimadzu SPD-40A (Shimadzu, Tokyo, Japan), a Dawn 8-angle laser light scattering detector having a 658 nm laser and an Optilab refractometer (Wyatt Technology Corp., Santa Barbara, USA). All detectors are thermostated at 30 °C. The polymer samples (100 µL injection volume at a concentration of 5 gL^{-1}) were eluted with phosphate buffer at a 1.0 $mL.min^{-1}$ flowrate. Phosphate buffer was prepared with Milli-Q grade water with 200 mM

sodium nitrate, 10 mM sodium phosphate and 200 ppm sodium azide at pH = 7 filtered through a 0.1 μm membrane filter. The *dn*/*dc* values used were calculated directly in the analysis software or were determined in the phosphate buffer at various polymer concentrations (from 0.2 to 2.0 gL^{-1}) using the Optilab refractometer (Wyatt Technology Corp., Santa Barbara, USA). The data were analyzed using the Astra software (v8.0.2.5, from Wyatt Technology Corp).

2.2.4.2. NMR Spectroscopy

A Bruker Advance III 600 MHz NMR spectrometer was used for collecting the ^1H solution NMR spectra of the polymer samples in D_2O. Samples collected after the synthesis of each block were dried in an oven at 50°C overnight and about 10 mg were dissolved in 1 mL D_2O for the characterization. Topspin 4.1.4 was used for the analysis of spectra obtained and chemical shifts δ in the figures are presented in ppm, with Tetramethylsilane (TMS) as the reference.

2.2.4.3. Elemental Analysis

Through Elemental Analysis, using a ThermoFisher Scientific spectrometer iCE 3000, the weight percentages in C, H, N, S of the samples were obtained (approximately 50 mg of samples were used for the measurement). The samples were dialysed before characterization using Milli-Q water for 3 days (involving six water exchanges) with a dialysis bag of a molecular weight cut off of 3.5 kDa to remove impurities (Carl Roth), and followed by freeze-drying.

2.2.4.4. Light Scattering

Polymer suspensions at 0.1 wt% in D_2O, stirred overnight and filtered using 0.45 μm PTFE membrane-based Millipore filters (0.22 μm PTFE filters were used for the respective buffer solutions) were characterized by light scattering using an ALV CGS3 goniometer with an ALV 5004 correlator (ALV GmbH, Langen, Germany). Multiple tau digital correlator in the instrument

allow measuring simultaneously static and dynamic light scattering. Further, the equipment also has a maximum output power of 23 mW and is endowed with a Helium-Neon laser, operating at a wavelength λ of 632.8 nm. The samples were analyzed at 22.5 ± 1 °C and at an angular range between 30° and 150°.

2.2.4.4.1. Static Light Scattering

Radii of gyration R_G and weight-averaged molecular weights M_w of the scattering objects could be extracted from static light scattering experiments following Zimm's approximation:

$$\frac{Kc}{\Delta R_\theta} = \frac{1}{M_w} + \frac{1}{3M_w} R_G^2 q^2 \qquad (1)$$

$$q = \frac{4\pi n}{\lambda_0} sin\frac{\theta}{2} \qquad (2)$$

$$K = \frac{4\pi^2}{\lambda_0^4 N_A}\left(n\frac{dn}{dc}\right)^2 \qquad (3)$$

where q is the scattering vector varying with scattering angle θ, while c and K are the concentration of the polymeric species and optical constant respectively. Also, the laser wavelength in vacuum, Avogadro's number, the refractive index of the solvent and the refractive index increment of the self-assembled structures are given as λ_0, N_A, n and $\frac{dn}{dc}$ (0.1 mLg^{-1}) respectively.

The Rayleigh ratio (ΔR_θ) could be derived using equation (4), upon experimentally finding the time-averaged scattering intensity <I> as a function of scattering vector q.

$$\Delta R_\theta = \frac{\langle I_{solution}\rangle - \langle I_{solvent}\rangle}{\langle I_{standard}\rangle}\left(\frac{n_{solvent}}{n_{standard}}\right)^2 RR_{standard} \qquad (4)$$

where the time-averaged scattering intensity of the solution, solvent and standard are expressed as $\langle I_{solution} \rangle$, $\langle I_{solvent} \rangle$ and $\langle I_{standard} \rangle$ respectively, while $n_{solvent}$ and $n_{standard}$ are the refractive index of the solvent and the toluene standard. $RR_{standard}$ (1.369×10^{-5} cm^{-1}) is the Rayleigh ratio of the toluene standard for a laser wavelength $\lambda = 632.8$ nm at 22.5 ± 1 °C.

2.2.4.4.2. Dynamic Light Scattering

Using dynamic light scattering (DLS), the scattering intensity as a function of time at a specific scattering vector q was determined. The intensity-time autocorrelation function, $g_2(q,\tau)$ as a function of time shift τ, could be derived from it and is related to the electric field-time autocorrelation function $g_1(q,\tau)$ through Siegert's equation, as depicted below:

$$g_2(q,\tau) = \frac{\langle I\,(q,t) I(q,t+\tau)\rangle}{\langle I\,(q,t)\rangle^2} = 1 + |g_1(q,\tau)|^2 \qquad (5)$$

where $I(q,t)$ and $I(q,t+\tau)$ stand for the scattering intensity at time t and $t + \tau$ respectively, while the temporal averaging over all the time t is represented by <>.

The electric field autocorrelation function $g_1(q,\tau)$ is connected to the translational diffusion coefficient D_t and could be extracted using the CONTIN method, developed by Provencher,[71,72] based on Laplace inverse. CONTIN is ideal for complex systems which are non-monodisperse:

$$g_1(q,\tau) = \int_0^\infty G(D_t).\, e^{-D_t.\tau/q^2}\, dD_t \qquad (6)$$

where $G(D_t)$ is the resulting distribution function of D_t.

The cumulant analysis, that studies the deviation of the electric field-time autocorrelation function from a mono-exponential by describing the logarithm of $g_1(q,\tau)$ at fixed q as a power series in τ,

could also be used to derive the mean translational diffusion coefficient $\overline{D}_t$ for simpler systems, with a quasi-monomodal distribution of population:

$$ln\big(g_1(q,\tau)\big) = \Gamma_0 - \Gamma_1.\tau + \frac{\Gamma_2}{2!}.\tau^2 - \frac{\Gamma_3}{3!}.\tau^3 \qquad (7)$$

where Γ_0, Γ_1, Γ_2 and Γ_3 are the cumulants. In cumulant analysis, the z-averaged translational diffusion coefficient $\overline{D}_t$ could be extracted through the relation using the first cumulant, $\Gamma_1 = \overline{D}_t q^2$, while the ratio $PDI = \frac{\Gamma_2}{\Gamma_1^2}$ gives the polydispersity index of the system.

To obtain the translational diffusion coefficient extrapolated at zero-angle D_0, independent of the scattering vector, the samples have to be studied at different angles θ. D_0 for the dilute solutions can be obtained using the linear approximation shown below (where C is a dimensionless constant depending on polydispersity and particle shape, adopting values between 0 and 0.33):[73]

$$\overline{D}_t = D_0\big(1 + C.R_g^2.q^2\big) \qquad (8)$$

D_0 can then be obtained as the intercept of the $\overline{D}_t(q^2)$ plot. In case where no angular dependency of $\overline{D}_t$ is observed, D_0 is collected via averaging $\overline{D}_t$ over the different scattering vectors.

Finally, using Stokes-Einstein relationship, the hydrodynamic radius R_H could be obtained from the D_0 value (as shown below).

$$R_H = \frac{k_B T}{6\pi\eta}\frac{1}{D_0} \qquad (9)$$

where k_B, T, η are Boltzmann constant, temperature and solvent viscosity respectively.

Additionally, $\frac{R_G}{R_H}$ ratio, indicating the particle shape, could also be determined by combining static and dynamic light scattering. $\frac{R_G}{R_H}$ ratio of ca. 0.78 indicate homogeneous spherical species and a deviation from these numerical value point at a distortion in shape.[74–76]

2.2.4.5. Small Angle Neutron Scattering (SANS)

The samples for small angle neutron scattering (SANS) were studied in 2 mm quartz cuvettes with D_2O as solvent. D_2O alone was measured for solvent subtraction. The effect of concentration was investigated using 1 to 5 wt.% solutions at pH = 5, while the effect of the pH was investigated using 1 wt% solutions at various pH (3 - 8). A H_2O calibrated pH meter was used for the measurement of pH in all samples. Using the formula pD = 0.929 × pH* + 0.42, where pH* is the reading given in a H_2O-calibrated pH meter, the pH of the colloidal solution in D_2O (pD) could be estimated.[77] No filtration was carried out before the measurement of samples by SANS.

All the SANS measurements were carried out using the D22 small angle scattering instrument at Institut Laue-Langevin (ILL), Grenoble, France. A circular neutron beam with a diameter of 13 mm was used. D22 has two distinct detectors, a fixed front detector and a rear detector, with a sample-to-detector distance of 1.4 m and 17.6 m respectively (with a collimation distance of 17.6 m), that, associated to a wavelength of the neutron beam λ=6 Å ($\Delta\lambda/\lambda$ = 0.1), allows the access to a wide q-range: 0.002 - 0.639 $Å^{-1}$. Both detectors are made of Reuter−Stokes tubes; the front and rear detectors feature 96 and 128 tubes respectively (each tube diameter is 8 mm, giving a pixel size of 8 mm × 8 mm). The two-dimensional multi detector data thus obtained were corrected for direct beam transmission, empty cell scattering, background scattering and detector efficiencies using the GRASP software.[78] The corrected signal was then finally scaled to absolute intensity and azimuthally-averaged prior to the subtraction of incoherent scattering from the result. Finally,

SANS data are systematically stitched with the static light scattering (SLS) derived Rayleigh ratio R_θ, to further extend the q range to the lowest possible values (from ca. 0.003 $Å^{-1}$ to 0.0007 $Å^{-1}$).

2.2.4.5.1. SANS Model

The SANS data were fitted by summing the contribution from micelles with a contribution from unmicellized, molecularly dispersed DHBC in solution:

$$I(q) = I_{micelles}(q) + I_{DHBC}(q) \qquad (10)$$

The contribution from spherical micelles, of radius *R*, can be written as follows:[79]

$$I_{micelles}(q) = AP_{sp}\ (q) \qquad (11)$$

with *A* the scale factor, and $P_{sph}(q)$ the form factor of the spheres.

The scale factor *A* depends on the number of objects per unit volume *n*, the contrast between the micelles and the solvent $\Delta\rho = \rho_{mic} - \rho_0$ and the volume of the micelles $V = \frac{4}{3}\pi R^3$:

$$A = n\Delta\rho^2 V^2 \qquad (12)$$

In our case, with only one contrast, we cannot extract both *n* and $\Delta\rho$, hence the scale factor was not studied further. To obtain details about the contrast associated with the micelle, finding its matching point with the solvent is key. Since, contrast variation studies were not carried out, this information is currently lacking.

The form factor of the sphere $P_{sph}(q) = P_{sph}(q, R, \sigma) = \langle F^2(q) \rangle$ depends on the radius of the sphere *R* and the polydispersity in size σ. $F(q)$ is the form factor amplitude and $\langle\rangle$ is the size distribution averaging depending on the polydispersity index σ. The form factor amplitude $F(q)$ is written as:

$$F(q) = \frac{3(\sin(qR) - (qR)\cos(qR))}{(qR)^3} \qquad (13)$$

In certain cases, the micelles are not spherical but elongated. Those data are fitted using a model of non-interacting cylinders,[80] in that case $I_{micelles}(q) = AP_{cyl}(q)$, with A the scale factor described in equation 12.

For rigid cylinders of cross-section radius R and length L and polydispersity over the cross-section σ, with $L \geq 5R$, $P_{cyl}(q)$ can be written as follows:[80,81]

$$P_{cyl}(q) = F_{cyl}^2(q) = < F_{CS}^2(q) > P_{rod}(q) \qquad (14)$$

with $F_{CS}(q, R) = \frac{2J_1(qR)}{qR}$ the form factor amplitude of the circular cross-section, depending on the Bessel function J_1, and $P_{rod}(q) = \frac{\pi L}{q}$ the form factor of an infinitely thin rod. <> stands again for the cross-section radius size distribution depending on the polydispersity index σ, while the polydispersity in length is neglected.

The intensity from the remaining DHBC can be written as follows:

$$I_{DHBC}(q) = A' P_{pol}(q, R_g, m) \qquad (15)$$

with P_{pol} the form factor of a polymer chain with excluded volume, with a radius of gyration R_g and a mass fractal (or Porod) exponent m.

The mass fractal m is related to the excluded volume parameter ν by $m = \frac{1}{\nu}$.

An analytical solution was provided by Hammouda in 1993:[82]

$$P_{pol}(q) = \frac{1}{\nu U^{1/2\nu}} \left[\gamma\left(\frac{1}{2\nu}, U\right) - \frac{1}{U^{1/2\nu}} \gamma\left(\frac{1}{\nu}, U\right) \right] \qquad (16)$$

with:

$$\gamma(x, U) = \int_0^U e^{-t} t^{x-1} dt \qquad (17)$$

and:

$$U = \frac{q^2 R_g^2 (2\nu + 1)(2\nu + 2)}{6} \qquad (18)$$

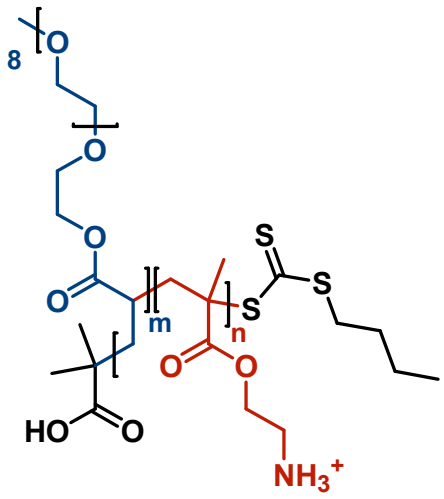
Above, $\gamma(x, U)$ is the incomplete gamma function.

Let us note that this model strictly applies for mass fractals $\frac{5}{3} \leq m \leq 3$ and has been devised for homopolymer chains and not a diblock copolymer. Here, our system is a DHBC with a comb-like structure for one of the blocks, hence we find high mass fractals $m \geq 3$. We nonetheless used this model as it is the currently only available model with an analytical solution that can describe our polymer chains in solution. Also, it is to be noted that the micellar solutions characterized contain unmicellized homo-polyelectrolytes, either from poly(acrylic acid) or poly(styrene sulphonate) sodium salts, depending on the micellization partner used, which is neither considered nor observed due to contrast.

2.3. RESULTS AND DISCUSSION

2.3.1. Block Copolymer P(OEGMEA)-*b*-P(AEMA)

The chemical structure of the newly developed double-hydrophilic block copolymer, P(OEGMEA)-*b*-P(AEMA), synthesized by RAFT polymerization, following the established protocol discussed in materials and methods, is depicted in **Scheme 2**.



***Scheme 2**. Structure of the P(OEGMEA)$_m$-b-P(AEMA)$_n$ copolymer*

2.3.1.1. SEC-MALLS Analysis

The SEC-MALLS data, depicting the overlap of chromatograms from three different detectors (UV, Light and dRI) for Pol. 1 (target of P(OEGMEA)$_{21}$-*b*-P(AEMA)$_{40}$) are provided in **Figure 1**. The profiles suggest a quasi-monomodal distribution of population, with a clear peak at ca. 8 min elution time seen on the three detectors, proving the two steps RAFT polymerization induced the formation of a single diblock copolymer and not two distinct homopolymers. The nearly symmetrical peaks with no prominent shoulders reveal that the polymer sample analyzed is homogeneous. The $PDI = \frac{M_w}{M_n}$ of 1.11 obtained is in complete agreement with expected values from RAFT polymerization, confirming the successful synthesis of the DHBC. The small but notable peak around ca. 12.5 min from dRI and UV indicate the possible presence of chain transfer agent BDMAT in the sample analyzed.

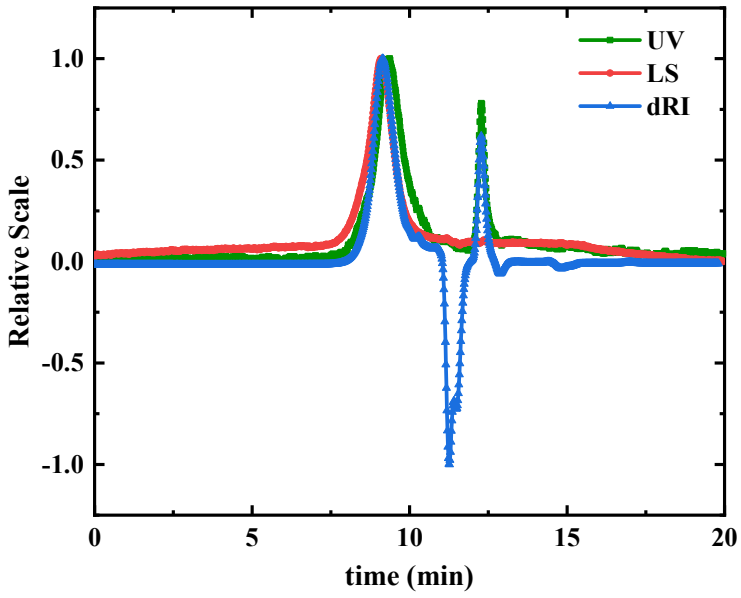


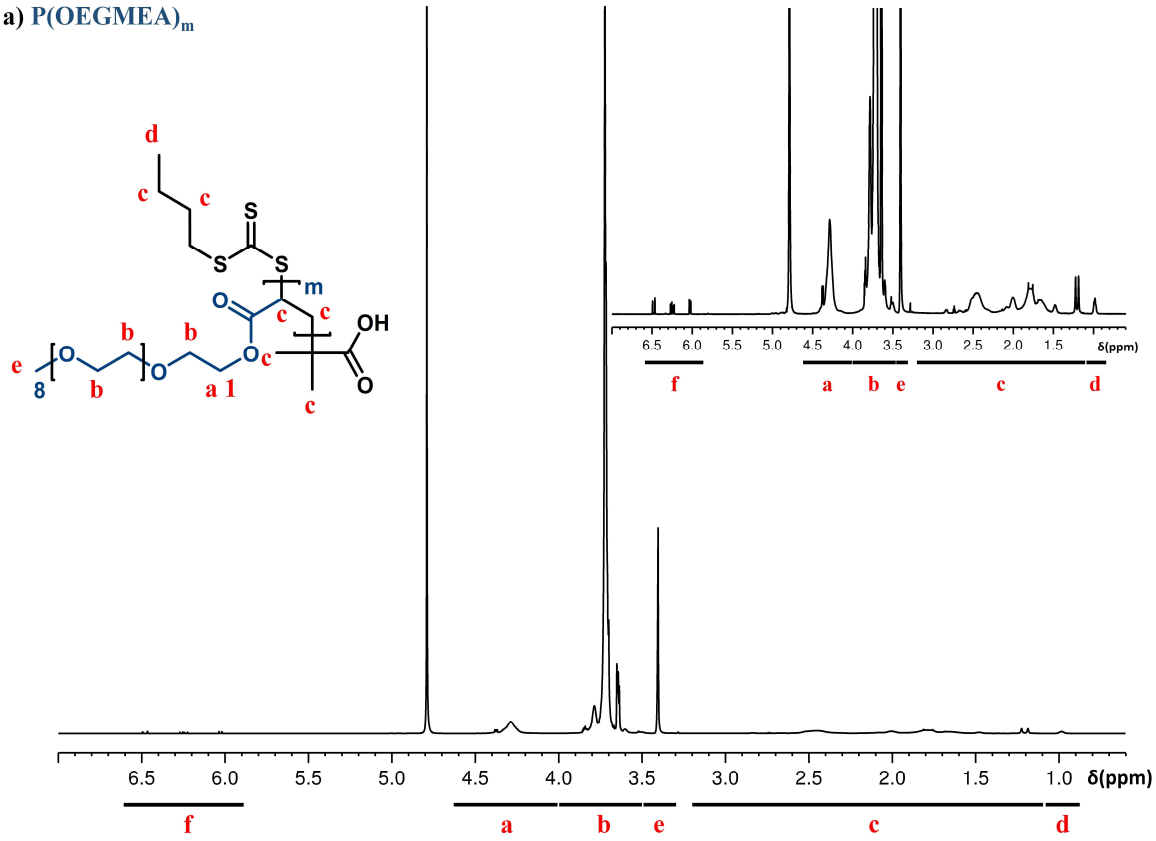
Figure 1. *SEC-MALLS analysis of P(OEGMEA)$_m$-b-P(AEMA)$_n$ copolymer (Pol. 1). The chromatographs obtained were normalized for proper comparison and indicate presence of a homogeneous monomodal distribution of the polymer with low polydispersity.*

2.3.1.2. NMR Analysis

^{1}H NMR spectra of a) P(OEGMEA) and b) P(OEGMEA)-*b*-P(AEMA) obtained by RAFT polymerization of Pol. 1 are displayed in **Figure 2**. The degree of polymerization (DP) of each block is obtained using the areas of the peak associated to protons highlighted with alphabetical letters. In both NMR spectra, the peaks in the range 0.2 – 3.2 ppm (labelled *c* in **Figure 2**) are primarily from the acrylate-based backbone of the polymer chain analyzed. The peaks between 3.2 - 4.4 ppm are related to the protons from the comb-like oligo(ethylene oxide) methyl ether side chains for the P(OEGMEA) spectrum, while they are associated to protons from both, the ethylene sites in the oligo(ethylene oxide) based chains of P(OEGMEA) and ethylene sites from the aminoethyl methacrylate groups in the P(AEMA) (area denoted using *a, b* and *e* together) for the

P(OEGMEA)-*b*-P(AEMA) spectrum. In detail, when studying the P(OEGMEA) spectrum (**Figure 2a**), the well separated peak depicted as *a* in the figure, at 4.30 ppm, is ascribed only to the two α-hydrogen atoms in the carbon adjacent to the ester bond of the side chain, while, in the P(OEGMEA)-*b*-P(AEMA) spectrum (**Figure 2b**), it has a contribution from the α-hydrogen atoms close to the ester bond in the aminoethyl methacrylate group of P(AEMA) block as well. Similarly, the peak in region *e*, **Figure 2a** is from the terminal methyl group in the oligo(ethylene oxide) based side chains while in **Figure 2b**, the same region also has contribution from the protons attached to the carbon next to the primary amine group in the P(AEMA) branches; both peaks are found at ca. 3.4 ppm, but the one corresponding to terminal methyl group (from P(OEGMEA)) shifts further downfield when compared to the signal from α-protons close to the primary amine in P(AEMA) due to higher electronegativity of oxygen relative to nitrogen group. Notably, the region *b* remains unchanged in both P(OEGMEA) and P(OEGMEA)-*b*-P(AEMA) spectra and is related to the other protons in side chains of the P(OEGMEA) block, and could be used as reference when needed. Finally, the region *f* in the P(OEGMEA) spectrum corresponds to the unreacted monomer species in the sample, which is absent in the P(OEGMEA)-*b*-P(AEMA) spectrum, owing to the prolonged dialysis carried out.

a) P(OEGMEA)$_m$



b) P(OEGMEA)$_m$-*b*-P(AEMA)$_n$ Pol. 1

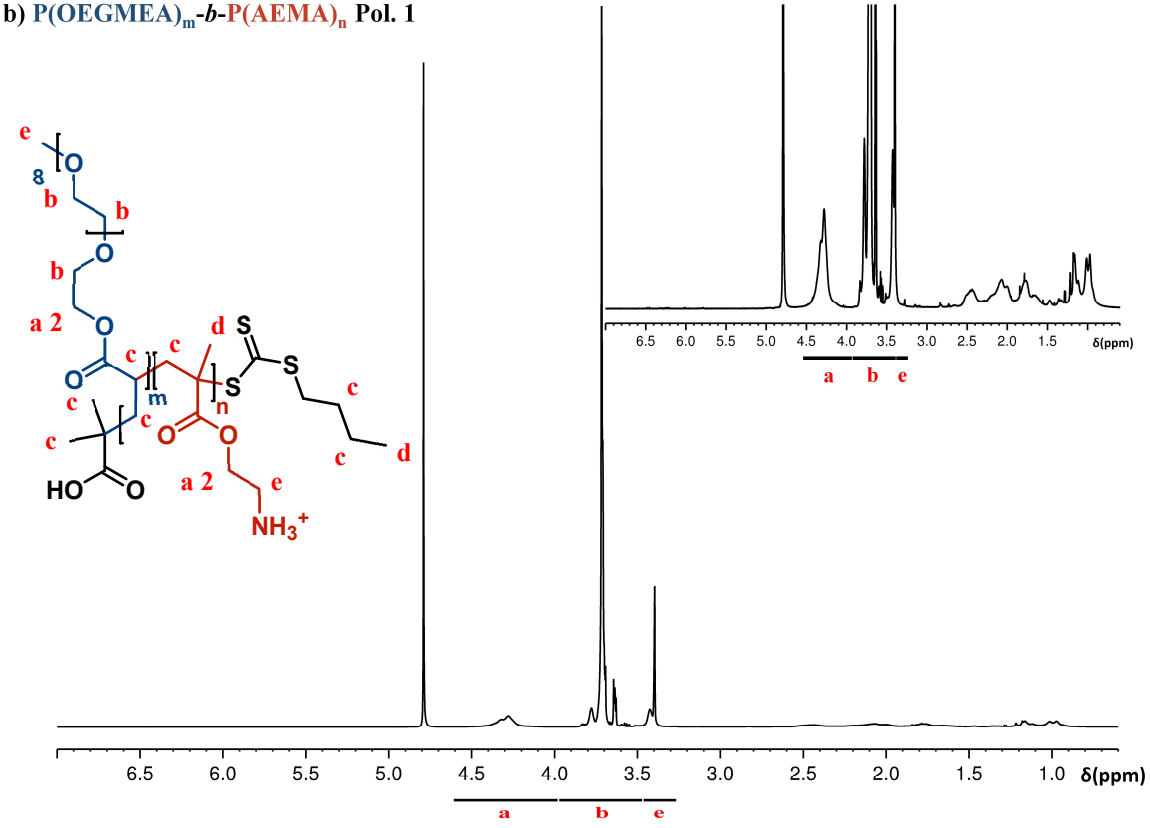


Figure 2. *NMR spectra of a) the P(OEGMEA) homopolymer and b) of the P(OEGMEA)-b-P(AEMA) diblock copolymer (Pol. 1). The degrees of polymerization of each block (21 for P(OEGMEA) and 23 for P(AEMA)) were calculated using the peaks highlighted using alphabetical letters. The insets, showing the chemical formula of each macromolecule, depict the hydrogen atoms attribution to each peak. In spectrum a, the peak labelled d (1 ppm) is used for calibration and the degree of polymerization of the homopolymer is found by finding the integral area of region c. The peaks in this region are from the acrylate backbone of the homopolymer. The signals in regions a, b, and e are from side chain and area f corresponds to free OEGMEA monomers. In spectrum b), the region b is used as the reference (3.5 - 4.0) and the peak area at a, corresponding to the α-hydrogens next to the ester in the side chains of both P(OEGMEA) and P(AEMA) blocks, is used for finding the number of units of the P(AEMA) block. Along with region a, the peaks at b, c, d, and e also have contribution from P(AEMA) block in spectrum b.*

In spectrum (a) of the P(OEGMEA) block, the peak at 1 ppm corresponds to the three protons attached to the terminal carbon in the backbone (shown by *d* in the figure), and is used for the calibration of the integral values in *a*, *b*, *c*, *e*, and *f* domains. The peaks in region *c* have a contribution of three protons from each OEGMEA monomer polymerizing and another ten protons from the chain ends, as depicted in **Figure 2**. Hence, using the equation $DP_{P(OEGMEA)} = m = \frac{c-10}{3}$, the degree of polymerization of P(OEGMEA) $DP_{P(OEGMEA)}$ could be obtained. In this particular case it was found to be 21 units. The narrow but notable set of peaks in the region *f* of spectrum (a), **Figure 2**, corresponding to the free OEGMEA monomers in the sample, has a low peak area (ca. 2.5) pointing at a high monomer conversion rate (ca. 95%). The homopolymer (OEGMEA) is not dialysed after its synthesis and hence, extracting the conversion rate is viable, unlike in the final copolymer, P(OEGMEA)-*b*-P(AEMA), studied only after dialysis.

In spectrum (b), corresponding to the entire block copolymer, P(OEGMEA)-*b*-P(AEMA), the NMR region highlighted as domain *b* is used for the calibration (from 4 to 3.5 ppm). This region of the spectrum, associated to a section of the protons in the side chain of the P(OEGMEA) block

(highlighted in **Figure 2b**), remains constant and does not evolve with the addition of the second block, making it a good reference range, as previously explained. The calibrated value of this domain *b*, obtained from the spectrum (a) is used to fix the integral value of this region in spectrum (b). Once this calibration is done, the peak area of the signal at 4.30 ppm (depicted as *a*, signal from the α-hydrogens next to the ester bond in the side chain of both P(OEGMEA) and P(AEMA) block) is measured, and the value obtained is subtracted for the contribution from the P(OEGMEA) side chain based α-hydrogens (obtained from the P(OEGMEA) spectrum). Finally, the value obtained is divided by two (number of α-hydrogen atoms attached to the carbon close to the ester group in each P(AEMA) side chain), to estimate the DP of the P(AEMA) block ($DP_{P(AEMA)} = n = \frac{a\,2 - a\,1}{2}$, *a 1* and *a 2* correspond to the peak area at 4.3 ppm for spectra (a) P(OEGMEA) and (b) P(OEGMEA)-*b*-P(AEMA) respectively). NMR analysis carried out on the copolymer, Pol. 1, gives a $DP_{P(AEMA)}$ of 23 units. Consequently, the Pol. 1 copolymer can be represented as P(OEGMEA)$_{21}$-*b*-P(AEMA)$_{23}$. From the degree of polymerization, the molecular weight of the entire copolymer is deduced to be 13.1 kDa (excluding the contribution from the terminal groups), with a share of 10.1 kDa and 3.0 kDa from P(OEGMEA) and P(AEMA) block respectively (overall molecular weight of the P(OEGMEA)$_{21}$-*b*-P(AEMA)$_{23}$ copolymer = 13.3 kDa). Let us note that according to this analysis, if the P(OEGMEA) block has reached the targeted DP (21), the second block is shorter than targeted (23 instead of 40). Nonetheless, the analysis of the second block relies on the calibration of the curve on the peak *b* at ca. 3.5 - 4 ppm, as we cannot rely on the peak *d* at 1 ppm anymore. Indeed, in the diblock, peak *d* is not only related to the protons of the terminal carbon group of the backbone (which can be damaged by the addition of the second block), but also on the three protons of the methyl groups in the backbone of the P(AEMA) block. And on the other side, peak *b*, associated purely to protons from the P(OEGMEA) block, is close to peak *e*

and hence does not fully return to the baseline. Hence, if NMR allows to extract $DP_{P(OEGMEA)}$ with great precision, the evaluation of $DP_{P(AEMA)}$ has some uncertainties. For this reason, NMR analysis are complemented with elemental analysis.

Another P(OEGMEA)-*b*-P(AEMA) copolymer was synthesized, labelled as Pol. 2. It was also characterized using NMR, yielding DPs of 25 and 17 units for P(OEGMEA) and P(AEMA) blocks respectively, for a target of 21 and 20. This copolymer with a shorter P(AEMA) block and a longer P(OEGMEA) was also used to study the self-assembling character along with $P(OEGMEA)_{21}$-*b*-$P(AEMA)_{23}$.

2.3.1.3. Elemental Analysis

Both batches of P(OEGMEA)-*b*-P(AEMA) were also characterized using elemental analysis (EA) for their CHNS composition (**Table 3** and **Table S1**). The main purpose here is to complement the NMR analysis, by estimating the degrees of polymerization of the second block of the DHBC in the macromolecules using the ratio between nitrogen and carbon atoms.

In P(OEGMEA)-*b*-P(AEMA), Pol. 1, the weight percentages measured in EA were 48.96% Carbon, 8.02% Hydrogen and 2.78% Nitrogen, giving atomic ratios of N/C = 0.049 and H/C = 1.96 respectively. By taking $DP_{P(OEGMEA)} = 21$ from the NMR, analysis, these atomic ratios give $DP_{P(AEMA)} = 32$, much higher than the value of 23 found by NMR analysis and closer to the target of 40. This gives $P(OEGMEA)_{21}$-*b*-$P(AEMA)_{32}$ for Pol. 1. Similarly, the weight percentages of Pol. 2 from elemental analysis (51.08%, 8.53% and 1.93% for Carbon, Hydrogen and Nitrogen respectively) were also used to determine the atomic ratios (N/C = 0.032 and H/C = 2.00) and consequently, the following polymerization degrees were estimated ($P(OEGMEA)_{25}$-*b*-$P(AEMA)_{22}$). **Table 1** summarizes the DPs found in NMR and elemental analysis and their

comparison with the targeted DPs for both DHBC. Due to the aforementioned imprecisions in the estimation of $DP_{P(AEMA)}$ in NMR, in the following sections we will the values found by combining both techniques to describe the polymers, i.e. P(OEGMEA)$_{21}$-*b*-P(AEMA)$_{32}$ for Pol. 1 and P(OEGMEA)$_{25}$-*b*-P(AEMA)$_{22}$ for Pol. 2. Finally, if results from elemental analysis are closer to the target, we still note a mismatch for high $DP_{P(AEMA)}$ between target and results. This suggests an incomplete polymerization of the second block at high molecular weights, which may be related to the instability of P(AEMA) at high temperature (the synthesis was performed at 80°C). Further tests would be required to see if this effect is ever more pronounced at even higher targets.

Sample name	N/C	S/C	H/C
Pol. 1	0.049	0.0047	1.96
Pol. 2	0.032	0.0020	2.00

Table 3. *Copolymers prepared (Pol. 1 and 2). For each sample atomic ratios calculated from EA is given (atomic ratios = N/C, S/C and H/C)*

2.3.2. Self-Assembly of P(OEGMEA)-*b*-P(AEMA) Copolymer

The ability of the P(OEGMEA)-*b*-P(AEMA) copolymers (Pol. 1 and 2) to form self-assembled nanostructures through electrostatic complexation between the positively charged block of the DHBC and negatively charged polyelectrolytes, such as the ionisable sodium poly(acrylate) and the poly(sodium styrene sulfonate), in aqueous medium was investigated. The charge ratio (ratio between acid groups and amine groups from polyelectrolyte and P(OEGMEA)-*b*-P(AEMA) copolymer respectively) used was ca. 1.1 for P(AA) based systems, while in P(SS) made system it was ca. 0.7. The obtained PIC micelles were characterized by light scattering and small angle neutron scattering.

2.3.2.1. Micelles Based on P(OEGMEA)$_{21}$-*b*-P(AEMA)$_{32}$ and PAANa 5.1 kDa

First, the self-assembling character of Agg. 1 (see **Table 2**), micelles made of Pol. 1, P(OEGMEA)$_{21}$-*b*-P(AEMA)$_{32}$, with poly(acrylic acid) sodium salt of 5.1 kDa (PAANa, DP of the polyelectrolyte = 54 units), was studied using static and dynamic light scattering (SLS/DLS), and small angle neutron scattering (SANS) (**Figure 3**).

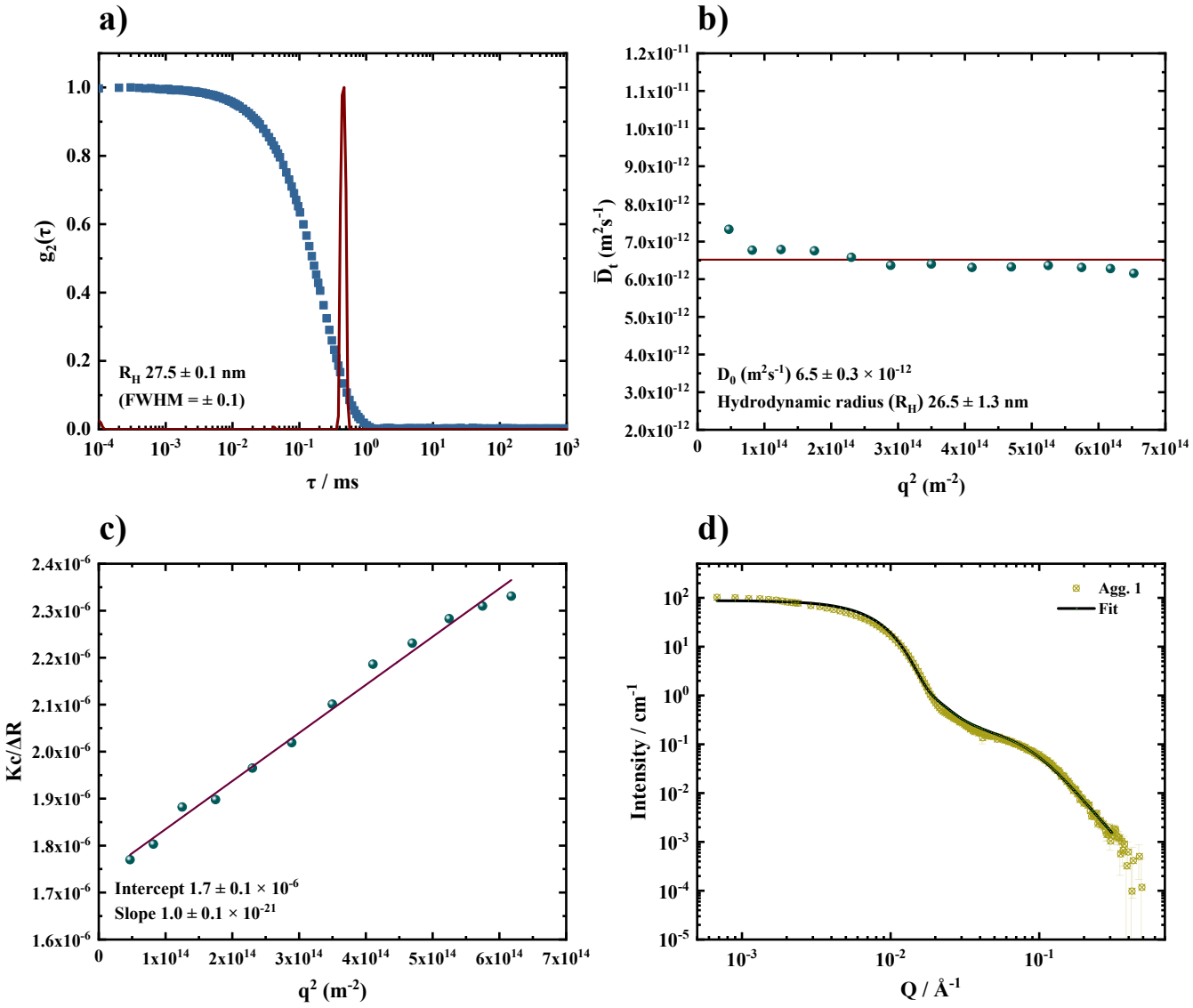


Figure 3. *Characteristics of the mixture of Agg. 1 at 0.1 wt%, and pH = 6 (a and b) DLS data with: (a) Intensity-time autocorrelation function $g_2(\tau)$ measured at a scattering angle $\theta = 90^o$ with the distribution of relaxation time acquired from the CONTIN fit (the hydrodynamic radius R_H and*

corresponding full width half maximum (FWHM) from the CONTIN analysis are given in inset), (b) Diffusion coefficient $\overline{D}_t$ as a function of q^2 from the second order cumulant analysis. In inset, the diffusion coefficient at the zero angle D_0 and its corresponding hydrodynamic radius R_H are given (c) Zimm plot from SLS data (d) merged SLS-SANS pattern of the same micelles but at 1 wt%. In black, the fit made using a combination of simple sphere and polymer chain with excluded volume in solution.

We firstly studied the behaviour of the system by DLS on samples at 0.1 wt% and pH = 6 in D_2O: the autocorrelation function $g_2(\tau)$ of intensity *vs* time and its associated relaxation time distributions at pH = 6 and a scattering angle 90° are depicted in **Figure 3a**. The CONTIN analysis gives a single peak referring to the formation of a stable well-defined structure. The hydrodynamic radius obtained from CONTIN for the sample stood at R_H = 27.5 ± 0.1 nm (FWHM ± 0.1). The sample was also measured at various scattering angles, and analyzed using the cumulant method, to measure more accurately the translational diffusion coefficient via the zero-angle averaging (see *Materials and Methods* and **Figure 3b**). D_0 (m^2s^{-1}) was found at (6.5 ± 0.3) × 10^{-12} m^2/s^{-1}, giving a hydrodynamic radius R_H = 26.5 ± 1.3 nm with a polydispersity index *PDI* = 1.06 ± 0.03.

The system was then investigated with SLS and the data obtained were fitted using the Zimm plot given in **Figure 3c**. The absence of multiple slopes in the Zimm plot confirms the monomodal distribution of the self-assembly. Through SLS, the radius of gyration R_G of the self-assembly could also be determined, using the equation $R_G = \sqrt{3.Mw.slope}$, with Mw being molecular weight of the self-assembly obtained from the intercept ($Mw = \frac{1}{Intercept}$). Although R_G can be calculated, Mw is not obtained because the $\frac{dn}{dc}$ value is not available from literature, and was not determined by us, too.

For a deeper understanding of the system, small angle neutron scattering (SANS) data of Agg. 1 was collected at 1 wt% and pH = 6 with D_2O as the solvent (**Figure 3d**). The SLS-SANS pattern of Agg. 1, at low q ($0.0007 < q < 0.001$ Å^{-1}) is typical for quasi spherical species, with a plateau at the lowest scattering vectors and a sudden decrease around ca. 0.010 - 0.020 Å^{-1}, followed by another shoulder at ca. 0.03 – 0.30 Å^{-1}. The absence of an upturn at the lowest scattering vector confirms the absence of aggregation. We ascribe the two notable plateaus in the SANS pattern to two populations of different sizes; a) the self-assembled polymeric micelles and b) free polymer chains, probably not contributing to micellar formation. While the first plateau of the SLS-SANS pattern (0.010 - 0.020 Å^{-1}) corresponds to the spherical micellar species, the second plateau can be assigned to the free polymer chains in the system. In the higher q values ($0.120 < q < 0.400$ Å^{-1}), associated to these free polymer chains, a power-law dependence is evidenced, $I \sim q^{-\alpha}$, with α = ca. 3.5, a value that is considerably higher than the value found in case of typical linear polymers in a good solvent ($\alpha = 5/3$). This is to be expected in the case of the comb-like architecture of the P(OEGMEA) block of the copolymer chains according to previously published results .[83]

The SANS pattern of the copolymer Pol. 1 without micellization partner (in 0.1 M NaCl solution in D_2O to screen out the charges, see **Figure S1** in supplementary information) was collected to confirm that the copolymer does not self-assemble spontaneously without an oppositely charged micellization partner. The steep upturn found at the low-q region of the SANS pattern from Pol. 1 alone, corresponds to an uncontrolled aggregation (different from the micellization seen in the samples labelled "Agg"). Further, the plateau limit at ca. 0.1 Å^{-1} of Pol. 1 corresponds to the free polymeric chains in the sample and upon comparing it with the SANS curve of the micellar system (at all pHs), overlaps well with the second shoulder observed, validating that this second shoulder corresponds to the free polymer chains in suspension coexisting with micelles.

Hence, data of micellar suspensions were fitted using a combination of these two contributions, spherical micelles and free polymer chains (see *Materials and Methods*). This model is well-suited to understand the dimension of the micelles and the free polymers. We could expect the micelles to exhibit a core-shell nature, with P(AEMA) and PAA forming the complex coacervate core and P(OEGMEA) forming the shell in agreement with previous works on amphiphilic or PIC micelles,[33,84,85] nonetheless, the strong contribution from the free polymers does not allow obtaining such information, hence a simple sphere model was used to describe the micelles. From the SANS fit, the radius R of the micelles is found at 19.5 ± 0.1 nm with a polydispersity in radius of 30 ± 1 %, while the radius of gyration R_g of the free individual P(OEGMEA)-*b*-P(AEMA) polymer chains is found to be 2.3 ± 0.1 nm (**Figure 3**). Let us note this R_g corresponds to the typical radius of gyration of the polymer chains in solution and not of the scattering objects (i.e. micelles) measured in SLS and labelled R_G.

The effect of pH on the micellization behaviour of Agg. 1 was further studied, in the pH range 3 - 8 (see **Figure 4**). The pH micellization range was obtained by studying the normalized scattering intensity as a function of pH (using DLS, **Figure 4a**). The scattering intensity is extremely low at pH = 3 and 4, strongly increases from pH = 5 to 6, before decreasing again at pH = 7 and 8. As the normalized scattered intensity is directly proportional to the number of scattering objects, we can estimate that micelles are formed at pH ranging from ca. 5 to 7, with an optimum at pH = 6. Let us note that this pH behaviour is in agreement with the formation of polyion complex micelles by electrostatic complexation between the two weak polyelectrolytes: the negatively charged acrylate functions (pKa (AA) is ca. 4.3)[86] of the PAA and the positively charged primary amine functions in the aminoethyl methacrylate (pKa of ca. 7.6).[87] Upon moving away from the optimum pH value of 5 - 7, micelles dissociate into individual polymer chains, resulting in a reduced scattered

intensity. The pH responsive character of the micellar suspension was further evidenced using the CONTIN analysis of the dynamic light scattering data at varying pHs (**Figure 4b**). In adequation with the normalized intensity, at pHs ranging from 5 to 7, a single well-defined population is observed, further validating that the optimal pH range for self-assembly is close to 6. The size distribution is the narrowest at pH = 6, indicating well-defined species and agreement with the normalized scattered intensity. The peak width increases as soon as pH deviates from this value, even in its vicinity (at pH = 5 and 7). The broadening of the size distribution indicates an increase of the polydispersity in size of the system. At extreme pHs (3, 4 and 8), multiple populations are readily observable, which further confirms that indeed the micelles are pH-sensitive and dissociate into free polymers and large aggregates when conditions are unfavourable.

SLS-SANS measurements at various pHs (3 - 8) were carried out to evidence the role of pH on the micelles and on the overall scattering intensity (**Figure 4c**). At all pHs, the signal exhibits a plateau at the smallest angles, proving the absence of very large aggregates. In the pH range 3 – 8, the scattering curves from the polymer solutions show a clear evolution, both in overall intensity and shape of the curve. The second plateau (shoulder) corresponding to the free polymers remain intact in all samples (ca. 0.1 $Å^{-1}$). However, the first plateau typically associated to the polymer micelles evolves significantly with the pH change. At pH = 3, polymer aggregates are evidenced by the presence of a plateau at small q ca. 0.001 – 0.005 $Å^{-1}$, a signal that largely disappears at pH = 4, indicating that the aggregates disappear. Even though pH = 3 has the highest scattering intensity at low q, the plateau around 0.001 – 0.005 $Å^{-1}$ suggests that the polymer aggregates formed in this case are not of individual micelles. The dimension of the species is also much larger after fitting of this curve and should be from a different population, potentially evolving from hydrogen bonding between free DHBCs and PAA homopolymers in acidic environment. Again, a

combination of simple sphere + free polymer was used to fit this data (**Figure S2**). The aggregates at pH = 3 is found with a radius of 54 ± 1 nm and a polydispersity of 40 ± 1 %, both parameters being significantly higher than the values reported for the same system at pH = 6 (considered as the optimal pH for micellization according to SLS/DLS). Further, upon moving from pH = 5 to 8, the signal from micelles is clearly observable and increases up to pH = 6, before decreasing again at higher pHs, in line with the result from light scattering. This again proves that the micelles are best formed starting from pH = 5, with an optimum value around pH = 6.

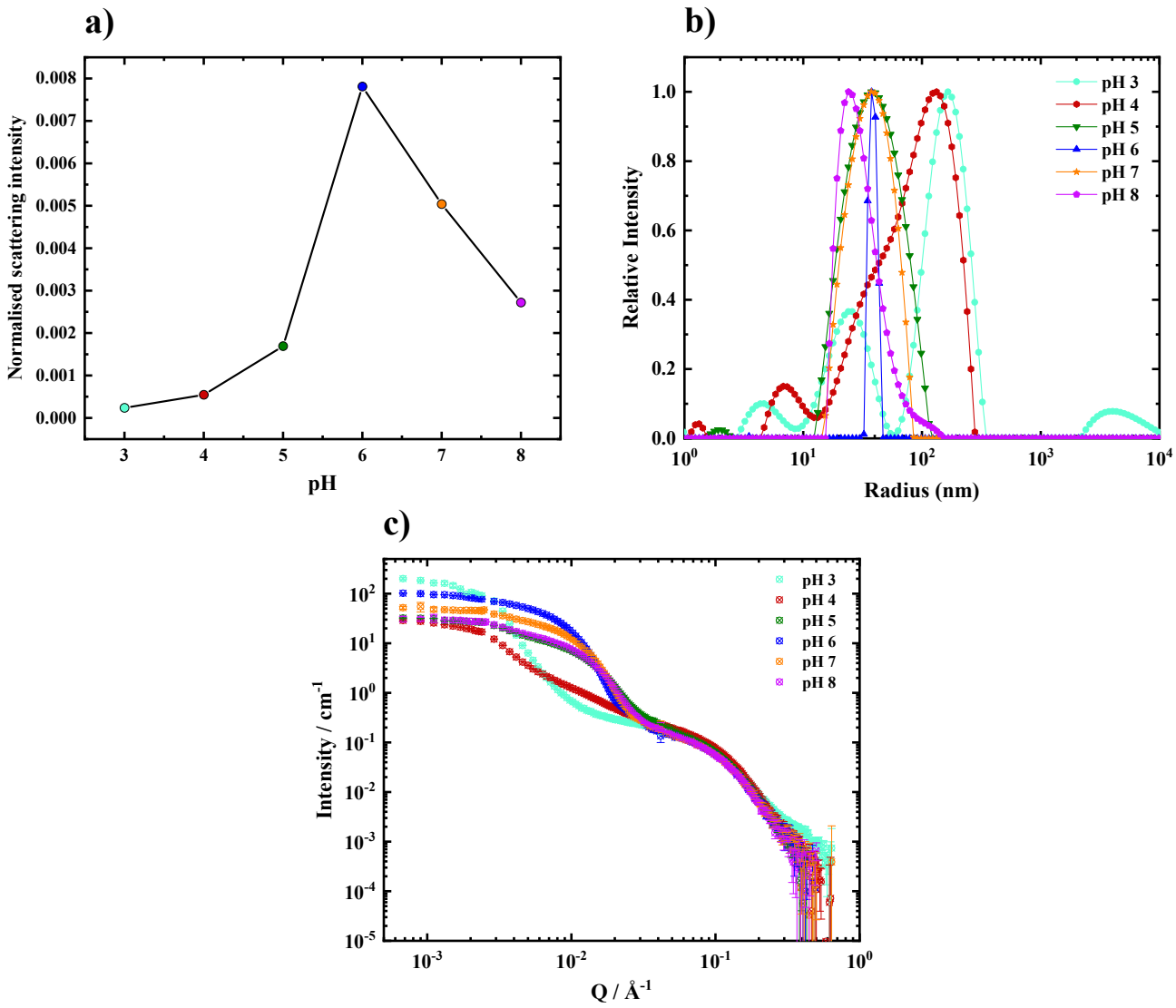


Figure 4. *(a, b) DLS analysis (at a scattering angle θ = 90°) and (c) merged SLS-SANS patterns*

of Agg. 1 micelle at various pH levels (3 - 8). The DLS analysis is comprised of (a) the normalized scattering light intensity and (b) the size distribution from the CONTIN analysis of $g_2(\tau)$.

2.3.2.2. Characterization of Other Systems Using Static & Dynamic Light Scattering and Small Angle Neutron Scattering

In order to investigate the role of the micellization partner and chain length of the P(OEGMEA)-*b*-P(AEMA) copolymer in the stability, shape and structure of the self-assembled micelles, three other micellar systems (Agg. 2 - 4, see **Table 2**) were also studied in detail using light and neutron scattering and compared with the previously studied Agg. 1.

As a reminder, the four 'Agg.' systems are: 1) $P(OEGMEA)_{21}$-*b*-$P(AEMA)_{32}$ & PAANa 5.1 kDa (DP = 54), 2) $P(OEGMEA)_{21}$-*b*-$P(AEMA)_{32}$ & PSSNa 1.1 kDa (DP = 5), 3) $P(OEGMEA)_{21}$-*b*-$P(AEMA)_{32}$ & PAANa 2.1 kDa (DP = 22) and 4) $P(OEGMEA)_{25}$-*b*-$P(AEMA)_{22}$ & PAANa 2.1 kDa (DP = 22).

It is to be noted that, even though the normalized scattering intensity at pH = 5 of Agg. 1 is relatively low when compared to the same system at pH = 6, in all other systems studied (Agg. 2 - 4) the scattering intensity at pH = 5 is significantly higher (**Table S2**). Hence, pH = 5 was considered as a suitable pH to compare micelles made for these four systems (**Figure 5** and **Table 4**). **Table 4** gives the averaged diffusion coefficient D_0, the corresponding hydrodynamic radius R_H and its associated polydispersity *PDI* obtained by DLS for all the four systems. Results indicate that the micellization agent used and copolymer chain length have an influence on the size and stability of the species derived. The size of the assemblies from $P(OEGMEA)_{21}$-*b*-$P(AEMA)_{32}$ & PAANa 5.1 kDa (Agg. 1) was found to be the smallest when compared to others (Agg. 2 - 4), while the largest size was found for Agg. 4, obtained by mixing $P(OEGMEA)_{25}$-*b*-$P(AEMA)_{22}$ &

PAANa 2.1 kDa. In all cases, the polydispersity in size *PDI* was ≤ 1.26, proving that well-defined species with a quasi-monomodal distribution are obtained.

Sample name	Diffusion coefficient D_0 (m²/s)	Hydrodynamic radius R_H (nm)	Polydispersity (PDI)
Agg. 1	$7.12 \pm 0.24 \times 10^{-12}$	24.3 ± 0.8	1.23 ± 0.03
Agg. 2	$5.75 \pm 0.13 \times 10^{-12}$	30.1 ± 0.7	1.26 ± 0.02
Agg. 3	$6.00 \pm 0.20 \times 10^{-12}$	28.8 ± 1.0	1.09 ± 0.03
Agg. 4	$3.51 \pm 0.10 \times 10^{-12}$	49.2 ± 1.4	1.19 ± 0.02

Table 4. *Diffusion coefficients D_0, corresponding hydrodynamic radii R_H and polydispersity indices ($PDI = \frac{M_w}{M_n}$) for Agg. 1 - 4 micelles (prepared with different DHBC and micellization partners) prepared at 0.1 wt% of DHBC in D_2O at pH = 5.*

Using SLS and SANS, the effect of concentration (1 - 5 wt%) on the shape and size of the micelles was studied in depth in all the four micellar systems. The absolute scattering intensity of the micellar solutions increases with concentration, as expected in all four sets (Agg. 1 - 4), due to the increase in number of scattering species, as depicted in **Figure 5**. Notably, even at 5 wt%, no feature related to inter micellar interaction was detected and hence the SANS data obtained have been fitted using a combination of simple cylinder or sphere models (depending on the system) and a free polymer chain model without structure factor, assuming the presence of two distinct populations. In all cases, the signal reaches a plateau at the smallest angles with no upturn, indicating that whatever the polymer or micellization agent used, no large aggregates are formed in solution.

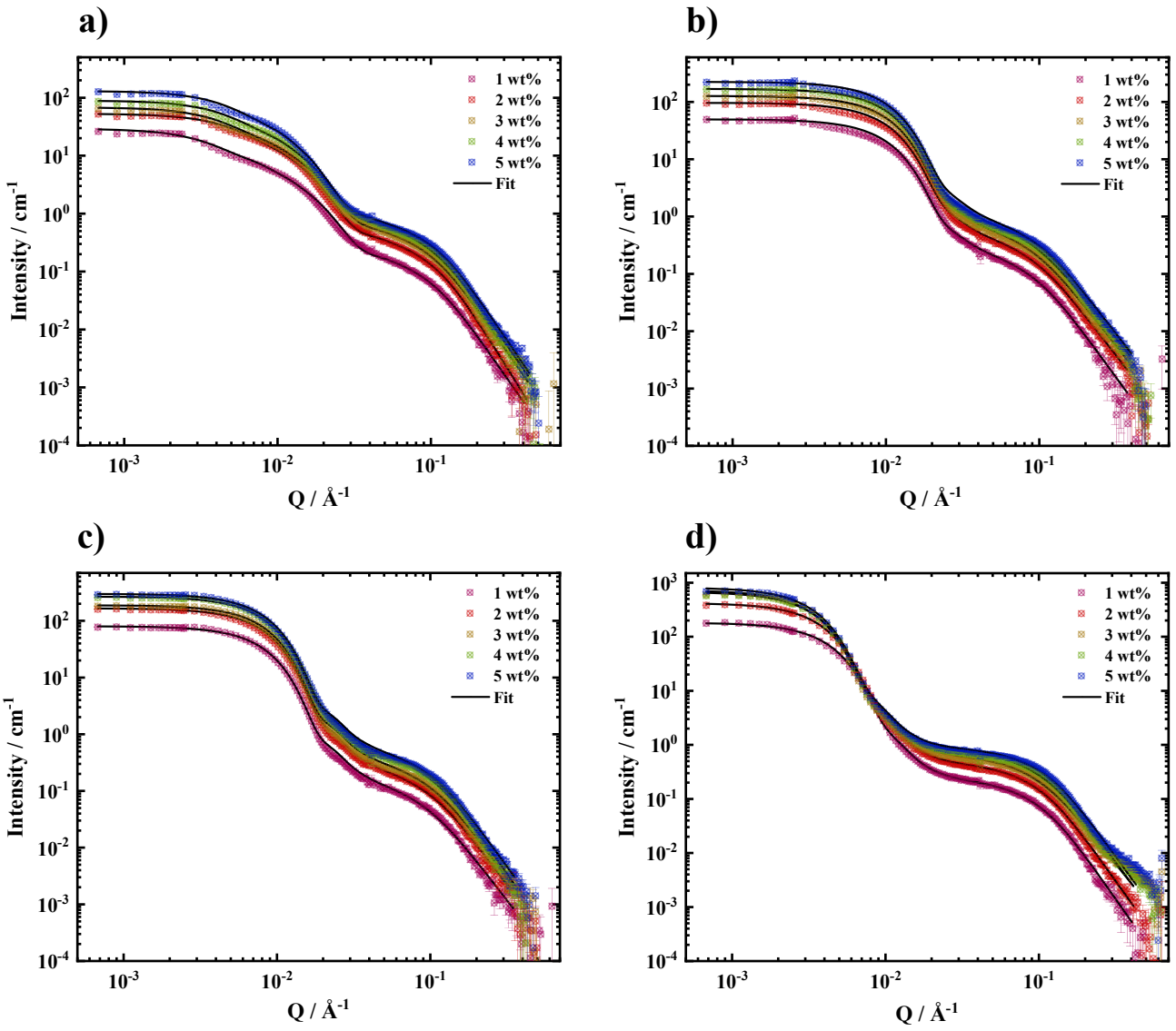


Figure 5. *Merged SLS-SANS patterns for micelles at different concentrations (1 - 5 wt%) at pH 5 in D_2O: (a) P(OEGMEA)$_{21}$-b-P(AEMA)$_{32}$ & PAANa 5.1 kDa (Agg. 1) (b) P(OEGMEA)$_{21}$-b-P(AEMA)$_{32}$ & PSSNa 1.1 kDa (Agg. 2) (c) P(OEGMEA)$_{21}$-b-P(AEMA)$_{32}$ & PAANa 2.1 kDa (Agg. 3) (d) P(OEGMEA)$_{25}$-b-P(AEMA)$_{22}$ & PAANa 2.1 kDa (Agg. 4). Fits were made using the model of Cylinders + free polymers for (a), and Spheres + free polymers for (b, c, d).*

In the case of P(OEGMEA)$_{21}$-*b*-P(AEMA)$_{32}$ & PAANa 5.1 kDa (Agg. 1) at pH = 5, the SLS-SANS patterns obtained are characteristic of elongated objects (**Figure 5a**). The signals at low q ($0.0007 < q < 0.001$ Å^{-1}) present a plateau followed by a power law dependence $I \sim q^{-\alpha}$ (ca. 0.007

$Å^{-1}$), with the value of α = ca. 1 for all concentrations, typical for elongated objects. At high q (at ca. 0.30 $Å^{-1}$), the data again show a power law dependence $q^{-\alpha}$ with an exponent value α ca. 4, coming from the comb like P(OEGMEA) block of the free copolymers in the system. On fitting the data obtained with the model of cylinder + free polymer chains, the radius of gyration R_G of the free individual polymer chains was determined and it remained nearly constant between 1 wt% and 5 wt% as anticipated (ca. 2.0 nm, **Figure 5a** and **Table S3**). Moving from 1 – 5 wt%, the exponent value α varied with values of 3.8, 4.3, 3.8, 3.9 and 3.9 respectively. While the radius of the elongated micelles is found to increase from 8.4 ± 0.1 nm to 10.3 ± 0.1 nm (with a polydispersity in radius at ca. 25% for all concentrations), the length of the micelles decreases from 138.2 ± 1 nm to 102.6 ± 1 nm, when concentration is increased from 1 wt% to 5 wt% (**Table S3**). This suggests that with concentration, the curvature of self-assembly increases. Let us note that these results indicate that the shape of the micelles is clearly pH dependent, as the same system at pH = 6 exhibited clear spherical morphology (see **Figure 5** and **section 3.2.1.**).

Further SLS-SANS measurements were carried out by replacing the negatively charged polyacrylate in the system with PSSNa 1.1 kDa, still mixed with Pol. 1 ($P(OEGMEA)_{21}$-*b*-$P(AEMA)_{32}$) (Agg. 2, **Figure 5b**). Upon changing the polyelectrolyte, SLS-SANS patterns exhibited signals typical of spheres instead of elongated entities. The plateau observed in the low q region ($0.0007 < q < 0.001$ $Å^{-1}$) at all concentrations, followed by a sudden decrease of intensity (ca. 0.010 $Å^{-1}$) is characteristic of quasi spherical objects in SANS, as previously stated. The type of micellization partner has no effect on the contribution of the free polymers, with a R_G fixed at 2 nm for all concentrations, and a power law dependence of ca. 3.5 (see **Table S3**). The scattering curves obtained above were fitted using a model which is a combination of simple sphere and free polymer. The radius R of the sphere associated to that of self-assembled micelles, at 1 wt% is

found to be 14.9 ± 0.1 nm and remains constant even with the increase in concentration until 5 wt%, suggesting species number to have no influence on the dimension of the population developed unlike the result observed with Agg. 1. Similarly, the polydispersity in size is found at 30 ± 1% for all concentrations.

The SLS-SANS patterns from the two other systems: P(OEGMEA)$_{21}$-*b*-P(AEMA)$_{32}$ & PAANa 2.1 kDa (Agg. 3) and P(OEGMEA)$_{25}$-*b*-P(AEMA)$_{22}$ & PAANa 2.1 kDa (Agg. 4) micelles are presented in **Figure 5c** and **Figure 5d** respectively. While P(OEGMEA)$_{21}$-*b*-P(AEMA)$_{32}$ & PAANa 2.1 kDa (Agg. 3) micelles were studied to further understand the influence of the micellization partner in the self-assembly, P(OEGMEA)$_{25}$-*b*-P(AEMA)$_{22}$ & PAANa 2.1 kDa (Agg. 4) solutions helped to investigate the effect of copolymer chain length in the dimension and stability of the species formed. At low q ($0.0007 < q < 0.001$ Å^{-1}), both micellar solutions, (Agg. 3 and Agg. 4), displayed a plateau (ca. 0.001 Å^{-1}) followed by a sudden drop in intensity at higher q values (ca. 0.007 and 0.003 for Agg. 3 and Agg. 4 respectively), characteristic of quasi-spherical species, and analogous to Agg. 2. A power law dependence of $I \sim q^{-\alpha}$ with an exponent value α ca. 3.5 - 4 is displayed in this context as well, for both systems at high q range (ca. 0.30 Å^{-1}, fitted values displayed in **Table S3**). The change of polymer between Agg. 1 - 3 and Agg. 4 has little influence on this parameter, which further hints at the role of the comb-like P(OEGMEA) block on this parameter.

The change of micellization agent from PSSNa 1.1 kDa to PAANa 2.1 kDa, keeping copolymer Pol. 1 (P(OEGMEA)$_{21}$-*b*-P(AEMA)$_{32}$) constant, showed no effect on the shape of the species made even though small variation in size could be noted. In both cases spherical structures are observed, unlike the P(OEGMEA)$_{21}$-*b*-P(AEMA)$_{32}$ & PAANa 5.1 kDa system, that presents elongated objects. In Agg. 3, the radius of gyration R_G is again found at ca. 2 nm in agreement with fits from

Agg. 1 and Agg. 2, while the radius of the sphere *R* is found at ca. 20 nm with a polydispersity in size again at ca. 25% at all concentrations (see **Table S3**). No significant change in shape and size of the micelles with concentration proves that the number of species in the vicinity does not influence the dimension of the population formed.

Also, changing the copolymer in micelles made with PAANa 2.1 kDa from P(OEGMEA)$_{21}$-*b*-P(AEMA)$_{32}$ (Agg. 3) to P(OEGMEA)$_{25}$-*b*-P(AEMA)$_{22}$ (Agg. 4) influences significantly the dimension of the species formed. Upon replacing the copolymer, the radius of the micellar spheres increased: at 1 wt%, it goes from 20.0 ± 0.1 nm (Agg. 3) to 36.0 ± 0.1 nm (Agg. 4). This trend is observed at all concentrations probed (see **Table S3** for the fitted values). Let us note that the radius of gyration R_G of the free polymer chains did not vary massively with the copolymer used as it was kept constant at ca. 2 nm, in agreement with the slight variations of DPs between the two DHBC. When P(OEGMEA)$_{25}$-*b*-P(AEMA)$_{22}$ is used (Agg. 4), the change in concentration surprisingly seems to play a crucial role in the size of the self-assembled species in this system. Moving from 1 – 3 wt%, the size of the population increase from 36.0 ± 0.1 nm to 46.7 ± 0.1 nm, before stabilizing and showing no further increase at 4 and 5 wt%, demonstrating that the number of species in suspension has an influence on the dimension of the self-assembled micelles formed until a certain point, before stabilisation. Further, by defining $r_{M_w} = \frac{M_w(P(OEGMEA))}{M_w(P(AEMA))}$ the molecular weight block ratio between the two blocks of the DHBC, we can observe that the increase in size when replacing Pol. 1 to Pol. 2 can be correlated to an increase in r_{M_w} from 2.4 to 4.2. This could be further explored in the future by designing DHBC with a $DP_{P(AEMA)}$ of 20 but two different $DP_{P(OEGMEA)}$, such as 21 and 42.

The overall scattering intensity at the lowest angles $I(q \to 0)$ of the micellar solutions made from Pol. 1 (P(OEGMEA)$_{21}$-*b*-P(AEMA)$_{32}$) with different micellization agents (PAANa 5.1 kDa, PSSNa 1.1 kDa and PAANa 2.1 kDa) at 1 wt% have been also compared (using the curves at 1 wt% in **Figure 5**). The highest scattering intensity is found for the sample with PAANa 2.1 kDa as the micelllisation partner (Agg. 3) followed by PSSNa 1.1 kDa (Agg. 2), and finally PAANa 5.1 kDa (Agg. 1). As the scattering intensity is dependent on the number of scattering objects, this proves that the highest number of micelles are formed in the system Agg. 3, when compared to others. The pH is fixed at 5 for the three samples; this proves that the micellization mechanism depends on the ionization rate of the micellization partner but also on its length. As proven by the pH variation studies presented in **Figure 4a**, PAA is probably only partially charged at pH = 5, as we are still in the vicinity of its pKa value (pKa (AA) = ca. 4.3),[86] while PSS is probably fully ionized at this pH (pKa (PSS) = ca. 1),[88,89] which would explain the higher scattering intensities for the micelles made with PSSNa 1.1 kDa versus PAANa 5.1 kDa as seen both in DLS (**Table S2)** and SANS (**Figure 5**). Nonetheless, the molecular weight of the polyelectrolyte has a strong influence as seen with the results from PAANa 2.1 kDa. While the use of smaller polyelectrolytes (PAANa 2.1 kDa, DP = 22) favours the formation of objects with higher curvature resulting in a spherical population, complexing agents with higher DP such as PAANa 5.1 kDa (DP = 54) gives elongated objects, even when the chemical nature of the polyelectrolyte used is the same. In spherical self-assemblies, the aggregation number is expected to be lesser than the value found in elongated structures, supporting the formation of more self-assembled objects, consequently, resulting a higher scattering intensity, as seen with the intensities of Agg. 1 and Agg. 3. Further investigations to fully comprehend the role of the micellization partner would require to study the role of pH for PAANa 2.1 kDa (DP = 22) and PSSNa 1.1 kDa (DP = 5), similarly to what has been

done with PAANa 5.1 kDa (DP = 54). Further, using a PSSNa 2.1 kDa (DP = 10) as micellization partner, the effect of polyelectrolyte bulkiness on the micelle shape could be studied, to have a complete picture.

In summary, the role of concentration in the shape and size of the micelles was studied in detail for different combinations of copolymer and micellization partner. While the systems such as P(OEGMEA)$_{21}$-*b*-P(AEMA)$_{32}$ & PAANa 5.1 kDa (Agg. 1) and P(OEGMEA)$_{25}$-*b*-P(AEMA)$_{22}$ & PAANa 2.1 kDa (Agg. 4) showed significant shape and size evolutions with concentration, spherical micelles from P(OEGMEA)$_{21}$-*b*-P(AEMA)$_{32}$ & PSSNa 1.1 kDa (Agg. 2) and P(OEGMEA)$_{21}$-*b*-P(AEMA)$_{32}$ & PAANa 2.1 kDa (Agg. 3) showed no significant changes, validating that the effect of concentration differs from one system to another. Further, while copolymer P(OEGMEA)$_{21}$-*b*-P(AEMA)$_{32}$ with PAANa 5.1 kDa (Agg. 1) built elongated structures at pH = 5, the same copolymer crafted spherical objects with PSSNa 1.1 kDa and PAANa 2.1 kDa, highlighting the importance of the micellization partner used. The degree of polymerization of the copolymer as well plays a considerable role in the micelles developed. By replacing P(OEGMEA)$_{21}$-*b*-P(AEMA)$_{32}$ (Pol. 1) with P(OEGMEA)$_{25}$-*b*-P(AEMA)$_{22}$ (Pol. 2), and keeping the micellization agent constant (PAANa 2.1 kDa), objects of higher dimension were made, suggesting to a possible influence of the molecular weight ratio between the two blocks that would be further explored in the future.

2.4. CONCLUSION

In this study, the synthesis and self-assembling properties of a newly developed amine rich double hydrophilic block copolymer, P(OEGMEA)-*b*-P(AEMA), has been discussed in-depth. The copolymer was synthesized via two-step RAFT polymerization using 4, 4′-azobis(4-cyano

pentanoic acid) (ACPA) as initiator and 2-(butylthiocarbonothioylthio)-2-methylpropanoic acid (BDMAT) as chain transfer agent for both blocks, and contains positively charged poly(aminoethyl methacrylate) P(AEMA) block along with a neutral comb like block poly(oligo(ethylene glycol) methyl ether acrylate) P(OEGMEA). The copolymer synthesized was at first characterized using Size Exclusion Chromatography with Multi-Angle Laser Light Scattering (SEC-MALLS) to collect information about the molecular weight and polydispersity index. Further, characterization using ^{1}H NMR and elemental analysis followed, in order to obtain the degree of polymerization of each block. P(OEGMEA)-*b*-P(AEMA) has the ability to electrostatically self-assemble with negatively charged polyelectrolytes (such as PAA and PSS) in aqueous medium under suitable pH forming well-defined micelles, by virtue of the positively charged P(AEMA) block.

Light and neutron scattering experiments were used to study the self-assembling character of P(OEGMEA)-*b*-P(AEMA) with oppositely charged micellization partners. The pH sensitive nature of the system was initially probed using light scattering and the results obtained were verified using neutron scattering measurements, varying the pH between 3 - 8. The formation of micelles was highly susceptible to pH variation, and the well-defined micelles were only found in the range 5 – 7 with an optimum value at pH = 6 in the case of $P(OEGMEA)_{21}$-*b*-$P(AEMA)_{32}$ and PAANa 5.1 kDa. Moving away from this optimal value led to the gradual dissociation of the micelles. Also, four different P(OEGMEA)-*b*-P(AEMA)/micellization partner systems were evaluated using SLS/DLS and SANS in order to evidence the role of the micellization agent used and the copolymer block length in the shape and size of the micelles formed. The scattering curves from SANS were fitted through the addition of two models; while the simple sphere or cylinder model corresponds to the micellar conformation, free polymer chain model is related to the

unmicellized polymer chains. Results show that P(OEGMEA)$_{21}$-*b*-P(AEMA)$_{32}$ & PAANa 5.1 kDa micelles are elongated structures at pH = 5 (while spherical species are obtained for the same system at pH = 6), while all the other systems studied exhibit spherical micelles with varying dimensions in the same conditions, proving that the micellization agent used and block length of the copolymer show significant impact on the shape and size of the species developed. Changing the polyelectrolyte from PAANa 5.1 kDa to PAANa 2.1 kDa while keeping the same copolymer P(OEGMEA)$_{21}$-*b*-P(AEMA)$_{32}$, the curvature of the self-assembled species increased significantly, causing a shift in the shape of the micelles from cylinder to sphere. This indicates that the length of the polyelectrolyte has a notable impact on the shape and size of the species developed. Similarly, upon changing the copolymer from P(OEGMEA)$_{21}$-*b*-P(AEMA)$_{32}$ to P(OEGMEA)$_{25}$-*b*-P(AEMA)$_{22}$ but using the same polyelectrolyte PAANa 2.1 kDa, the size of the species increases substantially even though the shape remains the same, hinting at the influence of the block ratio (P(OEGMEA)/P(AEMA)) on the species built. Further, studies were conducted to understand the impact of the chemical nature of the polyelectrolyte on the self-assembly. This was carried out by changing the polyelectrolyte to completely different PSSNa 1.1 kDa instead of PAANa (2.1 or 5.1 kDa) in presence of P(OEGMEA)$_{21}$-*b*-P(AEMA)$_{32}$. Interestingly, the micelles from PSS 1.1 kDa were significantly different both in term of shape and size compared to those made with PAANa 5.1 kDa; while PAANa 2.1 kDa-based micelles differed in size alone compared to PAANa 5.1 kDa-based micelles. SANS measurements were also carried out at different concentrations (1 – 5 wt%), for all systems, to study how sensitive the individual micellar shape and size are to species density in the solution. The concentration of the solution seems to influence the micellar dimension for some systems, while in others it showed no impact, suggesting that the effect of concentration on P(OEGMEA)-*b*-P(AEMA) self-assembly is contextual, varying with the system studied.

Depending on the dimension of the micelles made, the range and rate of inter-micellar interaction could vary significantly.

SUPPORTING INFORMATION

Normalized scattering intensity for all the polymer/micellization agent complexes investigated (light scattering); fitting parameters used for SANS curves (concentration series); SANS data of specific samples

ACKNOWLEDGMENTS

The authors would like to convey their genuine gratitude to the Physical Measurement Laboratory (Chemical Analysis Platform) at *Université de Montpellier*, France for the NMR and elemental analysis carried out. Also, the authors are very grateful to the Partnership for Soft Condensed Matter (PSCM) facilities at Grenoble, France for facilitating the preliminary characterization of the samples through light scattering experiments. This project has received funding from the European Union's Horizon 2020 research and innovation programme under the Marie Skłodowska-Curie grant agreement No 847439, through the InnovaXN scheme (Project XN2020-ILL30). SANS data obtained on D22 at ILL can be accessed under DOI: 10.5291/ILL-DATA.9-10-1760. This work benefited from the use of the SasView application, originally developed under NSF award DMR-0520547. SasView contains code developed with funding from the European Union's Horizon 2020 research and innovation programme under the SINE2020 project, grant agreement No 654000.

2.5. REFERENCES

(1) Corma, A. From Microporous to Mesoporous Molecular Sieve Materials and Their Use in Catalysis. *Chem. Rev.* **1997**, *97* (6), 2373–2420. https://doi.org/10.1021/cr960406n.

(2) Perego, C.; Millini, R. Porous Materials in Catalysis: Challenges for Mesoporous Materials. *Chem Soc Rev* **2013**, *42* (9), 3956–3976. https://doi.org/10.1039/C2CS35244C.

(3) Hartmann, M. Ordered Mesoporous Materials for Bioadsorption and Biocatalysis. *Chem. Mater.* **2005**, *17* (18), 4577–4593. https://doi.org/10.1021/cm0485658.

(4) Monson, P. A. Understanding Adsorption/Desorption Hysteresis for Fluids in Mesoporous Materials Using Simple Molecular Models and Classical Density Functional Theory. *Microporous Mesoporous Mater.* **2012**, *160*, 47–66. https://doi.org/10.1016/j.micromeso.2012.04.043.

(5) Sing, K. S. W. Adsorption Methods for the Characterization of Porous Materials. *Adv. Colloid Interface Sci.* **1998**, *76–77*, 3–11. https://doi.org/10.1016/S0001-8686(98)00038-4.

(6) Duan, L.; Wang, C.; Zhang, W.; Ma, B.; Deng, Y.; Li, W.; Zhao, D. Interfacial Assembly and Applications of Functional Mesoporous Materials. *Chem. Rev.* **2021**, *121* (23), 14349–14429. https://doi.org/10.1021/acs.chemrev.1c00236.

(7) Li, W.; Liu, J.; Zhao, D. Mesoporous Materials for Energy Conversion and Storage Devices. *Nat. Rev. Mater.* **2016**, *1* (6), 16023. https://doi.org/10.1038/natrevmats.2016.23.

(8) Vallet-Regí, M.; Schüth, F.; Lozano, D.; Colilla, M.; Manzano, M. Engineering Mesoporous Silica Nanoparticles for Drug Delivery: Where Are We after Two Decades? *Chem. Soc. Rev.* **2022**, *51* (13), 5365–5451. https://doi.org/10.1039/D1CS00659B.

(9) Yang, P.; Gai, S.; Lin, J. Functionalized Mesoporous Silica Materials for Controlled Drug Delivery. *Chem. Soc. Rev.* **2012**, *41* (9), 3679. https://doi.org/10.1039/c2cs15308d.

(10) Cai, Z.; Zhang, H.; Wei, Y.; Cong, F. Hyaluronan-Inorganic Nanohybrid Materials for Biomedical Applications. *Biomacromolecules* **2017**, *18* (6), 1677–1696. https://doi.org/10.1021/acs.biomac.7b00424.

(11) Gérardin, C.; Reboul, J.; Bonne, M.; Lebeau, B. Ecodesign of Ordered Mesoporous Silica Materials. *Chem. Soc. Rev.* **2013**, *42* (9), 4217. https://doi.org/10.1039/c3cs35451b.

(12) Ciesla, U.; Schüth, F. Ordered Mesoporous Materials. *Microporous Mesoporous Mater.* **1999**, *27* (2–3), 131–149. https://doi.org/10.1016/S1387-1811(98)00249-2.

(13) Velev, O. D.; Jede, T. A.; Lobo, R. F.; Lenhoff, A. M. Porous Silica via Colloidal Crystallization. *Nature* **1997**, *389* (6650), 447–448. https://doi.org/10.1038/38921.

(14) Stein, A.; Wang, Z.; Fierke, M. A. Functionalization of Porous Carbon Materials with Designed Pore Architecture. *Adv. Mater.* **2009**, *21* (3), 265–293. https://doi.org/10.1002/adma.200801492.

(15) Athens, G. L.; Shayib, R. M.; Chmelka, B. F. Functionalization of Mesostructured Inorganic–Organic and Porous Inorganic Materials. *Curr. Opin. Colloid Interface Sci.* **2009**, *14* (4), 281–292. https://doi.org/10.1016/j.cocis.2009.05.012.

(16) Park, M.; Komarneni, S. Stepwise Functionalization of Mesoporous Crystalline Silica Materials. *Microporous Mesoporous Mater.* **1998**, *25* (1–3), 75–80. https://doi.org/10.1016/S1387-1811(98)00173-5.

(17) Da'na, E. Adsorption of Heavy Metals on Functionalized-Mesoporous Silica: A Review. *Microporous Mesoporous Mater.* **2017**, *247*, 145–157. https://doi.org/10.1016/j.micromeso.2017.03.050.

(18) Soltani, S.; Khanian, N.; Rashid, U.; Yaw Choong, T. S. Fundamentals and Recent Progress Relating to the Fabrication, Functionalization and Characterization of Mesostructured Materials Using Diverse Synthetic Methodologies. *RSC Adv.* **2020**, *10* (28), 16431–16456. https://doi.org/10.1039/D0RA00440E.

(19) Valtchev, V.; Tosheva, L. Porous Nanosized Particles: Preparation, Properties, and Applications. *Chem. Rev.* **2013**, *113* (8), 6734–6760. https://doi.org/10.1021/cr300439k.

(20) Gottuso, A.; Armetta, F.; Cataldo, A.; Nardo, V. M.; Parrino, F.; Saladino, M. L. Functionalization of Mesoporous Silica Nanoparticles through One-Pot Co-Condensation in w/o Emulsion. *Microporous Mesoporous Mater.* **2022**, *335*, 111833. https://doi.org/10.1016/j.micromeso.2022.111833.

(21) Maria Chong, A. S.; Zhao, X. S.; Kustedjo, A. T.; Qiao, S. Z. Functionalization of Large-Pore Mesoporous Silicas with Organosilanes by Direct Synthesis. *Microporous Mesoporous Mater.* **2004**, *72* (1–3), 33–42. https://doi.org/10.1016/j.micromeso.2004.04.015.

(22) Huh, S.; Wiench, J. W.; Yoo, J.-C.; Pruski, M.; Lin, V. S.-Y. Organic Functionalization and Morphology Control of Mesoporous Silicas via a Co-Condensation Synthesis Method. *Chem. Mater.* **2003**, *15* (22), 4247–4256. https://doi.org/10.1021/cm0210041.

(23) Brunelli, N. A.; Venkatasubbaiah, K.; Jones, C. W. Cooperative Catalysis with Acid–Base Bifunctional Mesoporous Silica: Impact of Grafting and Co-Condensation Synthesis Methods on Material Structure and Catalytic Properties. *Chem. Mater.* **2012**, *24* (13), 2433–2442. https://doi.org/10.1021/cm300753z.

(24) Richard, J.; Phimphachanh, A.; Jamet-Fournier, A.; Cacciaguerra, T.; Dieudonné-George, P.; Cot, D.; Destarac, M.; Lacroix-Desmazes, P.; In, M.; Marcotte, N.; Gérardin, C. Dual Control of External Surface and Internal Pore Structure of Small Ordered Mesoporous Silica Particles Directed by Mixed Polyion Complex Micelles. *Microporous Mesoporous Mater.* **2022**, *338*, 111915. https://doi.org/10.1016/j.micromeso.2022.111915.

(25) Baccile, N.; Reboul, J.; Blanc, B.; Coq, B.; Lacroix-Desmazes, P.; In, M.; Gérardin, C. Ecodesign of Ordered Mesoporous Materials Obtained with Switchable Micellar Assemblies. *Angew. Chem.* **2008**, *120* (44), 8561–8565. https://doi.org/10.1002/ange.200802431.

(26) Yang, X.-Y.; Chen, L.-H.; Li, Y.; Rooke, J. C.; Sanchez, C.; Su, B.-L. Hierarchically Porous Materials: Synthesis Strategies and Structure Design. *Chem. Soc. Rev.* **2017**, *46* (2), 481–558. https://doi.org/10.1039/C6CS00829A.

(27) Molina, E.; Mathonnat, M.; Richard, J.; Lacroix-Desmazes, P.; In, M.; Dieudonné, P.; Cacciaguerra, T.; Gérardin, C.; Marcotte, N. pH-Mediated Control over the Mesostructure of Ordered Mesoporous Materials Templated by Polyion Complex Micelles. *Beilstein J. Nanotechnol.* **2019**, *10*, 144–156. https://doi.org/10.3762/bjnano.10.14.

(28) Bathfield, M.; Reboul, J.; Cacciaguerra, T.; Lacroix-Desmazes, P.; Gérardin, C. Thermosensitive and Drug-Loaded Ordered Mesoporous Silica: A Direct and Effective Synthesis Using PEO- *b* -PNIPAM Block Copolymers. *Chem. Mater.* **2016**, *28* (10), 3374–3384. https://doi.org/10.1021/acs.chemmater.6b00595.

(29) Di, A.; Schmitt, J.; Da Silva, M. A.; Hossain, K. M. Z.; Mahmoudi, N.; Errington, R. J.; Edler, K. J. Self-Assembly of Amphiphilic Polyoxometalates for the Preparation of Mesoporous Polyoxometalate-Titania Catalysts. *Nanoscale* **2020**, *12* (43), 22245–22257. https://doi.org/10.1039/D0NR05967F.

(30) Kim, S.; Bellouard, C.; Pasc, A.; Lamouroux, E.; Blin, J.-L.; Carteret, C.; Fort, Y.; Emo, M.; Durand, P.; Stébé, M.-J. Nanoparticle-Free Magnetic Mesoporous Silica with Magneto-Responsive Surfactants. *J. Mater. Chem. C* **2013**, *1* (42), 6930. https://doi.org/10.1039/c3tc31617c.

(31) Bastakoti, B. P.; Li, Y.; Miyamoto, N.; Sanchez-Ballester, N. M.; Abe, H.; Ye, J.; Srinivasu, P.; Yamauchi, Y. Polymeric Micelle Assembly for the Direct Synthesis of Functionalized Mesoporous Silica with Fully Accessible Pt Nanoparticles toward an Improved CO Oxidation Reaction. *Chem Commun* **2014**, *50* (65), 9101–9104. https://doi.org/10.1039/C4CC02556C.

(32) Li, C.; Li, Q.; Kaneti, Y. V.; Hou, D.; Yamauchi, Y.; Mai, Y. Self-Assembly of Block Copolymers towards Mesoporous Materials for Energy Storage and Conversion Systems. *Chem. Soc. Rev.* **2020**, *49* (14), 4681–4736. https://doi.org/10.1039/D0CS00021C.

(33) Witecka, A.; Schmitt, J.; Courtien, M.; Gérardin, C.; Rydzek, G. Hybrid Mesoporous Silica Materials Templated with Surfactant Polyion Complex (SPIC) Micelles for pH-Triggered Drug Release. *Microporous Mesoporous Mater.* **2024**, *365*, 112913. https://doi.org/10.1016/j.micromeso.2023.112913.

(34) Li, Y.; Bastakoti, B. P.; Malgras, V.; Li, C.; Tang, J.; Kim, J. H.; Yamauchi, Y. Polymeric Micelle Assembly for the Smart Synthesis of Mesoporous Platinum Nanospheres with Tunable Pore Sizes. *Angew. Chem. Int. Ed.* **2015**, *54* (38), 11073–11077. https://doi.org/10.1002/anie.201505232.

(35) Boudier, A.; Aubert-Pouëssel, A.; Gérardin, C.; Devoisselle, J.-M.; Bégu, S. pH-Sensitive Double-Hydrophilic Block Copolymer Micelles for Biological Applications. *Int. J. Pharm.* **2009**, *379* (2), 212–217. https://doi.org/10.1016/j.ijpharm.2009.05.032.

(36) Bathfield, M.; Warnant, J.; Gérardin, C.; Lacroix-Desmazes, P. Asymmetric Neutral, Cationic and Anionic PEO-Based Double-Hydrophilic Block Copolymers (DHBCs): Synthesis and Reversible Micellization Triggered by Temperature or pH. *Polym. Chem.* **2015**, *6* (8), 1339–1349. https://doi.org/10.1039/C4PY01502A.

(37) Khimani, M.; Patel, H.; Patel, V.; Parekh, P.; Vekariya, R. L. Self-Assembly of Stimuli-Responsive Block Copolymers in Aqueous Solutions: An Overview. *Polym. Bull.* **2020**, *77* (11), 5783–5810. https://doi.org/10.1007/s00289-019-03046-w.

(38) Hoogenboom, R.; Rogers, S.; Can, A.; Becer, C. R.; Guerrero-Sanchez, C.; Wouters, D.; Hoeppener, S.; Schubert, U. S. Self-Assembly of Double Hydrophobic Block Copolymers in Water–Ethanol Mixtures: From Micelles to Thermoresponsive Micellar Gels. *Chem. Commun.* **2009**, No. 37, 5582. https://doi.org/10.1039/b911858f.

(39) Richard, J.; Phimphachanh, A.; Schneider, J.; Nandi, S.; Laurent, E.; Lacroix-Desmazes, P.; Trens, P.; Devautour-Vinot, S.; Marcotte, N.; Gérardin, C. Integrated Process for Structuring

and Functionalizing Ordered Mesoporous Silica to Achieve Superprotonic Conductivity. *Chem. Mater.* **2022**, *34* (17), 7828–7836. https://doi.org/10.1021/acs.chemmater.2c01352.

(40) Warnant, J.; Reboul, J.; Aqil, A.; Cacciaguerra, T.; Jerome, C.; Gerardin, C. Nanostructured Silica Templated by Double Hydrophilic Block Copolymers with a Comb-like Architecture. *Powder Technol.* **2011**, *208* (2), 461–466. https://doi.org/10.1016/j.powtec.2010.08.043.

(41) Molina, E.; Warnant, J.; Mathonnat, M.; Bathfield, M.; In, M.; Laurencin, D.; Jérôme, C.; Lacroix-Desmazes, P.; Marcotte, N.; Gérardin, C. Drug–Polymer Electrostatic Complexes as New Structuring Agents for the Formation of Drug-Loaded Ordered Mesoporous Silica. *Langmuir* **2015**, *31* (47), 12839–12844. https://doi.org/10.1021/acs.langmuir.5b03221.

(42) Harada, A.; Kataoka, K. Novel Polyion Complex Micelles Entrapping Enzyme Molecules in the Core: Preparation of Narrowly-Distributed Micelles from Lysozyme and Poly(Ethylene Glycol)−Poly(Aspartic Acid) Block Copolymer in Aqueous Medium. *Macromolecules* **1998**, *31* (2), 288–294. https://doi.org/10.1021/ma971277v.

(43) El Jundi, A.; Buwalda, S. J.; Bakkour, Y.; Garric, X.; Nottelet, B. Double Hydrophilic Block Copolymers Self-Assemblies in Biomedical Applications. *Adv. Colloid Interface Sci.* **2020**, *283*, 102213. https://doi.org/10.1016/j.cis.2020.102213.

(44) Wibowo, A.; Osada, K.; Matsuda, H.; Anraku, Y.; Hirose, H.; Kishimura, A.; Kataoka, K. Morphology Control in Water of Polyion Complex Nanoarchitectures of Double-Hydrophilic Charged Block Copolymers through Composition Tuning and Thermal Treatment. *Macromolecules* **2014**, *47* (9), 3086–3092. https://doi.org/10.1021/ma500314d.

(45) Reboul, J.; Nugay, T.; Anik, N.; Cottet, H.; Ponsinet, V.; In, M.; Lacroix-Desmazes, P.; Gérardin, C. Synthesis of Double Hydrophilic Block Copolymers and Induced Assembly with Oligochitosan for the Preparation of Polyion Complex Micelles. *Soft Matter* **2011**, *7* (12), 5836. https://doi.org/10.1039/c1sm05230f.

(46) Gou, K.; Wang, Y.; Guo, X.; Wang, Y.; Bian, Y.; Zhao, H.; Guo, Y.; Pang, Y.; Xie, L.; Li, S.; Li, H. Carboxyl-Functionalized Mesoporous Silica Nanoparticles for the Controlled Delivery of Poorly Water-Soluble Non-Steroidal Anti-Inflammatory Drugs. *Acta Biomater.* **2021**, *134*, 576–592. https://doi.org/10.1016/j.actbio.2021.07.023.

(47) Xie, M.; Shi, H.; Ma, K.; Shen, H.; Li, B.; Shen, S.; Wang, X.; Jin, Y. Hybrid Nanoparticles for Drug Delivery and Bioimaging: Mesoporous Silica Nanoparticles Functionalized with

Carboxyl Groups and a near-Infrared Fluorescent Dye. *J. Colloid Interface Sci.* **2013**, *395*, 306–314. https://doi.org/10.1016/j.jcis.2013.01.001.

(48) Tsai, C.-H.; Chang, W.-C.; Saikia, D.; Wu, C.-E.; Kao, H.-M. Functionalization of Cubic Mesoporous Silica SBA-16 with Carboxylic Acid via One-Pot Synthesis Route for Effective Removal of Cationic Dyes. *J. Hazard. Mater.* **2016**, *309*, 236–248. https://doi.org/10.1016/j.jhazmat.2015.08.051.

(49) Chang, W.-C.; Deka, J. R.; Wu, H.-Y.; Shieh, F.-K.; Huang, S.-Y.; Kao, H.-M. Synthesis and Characterization of Large Pore Cubic Mesoporous Silicas Functionalized with High Contents of Carboxylic Acid Groups and Their Use as Adsorbents. *Appl. Catal. B Environ.* **2013**, *142–143*, 817–827. https://doi.org/10.1016/j.apcatb.2013.06.018.

(50) Yang, Q.; Liu, J.; Yang, J.; Kapoor, M. P.; Inagaki, S.; Li, C. Synthesis, Characterization, and Catalytic Activity of Sulfonic Acid-Functionalized Periodic Mesoporous Organosilicas. *J. Catal.* **2004**, *228* (2), 265–272. https://doi.org/10.1016/j.jcat.2004.09.007.

(51) Singh, S.; Kumar, A.; Nebhani, L.; Hazra, C. K. Sustainable Sulfonic Acid Functionalized Tubular Shape Mesoporous Silica as a Heterogeneous Catalyst for Selective Unsymmetrical Friedel–Crafts Alkylation in One Pot. *JACS Au* **2023**, *3* (12), 3400–3411. https://doi.org/10.1021/jacsau.3c00563.

(52) Marschall, R.; Rathouský, J.; Wark, M. Ordered Functionalized Silica Materials with High Proton Conductivity. *Chem. Mater.* **2007**, *19* (26), 6401–6407. https://doi.org/10.1021/cm071164i.

(53) Furtmair, M.; Timm, J.; Marschall, R. Sulfonation of Porous Materials and Their Proton Conductivity. *Microporous Mesoporous Mater.* **2021**, *312*, 110745. https://doi.org/10.1016/j.micromeso.2020.110745.

(54) Wang, J.; Feng, X.; Wen, S.; Zhan, D.; Zhu, X.; Ning, P.; Zhang, Y.; Mei, X. Recent Advances in Amine-Functionalized Silica Adsorbents for CO2 Capture. *Renew. Sustain. Energy Rev.* **2024**, *203*, 114724. https://doi.org/10.1016/j.rser.2024.114724.

(55) Dutcher, B.; Fan, M.; Russell, A. G. Amine-Based CO_2 Capture Technology Development from the Beginning of 2013—A Review. *ACS Appl. Mater. Interfaces* **2015**, *7* (4), 2137–2148. https://doi.org/10.1021/am507465f.

(56) Zhang, R.; Wang, X.; Liu, S.; He, L.; Song, C.; Jiang, X.; Blach, T. P. Discovering Inherent Characteristics of Polyethylenimine-Functionalized Porous Materials for CO_2 Capture. *ACS*

Appl. Mater. Interfaces **2019**, *11* (40), 36515–36524. https://doi.org/10.1021/acsami.9b08496.

(57) Terra, J. C. S.; Moores, A.; Moura, F. C. C. Amine-Functionalized Mesoporous Silica as a Support for on-Demand Release of Copper in the A^3 -Coupling Reaction: Ultralow Concentration Catalysis and Confinement Effect. *ACS Sustain. Chem. Eng.* **2019**, *7* (9), 8696–8705. https://doi.org/10.1021/acssuschemeng.9b00576.

(58) Yokoi, T.; Kubota, Y.; Tatsumi, T. Amino-Functionalized Mesoporous Silica as Base Catalyst and Adsorbent. *Appl. Catal. Gen.* **2012**, *421–422*, 14–37. https://doi.org/10.1016/j.apcata.2012.02.004.

(59) Aguado, J.; Arsuaga, J. M.; Arencibia, A.; Lindo, M.; Gascón, V. Aqueous Heavy Metals Removal by Adsorption on Amine-Functionalized Mesoporous Silica. *J. Hazard. Mater.* **2009**, *163* (1), 213–221. https://doi.org/10.1016/j.jhazmat.2008.06.080.

(60) Nayab, S.; Farrukh, A.; Oluz, Z.; Tuncel, E.; Tariq, S. R.; Rahman, H. U.; Kirchhoff, K.; Duran, H.; Yameen, B. Design and Fabrication of Branched Polyamine Functionalized Mesoporous Silica: An Efficient Absorbent for Water Remediation. *ACS Appl. Mater. Interfaces* **2014**, *6* (6), 4408–4417. https://doi.org/10.1021/am500123k.

(61) Wu, L.; Sun, J.; Lv, Z.; Chen, Y. In-Situ Preparation of Poly(Ether Imide)/Amino Functionalized Silica Mixed Matrix Membranes for Application in Enzyme Separation. *Mater. Des.* **2016**, *92*, 610–620. https://doi.org/10.1016/j.matdes.2015.12.108.

(62) Bagheri, E.; Ansari, L.; Abnous, K.; Taghdisi, S. M.; Charbgoo, F.; Ramezani, M.; Alibolandi, M. Silica Based Hybrid Materials for Drug Delivery and Bioimaging. *J. Controlled Release* **2018**, *277*, 57–76. https://doi.org/10.1016/j.jconrel.2018.03.014.

(63) Hu, J.; Zhang, G.; Ge, Z.; Liu, S. Stimuli-Responsive Tertiary Amine Methacrylate-Based Block Copolymers: Synthesis, Supramolecular Self-Assembly and Functional Applications. *Prog. Polym. Sci.* **2014**, *39* (6), 1096–1143. https://doi.org/10.1016/j.progpolymsci.2013.10.006.

(64) Lin, C.; Zhong, Z.; Lok, M. C.; Jiang, X.; Hennink, W. E.; Feijen, J.; Engbersen, J. F. J. Random and Block Copolymers of Bioreducible Poly(Amido Amine)s with High- and Low-Basicity Amino Groups: Study of DNA Condensation and Buffer Capacity on Gene Transfection. *J. Controlled Release* **2007**, *123* (1), 67–75. https://doi.org/10.1016/j.jconrel.2007.07.006.

(65) Mafra, L.; Čendak, T.; Schneider, S.; Wiper, P. V.; Pires, J.; Gomes, J. R. B.; Pinto, M. L. Amine Functionalized Porous Silica for CO2/CH4 Separation by Adsorption: Which Amine and Why. *Chem. Eng. J.* **2018**, *336*, 612–621. https://doi.org/10.1016/j.cej.2017.12.061.

(66) Ahmed, S.; Ramli, A.; Yusup, S. CO 2 Adsorption Study on Primary, Secondary and Tertiary Amine Functionalized Si-MCM-41. *Int. J. Greenh. Gas Control* **2016**, *51*, 230–238. https://doi.org/10.1016/j.ijggc.2016.05.021.

(67) Alidedeoglu, A. H.; York, A. W.; McCormick, C. L.; Morgan, S. E. Aqueous RAFT Polymerization of 2-aminoethyl Methacrylate to Produce Well-defined, Primary Amine Functional Homo- and Copolymers. *J. Polym. Sci. Part Polym. Chem.* **2009**, *47* (20), 5405–5415. https://doi.org/10.1002/pola.23590.

(68) Cheng, Q.; Huang, Y.; Zheng, H.; Wei, T.; Zheng, S.; Huo, S.; Wang, X.; Du, Q.; Zhang, X.; Zhang, H.-Y.; Liang, X.-J.; Wang, C.; Tang, R.; Liang, Z. The Effect of Guanidinylation of PEGylated Poly(2-Aminoethyl Methacrylate) on the Systemic Delivery of siRNA. *Biomaterials* **2013**, *34* (12), 3120–3131. https://doi.org/10.1016/j.biomaterials.2013.01.043.

(69) Bray, C.; Peltier, R.; Kim, H.; Mastrangelo, A.; Perrier, S. Anionic Multiblock Core Cross-Linked Star Copolymers via RAFT Polymerization. *Polym. Chem.* **2017**, *8* (36), 5513–5524. https://doi.org/10.1039/C7PY01062A.

(70) Lowe, A. B.; McCormick, C. L. Reversible Addition–Fragmentation Chain Transfer (RAFT) Radical Polymerization and the Synthesis of Water-Soluble (Co)Polymers under Homogeneous Conditions in Organic and Aqueous Media. *Prog. Polym. Sci.* **2007**, *32* (3), 283–351. https://doi.org/10.1016/j.progpolymsci.2006.11.003.

(71) Provencher, S. W. A Constrained Regularization Method for Inverting Data Represented by Linear Algebraic or Integral Equations. *Comput. Phys. Commun.* **1982**, *27* (3), 213–227. https://doi.org/10.1016/0010-4655(82)90173-4.

(72) Provencher, S. W. CONTIN: A General Purpose Constrained Regularization Program for Inverting Noisy Linear Algebraic and Integral Equations. *Comput. Phys. Commun.* **1982**, *27* (3), 229–242. https://doi.org/10.1016/0010-4655(82)90174-6.

(73) Akcasu, A.; Benmouna, M.; Han, C. Interpretation of Dynamic Scattering from Polymer Solutions. *Polymer* **1980**, *21* (8), 866–890. https://doi.org/10.1016/0032-3861(80)90242-6.

(74) Schweins, R.; Hollmann, J.; Huber, K. Dilute Solution Behaviour of Sodium Polyacrylate Chains in Aqueous NaCl Solutions. *Polymer* **2003**, *44* (23), 7131–7141. https://doi.org/10.1016/j.polymer.2003.07.005.

(75) Schweins, R.; Lindner, P.; Huber, K. Calcium Induced Shrinking of NaPA Chains: A SANS Investigation of Single Chain Behavior. *Macromolecules* **2003**, *36* (25), 9564–9573. https://doi.org/10.1021/ma0347722.

(76) Burchard, W. Static and Dynamic Light Scattering from Branched Polymers and Biopolymers. In *Light Scattering from Polymers*; Advances in Polymer Science; Springer Berlin Heidelberg: Berlin, Heidelberg, 1983; Vol. 48, pp 1–124. https://doi.org/10.1007/3-540-12030-0_1.

(77) Krężel, A.; Bal, W. A Formula for Correlating p K a Values Determined in D 2 O and H 2 O. *J. Inorg. Biochem.* **2004**, *98* (1), 161–166. https://doi.org/10.1016/j.jinorgbio.2003.10.001.

(78) Dewhurst, C. D. Graphical Reduction and Analysis Small-Angle Neutron Scattering Program: *GRASP*. *J. Appl. Crystallogr.* **2023**, *56* (5), 1595–1609. https://doi.org/10.1107/S1600576723007379.

(79) Guinier, A. *Small-Angle Scattering of X-rays; Wiley: New York, 1955*.

(80) Pedersen, J. S. Analysis of Small-Angle Scattering Data from Colloids and Polymer Solutions: Modeling and Least-Squares Fitting. *Adv. Colloid Interface Sci.* **1997**, *70*, 171–210. https://doi.org/10.1016/S0001-8686(97)00312-6.

(81) Onsager, L. The Effects of Shape on the Interaction of Colloidal Particles. *Ann. N. Y. Acad. Sci.* **1949**, *51* (4), 627–659. https://doi.org/10.1111/j.1749-6632.1949.tb27296.x.

(82) Hammouda, B. SANS from Homogeneous Polymer Mixtures: A Unified Overview. In *Polymer Characteristics*; Advances in Polymer Science; Springer-Verlag: Berlin/Heidelberg, 1993; Vol. 106, pp 87–133. https://doi.org/10.1007/BFb0025862.

(83) Warnant, J.; Marcotte, N.; Reboul, J.; Layrac, G.; Aqil, A.; Jerôme, C.; Lerner, D. A.; Gérardin, C. Physicochemical Properties of pH-Controlled Polyion Complex (PIC) Micelles of Poly(Acrylic Acid)-Based Double Hydrophilic Block Copolymers and Various Polyamines. *Anal. Bioanal. Chem.* **2012**, *403* (5), 1395–1404. https://doi.org/10.1007/s00216-012-5947-1.

(84) Houssein, D.; Warnant, J.; Molina, E.; Cacciaguerra, T.; Gérardin, C.; Marcotte, N. Mesoporous Silica Templated by Polyion Complex Micelles: A Versatile Approach for Controlling the Mesostructure. *Microporous Mesoporous Mater.* **2017**, *239*, 244–252. https://doi.org/10.1016/j.micromeso.2016.10.013.

(85) Schwiertz, D.; Angelina, J.; Zhang, H.; Barz, M. Miktoarm Star-Polypept(o)Ide-Based Polyion Complex Micelles for the Delivery of Large Nucleic Acids. *Biomacromolecules* **2024**, *25* (10), 6539–6554. https://doi.org/10.1021/acs.biomac.4c00695.

(86) Améndola, I. F.; Velasco, M. I.; Acosta, R. H.; Soler Illia, G. J. A. A.; Contreras, C. B. Smart Hybrid Copolymer-Coated Silica Nanosystems with Dual Responsiveness as a Carrier for Positive Charged Molecules. *Eur. Polym. J.* **2024**, *204*, 112717. https://doi.org/10.1016/j.eurpolymj.2023.112717.

(87) Thompson, K. L.; Read, E. S.; Armes, S. P. Chemical Degradation of Poly(2-Aminoethyl Methacrylate). *Polym. Degrad. Stab.* **2008**, *93* (8), 1460–1466. https://doi.org/10.1016/j.polymdegradstab.2008.05.013.

(88) Dickhaus, B. N.; Priefer, R. Determination of Polyelectrolyte pKa Values Using Surface-to-Air Tension Measurements. *Colloids Surf. Physicochem. Eng. Asp.* **2016**, *488*, 15–19. https://doi.org/10.1016/j.colsurfa.2015.10.015.

(89) Dong, H.; Du, H.; Wickramasinghe, S. R.; Qian, X. The Effects of Chemical Substitution and Polymerization on the p K_a Values of Sulfonic Acids. *J. Phys. Chem. B* **2009**, *113* (43), 14094–14101. https://doi.org/10.1021/jp906087c.

CHAPTER 3

Self-assembly of oppositely charged double hydrophilic block copolymers, tailoring the shape of the micelles

Ananthapadmanabhan Unnikrishnan,[1,2] Najet Mahmoudi,[3] William Chèvremont,[4] Gaulthier Rydzek,[2] Julien Schmitt,[2,5] Ralf Schweins[1] and Corine Gérardin[2]

[1] Institut Laue − Langevin, DS / LSS Group, 71 Avenue des Martyrs, CS 20156, Grenoble Cedex 9, F-38042, France

[2] Institut Charles Gerhardt, UMR 5253, CNRS-ENSCM-UM, University of Montpellier, Cedex, F-34295, France

[3] ISIS Neutron and Muon Source, Science and Technology Facilities Council, Rutherford Appleton Laboratory, Didcot OX11 0QX, United Kingdom

[4] ESRF, The European Synchrotron, 71 Avenue des Martyrs, Grenoble, 38043, France

[5] LSFC – Laboratoire de Synthèse et Fonctionnalisation des Céramiques, UMR 3080 CNRS/Saint-Gobain CREE, Saint-Gobain Research Provence, 550 Avenue Alphonse Jauffret, Cavaillon, France

3.1. INTRODUCTION

Block copolymers are a specific class of polymers, composed of distinct blocks with specific chemical nature, and have attracted keen attention in the recent past as structuring agents for building self-assembled nanostructures.[1–5] Due to the difference in hydrophilicity between the blocks, most exhibit an amphiphilic character, an attribute that could initiate their spontaneous self-assembly into micelles, vesicles or micro-phase separated matrices in solution if the chemical nature and length of each block in the copolymer is carefully refined.[5–8] A specific category of block copolymer is the double hydrophilic block copolymers (DHBCs), notable for their total hydrophilic nature.[9,10] Although they naturally lack an amphiphilic behaviour, some DHBCs can also self-assemble in reaction to external stimuli such as pH, ionic strength, temperature and nature of the solvent added.[10–15] The role of the stimulus is to induce an amphiphilic character to the copolymer by specifically reducing the hydrophilicity of one particular block while the other remains unaltered, making well-defined core-shell structures. Even though amphiphilicity driven self-assembly is the most conventional approach among DHBCs, ionic DHBCs, with one neutral block and one charged block, can also self-assemble through electrostatic complexation with entities (polyelectrolytes or metal ions) of opposite charge under specific conditions.[16–20] These nanostructures find applications in a wide range of domains including materials synthesis,[20,21] and medicine[22,23]. Among them, controlled material synthesis holds special significance since the properties of a material, including its mechanical and chemical character are tuned by its shape and structure.[24–26]

Through careful manipulation of the blocks, researchers have been able to develop DHBCs that act both as structuring and functionalization agents for the formation of ordered and chemically stable functional mesoporous silica materials. The introduced functionalities such as -COOH or

-SO_3H, are situated in the charged block of the DHBC-based templates, allowing their use in a large range of applications including super-protonic conductivity,[27] and drug delivery[28,29].

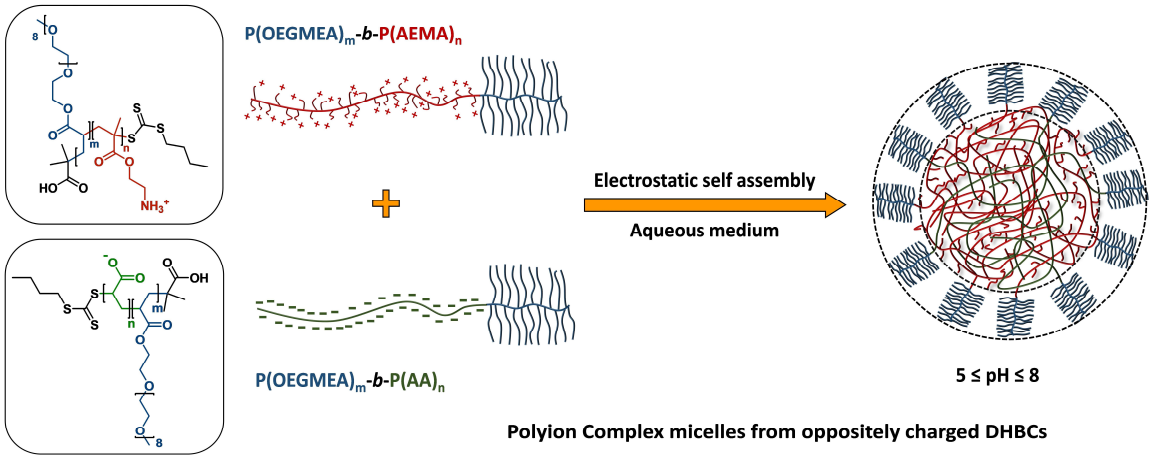
These DHBC-based micelles obtained by electrostatic complexation can be classified based on the complexation partner used. While Hybrid polyion complex (HPIC)[30–32] micelles use metal ions as the complexation partners, Polyion complex (PIC)[20,33] micelles are formed with polyelectrolytes. Polyion Complex (PIC) micelles, using a polyelectrolyte as complexation partner, are one of the most studied.[20,34–37] They find application in various domains including biosensors,[38] preparation of magnetic resonance imaging agents,[39] and drug delivery[40,41] due to their versatility in dimension and shape.[42–44] Among the PIC micelles built till date, micelles from negatively charged polyacid-based DHBCs, prepared by combining the copolymers electrostatically with different positively charged homopolymers, have been studied extensively.[45–47] Surprisingly, only a limited number of PIC micelles have been made using DHBCs containing cationic functionalities instead of anionic units: in most cases, these cationic DHBCs are made from either secondary, tertiary or quaternary functional groups of amine, such as poly(ethylenimine) PEI, poly(3-(methacrylamido)propyl)trimethylammonium chloride PMAPTAC, and poly(di-methylaminoethyl methacrylate) PAMA.[48–51] Making cationic DHBCs made of primary amine functions, with the potential to form PIC micelles, is still largely lacking; only a few examples are given in the literature.[50,52] The ability of primary amine DHBCs to form PIC micelles with gene, and also with other similar compounds have found them application as biological carrier systems, even though only a few of them are known. Previously, we have developed the synthesis of a DHBC bearing primary amines via simple RAFT polymerization and labelled $P(OEGMEA)_m$-*b*-$P(AEMA)_n$, made of a neutral poly(ethyleneoxidepolyacrylate) P(OEGMEA) block and a positively charged aminoethyl methacrylate P(AEMA) block (see *Chapter 2*).

Combining two DHBCs of opposite charges to build PIC micelles instead of using a complexation agent make self-assemblies with greater potential for functionalization and also helps in improving the stability of the species formed.[18,53,54] Similar to the addition of a complexation partner, the DHBC combination results in the efficient charge neutralization of the two charged blocks, resulting in a spontaneous micellization into core-shell structures with narrow size distribution, if appropriate block lengths are chosen in the copolymers used.[18] The hydrophilic block of the copolymers, in particular, has a pivotal role in the formation of a stable well-defined population, acting as a protective layer against random micellar aggregation followed by sedimentation.[55,56] In PIC micelles composed of oppositely charged DHBCs, the micellar corona is made of hydrophilic components of both DHBCs, offering higher stability when compared to self-assemblies with other complexation partners namely, homopolymers or multivalent metal-ions. Literature proves linear poly(ethylene glycol) to be the most widely used non-ionic hydrophilic block in the preparation of PIC micelles,[38,56,57] although alternatives including poly(N-isopropylacrylamide),[58] poly(N,N-dimethylacrylamide),[59] poly(poly(ethylene oxide) methyl ether methacrylate,[55] poly(acrylamide)[60] and poly(2-isopropyl-2-oxazoline)[61] are also reported. Combining two hydrophilic blocks unfolds greater opportunities for functional and structural optimization of the corona in the PIC micelles along with a higher stability.[62–65] Integrating identical hydrophilic blocks or two with different structures but with superior compatibility, ensures formation of a uniform corona, whereas limited affinity leads to phase separation and asymmetric structures.[65] Also, through a careful choice of hydrophilic blocks with distinct characters such as environmental responsiveness and biocompatibility, multiple functionalities could be introduced into the surface layer of the same self-assembly.[62] Forming PIC micelles using cationic and anionic DHBCs with branched hydrophilic block instead of linear framework, is also an interesting step forward. The difference

in architecture and length of the DHBCs has been found to affect the chain packing and, hence the morphology of the PIC micelles formed.[66–69] However, this effect of branching has not been reported for PIC micelles from oppositely charged comb-like DHBCs, and justify interest. A key aspect to characterize these PIC micelles is to do a careful analysis of their shape and aggregation using small angle scattering techniques.

In the present study, we report the formulation and characterization of a new fully DHBC based PIC micelle, prepared by combining the amine rich double hydrophilic block copolymer, $P(OEGMEA)_m$-*b*-$P(AEMA)_n$ described in *Chapter 2* with another double hydrophilic block copolymer containing carbonyl group from a poly(acrylic acid) P(AA) block, namely $P(OEGMEA)_m$-*b*-$P(AA)_n$ presented in *Chapter 1*.[20] Both $P(OEGMEA)_m$-*b*-$P(AEMA)_n$ and $P(OEGMEA)_m$-*b*-$P(AA)_n$, were synthesized through Reversible Addition Fragmentation Chain Transfer (RAFT) polymerization. The positively charged amine entities of the $P(OEGMEA)_m$-*b*-$P(AEMA)_n$ copolymer can electrostatically interact with the negatively charged carbonyl group of $P(OEGMEA)_m$-*b*-$P(AA)_n$ building well-defined objects **(Scheme 1)**. While the charged blocks (P(AA) and P(AEMA)) exhibit a linear nature, the neutral P(OEGMEA) block exhibits a comb-like architecture, which may impact the type of self-assembly they can form in solution. The copolymers synthesized were characterized using ^{1}H NMR and elemental analysis to acquire the degree of polymerization of each block and the self-assembled species were studied using light, neutron and X-ray scattering techniques. The ratio of charges between the two DHBCs (acid/amine = AA/NH_2) plays a critical role in the quality of self-assembly and hence was studied in detail using Small angle neutron and X-ray scattering (SANS/SAXS). Then, the effect of pH on the polymeric self-assembly was investigated in depth using light scattering (SLS/DLS) along with SANS, presenting the influence of acidic and alkaline environment on the structures developed.

Finally, the influence of DHBC block length in the shape and size of the polymeric structure was also investigated.



***Scheme 1**. General schematic representation of polyion complex micelles from oppositely charged DHBCs*

3.2. MATERIALS AND METHODS

3.2.1. Chemicals Used

Oligo(ethylene glycol) methyl ether acrylate (OEGMEA, 99%, M_n = 480 g/mol, 9 EO units on average), acrylic acid (AA, 99%, M_n = 72.06 g/mol), and 2-Aminoethyl methacrylate hydrochloride (AEMA, 90%, M_n = 165.62 g/mol), used in the polymer synthesis, were obtained from Sigma-Aldrich. Before every polymerization, the radical inhibitors were removed through adsorption using aluminum oxide purchased from Sigma-Aldrich. The initiator, 4,4′-azobis(4-cyano pentanoic acid) (ACPA, 98%) was also secured from Sigma-Aldrich whereas the chain transfer agent, 2-(butylthiocarbonothioylthio)-2-methylpropanoic acid (BDMAT) was synthesized according to already published protocol. All the chemical synthesis and sample preparations were carried out using Milli-Q water with a resistivity of 18.2 MΩ·cm at 25 °C. The pH of the samples was modified when required, using NaOH and HCl solutions (1M and 5M). The D_2O used for the

sample preparations in NMR, light scattering and small angle neutron scattering was also procured from Sigma-Aldrich.

3.2.2. P(OEGMEA)-*b*-P(AA) Synthesis

The DHBC Poly(oligoethylene glycol) methyl ether acrylate)-*b*-poly(acrylic acid) or P(OEGMEA)-*b*-P(AA), was synthesized through RAFT polymerization using oligo(ethylene glycol) methyl ether acrylate and acrylic acid as monomers for the first and second block respectively. The initiator and the chain transfer agent, used were 4,4′-azobis(4-cyano pentanoic acid) (ACPA) and 2-(butylthiocarbonothioylthio)-2-methylpropanoic acid (BDMAT) respectively. The protocol used is described in details in *Chapter 1 (Materials & Methods)*.

3.2.3. P(OEGMEA)-*b*-P(AEMA) Synthesis

DHBC poly(oligo(ethylene glycol) methyl ether acrylate)-*b*-poly(aminoethyl methacrylate) or P(OEGMEA)-*b*-P(AEMA) was also synthesized using RAFT polymerization with oligo(ethylene glycol) methyl ether acrylate and 2-aminoethyl methacrylate hydrochloride as monomers for the first and second block respectively. The initiator and chain transfer agent used were again 4,4′-azobis(4-cyano pentanoic acid) (ACPA) and 2-(butylthiocarbonothioylthio)-2-methylpropanoic acid (BDMAT) respectively. The synthesis protocol has been presented in detail in *Chapter 2 (Materials & Methods)*.

3.2.4. Sample Preparation

All sample preparations were carried out at room temperature. Since the micellar solutions were characterized through different techniques (light, neutron and X-ray scattering), the final concentration of the sample, and the solvent used varied accordingly. In neutron and light scattering, D_2O was used as the solvent, while in X-ray H_2O was the solvent used. Typically, in

neutron and X-ray scattering the samples prepared were at 1 wt%, with respect to P(OEGMEA)-*b*-P(AEMA) while in light scattering it was 0.1 wt%, unless stated otherwise. Keeping the above differences aside, the following procedure for sample preparation was similar in all the characterization techniques: a mixture of copolymers, $P(OEGMEA)_{21}$-*b*-$P(AEMA)_{32}$ and $P(OEGMEA)_{22}$-*b*-$P(AA)_{37}$, (Com. 1, see **Table 1**) was used as the model system for the basic micellar characterization including charge ratio (AA/NH_2, ratio between acid groups and amine groups of P(OEGMEA)-*b*-P(AA) and P(OEGMEA)-*b*-P(AEMA) respectively), concentration and pH studies.

A typical sample preparation procedure for Com. 1 at optimal conditions (pH = 5.5, AA/NH_2 = 1.1) is given here. As a first step, stock solutions of P(OEGMEA)-*b*-P(AEMA) and P(OEGMEA)-*b*-P(AA) were prepared in a suitable solvent. For light scattering experiments, the concentration of the stock solutions used were 2 wt% and 5 wt% for P(OEGMEA)-*b*-P(AEMA) and P(OEGMEA)-*b*-P(AA) respectively. In case of neutron/x-ray scattering, the concentration of P(OEGMEA)-*b*-P(AEMA) stock solution was 10 wt%, while for P(OEGMEA)-*b*-P(AA), concentration stood again at 5 wt%. To confirm that the stock solutions prepared were homogenous, low concentrations (≤ 10 wt%) were preferred whenever possible. Next, to a small vial containing P(OEGMEA)-*b*-P(AEMA) solution, required amount of P(OEGMEA)-*b*-P(AA) was added, so that the optimal charge ratio AA/NH_2 of 1.1 is reached. The overall mixture was then diluted with the solvent to attain the required concentration. Finally, the pH of the obtained system was adjusted to the target value, using HCl or NaOH solutions at 1M, and it was stirred overnight, before characterization.

The charge ratio and pH studies (2.5 – 9.5) were carried out to find the optimal conditions for micellization (Com. 1). The ratio AA/NH_2 along with pH could significantly affect the stability,

dimension and number of the species formed, as seen in micelles previously reported in literatures,[70] and hence was studied in detail.

Finally, the role of concentration on the shape and size of the self-assembly made at optimal pH and charge ratio conditions was investigated using neutron scattering, varying the concentration between 0.5 – 2.5 wt% with respect to P(OEGMEA)-*b*-P(AEMA). A few other micellar systems were also probed under these conditions using SANS alone to extract information about the effect of block length on the dimension of the self-assembly made (Com. 2 – Com. 4, ***Table 1***).

Sample name	**P(OEGMEA)-*b*-P(AEMA)**	**P(OEGMEA)-*b*-P(AA)**	**AA/NH_2 ratio**
Com. 1	$P(OEGMEA)_{21}$-*b*-$P(AEMA)_{32}$	$P(OEGMEA)_{22}$-*b*-$P(AA)_{37}$	1.1
Com. 2	$P(OEGMEA)_{21}$-*b*-$P(AEMA)_{32}$	$P(OEGMEA)_{27}$-*b*-$P(AA)_{50}$	1.3
Com. 3	$P(OEGMEA)_{25}$-*b*-$P(AEMA)_{22}$	$P(OEGMEA)_{22}$-*b*-$P(AA)_{37}$	1.3
Com. 4	$P(OEGMEA)_{25}$-*b*-$P(AEMA)_{22}$	$P(OEGMEA)_{27}$-*b*-$P(AA)_{50}$	1.5

Table 1. *Com. 1 - 4 sample composition with the corresponding AA/NH_2 ratio used*

3.2.5. Characterization Techniques

3.2.5.1. NMR Spectroscopy

^{1}H NMR measurements were carried using a Bruker Advance III 600 MHz NMR Spectrometer using D_2O as solvent. The polymeric samples synthesized were dried in an oven at 50 ^oC overnight and ca. 10 mg of the samples were dissolved in 1 mL of D_2O for characterization. The NMR data obtained were analyzed using Topspin 4.1.4 and the chemical shifts δ in the figures are displayed in ppm.

3.2.5.2. Elemental Analysis

Elemental analysis with a ThermoFisher Scientific spectrometer iCE 3000 extracted the atomic percentage of C, H, N, S in the samples. Approximately 50 mg of the polymeric samples were used for the analysis. Prior to characterization, the samples were dialysed against Milli-Q water for 3 days with six water exchanges, using a dialysis bag from Carl Roth, with a molar mass cut-off of 3.5 kDa. The samples thus obtained after dialysis were then freeze-dried, before being analyzed for their composition.

3.2.5.3. Small Angle Neutron Scattering (SANS)

Small Angle Neutron Scattering (SANS) measurements were carried out using 2 mm thick quartz cuvettes, with D_2O as the solvent. For all samples, the signal from D_2O alone was collected first. Samples were prepared following the protocol described above. Although solutions are prepared in D_2O, the pH of the solutions was measured using a pH meter calibrated using H_2O: the pH of the micellar solution in D_2O (pD) could be extracted following the equation $pD = 0.929 \times pH^* + 0.42$, where pH* is the direct reading of the H_2O-calibrated pH meter.[71] The samples were measured without prior filtration.

Small Angle Neutron Scattering (SANS) experiments were conducted at the Sans2d beamline of the Neutron and Muon Source, Rutherford Appleton Laboratory, Oxford, UK.

The small-angle neutron diffractometer at ISIS, Sans2d, used a 12 mm-diameter neutron beam at a wavelength range of 1.75 – 16.5 Å. An operational q-range of 0.004 – 1 $Å^{-1}$ was probed using the two 1 m^2 detectors (at 2.4 m and 4 m) in the instrument, with the q-resolution varying between ca. 2% to ca. 19% moving from the highest to lowest q-value, calculated using the Mildner Carpenter equation.[72] The collected raw data were always refined for transmissions, empty cell

scattering, background scattering, detector efficiencies, and averaged radially, using the Mantid Workbench software.[73] The averaged data were then converted to scattering cross-section data and set onto absolute scale, again using the Mantid software. Finally, the neutron data obtained were corrected for incoherent scattering.

3.2.5.4. Small Angle X-ray Scattering (SAXS)

The polymeric solutions for Small Angle X-ray Scattering (SAXS) were prepared in 1.5 mm quartz glass-capillaries, with H_2O as the solvent. All the samples measured were at 1 wt% with respect to P(OEGMEA)-*b*-P(AEMA) and the pH was adjusted to 5.5 in all measurements performed. Also, the suspensions were not filtered prior to the experiment and as a first step, the scattering from solvent alone was collected for background subtraction.

Small Angle X-ray Scattering (SAXS) measurements were performed at ID02 beamline in the European Synchrotron Radiation Facility, Grenoble, France. The instrument uses a monochromatic X-ray source with an incident photon wavelength of ca. 1 Å. The sample to detector distance of 1.5 m probed, offers access to the efficient q range of 0.005 – 0.5 $Å^{-1}$. The 2-Dimensional X-ray scattering patterns collected using Ravonix MX-170HS CCD detector of ID02 are initially corrected for the detector inefficiencies, and are azimuthally averaged before being normalized to absolute scattering intensity, to obtain the 1D plot, *I(q) vs q*. Finally, the contribution from solvent and sample thickness is also subtracted from the 1D SAXS pattern thus obtained using SAXSutilities, prior to data analysis.

3.2.5.5. Light Scattering

All light scattering measurements were carried out on a ALV CGS3 goniometer with an ALV 5004 correlator (ALV GmbH, Langen, Germany), using 0.1 wt% aqueous polymeric solutions. In order to ensure sample stability, the prepared samples were gently stirred overnight after the pH has been adjusted to the required value. The solutions were filtered prior to the measurements; using 0.45 μm or 0.22 μm PTFE membrane-based Millipore filters for samples and buffer solutions respectively. Static and dynamic light scattering were measured simultaneously, owing to the multiple tau digital correlator of the equipment. The instrument has a maximum output power of 23 mW and is equipped with a HeNe laser of wavelength λ = 632.8 nm. The measurements were carried out at 23.0 ± 1.0 °C with an angular range between 30° and 150°.

3.2.5.5.1. Static Light Scattering

Static light scattering data can be represented using Zimm's approximation, to derive the weight-averaged molecular weight M_w, and radius of gyration of the scattering species R_G (equation 1).

$$\frac{Kc}{\Delta R_\theta} = \frac{1}{M_w} + \frac{1}{3M_w} R_G^2 q^2 \qquad (1)$$

where K and c are the optical constant and concentration of the scattering species respectively, while q corresponds to the scattering vector that is related to the scattering angle θ. The optical constant K and scattering vector q can be extracted using equations 2 and 3:

$$K = \frac{4\pi^2}{\lambda_0^4 N_A}\left(n\frac{dn}{dc}\right)^2 \qquad (2)$$

$$q = \frac{4\pi n}{\lambda_0} sin\frac{\theta}{2} \qquad (3)$$

where the laser wavelength in vacuum, Avogadro's number, the refractive index of the solvent and the refractive index increment are denoted by λ_0, N_A, n and $\frac{dn}{dc}$ respectively.

Detection of time-averaged scattering intensity <*I*> as a function of scattering vector q, enables the calculation of Rayleigh ratio (ΔR_θ), using equation (4). In equation (4), $\langle I_{solution}\rangle$, $\langle I_{solvent}\rangle$ and $\langle I_{standard}\rangle$ correspond to the scattering intensities of the solution, solvent and standard (i.e. toluene) respectively. Also, $n_{solvent}$ and $n_{standard}$ are their respective refractive indexes and $RR_{standard}$ is the Rayleigh ratio of the toluene standard for λ = 632.8 nm at 23.0 ± 1.0 °C.

$$\Delta R_\theta = \frac{\langle I_{solution}\rangle - \langle I_{solvent}\rangle}{\langle I_{standard}\rangle}\left(\frac{n_{solvent}}{n_{standard}}\right)^2 RR_{standard} \qquad (4)$$

Upon plotting $\frac{\mathrm{Kc}}{\Delta R_\theta}$ against q^2, the molecular weight (M_w) of the objects can be derived from the intercept ($\frac{1}{Intercept}$) provided the refractive index increment value is known, while the radius of gyration is obtained from the slope ($R_G = \sqrt{3.M_w.slope}$).

3.2.5.5.2. Dynamic Light Scattering

In dynamic light scattering, the scattering intensity as a function of time, at a fixed scattering vector *q,* is studied. From the scattering intensity probed, the normalized intensity-time auto-correlation function $g_2(q,\tau)$, as a function of time shift τ, is obtained. Using Siegert's equation, the electric field-time auto-correlation function $g_1(q, \tau)$ is extracted:

$$g_2(q,\tau) = \frac{\langle I\,(q,t) I(q,t+\,\tau)\rangle}{\langle I\,(q,t)\rangle^2} = 1 + |g_1(q,\tau)|^2 \qquad (5)$$

In equation (5), $I(q,t)$ and $I(q,t+\,\tau)$ are the scattering intensity at time *t* and $t + \tau$ respectively and <> indicates temporal averaging over all the times *t*.

The translational diffusion coefficient D_t of an object is related to the electric field correlation function $g_1(q,\tau)$ and could be derived either through CONTIN or the cumulant analysis. While the CONTIN method is suitable for complex samples exhibiting multiple populations, the cumulant method is used for simpler systems with a quasi-monomodal distribution of population.

Provencher developed the CONTIN algorithm using Laplace inverse, and it relates the electric field autocorrelation function $g_1(q,\tau)$ of a system to the translational diffusion coefficient D_t, as depicted below:

$$g_1(q,\tau) \;= \int_0^\infty G(D_t).\, e^{-D_t.\tau/q^2} dD_t \qquad (6)$$

where $G(D_t)$ is the distribution function of translational diffusion coefficient D_t.

On the other side, the cumulant analysis, ideal for monomodal systems, defines the logarithm of $g_1(q,\tau)$ at specific q as a power sequence in τ

$$ln\big(g_1(q,\tau)\big) = \Gamma_0 - \Gamma_1.\tau + \frac{\Gamma_2}{2!}.\tau^2 - \frac{\Gamma_3}{3!}.\tau^3 \qquad (7)$$

where Γ_0, Γ_1, Γ_2 and Γ_3 are the cumulants offering insights typically into the average diffusion coefficient $\overline{D}_t$ and polydispersity index of the system studied. While the z-averaged translational diffusion coefficient $\overline{D}_t$ is associated to the first cumulant $\Gamma_1 = \overline{D}_t q^2$, the ratio of the second and square of the first cumulant gives the polydispersity in the system $PDI = \frac{\Gamma_2}{\Gamma_1^2}$.

Dynamic light scattering measurements carried out at multiple angles enable the determination of translational diffusion coefficient extrapolated to zero-angle D_0, independent of the scattering vector q. For dilute solutions, D_0 is derived using the linear approximation given below:

$$\overline{D}_t(q) = D_0\left(1 + C.R_g^2.q^2\right) \qquad (8)$$

In equation (8), R_g is radius of gyration of the self-assembly while C is a dimensionless constant related to polydispersity and shape of the particle, with a value between 0 and 0.33.[74]

Upon plotting $\overline{D}_t$ against q^2, if the system shows angular dependence, D_0 is obtained from the intercept and in case of no angular dependence D_0 could be determined by averaging $\overline{D}_t$ over the angular range.

Hydrodynamic radius R_H is related to translational diffusion coefficient extrapolated to zero-angle D_0 through the Stokes-Einstein relationship:

$$R_H = \frac{k_B T}{6\pi\eta}\frac{1}{D_0} \qquad (9)$$

In the Stokes-Einstein equation (9), k_B, T, η are Boltzmann constant, temperature and solvent viscosity respectively.

Further, combining both dynamic and static light scattering, a shape sensitive ratio, $\frac{R_G}{R_H}$ could be extracted. Spherical objects give $\frac{R_G}{R_H}$ = ca. 0.78, and a deviation from this value indicates a distortion in morphology.

3.2.6. Small Angle Scattering Model

The small angle neutron/X-ray scattering data (SANS/SAXS) collected were fitted using a model integrating the contribution from micelles with the contribution of individual polymer chains, not taking part in micellization.

$$I(q) = I_{micelles}(q) + I_{DHBC}(q) \qquad (10)$$

Micelles are then modelled either as polydisperse spheres or as flexible cylinders depending on the samples.

When spherical objects are obtained, the signal is modelled by polydisperse spheres of radius R and polydispersity in size σ:

$$I_{micelles}(q) = AP_{sp}\ (q, R, \sigma) \qquad (11)$$

where A and $P_{sph}(q)$ corresponds to the scale factor and polydisperse sphere form factor respectively.

The scale factor A, can be written as:

$$A = n\Delta\rho^2 V^2 \qquad (12)$$

depicting the influence of number of objects per unit volume n, the difference in contrast between the spheres and solvent $\Delta\rho = \rho_{mic} - \rho_0$, and the volume of the self-assembly $V = \frac{4}{3}\pi R^3$ in the scale factor A.

In the present study, the scale factor is not investigated in depth as the experiments were only carried out in one contrast, limiting the access to both n and $\Delta\rho$.

The form factor of a polydisperse sphere can be written as:

$$P_{sp}\ (q, R, \sigma) = < F^2(q, R) >_\sigma \qquad (13)$$

where *F(q,R)* is the form factor amplitude of a homogeneous monodisperse sphere and $<.>_\sigma$ is the integration over the polydispersity in size.

The form factor amplitude *F(q)* can be expressed as:

$$F(q, R) = \frac{3(\sin(qR) - (qR)\cos(qR))}{(qR)^3} \qquad (14)$$

The effect of the polydispersity is written as:

$$< F^2(q, R) >_\sigma = \int f_{SZ}\left(R, \frac{1}{\sigma^2} - 1\right)(F(q, R))^2\, dR$$

with $f_{SZ}\left(R, \frac{1}{\sigma^2} - 1\right)$ the Schulz-Zimm polydispersity distribution.[75]

When elongated micelles are monitored, they are modelled using a flexible cylindrical model.[76,77]. In those cases $I_{micelles}(q)$ is expressed as:

$$I_{micelles}(q) = AP_{fc}(q) \qquad (15)$$

with *A* again being the scale factor, defined similarly as prior.

For a flexible cylinder with cross-section radius *R*, length *L* (with $L \geq 5R$), and polydispersity over the cross-section σ, $P_{fc}(q)$ can be expressed as:

$$P_{fc}(q) = < F_{CS}^2(q) >_\sigma P_{fc}(q) \qquad (16)$$

where $F_{CS}(q, R) = \frac{2J_1(qR)}{qR}$ is the form factor amplitude of the circular monodisperse cross-section and is associated with the Bessel function J_1, and $P_{fc}(q)$ is the contribution from the flexible length of the cylinders and is related to both contour length L_C and Kuhn length b_{kuhn}. While contour

length L_C is the total length of the polymer chain, Kuhn length b_{kuhn} is twice the persistence length, a parameter indicating the rigidity of the chain analyzed.

The intensity of scattering from copolymers not contributing to micellization is given as:

$$I_{DHBC}(q) = A' P_{pol}(q, R_g, m) \qquad (17)$$

where, P_{pol} corresponds to the form factor of the polymer chain with excluded volume, while R_g and m depict the radius of gyration and mass fractal of the free species.

The mass fractal m is associated to the excluded volume v through $m = \frac{1}{v}$.

In 1993, Hammouda gave an analytical solution for the form factor P_{pol}:[78]

$$P_{pol}(q) = \frac{1}{vU^{1/2v}}\left[\gamma\left(\frac{1}{2v}, U\right) - \frac{1}{U^{1/2v}}\gamma\left(\frac{1}{v}, U\right)\right] \qquad (18)$$

where the general expression of $\gamma(x, U)$ is given by:

$$\gamma(x, U) = \int_0^U e^{-t} t^{x-1} dt \qquad (19)$$

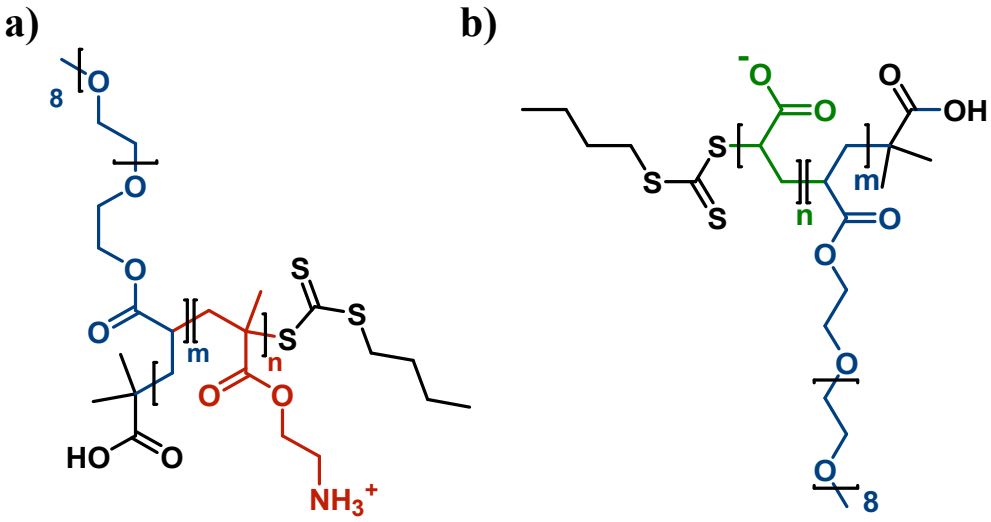
And the parameter U is given as:

$$U = \frac{q^2 R_g^2 (2v+1)(2v+2)}{6} \qquad (20)$$

The model used in his study was developed accounting homopolymers not block copolymers and strictly applies only for mass fractals between the range $\frac{5}{3} \leq m \leq 3$. Since the polymer chains used in our system hold a comb-like architecture, the mass fractals m obtained is ≥ 3. This model was still opted as it was the only available one giving information about the free polymer chain parameters in the solution.

3.3. RESULTS AND DISCUSSION

3.3.1. Block Copolymers; P(OEGMEA)-*b*-P(AEMA) & P(OEGMEA)-*b*-P(AA)



***Scheme 2**. Structure of the developed copolymers under study, (a) P(OEGMEA)$_m$-b-P(AEMA)$_n$ and (b) P(OEGMEA)$_m$-b-P(AA)$_n$*

Both DHBCs, P(OEGMEA)-*b*-P(AEMA) and P(OEGMEA)-*b*-P(AA), whose chemical compositions are depicted in **Scheme 1**, were synthesized using RAFT polymerization. While P(OEGMEA)-*b*-P(AEMA) copolymer was developed using a newly formulated protocol, as discussed in *Chapter 2*, P(OEGMEA)-*b*-P(AA) synthesis followed a well-established methodology already reported (*Chapter 1*).[79]

The chemical characterization of P(OEGMEA)-*b*-P(AEMA) was carried out using a combination of ^{1}H NMR and elemental analysis; complementing each other, and a degree of polymerization (DP) of 21 and 32 units for P(OEGMEA) and P(AEMA) blocks respectively was obtained (*Materials and Methods, Chapter 2*). This corresponds to a molecular weight for the polymer of 14.5 kDa (including the terminal groups), with a contribution of 10.1 kDa and 4.1 kDa from P(OEGMEA) and P(AEMA) block respectively (*Results and Discussion, Chapter 2*). The

chemical composition of P(OEGMEA)-*b*-P(AA) copolymer, was determined using ^{1}H NMR alone. The DP of P(OEGMEA) and P(AA) blocks were found to be 22 units and 37 units respectively (*Materials and Methods, Chapter 1* and **Figure S1** in supplementary information), associating with a molecular weight of 13.5 kDa for the entire copolymer (including the terminal groups), with a share of 10.6 kDa from P(OEGMEA) and 2.7 kDa from P(AA) block respectively.

Similarly, two other DHBC used were also characterized; a) an amine rich $P(OEGMEA)_{25}$-*b*-$P(AEMA)_{22}$ with a total molecular weight of 15.1 kDa (with a contribution of 12.0 kDa and 2.8 kDa from P(OEGMEA) and P(AEMA) respectively) b) an acrylate rich $P(OEGMEA)_{27}$-*b*-$P(AA)_{50}$ with a total molecular weight 16.8 kDa (with P(OEGMEA) and P(AA) share of 13.0 kDa and 3.6 kDa respectively).

3.3.2. Finding Optimal Micellization Conditions

The positively charged P(AEMA) block and the negatively charged P(AA) block of the DHBCs can interact electrostatically, leading to the self-assembly and formation of well-defined species in aqueous medium, studied by static/dynamic light scattering and small angle scattering measurements.

To begin with, we compare using small angle neutron scattering (SANS), the pattern of Com. 1 (see **Table 1**), a mixture of $P(OEGMEA)_{21}$-*b*-$P(AEMA)_{32}$ and $P(OEGMEA)_{22}$-*b*-$P(AA)_{37}$, made at pH = 5.5 and a ratio $AA/NH_2 = 1$, with the signal of both DHBCs alone in solution at the same concentration and pH (**Figure S2**). The pH was chosen as it is centred between the pKa of PAA[80] and PAEMA[81] while the charge ratio was chosen as it assumes a complete charge neutralisation. In the mixture, on top of a contribution at large angles (q = ca. 0.15 Å^{-1}) that is observed as well for both $P(OEGMEA)_{21}$-*b*-$P(AEMA)_{32}$ and $P(OEGMEA)_{22}$-*b*-$P(AA)_{37}$ alone and that we attribute

to the contribution of the polymer chains in solution, a large increase of the signal is seen at small angles, with a change in slope at ca. 0.03 $Å^{-1}$, indicating the formation of larger structures such as micellar aggregates. To control finely the formation of these aggregates and adjust their shape and size, we studied the influence of both the AA/NH_2 charge ratio and the pH on their structural features.

We first studied the influence of the charge ratio AA/NH_2 by studying samples made at a ratio of 0.7, 1.0 and 1.3 respectively (see **Figure 1**).

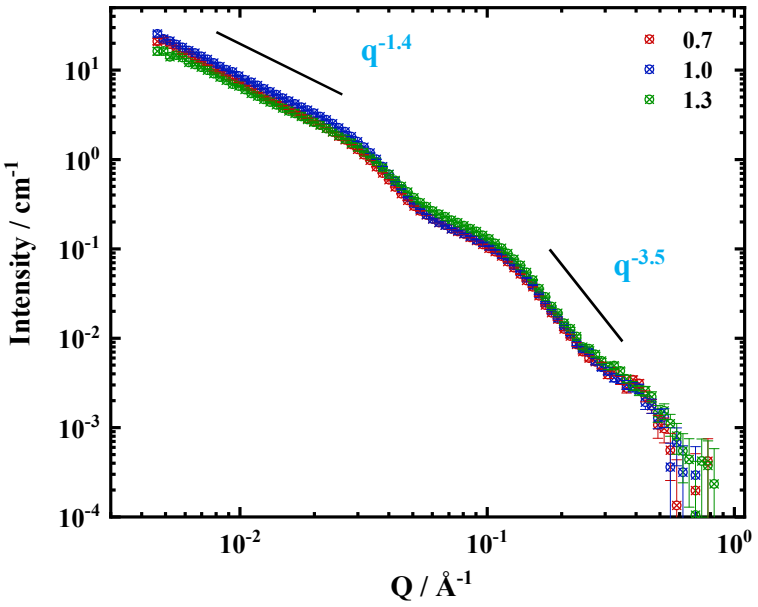


Figure 1. *SANS pattern of micelles from Com. 1 ($P(OEGMEA)_{21}$-b-$P(AEMA)_{32}$ with $P(OEGMEA)_{22}$-b-$P(AA)_{37}$) at varying charge ratio AA/NH_2 and pH = 5.5.*

The shape of the curve shows no noticeable difference at all three conditions studied, proving the charge ratio to have little influence on the dimension or shape of the population formed in the range studied. However, with the change in charge ratio used, the scattering intensity of the samples show a slight yet significant difference in low *q*. The highest intensity was found for AA/NH_2 = 1.0, followed by AA/NH_2 = 0.7 and finally, AA/NH_2 = 1.3. The intensity at zero angle

is related to the number of scattering objects, this indicates that the highest number of self-assembled species is found at charge ratio = 1.0, and a deviation from this value causes a reduction in the number of species formed, leading to a weaker scattering intensity. All the SANS curves obtained are characteristic of elongated objects with a signal at low q ($0.004 < q < 0.020$ Å^{-1}) that follows a $I \sim q^{-1.4}$, typical of elongated flexible particles.[76] No abrupt upturn is noted in the low q region of the SANS signal collected, suggesting an absence of larger aggregates at least in the probed q-range. At q ~ 0.03 Å^{-1}, a change of slope is observed, associated to the cross-section of the flexible cylinders, while the features at larger angles and especially the sharp decrease at ca. 0.15 Å^{-1} is attributed to the signal of polymer chains as seen by the comparison with the signal of polymers alone described above. At larger q, the signal decreases following $I \sim q^{-3.5}$ which is consistent with a signal from comb-like polymer chains in a good solvent with excluded volume, while the decrease would follow a $q^{-5/3}$ for a linear chain.[46]

Small angle X-ray scattering (SAXS) was used to complement and confirm the charge ratio (AA/NH_2) study from SANS (**Figure 2**). Using SAXS, the charge ratios were studied in finer increments of 0.1, ranging between 0.6 to 1.2, helping to choose the AA/NH_2 ratio for micellar studies with more accuracy. The curves obtained at all charge ratios except $AA/NH_2 = 0.6$, are characteristic of elongated structures, with an oscillation around ca. 0.03 Å^{-1}, in agreement with the SANS measurements. At the lowest charge ratio of 0.6, very low scattering intensity and no features corresponding to well defined population is obtained, indicating that below this limit, there is not enough P(OEGMEA)-*b*-P(AA) polymers to interact electrostatically with P(OEGMEA)-*b*-P(AEMA) and form micellar aggregates. For charge ratios ranging between 0.7 and 1.2, all samples exhibit a $I \sim q^{-\alpha}$ decrease below q ~ 0.03 Å^{-1}, with α ranging between 1.1 and 1.3. The absence of a plateau and the typical values of the slope hint at the formation of elongated

objects at all conditions. All the SAXS patterns show no presence of aggregation in the probed q-range; excluding the pattern from $AA/NH_2 = 0.9$, which exhibits an upturn in intensity at the smallest angles. This peculiar behaviour for this particular sample may be due to some problems in the subtraction of the empty capillary. Even though the curves do not evolve much in the charge ratio range probed, the highest scattering intensity could be attributed to the ratio = 1.1 and is therefore used for micellar studies to follow. Let us note the oscillation corresponding to the free polymers observed in SANS (ca. 0.15 $Å^{-1}$), is less pronounced in SAXS, due to a weaker contrast between polymeric species and solvent. Nonetheless, the change of slope characteristic of the object's cross-section observed at ca. 0.03 $Å^{-1}$ and the slope at ca. 1.4, seen in both techniques, indicate that changing the solvent from D_2O to H_2O has little influence on the type of structures obtained.

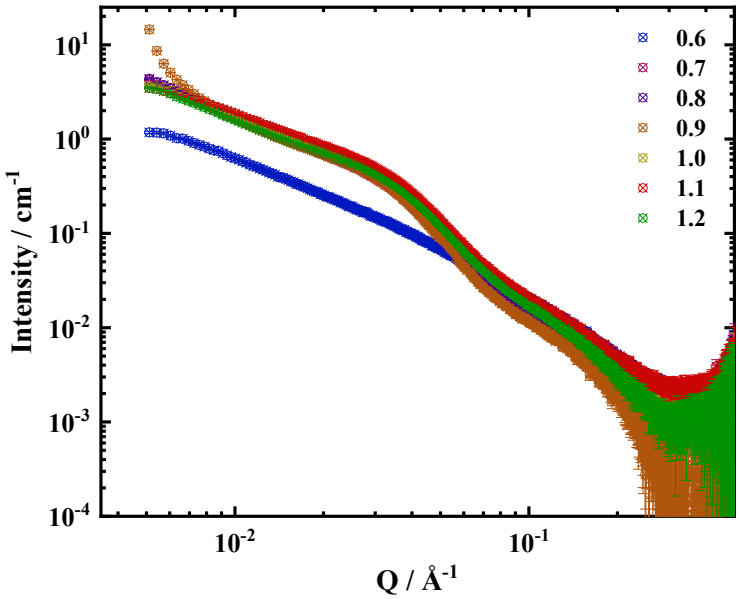


Figure 2. *SAXS pattern of micelles from Com. 1 at different charge ratios (AA/NH_2) ranging between 0.6 and 1.2, and pH = 5.5 in H_2O.*

Then, the pH sensitivity of the micelles made by Com. 1 at $AA/NH_2 = 1.1$, for pH ranging from 2.5 to 9.5 was investigated using both DLS and SANS (see **Figure 3**). **Figure 3a** gives the

normalized scattered intensity obtained in DLS on suspensions at 0.1 wt% in P(OEGMEA)-*b*-P(AEMA). The signal, very weak at pH = 2.5 ($I \sim 0.0025$), increases strongly with the pH up to pH = 5.5 ($I \sim 0.014$), before decreasing again up to pH = 7.5, with the last 3 pHs having similar normalized intensities at $I \sim 0.0025$. This suggests that at extreme pHs, polymers are dissociated in water, as either the PAA (in acidic) or PAEMA (in basic conditions) is uncharged, in agreement with their known pKa of 4.3 and 7.6 respectively.[80,81] The micellization pH range would hence be between 3.5 and 6.5, with an optimum at ca. pH = 5.5. These results are in complete agreement with the SANS data of the same system at 1 wt% in D_2O (**Figure 3b**). At pH = 2.5, the SANS pattern is similar to the one of polymers alone (see **Figure S2**), proving the absence of micelles at this pH. From pH = 3.5 onwards, the signal of larger, elongated structures gradually increases up to pH = 5.5, before decreasing again at higher pHs. Let us note that signals at pH = 7.5, 8.5 and 9.5 still exhibit a slope of $q^{-1.2}$, $q^{-1.1}$, and $q^{-1.4}$ respectively at small angles, indicating that a slight amount of micelles is still present at these pHs.

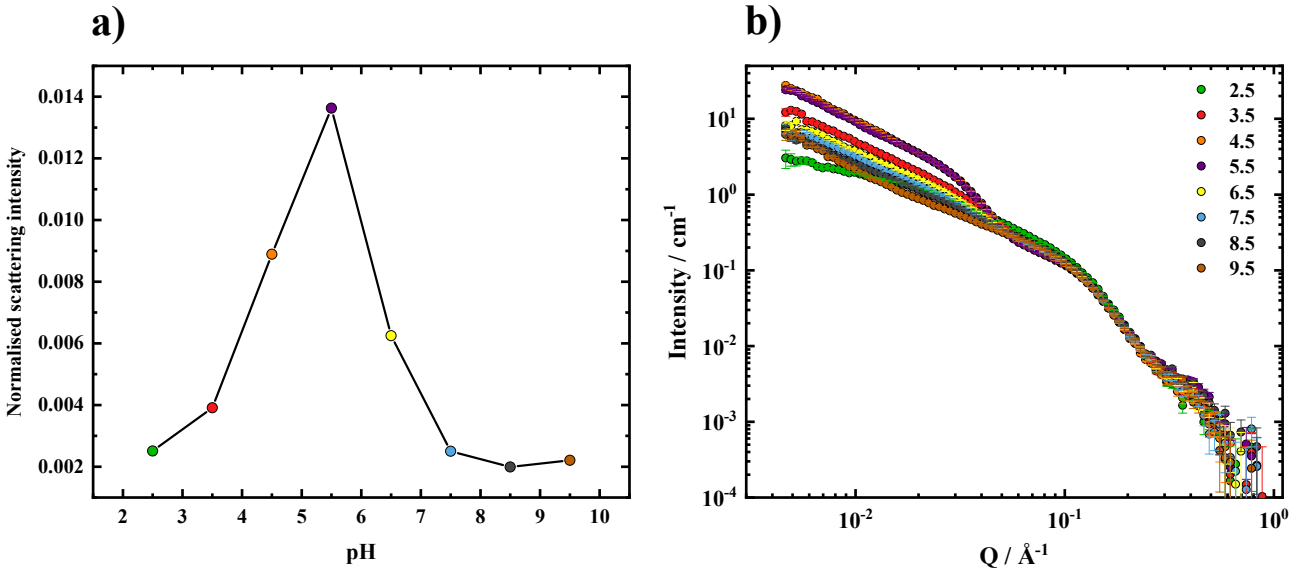


Figure 3. *(a) Normalized light scattering intensity of Com. 1 from DLS measurements at 0.1 wt% with respect to P(OEGMEA)-b-P(AEMA), charge ratio 1.1 and different pH conditions (2.5 - 9.5) and (b) SANS patterns of the same system at 1wt% in D_2O.*

3.3.3. Characterization of Micelles (Com. 1)

After optimising the micellization parameters (AA/NH_2 = 1.1 and pH = 5.5), self-assembly from Com. 1, was studied in greater depth using light, neutron and X-ray scattering.

The intensity-time autocorrelation function $g_2(\tau)$ of the system along with the distribution of relaxation time obtained has been displayed in **Figure 4a**. CONTIN analysis of the sample gives a single prominent signal with a distinct peak width, suggesting that the sample predominantly consists of only one well-defined population yet with a noticeable distribution in sizes, possibly due to the elongated nature of the object probed. The hydrodynamic radius of the species from CONTIN was found to be R_H = 60.5 ± 0.1 nm (FWHM ± 0.6).

The sample was also analyzed using the cumulant method (**Figure 4b**). The fitting with the cumulant analysis of the measurements made at different scattering angles enable extracting the translational diffusion coefficient extrapolated to zero-degree (D_0, see Materials and Methods). Using this technique of extrapolation, the translational diffusion coefficient D_0, was found to be (2.89 ± 0.05) × 10^{-12} m^2/s^{-1}, corresponding to a hydrodynamic radius of R_H = 63.3 ± 1.1 nm with a polydispersity index PDI = 1.36 ± 0.03.

Further, the sample was characterized via SLS and the data obtained were fitted using Zimm plot (see **Figure 4c**). The absence of multiple slopes in the plot suggest a monomodal distribution of population. Ideally, both the radius of gyration, $R_G = \sqrt{3.Mw.slope}$ and molecular weight, $Mw = \frac{1}{Intercept}$ could be derived from the plot. However, here Mw cannot be obtained because the $\frac{dn}{dc}$ is not available in the literature and was not experimentally determined by us.

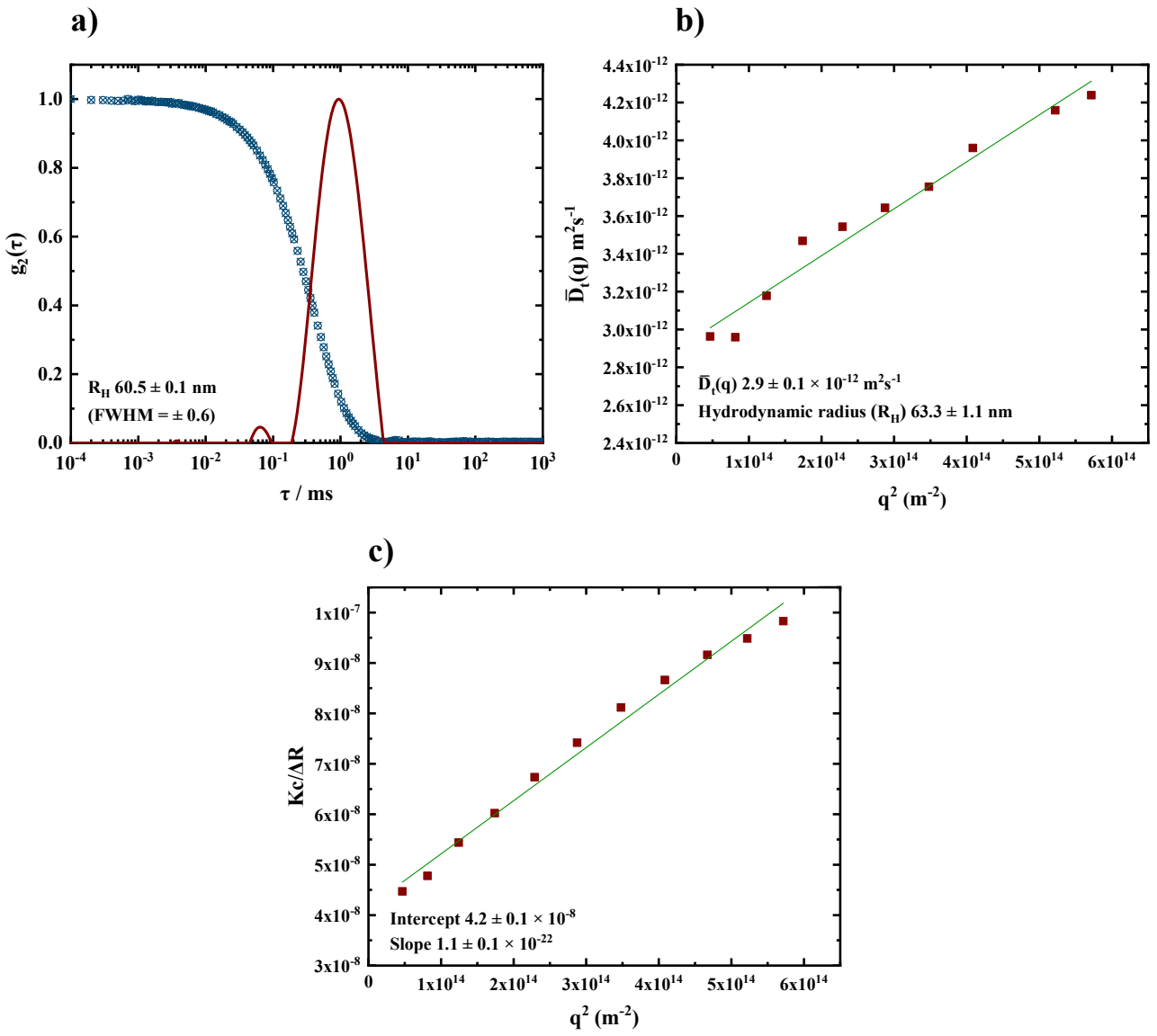


Figure 4. *SLS/DLS data of the self-assembly from Com. 1 at 0.1 wt% and pH = 5.5 in D_2O: (a) Intensity-time autocorrelation function $g_2(\tau)$ along with distribution of relaxation time resulting from the CONTIN analysis at a scattering angle of $\theta = 90^o$ (the CONTIN derived hydrodynamic radius R_H and full width half maximum (FWHM) also are given in inset), (b) Diffusion coefficient $\bar{D}_t(q)$ from the second order cumulant analysis plotted against the scattering vector q and in inset the diffusion coefficient at the zero angle D_0 and its corresponding hydrodynamic radius R_H are given (c) Zimm plot from the SLS data of the same system.*

The shape and size of the micelles of Com. 1 were characterized in both SANS (in D_2O) and SAXS (in H_2O) and results are given in **Figure 5**. Data were fitted using a combination of flexible cylinder and free polymer chain model as explained in *Materials and Methods*. Let us note that the q-range probed does not allow us to extract the overall length of the cylinders as the signal does not reach a plateau at the smallest angles studied and hence it was fixed arbitrarily at 150 nm.

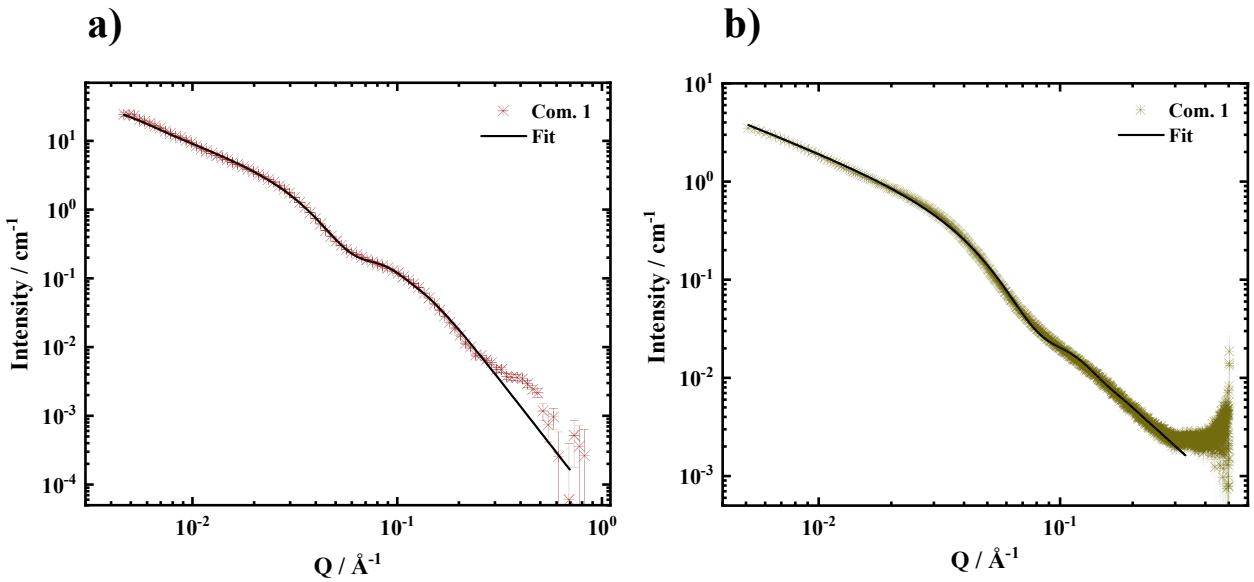


Figure 5. *(a) SANS and (b) SAXS patterns of Com. 1 (1 wt%) at pH = 5.5 and AA/NH_2 = 1.1. The solvent used are D_2O and H_2O respectively. In both (a) and (b), the fit made using a combination of flexible cylinder + free polymer chains is shown by black lines.*

The radius R of the flexible cylinder's cross-section was found to be 5.7 ± 0.1 nm with a polydispersity in size σ of 10 ± 1 %, while the radius of gyration R_g of the polymer chains was measured at 1.8 ± 0.1 nm, indicating the cylinders are indeed formed by the packing of several DHBCs. The Kuhn length b_{Kuhn} of the cylinders is found at 69.0 ± 2.0 nm. Evaluation of the system using SAXS delivers similar results. However, a difference in the dimension of the species obtained could be noted, probably due to solvent effect or the weaker contrast between objects and solvent. Indeed, the radius R of the polymer micelle is decreased at 4.3 ± 0.1 nm in SAXS with σ

13.0 ± 1.0 %. Regarding the polymer chains, the radius of gyration R_g is found at a similar value of 2.2 ± 0.1 nm.

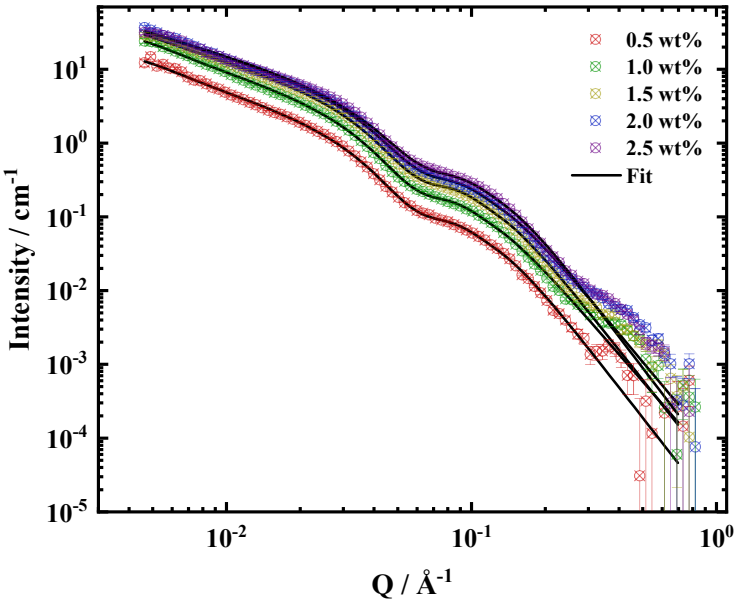


Figure 6. *SANS patterns of Com. 1 at pH = 5.5, AA/NH₂ = 1.1 and different concentrations (0.5 - 2.5%) in D₂O. In black, the fits made using the combination of flexible cylinder and free polymer chain.*

The influence of concentration on the size and shape of the polymeric self-assembly was investigated in SANS for concentration in P(OEGMEA)-*b*-P(AEMA) in the mixture ranging from 0.5 to 2.5 wt% (**Figure 6 & Table S1**). The overall increase in intensity with concentration, associated to a higher number of scattering objects, is expected. Indeed, the scale factor of both the flexible cylinders and the polymer chains increase linearly with concentration (see **Table S1**). 0.5 and 1 wt% show the same exact features, but above 1 wt% the slope observed in the small angle region ($q < 0.03$ Å^{-1}) decreases with concentration, from $q^{-1.4}$ to $q^{-1.2}$ at 2.5 wt%. This variation could be either due to a change in stiffness of the cylinders, or by the rise of repulsion between cylinders with concentration. Both effects would induce a decrease of the slope at small

angles and hence it is impossible to discriminate between those two effects. To avoid complexifying the model, data were fitted by adjusting the Kuhn length, without adding a structure factor.[77,82,83]

Indeed, according to the SANS fit, the Kuhn length is found to increase with concentration from ca. 69 nm to ca. 150 nm. On the other side, the Radius *R* of the cylinders see little variation with concentration, decreasing slightly from 5.7 ± 0.1 nm at 0.5 wt% to 5.3 ± 0.1 nm at 2.5 wt%. The radius of gyration R_g associated to the free polymeric objects in the suspension remains essentially the same (ca. 1.7 nm). Similar results have been reported for PIC micelles also made through electrostatic self-assembly.[84] The decrease in radius of the cylinders can be explained by a decrease of water content within the micelles with concentration, as previously observed for other PIC micelles.[84] Finally, it is to be noted that the power law dependence $I \sim q^{-\alpha}$, in the high q region of the SANS signals, associated to the comb-like polymer chains, is found at ca. 4 (**Table S1**). This value is slightly different from the one found for Com. 1, during the charge ratio studies (**Figure 1**). However, both values (3.5 and 4.0), corresponds to an abrupt interface between the micelle and solvent. It is far from the α expected from the linear chains in a good solvent ($\alpha = 5/3$), confirming the notable influence of comb-like architecture in the micelle formed.

3.3.4. Influence of the P(AEMA) and P(AA) Block Lengths on the Micelles

The copolymer chain length of P(OEGMEA)-*b*-P(AEMA) and P(OEGMEA)-*b*-P(AA) could have significant influence in the size and shape of the species made, as seen in previously reported polymer complexes.[85,86] In order to understand this effect, other micellar systems were prepared. All the new micellar suspensions prepared (Com. 2 - 4) were then measured using SANS at pH =

5.5 in D_2O and compared with Com. 1. The optimal ratio was found individually for each system (see **Figure S3**), before the effect of copolymer chain length was probed (**Figure 7 & Table S2**).

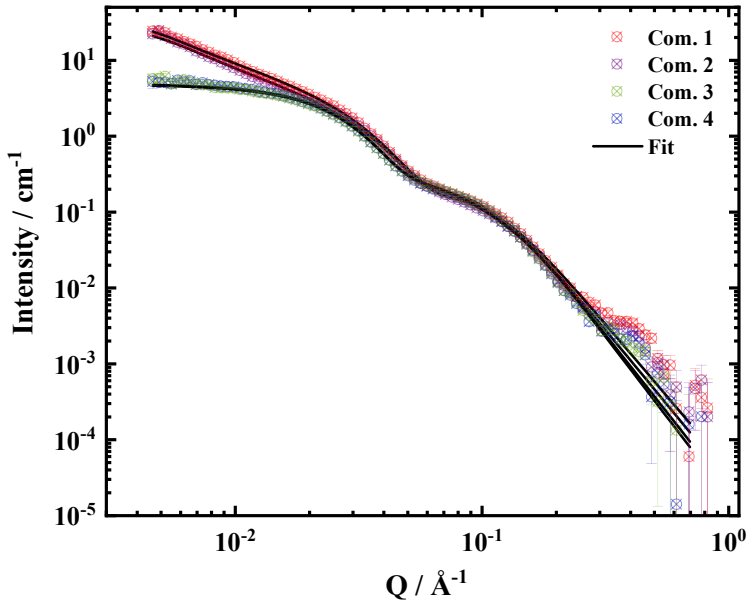


Figure 7. *Effect of copolymer chain length in the shape and size of the self-assembled population made, investigated using SANS at pH = 5.5 in D_2O (Com. 1 to 4, see Table 1). In black, the fits made using the combination of flexible cylinder/simple sphere and free polymer chain are depicted. Optimum charge ratios (AA/NH_2) discussed in table 1 was used for Com. 1 – 4 samples.*

SANS results revealed the P(AA) block length of the P(OEGMEA)-*b*-P(AA) copolymer to have a limited influence on the species formed. When increasing P(AA) from 37 to 50 (Com. 1 to 2), the SANS patterns overlap with little differences. Both patterns can be described with the model of flexible cylinders and polymer chains given in *Material and Methods* with similar values for the different parameters (see **Table S2**).

The influence of the P(AEMA) block length seems much more prominent, as is seen by the comparison between Com. 1 and Com. 3. While the SANS pattern of Com. 1 shows a $q^{-1.4}$ slope

for q < 0.03 $Å^{-1}$, the signal of Com. 3 (with a shorter P(AEMA) block of DP = 22 instead of DP = 32 found in Com. 1) exhibits a plateau characteristic of spherical objects. The SANS pattern was successfully fitted using a model of spheres and polymer chains (**Figure S4**, overlapping Com. 3 and the signal of both DHBCs used alone proves, similarly to Com. 1, that the contribution at q ≥ 0.15 $Å^{-1}$ is from the comb-like polymer chains). The ability of P(OEGMEA)$_{25}$-*b*-P(AEMA)$_{22}$ copolymer to craft spherical objects was confirmed using Com. 4 (made with a larger P(AA) block), whose SANS pattern completely overlap with Com. 3.

Fitting of Com. 3 and 4 gives a sphere radius *R* of 6.8 ± 0.1 nm with a polydispersity in size of 25 ± 1 %, while the radius of gyration R_g of the polymer chains also remains independent of the system analyzed at 1.8 ± 0.1 nm (**Table S2**).

The difference in shape of the species formed with varying block length of P(AEMA) could be associated with the notable impact it has on the block ratio of the polymers. We define $r_{M_w1} = \frac{M_w(P(OEGMEA))}{M_w(P(AEMA))}$ and $r_{M_w2} = \frac{M_w(P(OEGMEA))}{M_w(P(AA))}$ the molecular weight block ratios between the two blocks of each DHBC. r_{M_w1} is found to have a significant role in the size, shape and other properties of the micelle formed, while r_{M_w2} has little influence. One would expect both block ratios to have a strong influence on the self-assembly, since both the charged and neutral blocks manage very different responsibilities in a system; while the neutral hydrophilic block of the DHBC makes the corona of the micelle, playing a significant role in the stability and shape of the structure, the charged block enable complexation, influencing the size of the core. The balance between both blocks hence has a strong influence on the curvature of the core-shell interface, and the shape of the objects formed.

The block ratios found for P(OEGMEA)-*b*-P(AEMA) and P(OEGMEA)-*b*-P(AA) copolymers in Com. 1 – 4 are depicted in **Table 2**. It could be seen that, in Com. 1 and Com. 2, giving elongated

structures, block ratios found for P(OEGMEA)-*b*-P(AEMA) and P(OEGMEA)-*b*-P(AA) copolymers are significantly different from each other, while in Com. 3 and Com. 4, where spherical objects are made, the block ratios are more comparable. Hence, a study of the block ratios suggests that mixing copolymers of comparable block ratios give spherical objects, while a deviation in this can lead to reduced curvature in the self-assembly, and form elongated structures instead.

An alternative hypothesis is that for spherical objects to be obtained, block ratio of both DHBCs should be higher than ca. 3 - 3.5, as samples with a block ratio below this value (Com.1 and 2) form elongated objects while those above this value form spheres (Com. 3 and 4).

Concluding on the influence of the block ratios on the species formed would require further studies. For example, if mixing P(OEGMEA)-*b*-P(AA) copolymer having a block ratio of 2.4 with P(OEGMEA)-*b*-P(AEMA) of same block ratio gives spherical micelles, our first hypothesis would be validated, while the formation of elongated objects would hint more towards our second hypothesis.

Sample name	r_{M_w1}	r_{M_w2}
Com. 1	2.4	3.8
Com. 2	2.4	3.6
Com. 3	4.2	3.8
Com. 4	4.2	3.6

Table 2. *Block ratios calculated for P(OEGMEA)-b-P(AEMA) and P(OEGMEA)-b-P(AA) copolymers in various systems (Com. 1 – 4)*

However, it is interesting to note that, similar kind of results indicating the influence of block ratios on the self-assembly was also obtained when P(OEGMEA)-*b*-P(AEMA) was mixed with a homo-

polyelectrolyte instead of a DHBC (discussed in *Chapter 2*). Depending on the block ratio of P(OEGMEA)-*b*-P(AEMA) copolymer (ratio changed from 2.4 to 4.2) the dimension of the self-assembly showed evolution, when poly(acrylate) of DP = 22, was used as the micellization partner. This again indicate the influence block ratio of the polymer could have on a self-assembly. Even then, to make a proper comparison between the results from homo-polyelectrolyte based systems to fully DHBC based systems, more measurements are required.

3.4. CONCLUSION

In the present study, the electrostatic self-assembling nature of amine rich double hydrophilic block copolymer DHBC, P(OEGMEA)-*b*-P(AEMA), carrying positive charges, with oppositely charged carbonyl group containing DHBC, P(OEGMEA)-*b*-P(AA) has been discussed in detail. Copolymers, P(OEGMEA)-*b*-P(AEMA) and P(OEGMEA)-*b*-P(AA) were synthesized by RAFT polymerization, the copolymers synthesized are characterized using ^{1}H NMR and elemental analysis to extract the degree of polymerization (DP) of each block.

Neutron, X-ray and light scattering measurements were used to investigate the micellization properties of the P(OEGMEA)-*b*-P(AEMA) copolymer with P(OEGMEA)-*b*-P(AA). The optimal micellization conditions were found by studying the influence of the charge ratio between acrylate and amine functions AA/NH_2 of the two DHBCs and the influence of pH on the mixture of $P(OEGMEA)_{21}$-*b*-$P(AEMA)_{32}$ and $P(OEGMEA)_{22}$-*b*-$P(AA)_{37}$ (Com. 1). As a first step, the effect of charge ratio (AA/NH_2) between the amine species from P(AEMA) block and carbonyl groups from P(AA) in self-assembly was probed in depth, combining SANS and SAXS at an intermediate pH = 5.5 chosen. An optimal charge ratio of 1.1 was found, slightly different to the theoretical ratio of 1 to have a complete charge compensation. When largely away from this optimum (0.6),

no micelles are observed as there are not enough P(OEGMEA)-*b*-P(AA) chains to interact with P(OEGMEA)-*b*-P(AEMA) and allow micelle formation. Next, the effect of pH on the self-assembly of the polymeric structures was investigated, using a combination of SANS and DLS, varying the pH between 2.5 – 9.5. The formation of the polymeric self-assembly is highly influenced by the pH condition, with the well-defined species best formed at intermediate pH = 5.5, as assumed. The micelles gradually dissociate into individual polymeric chains when the pH deviates from this value. Once the optimal conditions for micellization (AA/NH_2 = 1.1 and pH = 5.5) were established, the polymeric self-assembly was fully characterized together both in light and x-ray/neutron scattering. The data collected from SAS were fitted with a combination model of flexible cylinder and polymer chain. Concentration studies were carried in SANS and results suggests either an increase in stiffness of the micellar cylinders or the emergence of interactions between cylinders without being possible to discriminate between both possibilities.

In order to study the effect of block length on the self-assembly made, three other systems along with Com. 1 were investigated, namely Com. 2 - 4. SANS measurements on Com. 1 and Com. 2 proved that the P(AA) block of the copolymer has little impact on the micelle made. Moving from Com. 1 to Com. 2, the block length of P(AA) increased but the elongated shape of the self-assembly remained the same. However, comparing Com. 1 with Com. 3 validates the notable impact of P(AEMA) block length has on the micelle formed. The shape of the species made changed to spherical conformation, with the decrease in P(AEMA) block length. The changing shape of the micelle with the P(AEMA) block length is associated to the significant influence it has on the block ratio. The micelles made from copolymers with comparable block length are found to be spherical while a too pronounced difference in the block ratio of the copolymers lead

to formation of elongated structures. This study proves that, through careful manipulation of the block ratio, self-assemblies of different morphologies could be achieved.

SUPPORTING INFORMATION

^{1}H NMR spectra of the P(OEGMEA)-*b*-(PAA) copolymer; SANS curves of micellar and polymer alone samples; fitting parameters associated with SANS curves (concentration and block length studies); dynamic light scattering data as a function of pH

ACKNOWLEDGMENTS

The authors would like to sincerely thank the Physical Measurement Laboratory (Chemical Analysis Platform) at *Université de Montpellier*, France for the polymer characterizations carried out using NMR and elemental analysis. Also, the authors extend their gratitude to the Partnership for Soft Condensed Matter (PSCM) facilities at Grenoble, France for facilitating the light scattering experiments. This project has received funding from the European Union's Horizon 2020 research and innovation programme under the Marie Skłodowska-Curie grant agreement No 847439, through the InnovaXN scheme (Project XN2020-ILL30). The authors deeply appreciate the Sans2d beamline of the Neutron and Muon Source, Rutherford Appleton Laboratory, Oxford, UK for the beam time provided (DOI: 10.5286/ISIS.E.RB2320268-1). All authors express their profound gratitude to ID02 beamline, European Synchrotron Radiation Facility, Grenoble, France (DOI: 10.15151/ESRF-ES-1371496482) for the allocation of beam time. This work benefited from the use of the SasView application, originally developed under NSF award DMR-0520547. SasView contains code developed with funding from the European Union's Horizon 2020 research and innovation programme under the SINE2020 project, grant agreement No 654000.

3.5. REFERENCES

(1) Kim, H.-C.; Park, S.-M.; Hinsberg, W. D. Block Copolymer Based Nanostructures: Materials, Processes, and Applications to Electronics. *Chem. Rev.* **2010**, *110* (1), 146–177. https://doi.org/10.1021/cr900159v.

(2) Bates, F. S.; Fredrickson, G. H. Block Copolymer Thermodynamics: Theory and Experiment. *Annu. Rev. Phys. Chem.* **1990**, *41* (1), 525–557. https://doi.org/10.1146/annurev.pc.41.100190.002521.

(3) Maekawa, S.; Seshimo, T.; Dazai, T.; Sato, K.; Hatakeyama-Sato, K.; Nabae, Y.; Hayakawa, T. Chemically Tailored Block Copolymers for Highly Reliable Sub-10-Nm Patterns by Directed Self-Assembly. *Nat. Commun.* **2024**, *15* (1), 5671. https://doi.org/10.1038/s41467-024-49839-0.

(4) Zou, Y.; Zhou, X.; Ma, J.; Yang, X.; Deng, Y. Recent Advances in Amphiphilic Block Copolymer Templated Mesoporous Metal-Based Materials: Assembly Engineering and Applications. *Chem. Soc. Rev.* **2020**, *49* (4), 1173–1208. https://doi.org/10.1039/C9CS00334G.

(5) Mai, Y.; Eisenberg, A. Self-Assembly of Block Copolymers. *Chem. Soc. Rev.* **2012**, *41* (18), 5969. https://doi.org/10.1039/c2cs35115c.

(6) Dau, H.; Jones, G. R.; Tsogtgerel, E.; Nguyen, D.; Keyes, A.; Liu, Y.-S.; Rauf, H.; Ordonez, E.; Puchelle, V.; Basbug Alhan, H.; Zhao, C.; Harth, E. Linear Block Copolymer Synthesis. *Chem. Rev.* **2022**, *122* (18), 14471–14553. https://doi.org/10.1021/acs.chemrev.2c00189.

(7) Ohtake, T.; Ito, H.; Toyoda, N. Amphiphilic Block Copolymer Surfactant-Containing Quaternized Pyridinium Salt Segments for Color Dispersion. *Polym. J.* **2022**, *54* (10), 1203–1211. https://doi.org/10.1038/s41428-022-00673-5.

(8) Sinsinbar, G.; Bindra, A. K.; Liu, S.; Chia, T. W.; Yoong Eng, E. C.; Loo, S. Y.; Lam, J. H.; Schultheis, K.; Nallani, M. Amphiphilic Block Copolymer Nanostructures as a Tunable Delivery Platform: Perspective and Framework for the Future Drug Product Development. *Biomacromolecules* **2024**, *25* (2), 541–563. https://doi.org/10.1021/acs.biomac.3c00858.

(9) Nabiyan, A.; Max, J. B.; Schacher, F. H. Double Hydrophilic Copolymers – Synthetic Approaches, Architectural Variety, and Current Application Fields. *Chem. Soc. Rev.* **2022**, *51* (3), 995–1044. https://doi.org/10.1039/D1CS00086A.

(10) El Jundi, A.; Buwalda, S. J.; Bakkour, Y.; Garric, X.; Nottelet, B. Double Hydrophilic Block Copolymers Self-Assemblies in Biomedical Applications. *Adv. Colloid Interface Sci.* **2020**, *283*, 102213. https://doi.org/10.1016/j.cis.2020.102213.

(11) Ge, Z.; Xie, D.; Chen, D.; Jiang, X.; Zhang, Y.; Liu, H.; Liu, S. Stimuli-Responsive Double Hydrophilic Block Copolymer Micelles with Switchable Catalytic Activity. *Macromolecules* **2007**, *40* (10), 3538–3546. https://doi.org/10.1021/ma070550i.

(12) Casse, O.; Shkilnyy, A.; Linders, J.; Mayer, C.; Häussinger, D.; Völkel, A.; Thünemann, A. F.; Dimova, R.; Cölfen, H.; Meier, W.; Schlaad, H.; Taubert, A. Solution Behavior of Double-Hydrophilic Block Copolymers in Dilute Aqueous Solution. *Macromolecules* **2012**, *45* (11), 4772–4777. https://doi.org/10.1021/ma300621g.

(13) Mountrichas, G.; Pispas, S. Synthesis and pH Responsive Self-Assembly of New Double Hydrophilic Block Copolymers. *Macromolecules* **2006**, *39* (14), 4767–4774. https://doi.org/10.1021/ma0605604.

(14) Al Nakeeb, N.; Willersinn, J.; Schmidt, B. V. K. J. Self-Assembly Behavior and Biocompatible Cross-Linking of Double Hydrophilic Linear-Brush Block Copolymers. *Biomacromolecules* **2017**, *18* (11), 3695–3705. https://doi.org/10.1021/acs.biomac.7b01094.

(15) Khimani, M.; Yusa, S.; Aswal, V. K.; Bahadur, P. Aggregation Behavior of Double Hydrophilic Block Copolymers in Aqueous Media. *J. Mol. Liq.* **2019**, *276*, 47–56. https://doi.org/10.1016/j.molliq.2018.11.135.

(16) Gineste, S.; Mingotaud, C. Double-Hydrophilic Block Copolymer–Metal Ion Associations: Structures, Properties and Applications. *Adv. Colloid Interface Sci.* **2023**, *311*, 102808. https://doi.org/10.1016/j.cis.2022.102808.

(17) Gérardin, C.; Sanson, N.; Bouyer, F.; Fajula, F.; Putaux, J.; Joanicot, M.; Chopin, T. Highly Stable Metal Hydrous Oxide Colloids by Inorganic Polycondensation in Suspension. *Angew. Chem. Int. Ed.* **2003**, *42* (31), 3681–3685. https://doi.org/10.1002/anie.200350917.

(18) Harada, A.; Kataoka, K. Polyion Complex Micelle Formation from Double-Hydrophilic Block Copolymers Composed of Charged and Non-Charged Segments in Aqueous Media. *Polym. J.* **2018**, *50* (1), 95–100. https://doi.org/10.1038/pj.2017.67.

(19) Insua, I.; Wilkinson, A.; Fernandez-Trillo, F. Polyion Complex (PIC) Particles: Preparation and Biomedical Applications. *Eur. Polym. J.* **2016**, *81*, 198–215. https://doi.org/10.1016/j.eurpolymj.2016.06.003.

(20) Witecka, A.; Schmitt, J.; Courtien, M.; Gérardin, C.; Rydzek, G. Hybrid Mesoporous Silica Materials Templated with Surfactant Polyion Complex (SPIC) Micelles for pH-Triggered Drug Release. *Microporous Mesoporous Mater.* **2024**, *365*, 112913. https://doi.org/10.1016/j.micromeso.2023.112913.

(21) Gérardin, C.; Reboul, J.; Bonne, M.; Lebeau, B. Ecodesign of Ordered Mesoporous Silica Materials. *Chem. Soc. Rev.* **2013**, *42* (9), 4217. https://doi.org/10.1039/c3cs35451b.

(22) Ando, T.; Vu, T. N.; Nishimura, T.; Takahashi, R.; Yusa, S. Synthesis and Characterization of Polyion Complex Micelles with Glycopolymer Shells for Drug Delivery Carriers. *Langmuir* **2024**, *40* (49), 26249–26258. https://doi.org/10.1021/acs.langmuir.4c03795.

(23) Luo, Y.; Yao, X.; Yuan, J.; Ding, T.; Gao, Q. Preparation and Drug Controlled-Release of Polyion Complex Micelles as Drug Delivery Systems. *Colloids Surf. B Biointerfaces* **2009**, *68* (2), 218–224. https://doi.org/10.1016/j.colsurfb.2008.10.014.

(24) Zhao, D.; Zhao, T. Pore Engineering for High Performance Porous Materials. *ACS Cent. Sci.* **2023**, *9* (8), 1499–1503. https://doi.org/10.1021/acscentsci.3c00916.

(25) Wang, A.; Ma, Y.; Zhao, D. Pore Engineering of Porous Materials: Effects and Applications. *ACS Nano* **2024**, *18* (34), 22829–22854. https://doi.org/10.1021/acsnano.4c08708.

(26) Björk, E. M.; Söderlind, F.; Odén, M. Tuning the Shape of Mesoporous Silica Particles by Alterations in Parameter Space: From Rods to Platelets. *Langmuir* **2013**, *29* (44), 13551–13561. https://doi.org/10.1021/la403201v.

(27) Richard, J.; Phimphachanh, A.; Schneider, J.; Nandi, S.; Laurent, E.; Lacroix-Desmazes, P.; Trens, P.; Devautour-Vinot, S.; Marcotte, N.; Gérardin, C. Integrated Process for Structuring and Functionalizing Ordered Mesoporous Silica to Achieve Superprotonic Conductivity. *Chem. Mater.* **2022**, *34* (17), 7828–7836. https://doi.org/10.1021/acs.chemmater.2c01352.

(28) Molina, E.; Warnant, J.; Mathonnat, M.; Bathfield, M.; In, M.; Laurencin, D.; Jérôme, C.; Lacroix-Desmazes, P.; Marcotte, N.; Gérardin, C. Drug–Polymer Electrostatic Complexes as New Structuring Agents for the Formation of Drug-Loaded Ordered Mesoporous Silica. *Langmuir* **2015**, *31* (47), 12839–12844. https://doi.org/10.1021/acs.langmuir.5b03221.

(29) Birault, A.; Molina, E.; Toquer, G.; Lacroix-Desmazes, P.; Marcotte, N.; Carcel, C.; Katouli, M.; Bartlett, J. R.; Gérardin, C.; Wong Chi Man, M. Large-Pore Periodic Mesoporous Organosilicas as Advanced Bactericide Platforms. *ACS Appl. Bio Mater.* **2018**, *1* (6), 1787–1792. https://doi.org/10.1021/acsabm.8b00474.

(30) Sanson, N.; Bouyer, F.; Destarac, M.; In, M.; Gérardin, C. Hybrid Polyion Complex Micelles Formed from Double Hydrophilic Block Copolymers and Multivalent Metal Ions: Size Control and Nanostructure. *Langmuir* **2012**, *28* (8), 3773–3782. https://doi.org/10.1021/la204562t.

(31) Layrac, G.; Gérardin, C.; Tichit, D.; Harrisson, S.; Destarac, M. Hybrid Polyion Complex Micelles from Poly(Vinylphosphonic Acid)-Based Double Hydrophilic Block Copolymers and Divalent Transition Metal Ions. *Polymer* **2015**, *72*, 292–300. https://doi.org/10.1016/j.polymer.2015.04.031.

(32) Gineste, S.; Lonetti, B.; Yon, M.; Giermanska, J.; Di Cola, E.; Sztucki, M.; Coppel, Y.; Mingotaud, A.-F.; Chapel, J.-P.; Marty, J.-D.; Mingotaud, C. Hybrid Polymeric Micelles Stabilized by Gallium Ions: Structural Investigation. *J. Colloid Interface Sci.* **2022**, *609*, 698–706. https://doi.org/10.1016/j.jcis.2021.11.077.

(33) Luo, Y.; Wang, A.; Yuan, J.; Gao, Q. Preparation, Characterization and Drug Release Behavior of Polyion Complex Micelles. *Int. J. Pharm.* **2009**, *374* (1–2), 139–144. https://doi.org/10.1016/j.ijpharm.2009.03.019.

(34) Pergushov, D. V.; Müller, A. H. E.; Schacher, F. H. Micellar Interpolyelectrolyte Complexes. *Chem. Soc. Rev.* **2012**, *41* (21), 6888. https://doi.org/10.1039/c2cs35135h.

(35) Sun, J.; Li, Z. Polyion Complexes via Electrostatic Interaction of Oppositely Charged Block Copolymers. *Macromolecules* **2020**, *53* (20), 8737–8740. https://doi.org/10.1021/acs.macromol.0c02031.

(36) Insua, I.; Zizmare, L.; Peacock, A. F. A.; Krachler, A. M.; Fernandez-Trillo, F. Polymyxin B Containing Polyion Complex (PIC) Nanoparticles: Improving the Antimicrobial Activity by Tailoring the Degree of Polymerisation of the Inert Component. *Sci. Rep.* **2017**, *7* (1), 9396. https://doi.org/10.1038/s41598-017-09667-3.

(37) Cabral, H.; Miyata, K.; Osada, K.; Kataoka, K. Block Copolymer Micelles in Nanomedicine Applications. *Chem. Rev.* **2018**, *118* (14), 6844–6892. https://doi.org/10.1021/acs.chemrev.8b00199.

(38) Bayó-Puxan, N.; Dufresne, M.-H.; Felber, A. E.; Castagner, B.; Leroux, J.-C. Preparation of Polyion Complex Micelles from Poly(Ethylene Glycol)-Block-Polyions. *J. Controlled Release* **2011**, *156* (2), 118–127. https://doi.org/10.1016/j.jconrel.2011.07.027.

(39) Shiraishi, K.; Kawano, K.; Maitani, Y.; Yokoyama, M. Polyion Complex Micelle MRI Contrast Agents from Poly(Ethylene Glycol)-b-Poly(l-Lysine) Block Copolymers Having Gd-DOTA; Preparations and Their Control of T1-Relaxivities and Blood Circulation Characteristics. *J. Controlled Release* **2010**, *148* (2), 160–167. https://doi.org/10.1016/j.jconrel.2010.08.018.

(40) Jiang, Y.; Lu, H.; Chen, F.; Callari, M.; Pourgholami, M.; Morris, D. L.; Stenzel, Martina. H. PEGylated Albumin-Based Polyion Complex Micelles for Protein Delivery. *Biomacromolecules* **2016**, *17* (3), 808–817. https://doi.org/10.1021/acs.biomac.5b01537.

(41) Jin, Q.; Cai, T.; Wang, Y.; Wang, H.; Ji, J. Light-Responsive Polyion Complex Micelles with Switchable Surface Charge for Efficient Protein Delivery. *ACS Macro Lett.* **2014**, *3* (7), 679–683. https://doi.org/10.1021/mz500290s.

(42) Takahashi, R.; Sato, T.; Terao, K.; Yusa, S. Reversible Vesicle–Spherical Micelle Transition in a Polyion Complex Micellar System Induced by Changing the Mixing Ratio of Copolymer Components. *Macromolecules* **2016**, *49* (8), 3091–3099. https://doi.org/10.1021/acs.macromol.6b00308.

(43) Anraku, Y.; Kishimura, A.; Oba, M.; Yamasaki, Y.; Kataoka, K. Spontaneous Formation of Nanosized Unilamellar Polyion Complex Vesicles with Tunable Size and Properties. *J. Am. Chem. Soc.* **2010**, *132* (5), 1631–1636. https://doi.org/10.1021/ja908350e.

(44) Li, Q.; Ye, L.; Zhang, A.; Feng, Z. The Preparation and Morphology Control of Heparin-Based pH Sensitive Polyion Complexes and Their Application as Drug Carriers. *Carbohydr. Polym.* **2019**, *211*, 370–379. https://doi.org/10.1016/j.carbpol.2019.01.089.

(45) Harada, A.; Kataoka, K. Novel Polyion Complex Micelles Entrapping Enzyme Molecules in the Core: Preparation of Narrowly-Distributed Micelles from Lysozyme and Poly(Ethylene Glycol)−Poly(Aspartic Acid) Block Copolymer in Aqueous Medium. *Macromolecules* **1998**, *31* (2), 288–294. https://doi.org/10.1021/ma971277v.

(46) Warnant, J.; Marcotte, N.; Reboul, J.; Layrac, G.; Aqil, A.; Jerôme, C.; Lerner, D. A.; Gérardin, C. Physicochemical Properties of pH-Controlled Polyion Complex (PIC) Micelles of Poly(Acrylic Acid)-Based Double Hydrophilic Block Copolymers and Various Polyamines. *Anal. Bioanal. Chem.* **2012**, *403* (5), 1395–1404. https://doi.org/10.1007/s00216-012-5947-1.

(47) Houssein, D.; Warnant, J.; Molina, E.; Cacciaguerra, T.; Gérardin, C.; Marcotte, N. Mesoporous Silica Templated by Polyion Complex Micelles: A Versatile Approach for Controlling the Mesostructure. *Microporous Mesoporous Mater.* **2017**, *239*, 244–252. https://doi.org/10.1016/j.micromeso.2016.10.013.

(48) Akiyama, Y.; Harada, A.; Nagasaki, Y.; Kataoka, K. Synthesis of Poly(Ethylene Glycol)-*Block* -Poly(Ethylenimine) Possessing an Acetal Group at the PEG End. *Macromolecules* **2000**, *33* (16), 5841–5845. https://doi.org/10.1021/ma000167c.

(49) Kataoka, K.; Harada, A.; Wakebayashi, D.; Nagasaki, Y. Polyion Complex Micelles with Reactive Aldehyde Groups on Their Surface from Plasmid DNA and End-Functionalized Charged Block Copolymers. *Macromolecules* **1999**, *32* (20), 6892–6894. https://doi.org/10.1021/ma990973n.

(50) Kakizawa, Y.; Kataoka, K. Block Copolymer Micelles for Delivery of Gene and Related Compounds. *Adv. Drug Deliv. Rev.* **2002**, *54* (2), 203–222. https://doi.org/10.1016/S0169-409X(02)00017-0.

(51) Ohno, S.; Ishihara, K.; Yusa, S. Formation of Polyion Complex (PIC) Micelles and Vesicles with Anionic pH-Responsive Unimer Micelles and Cationic Diblock Copolymers in Water. *Langmuir* **2016**, *32* (16), 3945–3953. https://doi.org/10.1021/acs.langmuir.6b00637.

(52) Cheng, Q.; Huang, Y.; Zheng, H.; Wei, T.; Zheng, S.; Huo, S.; Wang, X.; Du, Q.; Zhang, X.; Zhang, H.-Y.; Liang, X.-J.; Wang, C.; Tang, R.; Liang, Z. The Effect of Guanidinylation of PEGylated Poly(2-Aminoethyl Methacrylate) on the Systemic Delivery of siRNA. *Biomaterials* **2013**, *34* (12), 3120–3131. https://doi.org/10.1016/j.biomaterials.2013.01.043.

(53) Yusa, S.; Yokoyama, Y.; Morishima, Y. Synthesis of Oppositely Charged Block Copolymers of Poly(Ethylene Glycol) via Reversible Addition−Fragmentation Chain Transfer Radical Polymerization and Characterization of Their Polyion Complex Micelles in Water. *Macromolecules* **2009**, *42* (1), 376–383. https://doi.org/10.1021/ma8021162.

(54) Wibowo, A.; Osada, K.; Matsuda, H.; Anraku, Y.; Hirose, H.; Kishimura, A.; Kataoka, K. Morphology Control in Water of Polyion Complex Nanoarchitectures of Double-Hydrophilic Charged Block Copolymers through Composition Tuning and Thermal Treatment. *Macromolecules* **2014**, *47* (9), 3086–3092. https://doi.org/10.1021/ma500314d.

(55) Shovsky, A.; Varga, I.; Makuška, R.; Claesson, P. M. Formation and Stability of Water-Soluble, Molecular Polyelectrolyte Complexes: Effects of Charge Density, Mixing Ratio, and

Polyelectrolyte Concentration. *Langmuir* **2009**, *25* (11), 6113–6121. https://doi.org/10.1021/la804189w.

(56) Nakai, K.; Nishiuchi, M.; Inoue, M.; Ishihara, K.; Sanada, Y.; Sakurai, K.; Yusa, S. Preparation and Characterization of Polyion Complex Micelles with Phosphobetaine Shells. *Langmuir* **2013**, *29* (31), 9651–9661. https://doi.org/10.1021/la401063b.

(57) Kataoka, K.; Togawa, H.; Harada, A.; Yasugi, K.; Matsumoto, T.; Katayose, S. Spontaneous Formation of Polyion Complex Micelles with Narrow Distribution from Antisense Oligonucleotide and Cationic Block Copolymer in Physiological Saline. *Macromolecules* **1996**, *29* (26), 8556–8557. https://doi.org/10.1021/ma961217+.

(58) Read, E.; Lonetti, B.; Gineste, S.; Sutton, A. T.; Di Cola, E.; Castignolles, P.; Gaborieau, M.; Mingotaud, A.-F.; Destarac, M.; Marty, J.-D. Mechanistic Insights into the Formation of Polyion Complex Aggregates from Cationic Thermoresponsive Diblock Copolymers. *J. Colloid Interface Sci.* **2021**, *590*, 268–276. https://doi.org/10.1016/j.jcis.2021.01.028.

(59) Sotiropoulou, M.; Cincu, C.; Bokias, G.; Staikos, G. Water-Soluble Polyelectrolyte Complexes Formed by Poly(Diallyldimethylammonium Chloride) and Poly(Sodium Acrylate-Co-Sodium 2-Acrylamido-2-Methyl-1-Propanesulphonate)-Graft-Poly(N,N-Dimethylacrylamide) Copolymers. *Polymer* **2004**, *45* (5), 1563–1568. https://doi.org/10.1016/j.polymer.2003.12.048.

(60) Lindhoud, S.; Norde, W.; Cohen Stuart, M. A. Reversibility and Relaxation Behavior of Polyelectrolyte Complex Micelle Formation. *J. Phys. Chem. B* **2009**, *113* (16), 5431–5439. https://doi.org/10.1021/jp809489f.

(61) Park, J.-S.; Akiyama, Y.; Yamasaki, Y.; Kataoka, K. Preparation and Characterization of Polyion Complex Micelles with a Novel Thermosensitive Poly(2-Isopropyl-2-Oxazoline) Shell via the Complexation of Oppositely Charged Block Ionomers. *Langmuir* **2007**, *23* (1), 138–146. https://doi.org/10.1021/la061431j.

(62) Luo, Y.-L.; Yuan, J.-F.; Shi, J.-H.; Gao, Q.-Y. Synthesis and Characterization of Polyion Complex Micelles and Their Controlled Release of Folic Acid. *J. Colloid Interface Sci.* **2010**, *350* (1), 140–147. https://doi.org/10.1016/j.jcis.2010.06.014.

(63) Voets, I. K.; Moll, P. M.; Aqil, A.; Jérôme, C.; Detrembleur, C.; Waard, P. D.; Keizer, A. D.; Stuart, M. A. C. Temperature Responsive Complex Coacervate Core Micelles With a PEO

and PNIPAAm Corona. *J. Phys. Chem. B* **2008**, *112* (35), 10833–10840. https://doi.org/10.1021/jp8014832.

(64) De Santis, S.; Diana Ladogana, R.; Diociaiuti, M.; Masci, G. Pegylated and Thermosensitive Polyion Complex Micelles by Self-Assembly of Two Oppositely and Permanently Charged Diblock Copolymers. *Macromolecules* **2010**, *43* (4), 1992–2001. https://doi.org/10.1021/ma9026542.

(65) Voets, I. K.; Fokkink, R.; Hellweg, T.; King, S. M.; Waard, P. D.; Keizer, A. D.; Cohen Stuart, M. A. Spontaneous Symmetry Breaking: Formation of Janus Micelles. *Soft Matter* **2009**, *5* (5), 999–1005. https://doi.org/10.1039/B812793J.

(66) Steinschulte, A. A.; Gelissen, A. P. H.; Jung, A.; Brugnoni, M.; Caumanns, T.; Lotze, G.; Mayer, J.; Pergushov, D. V.; Plamper, F. A. Facile Screening of Various Micellar Morphologies by Blending Miktoarm Stars and Diblock Copolymers. *ACS Macro Lett.* **2017**, *6* (7), 711–715. https://doi.org/10.1021/acsmacrolett.7b00328.

(67) Chen, F.; Raveendran, R.; Cao, C.; Chapman, R.; Stenzel, M. H. Correlation between Polymer Architecture and Polyion Complex Micelle Stability with Proteins in Spheroid Cancer Models as Seen by Light-Sheet Microscopy. *Polym. Chem.* **2019**, *10* (10), 1221–1230. https://doi.org/10.1039/C8PY01565A.

(68) Harada, A.; Kataoka, K. Effect of Charged Segment Length on Physicochemical Properties of Core−Shell Type Polyion Complex Micelles from Block Ionomers. *Macromolecules* **2003**, *36* (13), 4995–5001. https://doi.org/10.1021/ma025737i.

(69) Gioldasis, C.; Gergidis, L. N.; Vlahos, C. Micellization through Complexation of Oppositely Charged Diblock Copolymers: Effects of Composition, Polymer Architecture, Salt of Different Valency, and Thermoresponsive Block. *J. Polym. Sci.* **2021**, *59* (2), 191–204. https://doi.org/10.1002/pol.20200754.

(70) Nakamura, N.; Mochida, Y.; Toh, K.; Fukushima, S.; Cabral, H.; Anraku, Y. Effect of Mixing Ratio of Oppositely Charged Block Copolymers on Polyion Complex Micelles for In Vivo Application. *Polymers* **2020**, *13* (1), 5. https://doi.org/10.3390/polym13010005.

(71) Krężel, A.; Bal, W. A Formula for Correlating p K a Values Determined in D 2 O and H 2 O. *J. Inorg. Biochem.* **2004**, *98* (1), 161–166. https://doi.org/10.1016/j.jinorgbio.2003.10.001.

(72) Mildner, D. F. R.; Carpenter, J. M. Optimization of the Experimental Resolution for Small-Angle Scattering. *J. Appl. Crystallogr.* **1984**, *17* (4), 249–256. https://doi.org/10.1107/S0021889884011468.

(73) Arnold, O.; Bilheux, J. C.; Borreguero, J. M.; Buts, A.; Campbell, S. I.; Chapon, L.; Doucet, M.; Draper, N.; Leal, R. F.; Gigg, M. A.; Lynch, V. E.; Markvardsen, A.; Mikkelson, D. J.; Mikkelson, R. L.; Miller, R.; Palmen, K.; Parker, P.; Passos, G.; Perring, T. G.; Peterson, P. F.; Ren, S.; Reuter, M. A.; Savici, A. T.; Taylor, J. W.; Taylor, R. J.; Tolchenov, R.; Zhou, W.; Zikovsky, J. Mantid - Data Analysis and Visualization Package for Neutron Scattering and $μSR$ Experiments. **2014**. https://doi.org/10.48550/ARXIV.1407.5860.

(74) Akcasu, A.; Benmouna, M.; Han, C. Interpretation of Dynamic Scattering from Polymer Solutions. *Polymer* **1980**, *21* (8), 866–890. https://doi.org/10.1016/0032-3861(80)90242-6.

(75) Manet, S.; Lecchi, A.; Impéror-Clerc, M.; Zholobenko, V.; Durand, D.; Oliveira, C. L. P.; Pedersen, J. S.; Grillo, I.; Meneau, F.; Rochas, C. Structure of Micelles of a Nonionic Block Copolymer Determined by SANS and SAXS. *J. Phys. Chem. B* **2011**, *115* (39), 11318–11329. https://doi.org/10.1021/jp200212g.

(76) Pedersen, J. S.; Schurtenberger, P. Scattering Functions of Semiflexible Polymers with and without Excluded Volume Effects. *Macromolecules* **1996**, *29* (23), 7602–7612. https://doi.org/10.1021/ma9607630.

(77) Chen, W.-R.; Butler, P. D.; Magid, L. J. Incorporating Intermicellar Interactions in the Fitting of SANS Data from Cationic Wormlike Micelles. *Langmuir* **2006**, *22* (15), 6539–6548. https://doi.org/10.1021/la0530440.

(78) Hammouda, B. SANS from Homogeneous Polymer Mixtures: A Unified Overview. In *Polymer Characteristics*; Advances in Polymer Science; Springer-Verlag: Berlin/Heidelberg, 1993; Vol. 106, pp 87–133. https://doi.org/10.1007/BFb0025862.

(79) Phimphachanh, A.; Chamieh, J.; Leclercq, L.; Harrisson, S.; Destarac, M.; Lacroix-Desmazes, P.; Gérardin, C.; In, M.; Cottet, H. Characterization of Diblock Copolymers by Capillary Electrophoresis: From Electrophoretic Mobility Distribution to Distribution of Composition. *Macromolecules* **2020**, *53* (1), 334–345. https://doi.org/10.1021/acs.macromol.9b01978.

(80) Améndola, I. F.; Velasco, M. I.; Acosta, R. H.; Soler Illia, G. J. A. A.; Contreras, C. B. Smart Hybrid Copolymer-Coated Silica Nanosystems with Dual Responsiveness as a Carrier for

Positive Charged Molecules. *Eur. Polym. J.* **2024**, *204*, 112717. https://doi.org/10.1016/j.eurpolymj.2023.112717.

(81) Thompson, K. L.; Read, E. S.; Armes, S. P. Chemical Degradation of Poly(2-Aminoethyl Methacrylate). *Polym. Degrad. Stab.* **2008**, *93* (8), 1460–1466. https://doi.org/10.1016/j.polymdegradstab.2008.05.013.

(82) Schmitt, J.; Calabrese, V.; Da Silva, M. A.; Lindhoud, S.; Alfredsson, V.; Scott, J. L.; Edler, K. J. TEMPO-Oxidised Cellulose Nanofibrils; Probing the Mechanisms of Gelation *via* Small Angle X-Ray Scattering. *Phys. Chem. Chem. Phys.* **2018**, *20* (23), 16012–16020. https://doi.org/10.1039/C8CP00355F.

(83) Ospennikov, A. S.; Gavrilov, A. A.; Artykulnyi, O. P.; Kuklin, A. I.; Novikov, V. V.; Shibaev, A. V.; Philippova, O. E. Transformations of Wormlike Surfactant Micelles Induced by a Water-Soluble Monomer. *J. Colloid Interface Sci.* **2021**, *602*, 590–601. https://doi.org/10.1016/j.jcis.2021.05.062.

(84) Mathonnat, M. Le rôle de l'eau dans la structuration des silices mésoporeuses par des complexes électrostatiques.

(85) Wang, J.; Si, J.; Zhu, J.; Nie, Y.; Lu, Y.; Chen, Y. Effect of Block Ratios on Self-Assembly Morphologies of Poly(ε-Caprolactone)-Block-Poly(Tert-Butyl Acrylate) Block Copolymer. *Polymer* **2023**, *284*, 126292. https://doi.org/10.1016/j.polymer.2023.126292.

(86) Sakamoto, S.; Sanada, Y.; Sakashita, M.; Nishina, K.; Nakai, K.; Yusa, S.; Sakurai, K. Chain-Length Dependence of Polyion Complex Architecture Bearing Phosphobetaine Block Explored Using SAXS and FFF-MALS. *Polym. J.* **2014**, *46* (9), 617–622. https://doi.org/10.1038/pj.2014.25.

GENERAL CONCLUSION

&

PERSPECTIVES

1. GENERAL CONCLUSION

In this PhD, we have studied the synthesis, characterization and micellization behaviour of amine-rich DHBC whose protonation leads to cationic moieties. The neutral block of the investigated DHBC is a comb-like ethylene oxide rich block, namely poly(oligo(ethylene glycol) methyl ether acrylate) (P(OEGMEA)), chosen for its ability to interact with silica and thereby to form functional mesoporous materials. We have developed two approaches to obtain these polymers:

1) by post-functionalization of a parent anionic DHBC, P(OEGMEA)-*b*-P(AA), containing a poly(acrylic acid) block and previously investigated in the team, via the so-called activation/amidation pathway. The original target was to obtain a DHBC with a partial amidation of carboxylic acid groups, hence exhibiting both primary amine and acrylate functions for applications requiring multi-functions. (*Chapter 1*)

2) by direct RAFT polymerization of the P(OEGMEA)-*b*-P(AEMA), with a second block composed of poly(2-aminoethyl methacrylate). In that path, the goal was to obtain a fully-aminated ionic block containing only primary amines. The challenges were to ensure the formation of this new diblock copolymer, control the degree of polymerization of each block and ensure the copolymer's capacity to form micelles in solution in presence of a homopolyanion (*Chapter 2*) or when mixed with P(OEGMEA)-*b*-P(AA) (*Chapter 3*).

Concerning the first approach, we presented in *Chapter 1* the method to modify the parent P(OEGMEA)-*b*-P(AA) polymer via the activation/amidation route, to graft N-Boc-ethylenediamine to the PAA backbone. This compound is further deprotected in acidic environment to remove the *tert*-butoxycabonyl group (Boc) and reveal the primary amine functions. We have seen that during activation, a side reaction induces the formation of tertiary

amines on the copolymer via the grafting of N-acyl urea derivatives on PAA's carboxylic acids. The final partially aminated DHBC hence exhibits an ionic block with a random sequence of acrylate, primary and tertiary amines species. A typical modification rate of 15 – 34 % in primary and 13 – 32 % in tertiary amines is obtained. This proves the method is suitable for a partial grafting of the polymer.

Further, the introduction of the tertiary amines allows electrostatic complexation with acrylate groups, letting the modified DHBC form micelles in solution. The micellization behaviour was studied in detail as a function of pH and concentration. Notably, we have observed by studying the scattered intensity as a function of pH in DLS the existence of an optimal pH of ca. 5 - 6 for the micelle formation, associated with the highest scattered intensity, and a slow micelle dissociation when deviating from this pH. Notably, micelles were not formed for pH ≤ 2. Finally, the shape of the micelles was studied with SANS and modelled using the polymer micelles model, proving this model is suitable to describe micellar structure made of DHBC. This self-assembling mechanism associated to the 3 different functions present on the polymer allows for a very versatile DHBC, that could be used for the design of multi-functional mesoporous materials.

Regarding the second approach, we have presented in *Chapter 2* the synthesis pathway to obtain the targeted P(OEGMEA)-*b*-P(AEMA), using RAFT polymerization. The monomers chosen allowed to use the same chain transfer agent and the same initiator for both block polymerizations. SEC-MALLS analysis proved that a DHBC was indeed formed and not two separate blocks, and the polydispersity found Mw/Mn = 1.11 is in agreement with typical polymers obtained from RAFT, proving the synthesis pathway to be successful. We have prepared two DHBC with two target degrees of polymerization (DPs) for the P(AEMA) block: 40 and 20. We noted that the analysis of the polymers by ^{1}H-NMR and elemental analysis gave slightly different DP estimates,

with values of 22 and 17 (NMR) versus 32 and 22 (elemental analysis) for both polymers synthesized. We explain this inconsistency by the complexity of the NMR pattern when the two blocks are present and the difficulty to find a proper calibration, but this will require further work in the future. We note that if obtained DPs are close to the target, according to elemental analysis, the higher the targeted DP, the more important is the mismatch. This could be due to the possible temperature-sensitive hydrolysis of P(AEMA) at high temperature, and further improvement on the synthesis protocol, notably to use initiators that work at lower temperature, should be explored. Still, we successfully design a simple polymerization protocol to obtain P(OEGMEA)-*b*-P(AEMA) with reasonable control over the DP of the second block.

This new DHBC has been mixed with polyacids, namely poly(acrylic acid) (PAA) and polystyrene sulfonate (PSS), to form micelles by electrostatic complexation with the P(AEMA) block. We studied the effect of type of polyacid used as micellization partner, of the molecular weight of the polyacid used (PAA) and of the P(AEMA) block length on the shape and size of the micelles. The micelles obtained evidenced a clear pH sensitivity as seen by DLS, with an optimum at pH = 6 and a complete dissociation for pH $\leq$ 3 - 4. Interestingly, SANS patterns as a function of pH have demonstrated a shape variation with pH, with elongated micelles seen at pH = 5 versus spherical micelles observed at pH = 6 for the system studied. This could be related to an incomplete deprotonation of the acrylate groups of the PAA used as micellization agent at pH = 5.

We have seen that at pH = 5, changing the type or length of polyacid used can also induce a shape (from cylinders to spheres) or size change. Contrarily to the micelles studied in *Chapter 1*, the SANS data studied in *Chapter 2* could not be fitted using a model of "polymer micelles". Instead, we fitted successfully the data by summing the contribution from simple spheres or cylinders to describe the micelles with the addition of a signal of polymer chains to reproduce the scattering at

high angles. This model was chosen because the comparison between the signal of P(OEGMEA)-*b*-P(AEMA) alone and in presence of PAA showed that the two scattering intensities overlap completely at large angles. However, this model raises a fundamental question: assuming this contribution to come from free DHBC polymer chains (i.e. a fraction not participating to the micelle formation), cannot be reconciled with the lack of intensity decrease compared to the signal of free DHBC, as this would suggest that almost no DHBC participates to the micelle formation. This is however in complete opposition to the DLS and SLS measurements where only the signal of micelles could be measured. An alternative to be explored in the future is to consider this contribution at large angles being associated to the comb-like architecture of the P(OEGMEA) block forming the corona of the micelles, which in that particular case is not well-reproduced with the model of "polymer micelles" that assumes a linear block.

Finally, we have studied in *Chapter 3* the formation of dual-DHBC PIC micelles by mixing P(OEGMEA)-*b*-P(AEMA) synthesized in *Chapter 2* with P(OEGMEA)-*b*-P(AA) used in *Chapter 1*. We showed that, similarly to regular PIC micelles, and in accordance with other systems reported in literature, micelles can be formed. We have carefully studied the optimal conditions for micelle formation, in terms of charge ratio between the positive ammonium and negative acrylate groups and pH. Similar trends in terms of behaviour as a function of pH can be seen in these mixtures. More interestingly, the shape of the micelles, studied in SANS and SAXS, evolves from flexible cylinders to spheres depending on the P(AEMA) block length. The effect of the P(AA) block length is less obvious, although the range of block lengths probed for this DHBC is limited. Two hypotheses can explain the deviation from the spherical shape, related to the block ratio of the DHBCs (i.e. the ratio between the molecular weight of the neutral block over the ionic block). This deviation is either related to a too anisotropic block ratio for one of the DHBC (i.e. a

too short neutral block to ensure a spherical curvature to the micelles), or a too strong mismatch between the block ratios of the two DHBCs. Further studies with other block ratios would help discriminate between these hypotheses.

In conclusion, this PhD allowed to successfully design two methods to obtain amine rich DHBC, either with only a partial grafting of amine pending groups over an acrylate backbone, or via a direct RAFT polymerization to obtain a fully aminated ionic block. Both approaches allowed for micelle formation and hence will be considered as structuring and functionalization agents for the formation of mesoporous materials.

2. PERSPECTIVES

The work developed in this manuscript paves the way for the use of cationic-DHBC for the design of functional mesoporous materials. To reach this ambitious goal, several aspects regarding the synthesis of these DHBC, their characterization and their use as templating agent should be further explored in the future.

2.1. Synthesis

2.1.1. Modification of a Parent Double Hydrophilic Block Copolymer (*Chapter 1*)

1) The unexpected incorporation of N-acyl urea to the comb-like copolymer P(OEGMEA)-*b*-P(AA) is an interesting development in itself and could find potential application in different fields including water purification, species separation, and drug delivery. Indeed, amine rich polymers can be used in devices to remove anionic contaminants from water due to their cationic behavior.[1–3] What truly sets amine rich materials apart is their extensive application in medicine.[6–8] Amine bearing polymers have been found to be excellent drug carriers, and their impressive applications have been reported more than once.[9–11] Contrarily to CO_2 adsorption where primary amines are

favoured, these applications could be performed with tertiary amines present in N-acyl urea, hence micelles made of P(OEGMEA)-*b*-P(AA/N-acyl) should be studied as nanocarriers. This would require a better control of the degree of N-acyl urea grafting. This could be achieved by studying the modification of the parent polymer with EDC only, notably by probing the effect of the excess of EDC in the mixture onto the modification rate.

2) Despite their high potential, notably in CO_2 or CH_4 capture or in drug delivery, primary amine bearing DHBCs are not found often, largely due to the lack of a simple preparation protocol. Via the protocol developed here, we reached conversion rates in primary amines of ca. 15 to 30%. This relatively low value can be explained by the O-acyl urea to N-acyl urea rearrangement which prevents the successful activation of the polymer and hence its amidation with N-Boc ethylene diamine. Hence, one future key perspective is to adjust the synthesis conditions to mitigate or even prevent the formation of N-acyl urea and hence improve the yield in N-Boc-ethylenediamine grafting. This could be achieved by working in anhydrous conditions (selecting the right carbodiimide for syntheses in non-aqueous solvents), or by adding 4-Dimethylaminopyridine (DMAP) as an EDC catalyst. First tests of the latter were performed, and amidation rates of ca. 30 - 40 % were achieved.

3) Although the chapter focusses on the modification of P(OEGMEA)-*b*-P(AA) copolymer through the grafting of N-acyl urea and primary amine groups, the possibilities extend beyond this. Other functionalities could also be introduced to the P(OEGMEA)-*b*-P(AA) copolymer, in the same fashion. Hydrophobic entities grafted onto poly(acrylic acid) for inducing self-assembly in the polymer is a classic example for the modifications carried out till date.[15] Introducing biologically relevant compounds to the P(OEGMEA)-*b*-P(AA) copolymer also seems like a promising step forward. The high biocompatibility of P(OEGMEA)-*b*-P(AA) makes it a perfect

starting material for post-synthesis modification for biological systems.[16,17] Inclusion of active compounds into the polymer; for instance, cyclodextrin[18] which enhances the solubility of drugs, seems viable through this exciting route, and justifies interest.

2.1.2. Direct Synthesis of Amine Rich Double Hydrophilic Block Copolymer (*Chapter 2*)

1) Results from this PhD prove the feasibility to design P(OEGMEA)-b-P(AEMA) via RAFT polymerization in aqueous medium. Nonetheless the main shortcoming of our work lies in the discrepancy between the degree of polymerizations (DP) of the P(AEMA) obtained via the ^{1}H NMR and elemental analyses. For targets of 20 and 40 respectively, elemental analysis results give DP of 22 and 32 respectively, while we found 17 and 22 in ^{1}H NMR. The discrepancy could be due to the complex NMR patterns, having contributions of both blocks, that may prevent the perfect integration of the P(AEMA) related peaks. We started in the group some more detailed studies of the P(AEMA) homopolymer via NMR and SEC-MALLS, to better characterize it. Notably, the importance of dialysis was evidenced in SEC-MALLS, suggesting the presence of residual monomers or incomplete polymerization. A simple study to try to better characterize the DP of the diblock copolymer would be to start the polymerization from the P(AEMA) block instead of the, well-known and controlled, P(OEGMEA) block. This would allow for a simpler interpretation of the NMR pattern regarding the P(AEMA) block. The main difficulty would be to have a sufficiently trustworthy calibration for the analysis of the second block. Finally, P(AEMA) can become highly unstable at high temperatures, which could explain the lower DPs found especially at high targets. Hence finding alternative initiators that would allow to work at lower synthesis temperatures would be beneficial. A promising candidate is 2,2'-Azobis[2-(2-imidazolin-2-yl)propane] Dihydrochloride (VA44), which could be used for the polymerization of P(AEMA) at 50°C instead of 80°C.

2) The synthesis could be extended to poly(acrylamide) blocks instead of P(AEMA). The higher stability of poly(acrylamide) towards hydrolysis than poly(amine acrylate), make them the ideal subsequent development.

2.2. Characterization of Self-Assemblies

1) In this manuscript, micelles made of different DHBC were extensively studied as a function of pH and concentration, using SANS and/or SAXS. Due to the nature of the micelles investigated, we expected to need core-shell models to describe them accurately. Hence one of the main axis of improvement would lie in the careful examination of this possible core-shell organization using contrast variation techniques. The difference in scattering length density (SLD) between the objects, or in our case core and shell, which is a parameter associated with the neutron scattering ability, is the basis of contrast variation technique. We have made significant tests by varying the D_2O/H_2O ratio of the solutions, but those results were mainly unsuccessful due to the limited difference in SLD between the two hydrogenated blocks of the DHBCs and the micellization partner (when present) and the high amount of water expected in both core and shell. Due to the large difference in SLD between deuterium and hydrogen, a deuteration of one of the blocks of the DHBC and/or the micellization partner could allow to differentiate the signal of the core from the one of the shell. This could be applied for both the aminated self-assemblies discussed in *Chapter 1* P(OEGMEA)-*b*-P(AA-*s*-(Acyl urea)-*s*-(AA/NH_2)) and *Chapter 2* P(OEGMEA)-*b*-P(AEMA). However, ultimately finding the required deuterated monomers could prove to be a limiting factor. Concerning *Chapter 2*, a possibility would lie in using a commercial deuterated PAA as micellization partner.

2) All small angle scattering data (SAS) collected during this project were fitted with a carefully chosen model, to extract detailed information about the systems. Models used were chosen based

on the sample probed. In *Chapter 1*, electrostatic interaction within the copolymer leads to the self-assembly. For that reason, we expect the entire signal to derive from a single population. A polymer micelle model was hence used to fit the SANS data in this context. In *Chapter 2* and *3*, the micelles are formed through the electrostatic interaction between two oppositely charged species, and one may expect multiple populations even after self-assembly, due to the presence of unmicellized entities. SAS data for these samples were examined by fitting them with a combination of two models; a simple sphere/(flexible) cylinder model associated with the shape of the micelle and a free polymer model linked to all polymer chains. It should be noted that, polyelectrolytes comparable to PAANa and PSSNa used as micellization partner, cannot be probed using SAS, due to their negligible contrast and were not considered while choosing the model for fitting. This sum of two contributions is consistent as well with the SAS patterns of unmicellized DHBC, where the contribution measured overlaps well with the signal observed at large angles in micellar suspensions. Nonetheless, this model has a severe shortcoming: if the contribution from polymer chains are from unmicellized DHBC, its intensity is very high, within the same range than the signal from DHBC without micellization partner. This would lead to a very low amount of DHBC to be used to form the micelles, typically below 20%, which is completely inconsistent with the DLS data. An alternative is that this contribution at large angles is from the comb-like P(OEGMEA) block composing the corona. We have tried to fit the data from *Chapter 2* with the 'polymer micelles' model used in *Chapter 1* but fits failed to reproduce well the data. This may be due to the fact that both the polymer micelles and free polymer chains models used in this PhD were built for linear block copolymers and not comb-like structures with a more abrupt interface between micelles and solvent. Consequently, these models fail to fully reproduce the scattering behaviour of the samples in the high-q region. In the future, it would hence be interesting to

develop models for diblock polymer chains and polymer micelles with a comb-like architecture in one of the blocks.

2.3. Porous Material Synthesis

In the future, the main perspective is to use both types of aminated DHBCs to form functional mesoporous materials in presence of a silica precursor such as tetraethyl orthosilicate (TEOS). If first tests still need to be carried, special care should be taken regarding the following point: primary amine groups are recognized for their good nucleophilic and alkaline nature, along with lower steric hindrance. These characters make primary amine-based DHBC an efficient precursor in the syntheses of polyion complex micelles. While the nucleophilicity and lesser steric-hindrance helps functionalization if needed, the basicity of the amine promotes electrostatic self-assembly. However, studies on its ability to craft ordered and functionalized mesoporous materials is still lacking. The primary amine groups could potentially interact with the acidic hydroxyl groups (-OH) in the silica material, during the material synthesis, causing disturbance to the structure and functionalization of the final product. Functional materials synthesized from copolymers bearing secondary, tertiary and quaternary amine should be safer in this aspect, due to the diminished basicity. Fine tuning the protocol for material synthesis could potentially help us to go around this shortcoming of primary amine copolymers but it requires further comprehensive studies.

Annex 1 - Supporting information for Chapter 1

Synthesis of a double-hydrophilic block copolymer with a multifunctional block: spontaneous formation of polyion complex micelles from a single cationic-anionic copolymer

Ananthapadmanabhan Unnikrishnan,[1,2] Mateus Garcia Rodolfo[2], Najet Mahmoudi,[3] Gaulthier Rydzek,[2] Julien Schmitt,[2,4] Ralf Schweins[1] and Corine Gerardin[2]

[1] Large Scale Structures Group, Institut Laue − Langevin, 71 Avenue des Martyrs, CS 20156, Grenoble Cedex 9, 38042, France

[2] Institut Charles Gerhardt, UMR 5253, CNRS-ENSCM-UM, University of Montpellier, Cedex, F-34295, France

[3] ISIS Neutron and Muon Source, Science and Technology Facilities Council, Rutherford Appleton Laboratory, Didcot OX11 0QX, United Kingdom

[4] LSFC – Laboratoire de Synthèse et Fonctionnalisation des Céramiques, UMR 3080 CNRS/Saint-Gobain CREE, Saint-Gobain Research Provence, 550 Avenue Alphonse Jauffret, Cavaillon, France

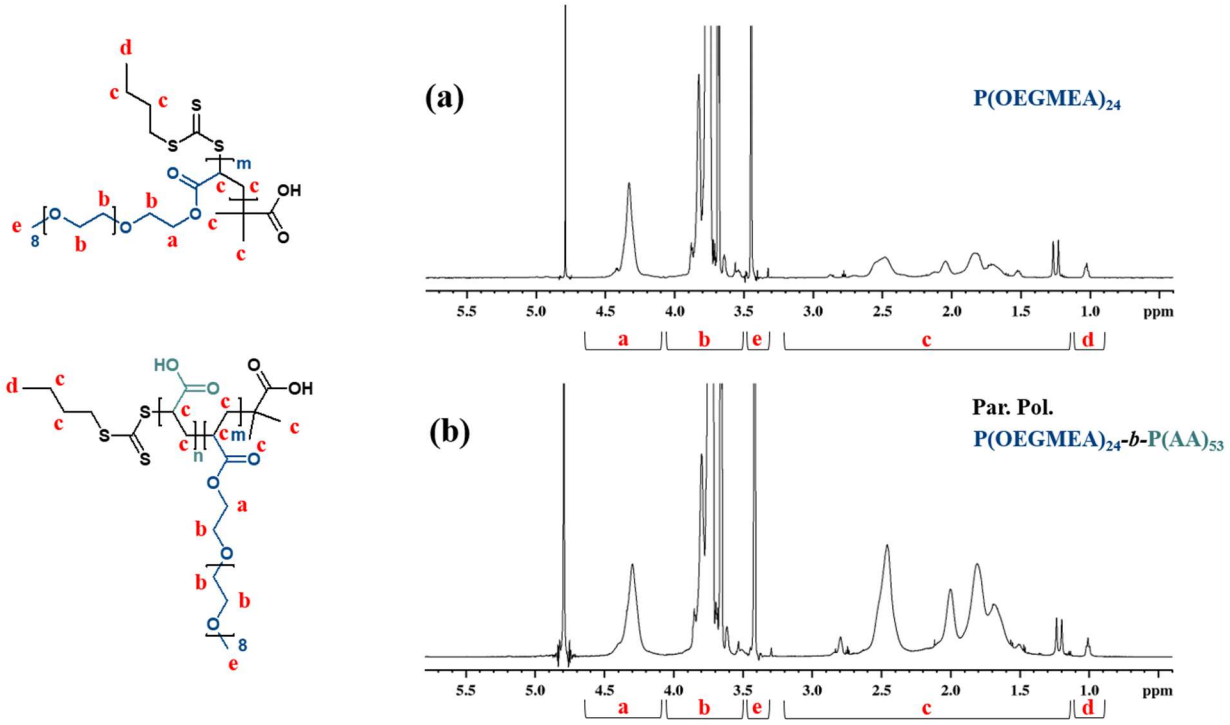


Figure S1. *^{1}H NMR spectra of (a) P(OEGMA)$_m$ (b) P(OEGMA)$_m$-b-P(AA)$_n$ (Par. Pol.) obtained after RAFT polymerization. The degree of polymerization (DP) of each block was characterized using the peaks highlighted (through alphabetical characters). The insets, presenting the chemical formula of each polymer, show to which protons each highlighted peak corresponds to. The peaks at 1 ppm (highlighted using "d") corresponds to the three protons attached to the terminal carbon in the backbone for both (a) and (b) while the peak area in the up shield (1.2 - 3.2) presents the protons in the backbone of P(OEGMEA) of (a) and, in (b) is the contribution from the backbone of the entire copolymer (P(OEGMEA)-b-P(AA)). The peak area highlighted using a, b and e is the contribution from the hydrogens in the side chain of the P(OEGMEA) block. The DP was found to be 24 and 53 for P(OEGMEA) and P(AA) blocks respectively, (P(OEGMA)$_{24}$-b-P(AA)$_{53}$).*

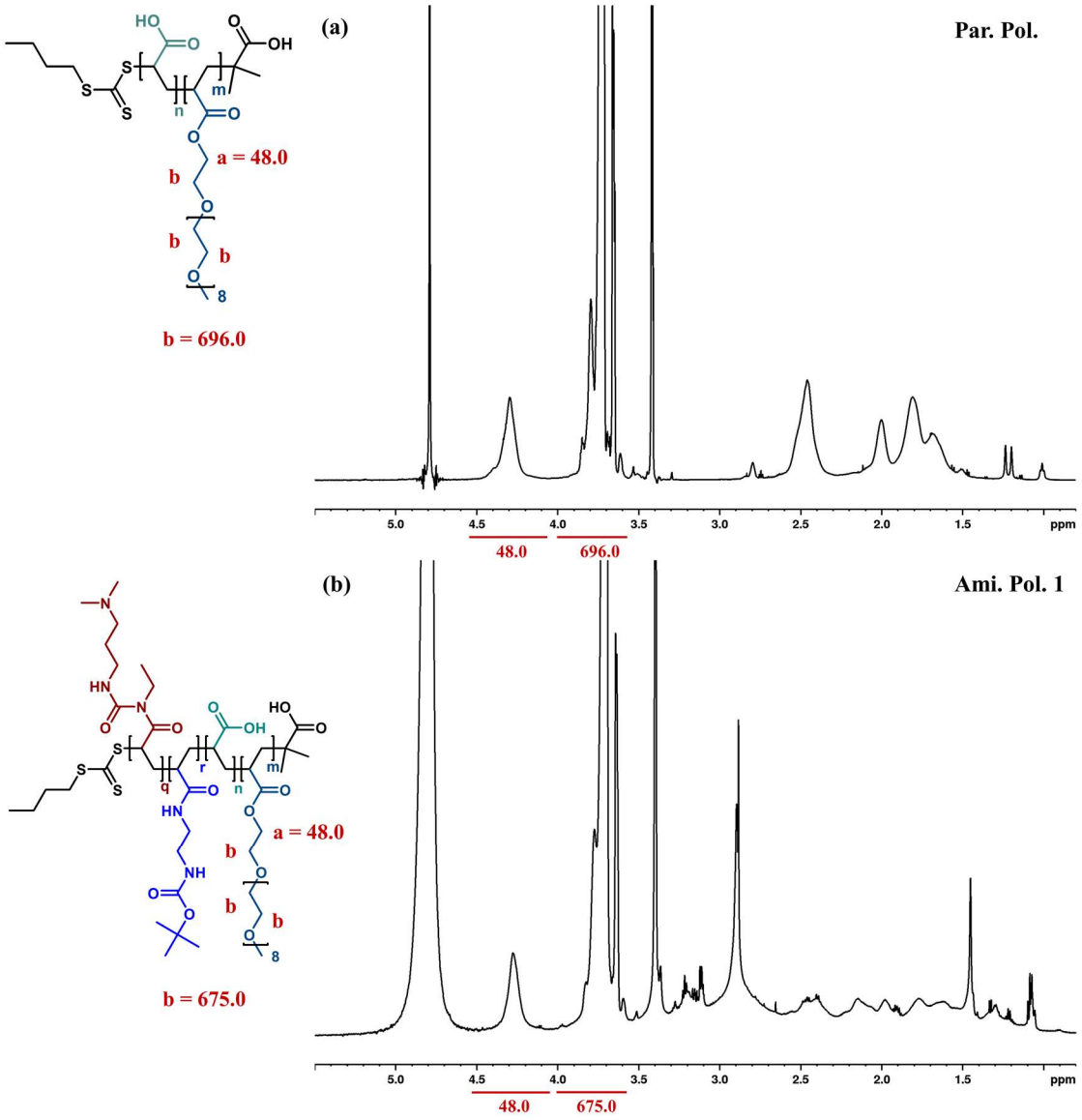


Figure S2. *^{1}H NMR spectra of (a) P(OEGMEA)$_{24}$-b-P(AA)$_{53}$ (Par. Pol.) and (b) P(OEGMEA)$_{24}$-b-P((AA)$_{28}$-s-(Acyl urea)$_{17}$-s-(N-Boc)$_{8}$) (Ami. Pol. 1). The peak at 1 ppm (in spectrum (a)) corresponds to the three protons attached to the terminal carbon in the backbone while the peak area in the up shield (1.2 - 3.2) is the contribution from the backbone of the entire copolymer (P(OEGMEA)-b-P(AA)) in (a) and it is the contribution from P(OEGMEA)-b-P((AA)-s-(Acyl urea)-s-(N-Boc)) backbone in (b). The range 3.2 - 4.4 is ascribed to the protons from the oligo(ethylene oxide) methyl ether comb in the POEGMEA block for both (a) and (b). The distinct*

peak at 4.30 ppm in the spectra (a) and (b) is the contribution from the α-hydrogens adjacent to the ester bond in POEGMEA. This peak at 4.30 ppm is used as the reference to find the peak area between 3.6 – 4.0 before and after the amidation reaction, to confirm that the comb structure of the POEGMA block is not destroyed. Consistent values (696.0 and 675.0 for (a) and (b) respectively) indicate the copolymer to be unharmed by the modification carried out.

Sample name	Elemental Analysis (EA)							
	%C	Deviation (abs.)	%H	Deviation (abs.)	%N	Deviation (abs.)	%S	Deviation (abs.)
Act. Pol.	46.95	0.17	8.79	0.04	6.08	0.02	0.15	0.01
Ami. Pol. 1	48.84	0.01	9.28	0.06	7.52	0.01	0.01	0.01
Ami. Pol. 2	51.78	0.05	8.57	0.02	7.84	0.08	0.17	0.04
Ami. Pol. 3	47.32	0.19	8.73	0.22	6.07	0.02	0.01	0.02
Ami. Pol. 4	50.38	0.19	8.43	0.01	6.53	0.05	0.09	0.03

Table S1. *Composition measurement in weight % of P(OEGMEA)-b-P(AA-s-(AA-NHS)-s-(Acyl urea)) (Act. Pol.) and P(OEGMEA)-b-P(AA-s-(Acyl urea)-s-(N-Boc)) (Ami. Pol. 1 - 4) batches by Elemental Analysis (EA).*

Sample name	Condition for deprotection (acid, reaction time)	Elemental Analysis (EA)							
		%C	Deviation (abs.)	%H	Deviation (abs.)	%N	Deviation (abs.)	%S	Deviation (abs.)
De. Pol. 1	TCA, 1 hour	50.77	0.11	8.95	0.17	6.79	0.05	0.07	0.01
De. Pol. 2	TCA, 1 hour	51.51	1.88	8.87	0.01	6.85	0.01	0.11	0.02
De. Pol. 3	TCA, 1 day	52.31	0.04	8.93	0.05	7.29	0.09	0.06	0.09
De. Pol. 4	HCl, 1 day	51.30	0.16	8.70	0.09	6.94	0.12	0.13	0.02

Table S2. *Composition measurement in weight % from elemental analysis of De. Pol. 1 – 4 deprotected samples.*

Comparing the methods for deprotection

Different protocols for deprotection, using TCA for 1h (De. Pol. 2, similar to the method used for Ami. Pol. 1 above), TCA for 1 day (De. Pol. 3) and HCl for 1 day (De. Pol. 4) were studied in detail using Ami. Pol. 2 (see **Table 1**). The deprotection was once again explored using ^{1}H NMR. The deprotection was successfully done, using all methodologies attempted, with the removal of the 1.47 ppm peak associated to Boc (**Figure S3**). Even though, a 1 M hydrochloric acid solution could also be used, instead of TCA for freeing the amine species in the copolymer, HCl being a stronger acid when compared to TCA, using it could possibly destroy the polyester side chain in the copolymers. Also, using TCA for a longer time could lead to the same, as polyester chains in the copolymer is susceptible to acid hydrolysis. Elemental analysis was used to determine the Nitrogen content in the copolymers after deprotection. The N/C ratio was ca. 0.116 (the average of three N/C values) for the products obtained through the above routes while the H/C was found to be ca. 2.10. The slight disparity in the N/C and H/C ratio from EA compared to the theoretical calculated values from NMR (N/C 0.103 and H/C 1.88) is most likely due to the impurities.

Both the rigorous methodologies, i) the use of a stronger acid 1 M HCl for 1 day and ii) the TCA deprotection for a longer time, could potentially rupture the side chain in the copolymer, however, this does not restrict the copolymer from crafting well-defined spherical species, just like the 1-hour TCA deprotected macromolecules studied above. Typically, the copolymers from the above deprotected routes were characterized in SANS at 1 wt% (solution at pH = 5 in D_2O, **Figure S4** and **Table S3**) for studying their micellar behaviour, however, the sample deprotected using TCA for 1 hour was studied at 2 wt%. The scattering curves exhibit the same pattern whatever the deprotection method being used. Although the treatments using TCA and HCl for 1 day did not

prevent the micellization of the polymer after deprotection, the 1h treatment with TCA remains the most efficient method to ensure Boc removal without damaging the polymer.

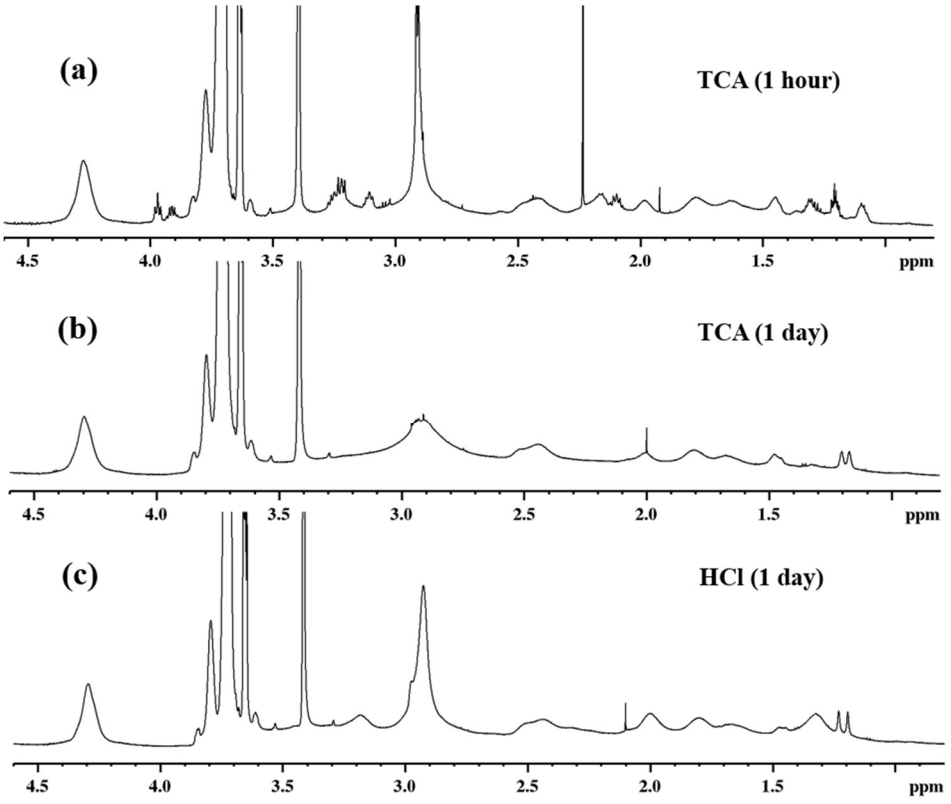


Figure S3. *^{1}H NMR spectra of De. Pol. 2 - 4, from the deprotection of Ami. Pol. 2. Deprotection made using (a) TCA 1 hour (De. Pol. 2) (b) TCA 1 day (De. Pol. 3) (c) HCl 1 day (De. Pol. 4).*

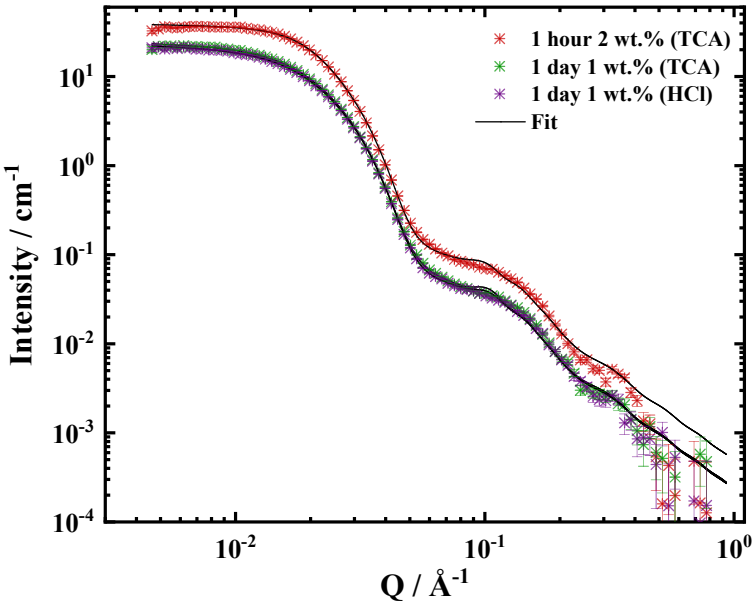


Figure S4. *SANS patterns of deprotected polymers, De. Pol. 2 – 4 micelles. In red, De. Pol. 2 (TCA 1 hour), in green, De. Pol. 3 (TCA 1 day), and in violet, De. Pol. 4 (HCl 1 day).*

Sample name	Condition for deprotection (acid, reaction time)	Scale (std. error)	Radius R nm (std. error)	Radius of gyration R_g nm (std. error)	Volume of shell v_{shell} nm^3 (std. error)	Polydispersity σ % (std. error)	Structural factor	
							Volume fraction % (std. error)	Hard sphere radius nm (std. error)
De. Pol. 2	TCA, 1 hour	0.31×10^{-6} (0.01×10^{-6})	6.5 (0.1)	3.2 (0.1)	0.73×10^{2} (0.01×10^{2})	13 (1)	6 (1)	14.8 ± 0.3
De. Pol. 3	TCA, 1 day	0.16×10^{-6} (0.01×10^{-6})	6.2 (0.1)	3.3 (0.1)	0.69×10^{2} (0.01×10^{2})	13 (1)	2 (1)	16.7 ± 0.6
De. Pol. 4	HCl, 1 day	0.16×10^{-6} (0.01×10^{-6})	6.1 (0.1)	3.3 (0.1)	0.68×10^{2} (0.01×10^{2})	14 (1)	2 (1)	16.4 ± 0.5

Table S3*. List of parameters obtained from the SANS data fitting of deprotected De. Pol. 2 – 4 micelles.*

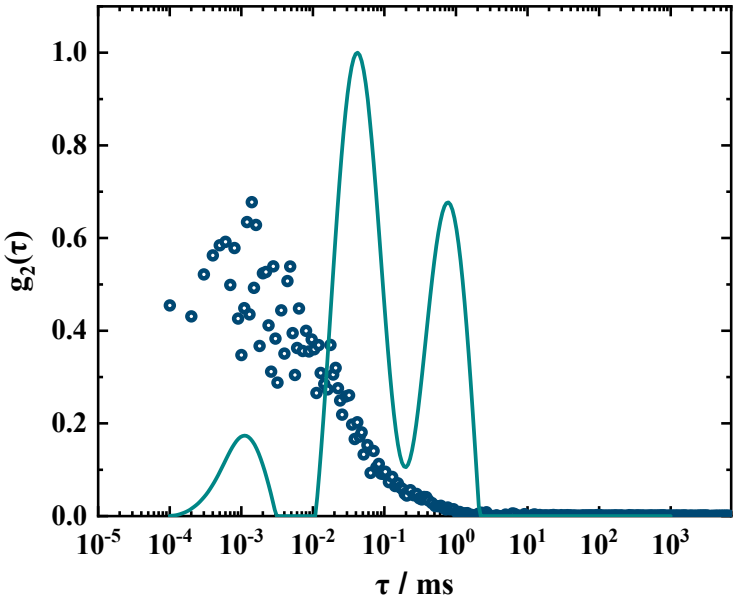


Figure S5. *(a) Intensity-time autocorrelation function $g_2(\tau)$ of Par. Pol., $P(OEGMEA)_{24}$-b-$P(AA)_{53}$, at 0.1 wt% and pH = 5 in H_2O (0.1 M NaCl), measured at a scattering angle $\theta = 90^{o}$ and its related relaxation time distribution using the CONTIN analysis. The very noisy correlation highlights that no clear scattering objects could be detected, referring to the inability of the copolymer to self-assemble spontaneously without a micellization partner or suitable modifications of the PAA block.*

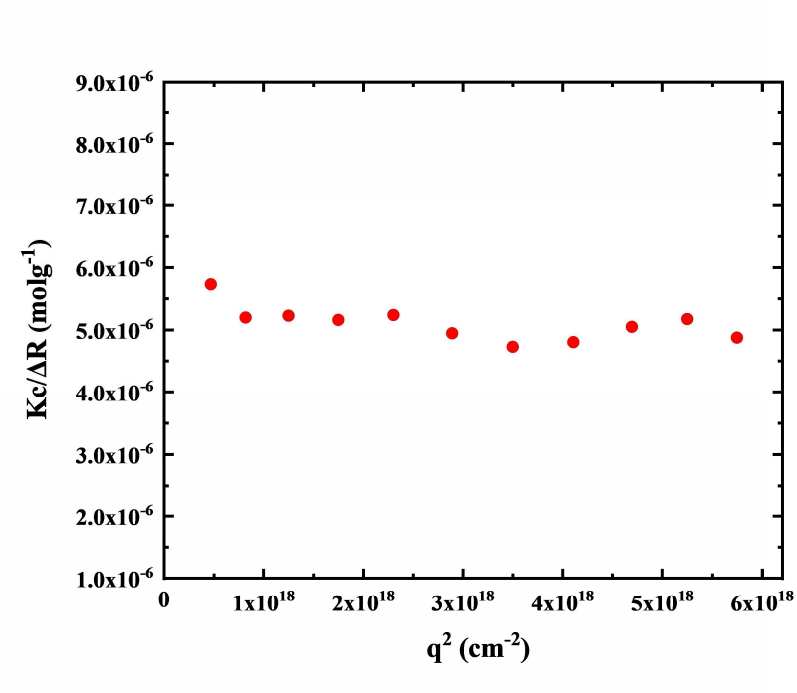


Figure S6. *Zimm plot from SLS data associated to Act. Pol. micelles in 0.1 wt% H_2O at pH 5.*

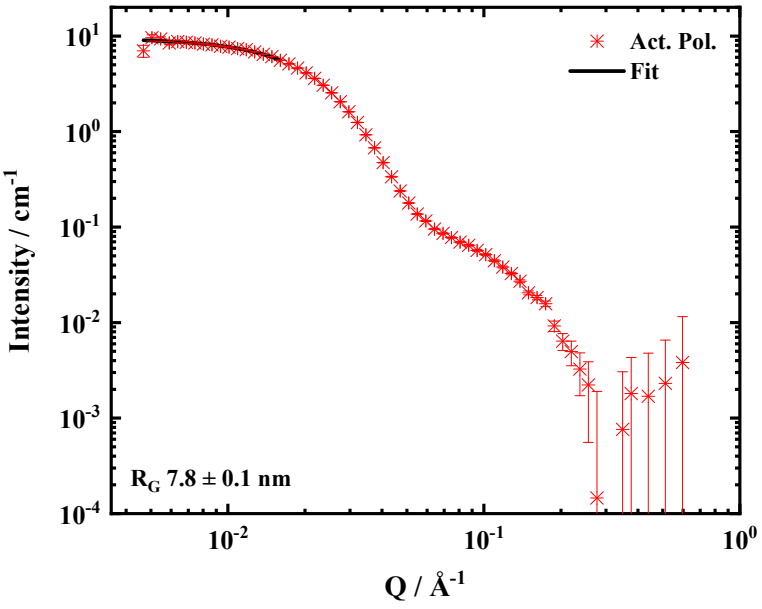


Figure S7. *Guinier fit of polymeric micelles from Act. Pol. using SANS data at 1 wt% and pH 5 in D_2O (R_G found to be 7.8 ± 0.1 nm).*

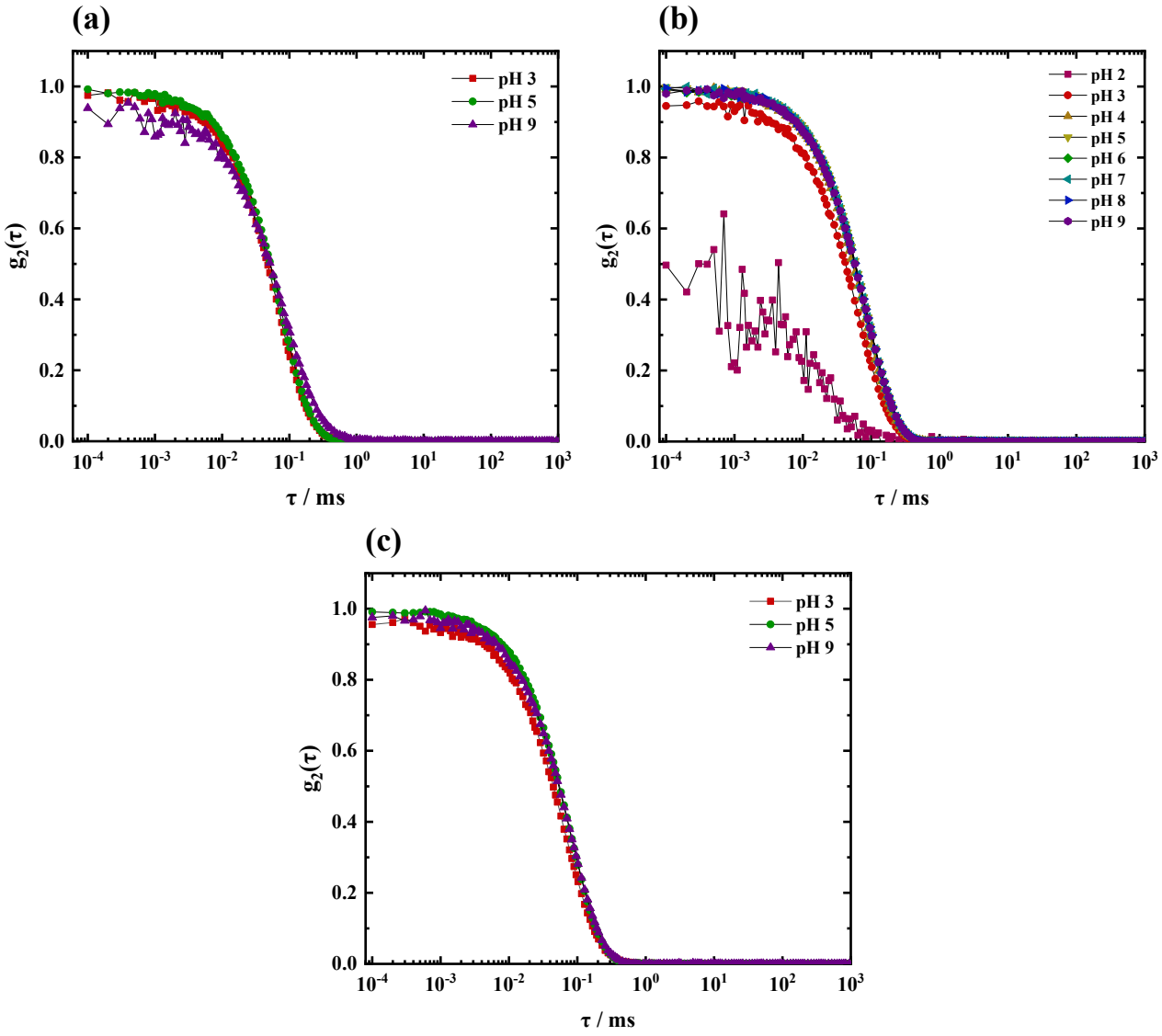


Figure S8. *Intensity-time autocorrelation functions $g_2(\tau)$ studied at a scattering angle of $\theta = 90°$ for micelles at 0.1 wt% in H_2O and various pH; (a) Act. Pol. (b) Ami. Pol. 1 (c) De. Pol. 1.*

Sample name	Chemical composition	Light scattering		Neutron scattering		
		Hydrodynamic radius R_H nm (std. error)	Full width half maximum FWHM	Radius R nm (std. error)	Radius of gyration R_g nm (std. error)	Polydispersity σ % (std. error)
Act. Pol.	$P(OEGMEA)_{24}$-*b*-$P((AA)_{25}$-*s*-$(AA\text{-}NHS)_{17}$-*s*-$(Acyl\ urea)_{11})$	13.4 (0.1)	0.3	5.2 (0.3)	1.8 (0.2)	36 (1)
Ami. Pol. 1	$P(OEGMEA)_{24}$-*b*-$P((AA)_{28}$-*s*-$(Acyl\ urea)_{17}$-*s*-$(N\text{-}Boc)_8)$	14.6 (0.1)	0.2	6.3 (0.1)	3.3 (0.1)	13 (2)
Ami. Pol. 2	$P(OEGMEA)_{24}$-*b*-$P((AA)_{28}$-*s*-$(Acyl\ urea)_{17}$-*s*-$(N\text{-}Boc)_8)$	---	---	6.7 (0.1)	3.6 (0.1)	14 (2)
Ami. Pol. 3	$P(OEGMEA)_{24}$-*b*-$P((AA)_{23}$-*s*-$(Acyl\ urea)_{12}$-*s*-$(N\text{-}Boc)_{18})$	---	---	3.5 (0.2)	3.0 (0.1)	48 (2)
Ami. Pol. 4	$P(OEGMEA)_{24}$-*b*-$P((AA)_{32}$-*s*-$(Acyl\ urea)_7$-*s*-$(N\text{-}Boc)_{14})$	---	---	4.1 (0.3)	2.8 (0.1)	46 (3)
De. Pol. 1	$P(OEGMEA)_{24}$-*b*-$P((AA)_{28}$-*s*-$(Acyl\ urea)_{17}$-*s*-$(AA/NH_2)_8)$	13.8 (0.1)	0.3	5.3 (0.1)	3.5 (0.1)	17 (1)
De. Pol. 2	$P(OEGMEA)_{24}$-*b*-$P((AA)_{30}$-*s*-$(Acyl\ urea)_{17}$-*s*-$(AA/NH_2)_6)$	---	---	6.5 (0.1)	3.2 (0.1)	13 (1)
De. Pol. 3	$P(OEGMEA)_{24}$-*b*-$P((AA)_{30}$-*s*-$(Acyl\ urea)_{17}$-*s*-$(AA/NH_2)_6)$	---	---	6.2 (0.1)	3.3 (0.1)	13 (1)
De. Pol. 4	$P(OEGMEA)_{24}$-*b*-$P((AA)_{30}$-*s*-$(Acyl\ urea)_{17}$-*s*-$(AA/NH_2)_6)$	---	---	6.1 (0.1)	3.3 (0.1)	14 (1)

Table S4. *Consolidation of small angle neutron scattering and dynamic light scattering data on the dimension of the self-assemblies formed.*

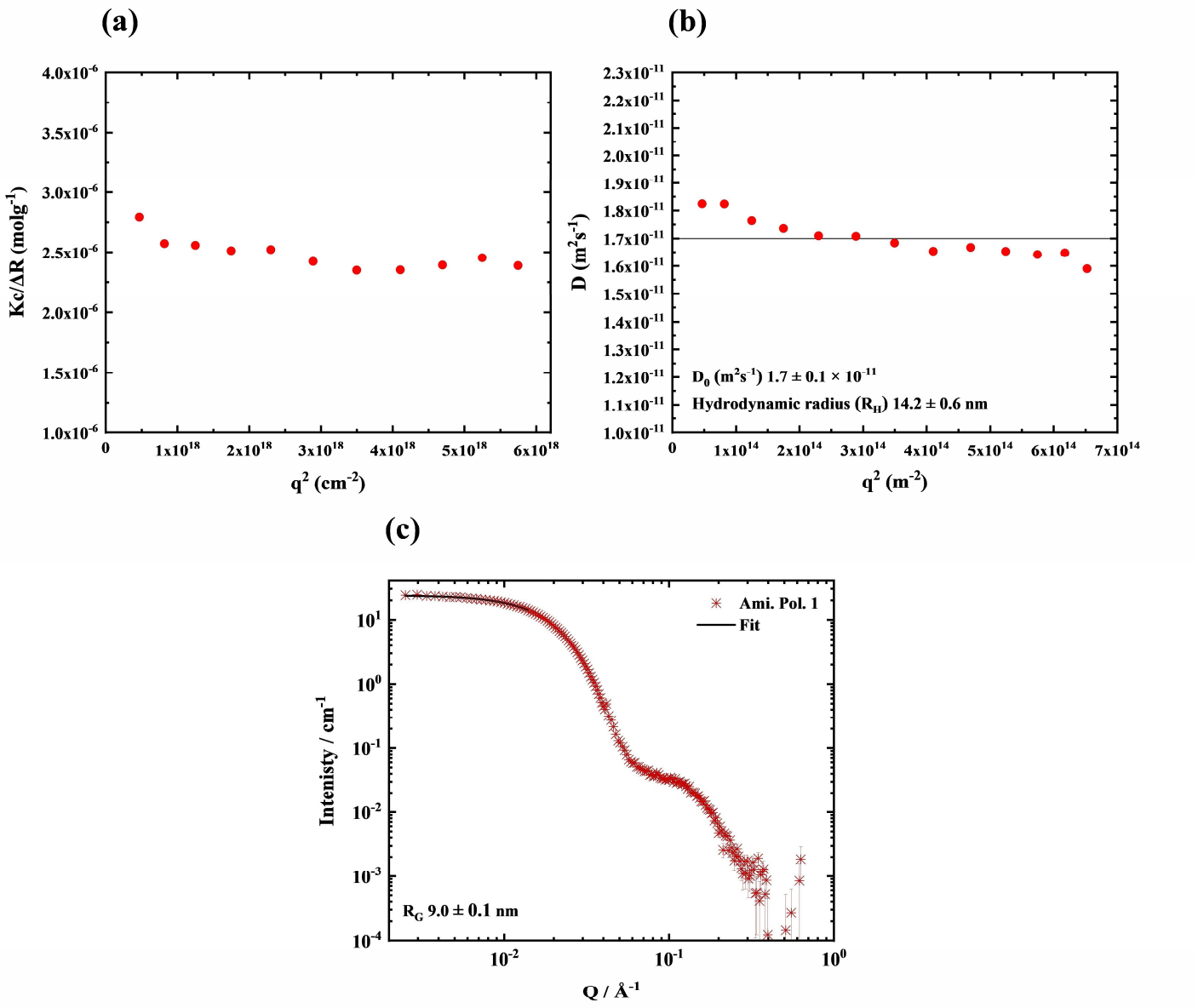
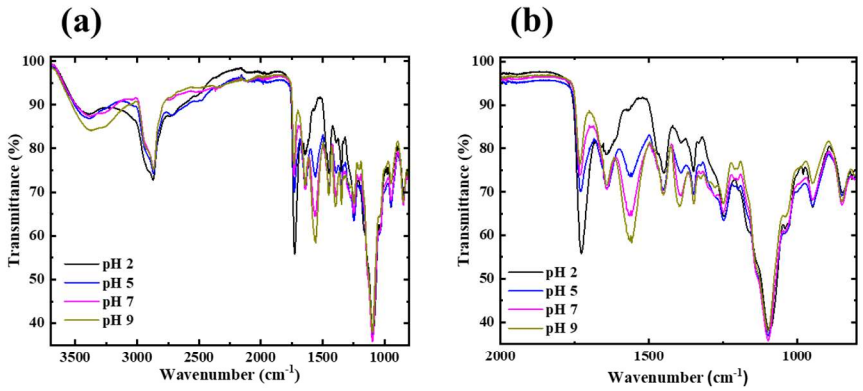


Figure S9. *(a) Zimm plot from SLS data (b) Plot of the Diffusion coefficient (D) as a function of scattering vector (q^2) of Ami. Pol. 1 micelles at pH 5 in H_2O from the second order cumulant analysis (in inset are given the diffusion coefficient D_0 from averaging and the corresponding hydrodynamic radius R_H) (c) SANS pattern of micelles from Ami. Pol. 1 at pH 5 and D_2O as the solvent. In black, the fit made using the Guinier approximation at low q is given (in inset, the value of R_G found from the fit).*



(c)

Main vibration bands (cm^{-1})	3200-3600	2800-3000	1600-1700	1560	1450	1400	1000-1200
Attributions	O-H (s) N-H (s)	C-H (s)	C=O (s)	C=O (s) in COO- N-H (b)	C-OH (b)	C=O (s) in COO-	C-O (s) C-N (s)

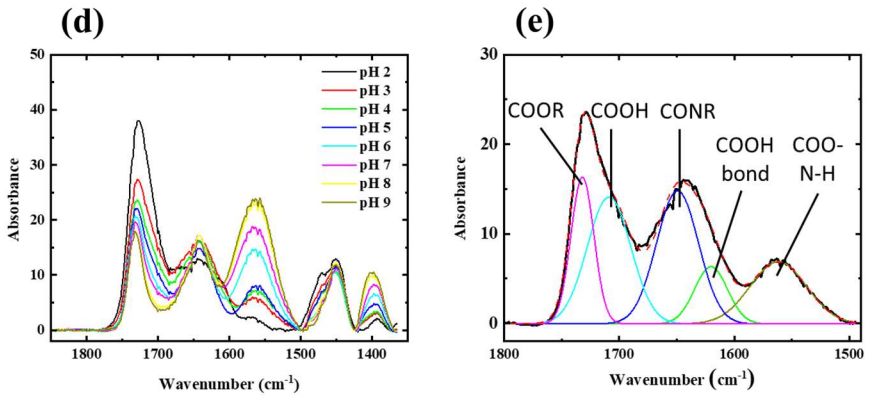


Figure S10. *ATR-FTIR analysis of the amidated copolymer as a function of pH. Overview spectra (a) and fingerprint region (b) measured by ATR-FTIR of Ami. Pol. 5 freeze-dried at pH 2 to 9. (c) Attribution of the main bands to vibrational modes. (d) Evolution of the baseline-corrected absorbance measured in the carbonyl region as a function of pH. (e) Example of spectrum deconvolution, corresponding to pH 5 conditions, displaying carbonyl stretching bands from ester, carboxylic acid, amide, bound carboxylic acid and carboxylate moieties as well as N-H bending from amides.*

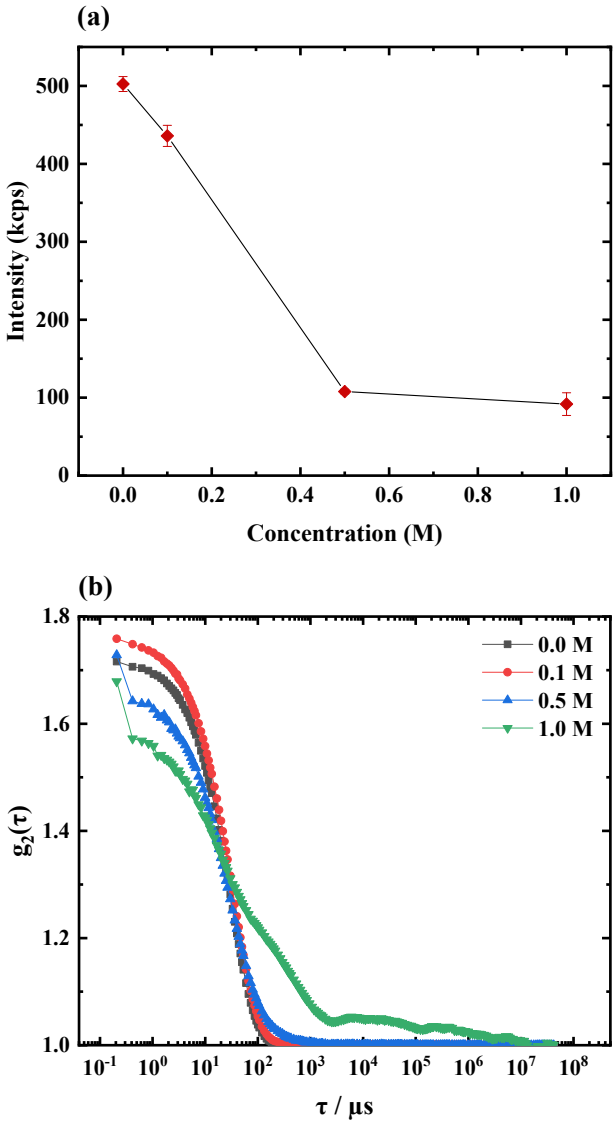


Figure S11. *DLS measurements of Ami. Pol. 5 at 0.1 wt% and pH = 5 as a function of salt concentration: (a) Averaged scattered intensity (b) the associated correlation functions in intensity* $g_2(\tau)$.

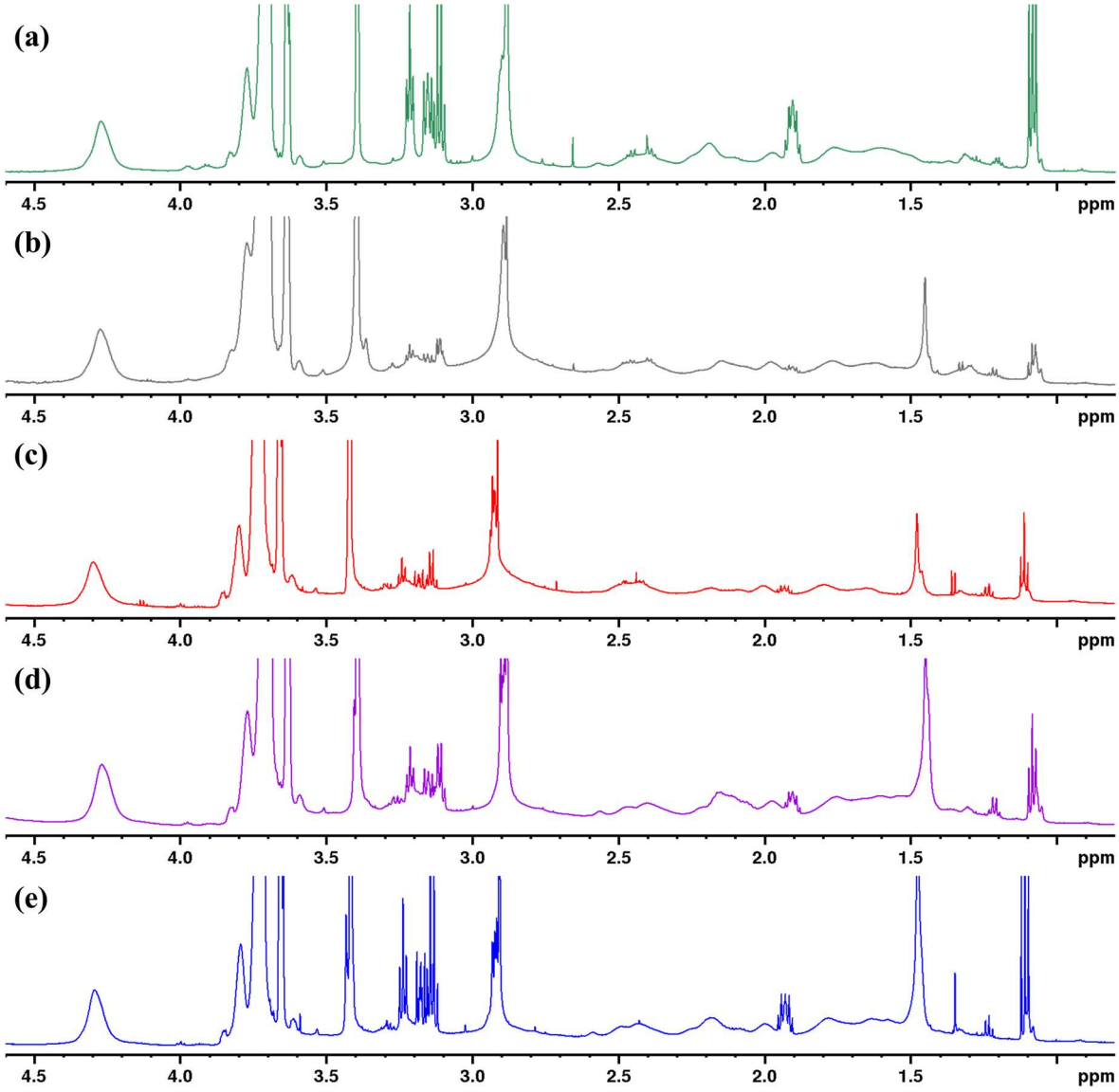


Figure S12. *^{1}H NMR spectra of (a) Act. Pol., (b) Ami. Pol. 1, (c) Ami. Pol. 2, (d) Ami. Pol. 3, and (e) Ami. Pol. 4.*

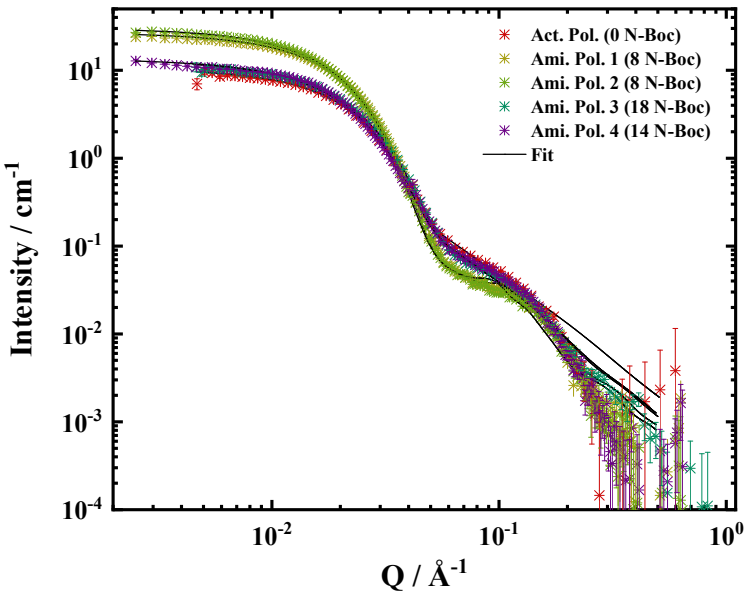


Figure S13. *Effect of N-Boc content in the shape of the self-assembled species formed, studied using SANS. In inset, the name of the polymers used, and in parenthesis, the number of N-Boc units in the polymers. In black, the fits made using the polymer micelle model are given.*

Sample name	Scale (std. error)	Radius R nm (std. error)	Radius of gyration R_g nm (std. error)	Volume of shell v_{shell} nm^3 (std. error)	Polydispersity σ % (std. error)
Act. Pol.	0.48×10^{-7} (0.03×10^{-7})	5.2 (0.3)	1.8 (0.2)	0.14×10^{3} (0.02×10^{3})	36 (1)
Ami. Pol. 1	0.14×10^{-6} (0.01×10^{-6})	6.3 (0.1)	3.3 (0.1)	0.72×10^{2} (0.01×10^{2})	13 (2)
Ami. Pol. 2	0.14×10^{-6} (0.01×10^{-6})	6.7 (0.1)	3.6 (0.1)	0.77×10^{2} (0.01×10^{2})	14 (2)
Ami. Pol. 3	0.84×10^{-7} (0.04×10^{-7})	3.5 (0.2)	3.0 (0.1)	0.12×10^{3} (0.01×10^{3})	48 (2)
Ami. Pol. 4	0.67×10^{-7} (0.07×10^{-7})	4.1 (0.3)	2.8 (0.1)	0.16×10^{3} (0.01×10^{3})	46 (3)

Table S5*. List of parameters obtained from the SANS data fitting of Act. Pol. and Ami. Pol. 1 – 4 micelles associated to* ***Figure S13****. No structure factor was required to fit the data.*

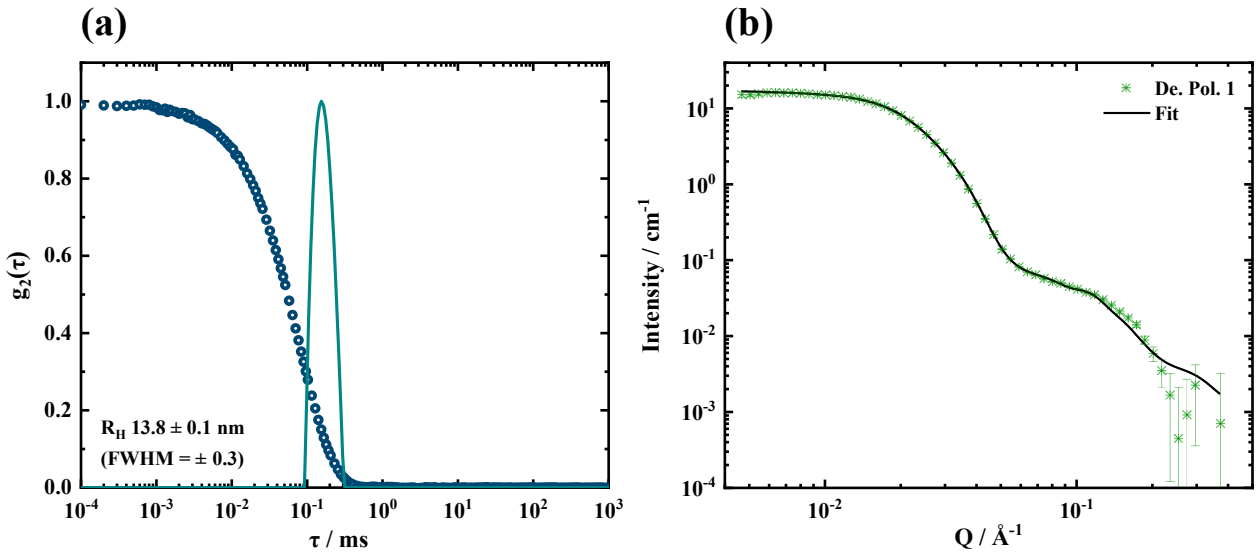


Figure S14. *(a) Intensity-time autocorrelation function $g_2(\tau)$ of De. Pol. 1 at 0.1 wt% and pH 5 in H_2O, measured at a scattering angle $\theta = 90^o$ and related relaxation time distribution from CONTIN method (in inset, hydrodynamic radius R_H and full width at half maximum (FWHM) from the CONTIN analysis are given) (b) SANS pattern of micelles from the same sample at 1 wt% in D_2O (pH 5). In black, the fit made using the polymer micelle model.*

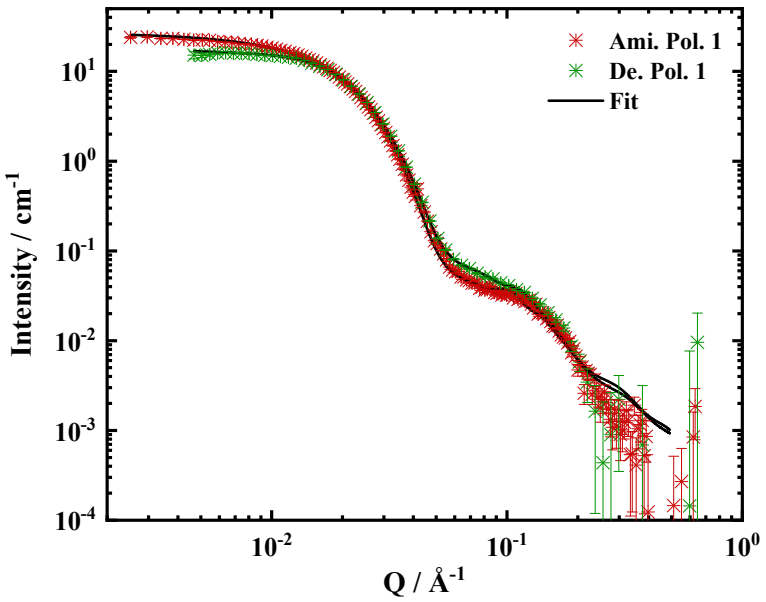


Figure S15. *SANS patterns of Ami. Pol. 1 and De. Pol. 1 micelles at pH 5 (1 wt% in D_2O). Ami. Pol. 1 is depicted using colour red while the green colour is for De. Pol. 1 micelles. The fit using the polymer micelle model is shown as black lines.*

Annex 2 - Supporting information for Chapter 2

Design of primary amine-based double-hydrophilic block copolymer: from their synthesis to the formation of polyion complex micelles by electrostatic complexation with polyacids

Ananthapadmanabhan Unnikrishnan,[1,2] Lynn Obeid,[1] Amna Korbi,[2] Gaulthier Rydzek,[2] Julien Schmitt,[2,3] Ralf Schweins[1] and Corine Gérardin[2]

[1] Institut Laue − Langevin, DS / LSS Group, 71 Avenue des Martyrs, CS 20156, Grenoble Cedex 9, F-38042, France

[2] Institut Charles Gerhardt, UMR 5253, CNRS-ENSCM-UM, University of Montpellier, Cedex, F-34295, France

[3] LSFC – Laboratoire de Synthèse et Fonctionnalisation des Céramiques, UMR 3080 CNRS/Saint-Gobain CREE, Saint-Gobain Research Provence, 550 Avenue Alphonse Jauffret, Cavaillon, France

Sample name	Block copolymer	Elemental Analysis (EA)							
		%C	Deviation (abs.)	%H	Deviation (abs.)	%N	Deviation (abs.)	%S	Deviation (abs.)
Pol. 1	P(OEGMEA)-*b*-P(AEMA)	48.96	0.23	8.02	0.29	2.78	0.17	0.61	0.07
Pol. 2	P(OEGMEA)-*b*-P(AEMA)	51.08	0.06	8.53	0.03	1.93	0.06	0.28	0.39

Table S1. *Elemental weight fractions of C, H, N, and S of the two P(OEGMEA)$_m$-b-P(AEMA)$_n$ polymers obtained by Elemental analysis.*

Sample name	Block copolymer (number of units from EA)	Polyelectrolyte with molecular weight (kDa)	Normalised scattering intensity
Agg. 1	P(OEGMEA)$_{21}$-*b*-P(AEMA)$_{32}$	PAA 5.1	0.00169
Agg. 2	P(OEGMEA)$_{21}$-*b*-P(AEMA)$_{32}$	PSS 1.1	0.00509
Agg. 3	P(OEGMEA)$_{21}$-*b*-P(AEMA)$_{32}$	PAA 2.1	0.00651
Agg. 4	P(OEGMEA)$_{25}$-*b*-P(AEMA)$_{22}$	PAA 2.1	0.00457

Table S2. *Normalized scattering intensity at pH = 5 for all the polymer/micellization agent complexes studied (0.1 wt%). The scattering value obtained is very high in all the systems (Agg. 2 - 4), except in the case of Pol. 1 with PAA 5.1 kDa micelles (Agg. 1). Hence, pH = 5 was considered as a suitable pH for comparison studies.*

Sample name	Concentration wt%	Scale Cylinder/Sphere (std. error)	Radius R nm (± 0.1)	Length L nm (± 1)	Polydispersity in radius σ % (± 1)	Scale Polymer exclusion volume (± 0.1)	Radius of gyration R_g nm (± 0.1)	Exponent α (± 0.1)
$P(OEGMEA)_{21}$-*b*-$P(AEMA)_{32}$ + PAANa 5.1 (Agg. 1)	**Cylinder + Free polymer**							
	1	0.22×10^{-3} (± 0.01×10^{-3})	8.4	138.2	25	0.21	2.1	3.8
	2	0.47×10^{-3} (± 0.01×10^{-3})	9.5	93.1	25	0.43	2.0	4.3
	3	0.57×10^{-3} (± 0.01×10^{-3})	8.9	111.3	25	0.62	2.1	3.8
	4	0.71×10^{-3} (± 0.01×10^{-3})	9.5	103.6	26	0.76	2.0	3.9
	5	0.89×10^{-3} (± 0.01×10^{-3})	10.3	102.6	26	0.86	2.0	3.9
$P(OEGMEA)_{21}$-*b*-$P(AEMA)_{32}$ + PSSNa 1.1 (Agg. 2)	**Sphere + Free polymer**							
	1	0.53×10^{-3} (± 0.01×10^{-3})	14.9	---	30	0.27	2.2	3.7
	2	0.10×10^{-2} (± 0.01×10^{-2})	14.9	---	30	0.50	2.2	3.5
	3	0.13×10^{-2} (± 0.01×10^{-2})	14.9	---	30	0.72	2.2	3.4
	4	0.18×10^{-2} (± 0.01×10^{-2})	14.9	---	30	0.92	2.2	3.4
	5	0.24×10^{-2} (± 0.01×10^{-2})	14.9	---	30	1.01	2.1	3.5
$P(OEGMEA)_{21}$-*b*-$P(AEMA)_{32}$ + PAANa 2.1 (Agg. 3)	**Sphere + Free polymer**							
	1	0.43×10^{-3} (± 0.01×10^{-3})	20.0	---	24	0.15	2.2	3.5
	2	0.89×10^{-3} (± 0.01×10^{-3})	20.0	---	24	0.27	2.0	3.6
	3	0.10×10^{-2} (± 0.01×10^{-2})	20.0	---	24	0.36	2.0	3.7
	4	0.14×10^{-2} (± 0.01×10^{-2})	20.0	---	25	0.52	2.0	3.9
	5	0.16×10^{-2} (± 0.01×10^{-2})	20.0	---	24	0.57	2.0	3.8
$P(OEGMEA)_{25}$-*b*-$P(AEMA)_{22}$ + PAANa 2.1 (Agg. 4)	**Sphere + Free polymer**							
	1	0.14×10^{-3} (± 0.01×10^{-3})	36.0	---	30	0.24	2.0	4.1
	2	0.22×10^{-3} (± 0.01×10^{-3})	40.7	---	30	0.47	2.0	4.0
	3	0.25×10^{-3} (± 0.01×10^{-3})	46.7	---	30	0.66	2.0	3.6
	4	0.26×10^{-3} (± 0.01×10^{-3})	45.2	---	30	0.81	1.9	3.9
	5	0.29×10^{-3} (± 0.01×10^{-3})	46.1	---	30	0.91	1.8	3.9

Table S3. *Parameters obtained from the SANS data fitting using a combination of simple cylinder/sphere and free polymer for Agg. 1 – 4 suspensions at 1 wt% in D_2O (pH = 5 and concentration 1 – 5 wt%).*

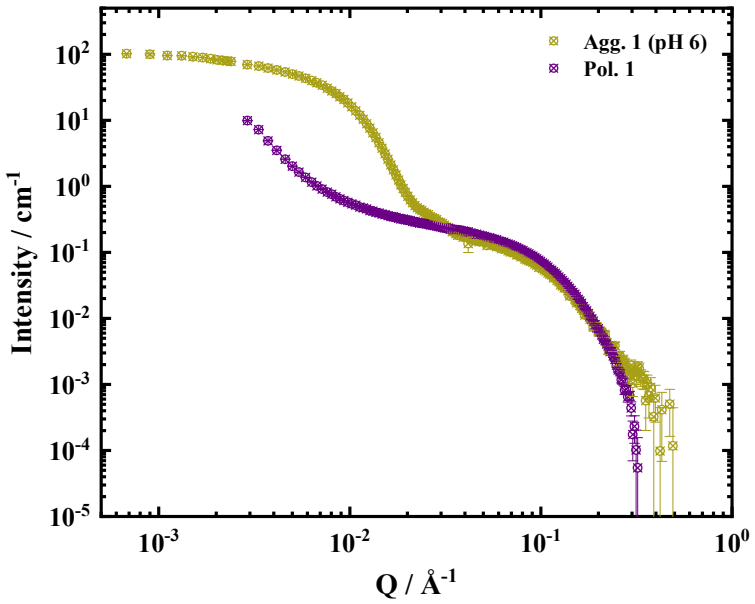


Figure S1. *SANS patterns of Pol. 1 (P(OEGMEA)$_{21}$-b-P(AEMA)$_{32}$) in D_2O (with 0.1 M NaCl), overlapped with the scattering curve of Agg. 1 (*P(OEGMEA)$_{21}$-*b*-P(AEMA)$_{32}$ + PAA 5.1 kD*) at pH = 6 in D_2O. The scattering from Pol. 1 show aggregation at low q, while in the high q, an oscillation (q = ca. 0.1 $Å^{-1}$) following power law is evident. In Agg. 1, a clear plateau formed in low q confirm no uncontrolled aggregations in the system. Agg. 1 gives two oscillations; a) at low q corresponding to micelles b) at high q associated to free polymers in the system. The second oscillation of the Agg. 1 overlaps well with the oscillation from Pol. 1 at ca. 0.1 $Å^{-1}$. This confirm that the second oscillation is indeed from the free polymer chains in the micellar solution rather than from the self-assembled structures. A small decrease of the intensity of this contribution at q = ca. 0.1 $Å^{-1}$ in Agg. 1 compared to Pol. 1 (both made at 1wt% in polymer) indicates that a fraction of polymer chains are being used for micellization once the polyelectrolyte is introduced in the system.*

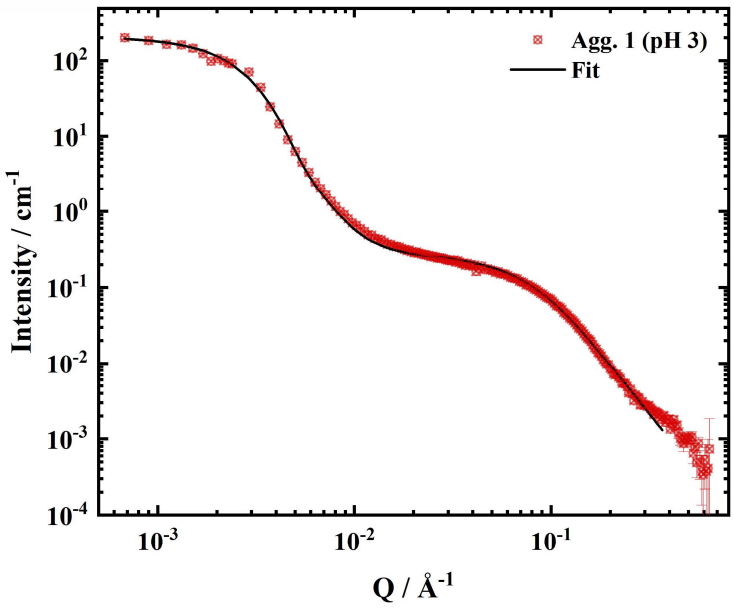


Figure S2. *SANS pattern of the self-assembly from Agg. 1 (pH = 3 and 1 wt%) in D_2O. In black, the fit made using the model (combination of sphere + free polymer).*

Annex 3 - Supporting information for Chapter 3

Self-assembly of oppositely charged double hydrophilic block copolymers, tailoring the shape of the micelles

Ananthapadmanabhan Unnikrishnan,[1,2] Najet Mahmoudi,[3] William Chèvremont,[4] Gaulthier Rydzek,[2] Julien Schmitt,[2,5] Ralf Schweins[1] and Corine Gérardin[2]

[1] Institut Laue − Langevin, DS / LSS Group, 71 Avenue des Martyrs, CS 20156, Grenoble Cedex 9, F-38042, France

[2] Institut Charles Gerhardt, UMR 5253, CNRS-ENSCM-UM, University of Montpellier, Cedex, F-34295, France

[3] ISIS Neutron and Muon Source, Science and Technology Facilities Council, Rutherford Appleton Laboratory, Didcot OX11 0QX, United Kingdom

[4] ESRF, The European Synchrotron, 71 Avenue des Martyrs, Grenoble, 38043, France

[5] LSFC – Laboratoire de Synthèse et Fonctionnalisation des Céramiques, UMR 3080 CNRS/Saint-Gobain CREE, Saint-Gobain Research Provence, 550 Avenue Alphonse Jauffret, Cavaillon, France

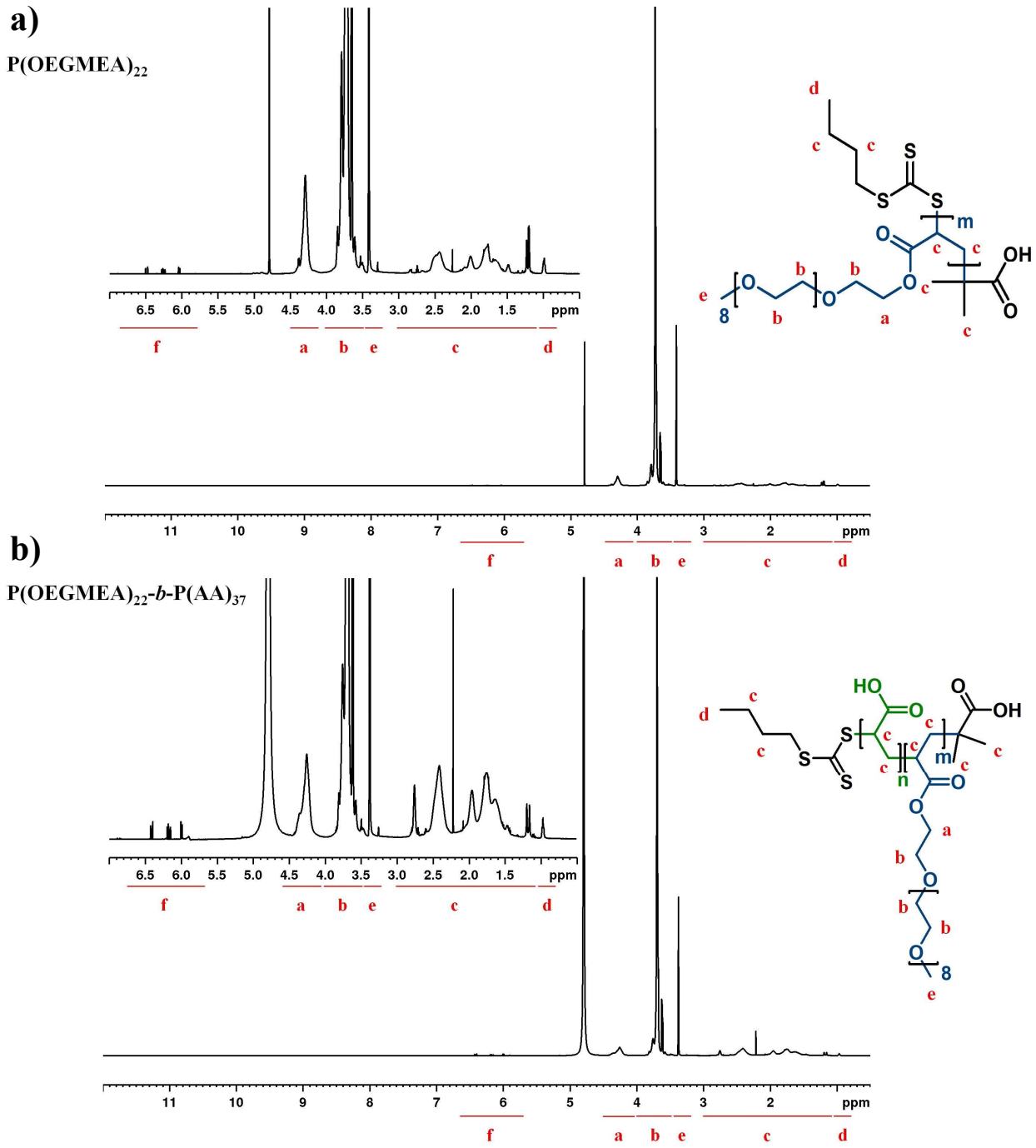

a)
P(OEGMEA)22
6.5 6.0 5.5 5.0 4.5 4.0 3.5 3.0 2.5 2.0 1.5 ppm
f a b e c d
11 10 9 8 7 6 5 4 3 2 ppm
f a b e c d
b)
P(OEGMEA)22-b-P(AA)37
6.5 6.0 5.5 5.0 4.5 4.0 3.5 3.0 2.5 2.0 1.5 ppm
f a b e c d
11 10 9 8 7 6 5 4 3 2 ppm
f a b e c d

Figure S1. *^{1}H NMR spectra of (a) $P(OEGMEA)_m$ (b) $P(OEGMEA)_m$-b-$P(AA)_n$ polymers synthesized through RAFT polymerization is depicted. The DP of each block was found using the peaks marked using alphabetical letters. In insets, the chemical formula of $P(OEGMEA)_m$ (b) $P(OEGMEA)_m$-b-$P(AA)_n$ are given and display which protons each highlighted signal corresponds to. The signal at 1 ppm (highlighted using "d") is associated with the three hydrogens species attached to the terminal carbon in the backbone for both (a) and (b). The peak area between 1.2 - 3.2 ppm presents the protons in the backbone of P(OEGMEA) of (a) and, in (b) is the contribution from the backbone of the total copolymer P(OEGMEA)-b-P(AA). The contribution from the protons in the side chains of P(OEGMEA) block is highlighted using a, b and e. The DP was identified to be 22 and 37 for P(OEGMEA) and P(AA) blocks respectively, $P(OEGMEA)_{22}$-b-$P(AA)_{37}$.*

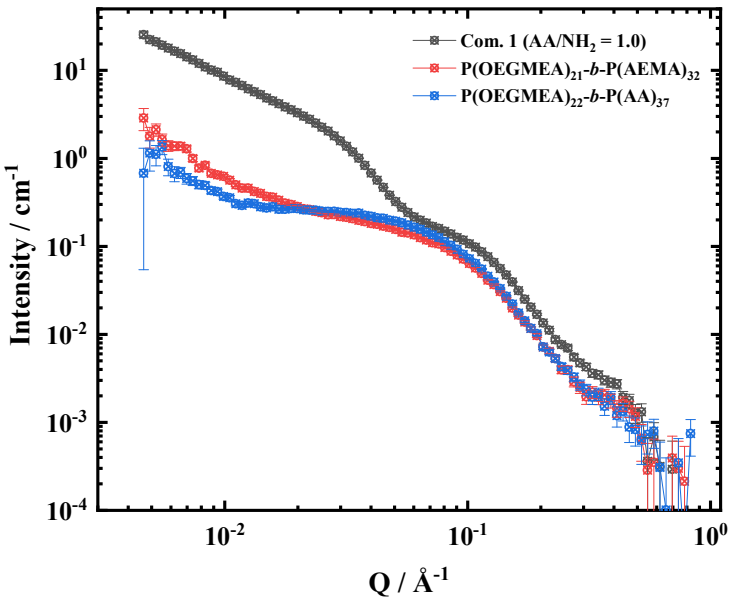


Figure S2. *Overlapping SANS pattern of micelles from Com. 1 (AA/NH_2 = 1.0, 1 wt% in terms of $P(OEGMEA)_{21}$-b-$P(AEMA)_{32}$) with its constituent polymers; $P(OEGMEA)_{21}$-b-$P(AEMA)_{32}$ and $P(OEGMEA)_{22}$-b-$P(AA)_{37}$ (1 wt%) at pH = 5.5 in D_2O.*

Sample name	Concentration wt%	Scale Cylinder	Radius R nm	Kuhn length L nm	Polydispersity in radius σ %	Scale Polymer exclusion volume	Radius of gyration R_g nm	Exponent α
$P(OEGMEA)_{21}$-*b*-$P(AEMA)_{32}$ + $P(OEGMEA)_{22}$-*b*-$P(AA)_{37}$ (Com. 1)	**Flexible cylinder + Free polymer**							
	0.5	0.51 ± 0.01 × 10^{-3}	5.7 ± 0.1	68.5 ± 2.2	11 ± 1	0.15 ± 0.01	1.8 ± 0.1	4.3 ± 0.1
	1.0	0.96 ± 0.01 × 10^{-3}	5.7 ± 0.1	69.0 ± 1.6	10 ± 1	0.29 ± 0.01	1.8 ± 0.1	3.8 ± 0.1
	1.5	0.14 ± 0.01 × 10^{-2}	5.6 ± 0.1	102.0 ± 5.6	9 ± 1	0.43 ± 0.01	1.7 ± 0.1	4.2 ± 0.1
	2.0	0.17 ± 0.01 × 10^{-2}	5.5 ± 0.1	150.0 (fixed)	10 ± 1	0.54 ± 0.01	1.7 ± 0.1	4.0 ± 0.1
	2.5	0.18 ± 0.01 × 10^{-2}	5.3 ± 0.1	150.0 (fixed)	10 ± 1	0.63 ± 0.01	1.7 ± 0.1	4.4 ± 0.1

Table S1. *Parameters obtained from the SANS data fitting using a combination of flexible cylinder and free polymer for Com. 1 suspensions in D_2O (pH = 5.5, concentration 0.5 – 2.5 wt%, AA/NH_2 = 1.1 and L_c fixed at 150 nm).*

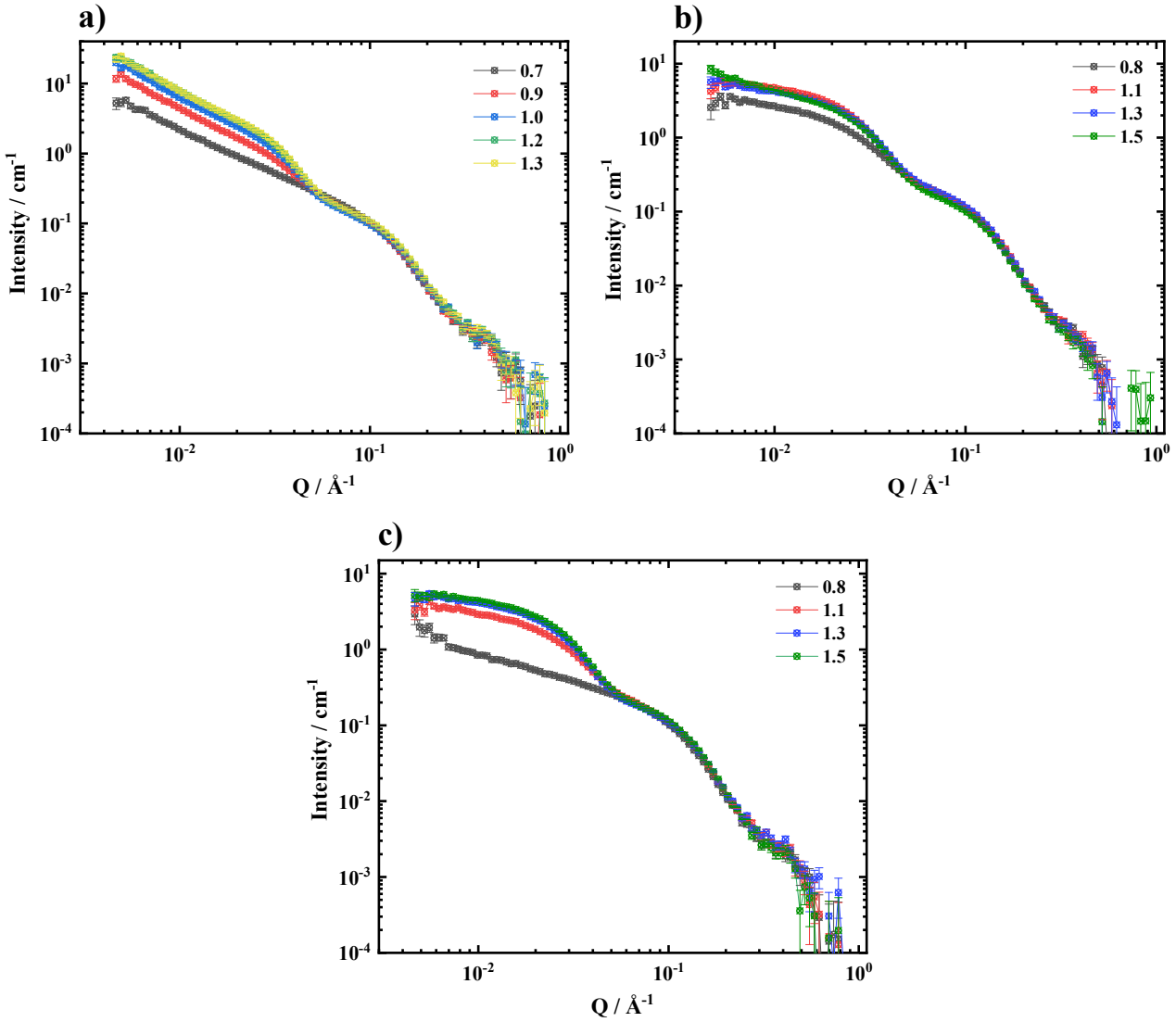


Figure S3. *Charge ratio study on different micelles from P(OEGMEA)-b-P(AEMA) and P(OEGMEA)-b-P(AA) (Com. 2 – 4, 1 wt% in terms of P(OEGMEA)-b-P(AEMA)) at pH = 5.5 in D_2O; a) Com. 2, b) Com. 3, c) Com. 4.*

Sample name	Scale Cylinder/Sphere	Radius R nm	Kuhn length L nm	Polydispersity in radius σ %	Scale Polymer exclusion volume	Radius of gyration R_g nm	Exponent α
Flexible cylinder + Free polymer							
Com. 1	$0.96 \pm 0.01 \times 10^{-3}$	5.7 ± 0.1	69.0 ± 1.6	10 ± 1	0.29 ± 0.01	1.8 ± 0.1	3.8 ± 0.1
Com. 2	$0.87 \pm 0.01 \times 10^{-3}$	5.5 ± 0.1	59.2 ± 1.2	10 ± 1	0.26 ± 0.01	1.8 ± 0.1	4.0 ± 0.1
Simple sphere + Free polymer							
Com. 3	$0.67 \pm 0.01 \times 10^{-3}$	6.8 ± 0.1	----	25 ± 1	0.29 ± 0.01	1.8 ± 0.1	4.1 ± 0.1
Com. 4	$0.70 \pm 0.01 \times 10^{-3}$	6.8 ± 0.1	----	25 ± 1	0.27 ± 0.01	1.8 ± 0.1	4.3 ± 0.1

Table S2. *Parameters obtained from the SANS data fitting using a combination of flexible cylinder/simple sphere and free polymer for Com. 1 - 4 suspensions at 1 wt% in D_2O (pH = 5.5, for optimal AA/NH_2 corresponding to each system refer Table 1, L_c fixed at 150 nm for cylinder).*

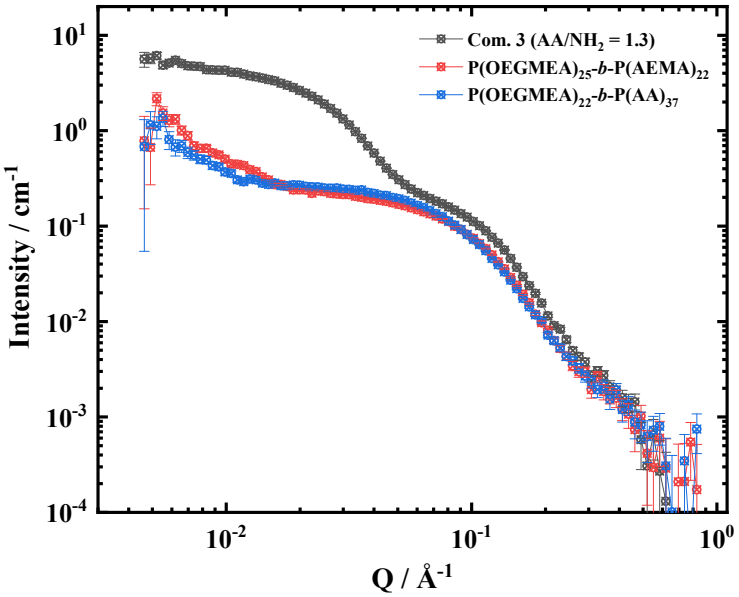


Figure S4. *Overlapping SANS pattern of micelles from Com. 3 (AA/NH_2 = 1.3, 1 wt% in terms of $P(OEGMEA)_{25}$-b-$P(AEMA)_{22}$) with its constituent polymers; $P(OEGMEA)_{25}$-b-$P(AEMA)_{22}$ and $P(OEGMEA)_{22}$-b-$P(AA)_{37}$ (1 wt%) at pH = 5.5 in D_2O.*

Light scattering data of Com. 1 micelles as a function of pH

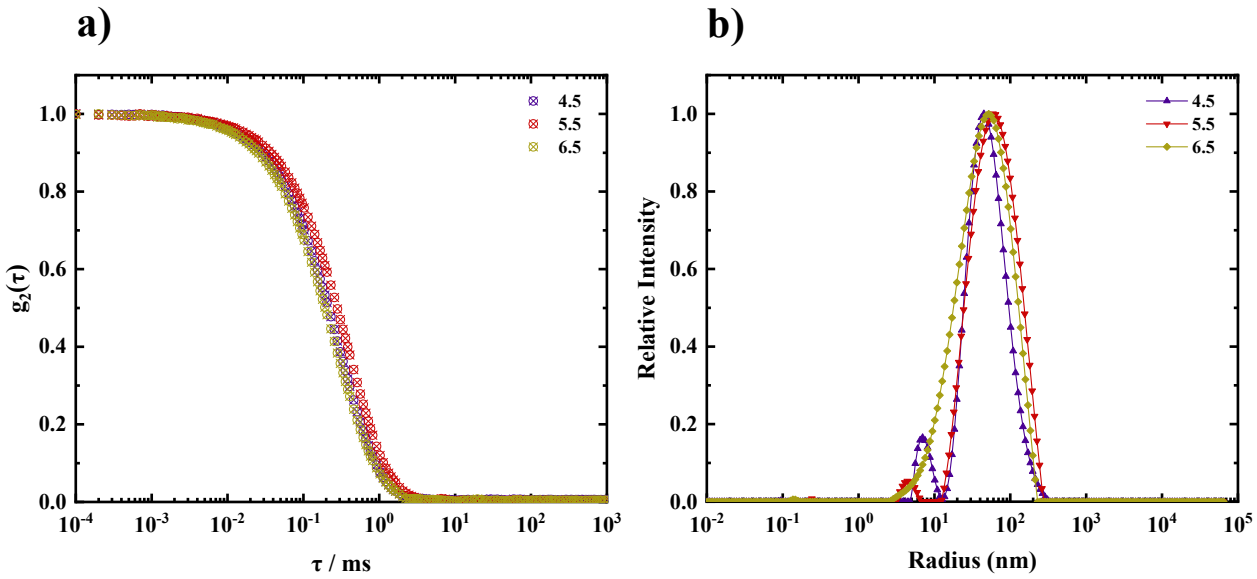


Figure S5. *Dynamic light scattering data of the self-assembly from Com. 1 at 0.1 wt% and different pHs (4.5 – 6.5) in D_2O: (a) Intensity time autocorrelation function $g_2(\tau)$ of the self-assembly at various pH conditions combined (scattering angle $\theta = 90^o$) (b) size distribution from the intensity time autocorrelation function $g_2(\tau)$ at a scattering angle of $\theta = 90^o$ analyzed using CONTIN (the data has been split between figures for easy visualisation and interpretation in both (a) and (b)).*

More inferences on the effect of pH in micellization could be derived upon comparing the intensity time auto-correlation function $g_2(\tau)$, at different pH values (4.5 – 6.5, **Figure S5a**). The correlation functions depicted are found to have a clear signal-to-noise ratio along with the baseline stability, implying sufficient scattering from the objects. The correlation function at all pHs predominantly seems to follow a single exponential decay, which would ideally point at the presence of one stable well-defined population.

Further, the correlation functions obtained were fitted using CONTIN method (pH = 4.5 – 6.5, **Figure S5b**). A monomodal distribution of size is obtained for all three pHs, but with varying peak width. At the intermediate pH = 5.5, a single well-defined signal is obtained, with a relatively low

polydispersity compared to others, proving it to be the most ideal pH for micellization. Moving away from pH = 5.5, either the peak width of the sample increase significantly or give rise to other notable peaks, hinting at the dissociation of the self-assembled population (see **Figure S5b)**. At pH = 4.5, the peak width is lowest among the studied, suggesting micellar formation. However, the presence of another notable population at ca. 10 nm, prove pH = 4.5 to be acceptable but not ideal. The increase in polydispersity is significant at pH = 6.5, proving the formation of no stable population but presence of either individual polymeric chains or random aggregates.

pH	Particle hydrodynamic radius R_H (width) nm	PDI M_w/M_n
4.5	37.4 (22.2)	1.35
5.5	48.3 (28.1)	1.34
6.5	33.9 (20.9)	1.38

Table S3. *Particle hydrodynamic radius R_H (nm) and associated polydispersity index (PDI) derived from the cumulant analysis of the intensity-time autocorrelation function $g_2(\tau)$ at a scattering angle of $\theta = 90^o$ for the self-assembly from P(OEGMEA)$_{21}$-b-P(AEMA)$_{32}$ at 0.1 wt% in D_2O with P(OEGMEA)$_{22}$-b-P(AA)$_{37}$ (Com. 1), varying pH between 4.5 - 6.5.*

The auto-correlation function at pHs 4.5 – 6.5 were also fitted using the cumulant to collect more information about the particle hydrodynamic radius and polydispersity in the system (**Table S3**). Depending on the pH used, the dimensions of species formed show considerable fluctuation. At pH = 5.5, the highest R_H of ca. 48 nm was recorded, which reduces moving either to pH = 4.5 or 6.5. Also, among the fitted data, the lowest polydispersity was seen at pH = 5.5. The highest particle hydrodynamic radius along with the lowest polydispersity found, confirms that the micellar species are best formed at pH = 5.5.